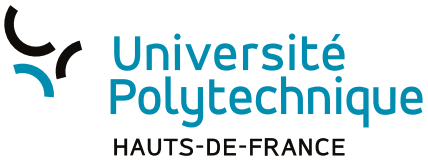

Cooperative distributed navigation for wheeled mobile robots using the Vector Field Orientation approach under time constraints

PhD dissertation

Rafał Mateusz SOBAŃSKI

The research was conducted under the joint supervision of:

prof. Maciej Marcin MICHAŁEK

Institute of Automatic Control and Robotics,
Poznan University of Technology

prof. Michael DEFOORT

CNRS, UMR 8201-LAMIH,
Université Polytechnique Hauts-de-France

2026

Cooperative distributed navigation for wheeled mobile robots using the Vector Field Orientation approach under time constraints

PhD dissertation
Rafał Mateusz SOBAŃSKI

Abstract

This doctoral dissertation is focused on the development of control algorithms within the *Vector Field Orientation* (VFO) methodology for nonholonomic mobile robots and distributed multi-vehicle systems composed of nonholonomic vehicles, which simultaneously take into account task execution time constraints and control input constraints.

This work uses the concept of *fixed-time stability*, which guarantees that the system's errors will converge to zero within a fixed time, which is upper-bounded by a certain constant value. Furthermore, the value of this upper bound is independent of a particular initial condition and holds for all initial conditions belonging to a certain set of admissible initial conditions. In this dissertation, due to the simultaneous consideration of time constraints and control input constraints, the use of a 'local' estimation of this upper bound is proposed.

The control algorithms developed are dedicated to unicycle-like mobile robots and were designed based on a two-stage control design approach, which means that a *nominal* control law is first designed, which does not guarantee satisfaction of the imposed constraints on the control inputs, and then a scaling procedure is performed to rescale the control signal values in order to satisfy the constraints.

This dissertation presents control laws for two control problems defined for a nonholonomic mobile robot, namely the set-point stabilization problem and the path-following problem with a nonparametrized reference path. Furthermore, two control algorithms for a nonholonomic multi-vehicle system are proposed, which address the problem of distributed formation control. The stability of the proposed algorithms has been formally proven, and the performance was verified by numerical simulations and experimental tests using physical mobile robots.

Kooperatywna rozproszona nawigacja dla kołowych robotów mobilnych z wykorzystaniem metodyki orientowania pól wektorowych (VFO) w obecności ograniczeń czasowych

Rozprawa doktorska
Rafał Mateusz SOBAŃSKI

Streszczenie

Niniejsza rozprawa doktorska poświęcona jest opracowaniu algorytmów sterowania w ramach metodyki orientowania pól wektorowych (VFO, ang. *Vector Field Orientation*) dla nieholonomicznych robotów mobilnych oraz rozproszonych systemów wielopojazdowych złożonych z pojazdów nieholonomicznych, które jednocześnie uwzględniają ograniczenia czasu wykonania zadania oraz ograniczenia wejść sterujących.

W pracy wykorzystano koncept stabilności w czasie ustalonym (ang. *fixed-time stability*), który zakłada, że zbieżność błędów systemu do zera nastąpi w skończonym czasie, który jest odgórnie ograniczony przez pewną stałą wartość. Ponadto, wartość tegoż górnego ograniczenia jest niezależna od poszczególnego warunku początkowego i jest słuszna dla wszystkich warunków początkowych należących do pewnego zbioru dopuszczalnych warunków początkowych. W niniejszej rozprawie, ze względu na jednoczesne rozważanie ograniczeń czasu i ograniczeń wejść sterujących, zaproponowano wykorzystanie pewnego „lokalnego" szacowania tegoż górnego ograniczenia.

Opracowane algorytmy sterowania są dedykowane dla robota mobilnego typu monocykl i zostały zaprojektowane w oparciu o dwuetapową ideę projektowania sterowań, to znaczy najpierw projektowane jest *nominalne* prawo sterowania, które nie gwarantuje spełnienia nałożonych ograniczeń wejść sterujących, a następnie wykonywana jest procedura skalowania, która skaluje wartości sygnałów sterujących w celu spełnienia nałożonych ograniczeń.

W niniejszej rozprawie przedstawiono prawa sterowania dla dwóch problemów sterowania zdefiniowanych dla nieholonomicznego robota mobilnego, a mianowicie problemu podążania wzdłuż nieparametryzowanej ścieżki referencyjnej oraz problemu sterowania do punktu. Ponadto zaproponowano dwa algorytmy sterowania dla nieholonomicznego systemu wielopojazdowego, które rozwiązują problem rozproszonego tworzenia formacji. Stabilność proponowanych algorytmów została formalnie wykazana, a wydajność została zweryfikowana za pomocą symulacji numerycznych oraz testów eksperymentalnych z wykorzystaniem fizycznych robotów mobilnych.

Kooperatywna rozproszona nawigacja dla kołowych robotów mobilnych z wykorzystaniem metodyki orientowania pól wektorowych (VFO) w obecności ograniczeń czasowych

Rozprawa doktorska
Rafał Mateusz SOBAŃSKI

Streszczenie rozszerzone

Niniejsza rozprawa doktorska poświęcona jest opracowaniu algorytmów sterowania w ramach metodyki orientowania pól wektorowych (VFO, ang. *Vector Field Orientation*, zobacz [2]) dla nieholonomicznych robotów mobilnych oraz rozproszonych systemów wielopojazdowych złożonych z pojazdów nieholonomicznych, które jednocześnie uwzględniają ograniczenia czasu wykonania zadania oraz ograniczenia wejść sterujących.

W pracy wykorzystano koncept stabilności w czasie ustalonym (ang. *fixed-time stability*) zdefiniowany w [5]. Koncept ten zakłada, że zbieżność błędów systemu do zera nastąpi w skończonym czasie t_s, który jest odgórnie ograniczony przez pewną stałą wartość T_c. Ponadto, wartość tegoż górnego ograniczenia T_c jest niezależna od konkretnego warunku początkowego $\boldsymbol{z}_0$ i jest słuszna dla wszystkich warunków początkowych należących do pewnego zbioru $\mathcal{V} \subseteq \mathbb{R}^n$ dopuszczalnych warunków początkowych. Zgodnie z [5], badanie stabilności w czasie ustalonym punktu równowagi danego systemu opiera się na wykorzystaniu metody Lapunowa, to znaczy na znalezieniu takiej dodatnio określonej funkcji $V(\boldsymbol{z})$ której pochodna czasowa jest ograniczona następującym wyrażeniem:

$$\dot{V}(\boldsymbol{z}) \leq -\beta_1 V^{P_1}(\boldsymbol{z}) - \beta_2 V^{P_2}(\boldsymbol{z}), \tag{1}$$

gdzie $\beta_1 > 0$, $\beta_2 > 0$, $P_1 \in (0, 1)$, oraz $P_2 > 1$. Następnie, w oparciu o uzyskane wartości $\beta_1, \beta_2, P_1, P_2$ oraz o odpowiedni lemmat sformułowany na przykład w [1, 4] można oszacować wartość górnego ograniczenia T_c czasu ustalania t_s. W niniejszej rozprawie, ze względu na jednoczesne rozważanie ograniczeń czasu i ograniczeń wejść sterujących, zaproponowano wykorzystanie pewnego „lokalnego" szacowania, które pozwala uzyskać wartość T_c słuszną dla konkretnego zbioru $\mathcal{V} \subset \mathbb{R}^n$ warunków początkowych i zależną od największej normy warunku początkowego z rozważanego zbioru.

Opracowane algorytmy sterowania są dedykowane dla robota mobilnego typu monocykl, którego model kinematyczny może być zapisany następująco:

$$\dot{\boldsymbol{q}} \triangleq \boldsymbol{G}(\boldsymbol{q})\boldsymbol{u} = \begin{bmatrix} 1 & 0 \\ 0 & \cos\theta \\ 0 & \sin\theta \end{bmatrix} \begin{bmatrix} u_1 \\ u_2 \end{bmatrix} = \boldsymbol{g}_1 u_1 + \boldsymbol{g}_2(\theta) u_2, \tag{2}$$

gdzie $\boldsymbol{q} = \begin{bmatrix} \theta & x & y \end{bmatrix}^\top$ jest wektorem konfiguracyjnym zawierającym pozycję (x, y) punktu prowadzenia pojazdu umieszczonego pośrodku osi łączącej koło prawe i lewe

robota, oraz kąt θ wyrażający orientację robota w układzie globalnym (por. Rys. 1). Wejścia sterujące $\boldsymbol{u} = \begin{bmatrix} u_1 & u_2 \end{bmatrix}^\top$ w przypadku robota typu monocykl są interpretowane jako prędkość kątowa u_1 oraz prędkość postępowa u_2 punktu prowadzenia pojazdu. W pracy przyjęto, że wejścia sterujące są ograniczone, to znaczy $\boldsymbol{u} \in \mathscr{U} \subset \mathbb{R}^2$, gdzie $\mathscr{U} \triangleq \{\boldsymbol{u} : |u_1| \leq u_{1M}, |u_2| \leq u_{2M}\}$ jest zbiorem dopuszczalnych wejść sterujących, natomiast u_{1M} i u_{2M} są wybierane przez projektanta i oznaczają odpowiednio największą dozwoloną wartość bezwzględną prędkości kątowej i postępowej (por. Rys. 2).

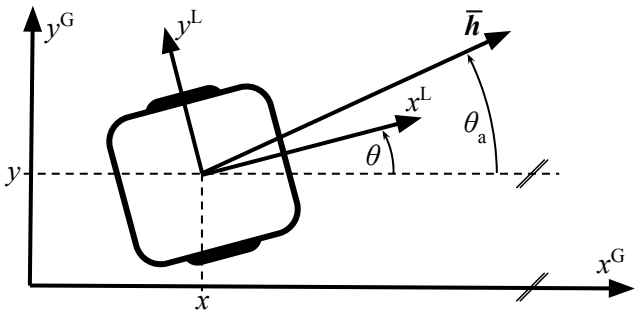

Rysunek 1: Dwukołowy robot mobilny typu monocykl.

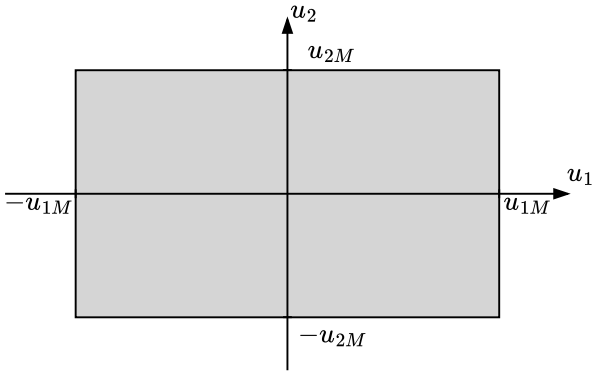

Rysunek 2: Zbiór $\mathscr{U}$ dopuszczalnych wejść sterujących.

W rozprawie wykorzystano dwuetapową ideę projektowania sterowań, to znaczy najpierw projektowane jest *nominalne* prawo sterowania $\boldsymbol{u}_N \in \mathbb{R}^2$ które nie gwarantuje spełnienia nałożonych ograniczeń wejść sterujących, a następnie wykonywana jest procedura skalowania (zobacz, np. [3]), która wykorzystuje funkcję skalującą s do przeskalowania nominalnych wartości sygnałów sterujących w celu uzyskania prawa sterowania $\boldsymbol{u} = s\boldsymbol{u}_N \in \mathscr{U}$ spełniającego nałożone ograniczenia. Wykorzystana procedura skalowania gwarantuje, że kierunek i zwrot *nominalnego* wektora sygnałów sterujących zostanie zachowany.

Metodyka VFO została opublikowana w [2]. Opiera się ona na intuicyjnych geometrycznych zależnościach, a jej kluczowym elementem jest tak zwane wektorowe pole zbieżności definiowane następująco:

$$\boldsymbol{h} = \begin{bmatrix} h_\theta \\ \bar{\boldsymbol{h}} \end{bmatrix} = \begin{bmatrix} h_\theta \\ h_x \\ h_y \end{bmatrix}, \tag{3}$$

które dla każdego punktu przestrzeni konfiguracyjnej wskazuje pożądany kierunek zbieżności gwarantujący realizację wybranego zadania ruchu. Sposób zdefiniowania pola $\boldsymbol{h}$ determinuje zadanie, które będzie wykonywane. Innym charakterystycznym elementem metodyki VFO jest tak zwana orientacja pomocnicza θ_a, która oznacza orientację pozycyjnej części $\bar{\boldsymbol{h}}$ wektorowego pola zbieżności $\boldsymbol{h}$ w układzie globalnym (por. Rys. 1). Ogólna postać prawa sterowania VFO może być zapisana następująco:

$$u_1 \triangleq h_\theta, \tag{4}$$

$$u_2 \triangleq \boldsymbol{h}^\top \boldsymbol{g}_2(\theta), \tag{5}$$

gdzie u_1 nazywane jest sterowaniem orientującym, gdyż odpowiada za zmianę orientacji robota na orientację zgodną z pozycyjną częścią $\bar{\boldsymbol{h}}$ wektorowego pola zbieżności, natomiast u_2 nazywane jest sterowanie popychającym, ponieważ jego celem jest pchnięcie robota wzdłuż wektorowego pola zbieżności.

Niniejsza rozprawa zawiera cztery algorytmy sterowania opracowane z wykorzystaniem metodyki VFO i konceptu stabilności w czasie ustalonym. Dwa z zaproponowanych algorytmów dedykowane są dla pojedynczego nieholonomicznego robota mobilnego i pozwalają rozwiązać następujące problemy sterowania:

- *sterowanie do punktu* (por. [9]) – zadanie polega na zagwarantowaniu, że robot osiągnie zadaną stałą konfigurację. W rozprawie przedstawiono syntezę prawa sterowania wraz z formalnym dowodem stabilności w czasie ustalonym, oraz metodą pozwalającą znaleźć *a priori* maksymalne możliwe wartości bezwzględne nominalnych sygnałów sterujących dla warunków początkowych należących do pewnego zbioru dopuszczalnych warunków początkowych. Działanie zaproponowanego algorytmu zostało przetestowane poprzez symulacje numeryczne i testy eksperymentalne z wykorzystaniem fizycznego robota mobilnego.
- *odtwarzanie ścieżki referencyjnej* (por. [10]) – zadanie polega na zagwarantowaniu, że robot dojedzie do zadanej ścieżki referencyjnej w skończonym czasie i następnie będzie się nią poruszał ze stałą prędkością postępową. W pracy przedstawiono syntezę prawa sterowania wraz z formalną analizą stabilności, oraz wyniki symulacji numerycznych i testów eksperymentalnych wykorzystujących fizycznego robota mobilnego.

Algorytmy sterowania dedykowane dla rozproszonych systemów wielopojazdowych (por. [6]) skupiały się na realizacji zadania tworzenia zadanej formacji. W rozprawie przedstawiono dwie propozycje rozwiązania tego problemu:

- *podejście wykorzystujące rozproszone obserwatory* (por. [7, 8]) – zaproponowano wykorzystanie rozproszonych obserwatorów, których zadaniem jest obliczenie dla każdego z pojazdów zadanej konfiguracji pozwalającej na utworzenie formacji o kształcie zdefiniowanym przez projektanta. Obserwatory wykorzystują informację o konfiguracji początkowej danego pojazdu i o konfiguracjach początkowych pojazdów, które mogą się z nim wymieniać informacjami. To podejście wykorzystuje pewien dwuetapowy proces sterowania: najpierw rozproszone obserwatory estymują zadane konfiguracje, a następnie na każdym z pojazdów zostaje uruchomione prawo sterowania pozwalające zrealizować zadanie stabilizacji w punkcie. Stabilność w czasie ustalonym zaproponowanych obserwatorów została formalnie wykazana, a działanie algorytmu zostało zweryfikowane poprzez symulacje numeryczne.

- *podejście wykorzystujące mechanizm konsensusu* – mechanizm konsensusu polega na pewnego rodzaju negocjacjach w wyniku których pojazdy uzgadniają wspólną wartość pewnej zmiennej. W przypadku zadania tworzenia formacji zmienna ta związana jest z pozycją punktu wokół którego pojazdy utworzą formację o kształcie zadanym przez projektanta. W zaproponowanym algorytmie sterowania pojazdy wykonują ruch w celu utworzenia zadanej formacji mimo, że aż do zakończenia ruchu nie jest wiadome gdzie ta formacja zostanie utworzona (zaletą tego podejścia jest jeden etap sterowania w porównaniu do dwóch etapów w przypadku podejścia wykorzystującego obserwatory). W rozprawie przedstawiono syntezę algorytmu sterowania wraz z formalnym dowodem stabilności oraz metodą rozproszonego uzgadniania najmniejszej wartości funkcji skalującej s generowanej przez pojazdy wchodzące w skład systemu, która potrzebna jest do poprawy jakości działania algorytmu sterowania i formalnego wykazania stabilności. Działanie algorytmu zostało przetestowane poprzez symulacje numeryczne oraz testy eksperymentalne.

W rozprawie został także zawarty przegląd literatury wskazujący na nowość i wkład zaproponowanych rozwiązań, oraz dyskusja dotycząca dalszych możliwości rozwoju.

Bibliografia

[1] R. Aldana-López, D. Gómez-Gutiérrez, E. Jiménez-Rodríguez, J. D. Sánchez-Torres, and M. Defoort, "Enhancing the settling time estimation of a class of fixed-time stable systems," *International Journal of Robust and Nonlinear Control*, vol. 29, no. 12, pp. 4135–4148, 2019.

[2] M. Michałek and K. Kozłowski, "Vector-Field-Orientation feedback control method for a differentially driven vehicle," *IEEE Transactions on Control Systems Technology*, vol. 18, no. 1, pp. 45–65, 2010.

[3] G. Oriolo, A. De Luca, and M. Vendittelli, "WMR control via dynamic feedback linearization: design, implementation, and experimental validation," *IEEE Transactions on Control Systems Technology*, vol. 10, no. 6, pp. 835–852, 2002.

[4] S. Parsegov, A. Polyakov, and P. Shcherbakov, "Nonlinear fixed-time control protocol for uniform allocation of agents on a segment," in *2012 IEEE 51st IEEE Conference on Decision and Control (CDC)*, 2012, pp. 7732–7737.

[5] A. Polyakov, "Nonlinear feedback design for fixed-time stabilization of linear control systems," *IEEE Transactions on Automatic Control*, vol. 57, no. 8, pp. 2106–2110, 2012.

[6] W. Ren and R. W. Beard, *Distributed Consensus in Multi-vehicle Cooperative Control: Theory and Applications*. London: Springer London, 2008.

[7] R. M. Sobański, M. Defoort, and M. M. Michałek, "Decentralized predefined-time leaderless consensus-formation VFO control for nonholonomic multi-agent systems," in *2024 13th International Workshop on Robot Motion and Control (RoMoCo)*, 2024, pp. 136–141.

[8] ——, "Observer-based fixed-time VFO control algorithm for leaderless multi-vehicle systems with directed communication topology," in *22nd Polish Control Conference*, 2026, (zaakceptowany).

[9] R. M. Sobański, M. M. Michałek, and M. Defoort, "Fixed-time VFO control design for nonholonomic mobile robots with constrained control inputs," *IEEE Transactions on Cybernetics*, vol. 55, no. 7, pp. 3038–3050, 2025.

[10] ——, "Fixed-time path-following VFO control design for a unicycle-like mobile robot with constrained control inputs," in *23rd IFAC World Congress*, 2026, (zaakceptowany).

Navigation distribuée coopérative pour robots mobiles en utilisant une approche d'orientation de champ vectoriel (VFO) sous contraintes de temps

Thèse de doctorat

Rafał Mateusz SOBAŃSKI

Résumé

La présente thèse de doctorat est consacrée à l'élaboration d'algorithmes de commande dans le cadre de la méthodologie d'orientation des champs vectoriels (VFO, en anglais *Vector Field Orientation*) pour les robots mobiles non holonomes et les systèmes multi-véhicules distribués composés de véhicules non holonomes, qui tiennent compte à la fois des contraintes sur le temps d'exécution de la tâche et des contraintes sur les entrées de commande.

Ce travail s'appuie sur le concept de stabilité en temps fixe (en anglais *fixed-time stability*), qui suppose que la convergence des erreurs du système vers zéro se produira en un temps fini, limité a priori par une certaine valeur constante. De plus, la valeur de cette limite supérieure est indépendante de la condition initiale particulière et vaut pour toutes les conditions initiales appartenant à un certain ensemble de conditions initiales admissibles. Dans la présente thèse, compte tenu de la prise en compte simultanée des contraintes de temps et des contraintes sur les entrées de commande, il est proposé d'utiliser une estimation « locale » de cette limite supérieure.

Les algorithmes de commande développés sont destinés à un robot mobile de type unicycle et ont été conçus selon une approche de conception en deux étapes : on commence par concevoir une loi de commande nominale, qui ne garantit pas le respect des contraintes imposées aux entrées de commande, puis une procédure de mise à l'échelle est effectuée, qui redimensionne les valeurs des signaux de commande afin de respecter les contraintes imposées.

Cette thèse présente des lois de commande pour deux problèmes de commande définis pour un robot mobile non holonome, à savoir le problème du suivi d'une trajectoire de référence non paramétrée et le problème de la stabilisation en un point donné. De plus, deux algorithmes de commande pour un système multi-véhicules non holonomes sont proposés, qui résolvent le problème de la formation de formation distribuée. La stabilité des algorithmes proposés a été formellement démontrée, et leur performance a été vérifiée à l'aide de simulations numériques et de tests expérimentaux utilisant des robots mobiles physiques.

Navigation distribuée coopérative pour robots mobiles en utilisant une approche d'orientation de champ vectoriel (VFO) sous contraintes de temps

Thèse de doctorat
Rafał Mateusz SOBAŃSKI

Résumé détaillé

La présente thèse de doctorat est consacrée à l'élaboration d'algorithmes de commande dans le cadre de la méthodologie d'orientation des champs vectoriels (VFO, en anglais *Vector Field Orientation*, voir [2]) pour les robots mobiles non holonomes et les systèmes multi-véhicules distribués composés de véhicules non holonomes, qui tiennent compte à la fois des contraintes sur le temps d'exécution de la tâche et des contraintes sur les entrées de commande.

Ce travail utilise le concept de stabilité en temps fixe (en anglais *fixed-time stability*) défini dans [5]. Ce concept suppose que la convergence des erreurs du système vers zéro se produira en un temps fini t_s, qui est limité par une certaine valeur constante T_c. De plus, la valeur de cette borne supérieure T_c est indépendante de la condition initiale particulière $\boldsymbol{z}_0$ et vaut pour toutes les conditions initiales appartenant à un certain ensemble $\mathcal{V} \subseteq \mathbb{R}^n$ de conditions initiales admissibles. Selon [5], l'étude de la stabilité en régime permanent d'un point d'équilibre d'un système donné peut reposer sur l'utilisation de la méthode de Lapunov, c'est-à-dire sur la recherche d'une fonction définie positive, radialement bornée, $V(\boldsymbol{z})$ dont la dérivée temporelle est bornée par l'expression suivante :

$$\dot{V}(\boldsymbol{z}) \leq -\beta_1 V^{P_1}(\boldsymbol{z}) - \beta_2 V^{P_2}(\boldsymbol{z}), \tag{1}$$

où $\beta_1 > 0$, $\beta_2 > 0$, $P_1 \in (0, 1)$, et $P_2 > 1$. Ensuite, à partir des valeurs obtenues $\beta_1, \beta_2, P_1, P_2$ et d'un lemme approprié formulé par exemple dans [1, 4], on peut estimer la valeur de la borne supérieure T_c du temps de stabilisation t_s. Dans la présente thèse, compte tenu de la prise en compte simultanée des contraintes de temps et des contraintes sur les entrées de commande, nous proposons d'utiliser une estimation dite « locale », qui permet d'obtenir une valeur de T_c valable pour un ensemble concret $\mathcal{V} \subset \mathbb{R}^n$ de conditions initiales et dépendant de la plus grande valeur de la norme de la condition initiale parmi l'ensemble considéré.

Les algorithmes de commande développés sont destinés à un robot mobile de type unicycle, dont le modèle cinématique peut s'écrire comme suit :

$$\dot{\boldsymbol{q}} \triangleq \boldsymbol{G}(\boldsymbol{q})\boldsymbol{u} = \begin{bmatrix} 1 & 0 \\ 0 & \cos\theta \\ 0 & \sin\theta \end{bmatrix} \begin{bmatrix} u_1 \\ u_2 \end{bmatrix} = \boldsymbol{g}_1 u_1 + \boldsymbol{g}_2(\theta) u_2, \tag{2}$$

où $\boldsymbol{q} = \begin{bmatrix} \theta & x & y \end{bmatrix}^\top$ est le vecteur de configuration contenant la position (x, y) du point de guidage du véhicule situé au milieu de l'axe reliant les roues droite et gauche du robot, ainsi que l'angle θ exprimant l'orientation du robot dans le repère global

(voir Fig. 1). Les entrées de commande $\boldsymbol{u} = \begin{bmatrix} u_1 & u_2 \end{bmatrix}^\top$ dans le cas d'un robot de type unicycle sont interprétées comme la vitesse angulaire u_1 et la vitesse linéaire u_2 du point de guidage du véhicule. Dans cette thèse, on suppose que les entrées de commande sont limitées, c'est-à-dire que $\boldsymbol{u} \in \mathscr{U} \subset \mathbb{R}^2$, où $\mathscr{U} \triangleq \{\boldsymbol{u} : |u_1| \leq u_{1M}, |u_2| \leq u_{2M}\}$ est l'ensemble des entrées de commande admissibles, tandis que u_{1M} et u_{2M} sont choisis par le concepteur et désignent respectivement la valeur absolue maximale autorisée de la vitesse angulaire et de la vitesse linéaire (voir Fig. 2).

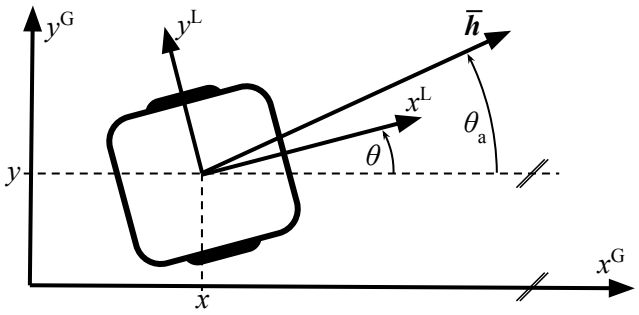

FIGURE 1 – Robot mobile à deux roues de type unicycle.

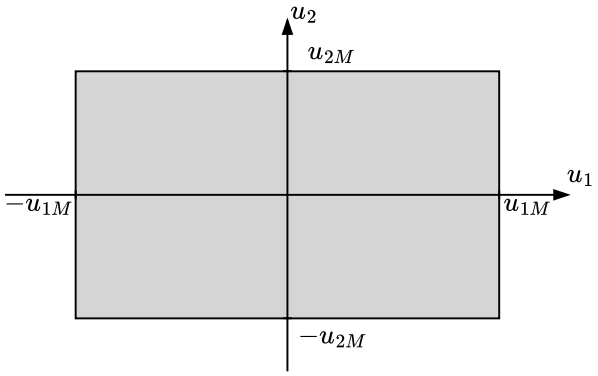

FIGURE 2 – L'ensemble $\mathscr{U}$ des entrées de commande admissibles.

Cette thèse s'appuie sur une approche en deux étapes de la conception des lois de commande : on commence par concevoir une loi de commande *nominale* $\boldsymbol{u}_N \in \mathbb{R}^2$ qui ne garantit pas le respect des contraintes imposées sur les entrées de commande, puis on applique une procédure de mise à l'échelle (voir, par exemple, [3]), qui utilise la fonction de mise à l'échelle s pour redimensionner les valeurs nominales des signaux de commande afin d'obtenir une loi de commande $\boldsymbol{u} = s\boldsymbol{u}_N \in \mathscr{U}$ respectant les contraintes imposées. La procédure de mise à l'échelle utilisée garantit que la direction et l'orientation du vecteur *nominal* des signaux de commande sont conservées.

La méthodologie VFO a été publiée pour la première fois dans [2]. Elle repose sur des relations géométriques intuitives, et son élément clé est ce qu'on appelle le champ vectoriel de convergence, défini comme suit :

$$\boldsymbol{h} = \begin{bmatrix} h_\theta \\ \bar{\boldsymbol{h}} \end{bmatrix} = \begin{bmatrix} h_\theta \\ h_x \\ h_y \end{bmatrix}, \tag{3}$$

qui, pour chaque point de l'espace, indique la direction de convergence souhaitée garantissant la réalisation de la tâche de mouvement choisie. La manière dont le champ $\boldsymbol{h}$ est défini détermine la tâche qui sera exécutée. Un autre élément caractéristique de la méthodologie VFO est ce qu'on appelle l'orientation auxiliaire θ_a, qui désigne l'orientation de la partie relative à la position $\bar{\boldsymbol{h}}$ du champ de convergence vectoriel $\boldsymbol{h}$ dans le repère global (voir Fig. 1). La forme générale de la loi de commande VFO peut s'écrire comme suit :

$$u_1 \triangleq h_\theta, \tag{4}$$

$$u_2 \triangleq \boldsymbol{h}^\top \boldsymbol{g}_2(\theta), \tag{5}$$

où u_1 est appelé commande d'orientation, car elle est chargée de faire pivoter le robot selon une orientation conforme à la composante de position $\bar{\boldsymbol{h}}$ du champ vectoriel de convergence, tandis que u_2 est appelé commande de poussée, car son objectif est de pousser le robot le long du champ vectoriel de convergence.

La présente thèse présente quatre algorithmes de commande élaborés à l'aide de la méthodologie VFO et du concept de stabilité en temps fixe. Deux des algorithmes proposés sont destinés à un robot mobile non holonome seul et permettent de résoudre les problèmes de commande suivants :

- *stabilisation en un point* (voir [9]) – le problème consiste à garantir que le robot atteigne une configuration fixe prédéfinie. Cette thèse présente une synthèse de la loi de commande accompagnée d'une preuve formelle de stabilité en temps fini, ainsi qu'une méthode permettant de déterminer *a priori* les valeurs absolues maximales possibles des signaux de commande nominaux pour des conditions initiales appartenant à un certain ensemble de conditions initiales admissibles. Le fonctionnement de l'algorithme proposé a été testé par des simulations numériques et des essais expérimentaux à l'aide d'un robot mobile physique.
- *suivi d'un chemin de référence* (voir [10]) – la tâche consiste à garantir que le robot atteigne un chemin de référence spécifié, en un temps fini, puis qu'il le suive à une vitesse d'avancement constante. Cette thèse présente la synthèse de la loi de commande ainsi qu'une analyse formelle de la stabilité, et les résultats de simulations numériques et d'essais expérimentaux utilisant un robot mobile physique.

Les algorithmes de commande dédiés aux systèmes multi-véhicules distribués ont été développés afin d'assurer la réalisation de la tâche consistant à former une formation prédéfinie (voir [6]). La thèse présente deux propositions pour résoudre ce problème :

- *approche utilisant des observatoires distribués* (voir [7, 8]) – il a été proposé d'utiliser des observateurs distribués dont la tâche consiste à calculer, pour chaque véhicule, une configuration prédéfinie assurant la réalisation d'une formation dont la forme est définie par le concepteur. Les observateurs utilisent les informations relatives à la configuration initiale d'un véhicule donné et aux configurations initiales des véhicules avec lesquels il peut échanger des informations. Cette approche utilise un processus de contrôle en deux étapes : tout d'abord, les observateurs distribués estiment les configurations données, puis une loi de contrôle est appliquée sur chaque véhicule afin de réaliser la tâche de stabilisation en un point donné. La stabilité en temps fixe des observateurs

proposés a été formellement démontrée, et le fonctionnement de l'algorithme a été vérifié par des simulations numériques.

- *approche utilisant un mécanisme de consensus* – le mécanisme de consensus repose sur une forme de négociation à l'issue de laquelle les véhicules s'accordent sur une valeur commune pour une variable donnée. Dans le cas d'une tâche de génération de formation, cette variable est liée à la position du point autour duquel les véhicules réaliseront une formation dont la forme est définie par le concepteur. Dans l'algorithme de contrôle proposé, les véhicules effectuent un mouvement afin de réaliser la formation spécifiée, bien que l'emplacement de cette formation ne soit pas connu avant la fin du mouvement (l'avantage de cette approche réside dans le fait qu'elle ne comporte qu'une seule étape de contrôle, contre deux dans le cas de l'approche utilisant des observateurs). La thèse présente une synthèse de l'algorithme de commande, accompagnée d'une preuve formelle de stabilité, ainsi qu'une méthode de recherche distribuée de la valeur minimale de la fonction d'échelle s générée par les véhicules composant le système, nécessaire pour garantir le respect des contraintes sur l'algorithme de commande et démontrer formellement sa stabilité. Le fonctionnement de l'algorithme a été testé par des simulations numériques et des essais expérimentaux.

La thèse comprend également une revue de la littérature mettant en évidence la nouveauté et l'apport des solutions proposées, ainsi qu'une discussion sur les perspectives de développement futures.

Bibliographie

[1] R. Aldana-López, D. Gómez-Gutiérrez, E. Jiménez-Rodríguez, J. D. Sánchez-Torres, and M. Defoort, "Enhancing the settling time estimation of a class of fixed-time stable systems," *International Journal of Robust and Nonlinear Control*, vol. 29, no. 12, pp. 4135–4148, 2019.

[2] M. Michałek and K. Kozłowski, "Vector-Field-Orientation feedback control method for a differentially driven vehicle," *IEEE Transactions on Control Systems Technology*, vol. 18, no. 1, pp. 45–65, 2010.

[3] G. Oriolo, A. De Luca, and M. Vendittelli, "WMR control via dynamic feedback linearization : design, implementation, and experimental validation," *IEEE Transactions on Control Systems Technology*, vol. 10, no. 6, pp. 835–852, 2002.

[4] S. Parsegov, A. Polyakov, and P. Shcherbakov, "Nonlinear fixed-time control protocol for uniform allocation of agents on a segment," in *2012 IEEE 51st IEEE Conference on Decision and Control (CDC)*, 2012, pp. 7732–7737.

[5] A. Polyakov, "Nonlinear feedback design for fixed-time stabilization of linear control systems," *IEEE Transactions on Automatic Control*, vol. 57, no. 8, pp. 2106–2110, 2012.

[6] W. Ren and R. W. Beard, *Distributed Consensus in Multi-vehicle Cooperative Control : Theory and Applications*. London : Springer London, 2008.

[7] R. M. Sobański, M. Defoort, and M. M. Michałek, "Decentralized predefined-time leaderless consensus-formation VFO control for nonholonomic multi-agent systems," in *2024 13th International Workshop on Robot Motion and Control (RoMoCo)*, 2024, pp. 136–141.

[8] ——, "Observer-based fixed-time VFO control algorithm for leaderless multi-vehicle systems with directed communication topology," in *22nd Polish Control Conference*, 2026, (accepté).

[9] R. M. Sobański, M. M. Michałek, and M. Defoort, "Fixed-time VFO control design for nonholonomic mobile robots with constrained control inputs," *IEEE Transactions on Cybernetics*, vol. 55, no. 7, pp. 3038–3050, 2025.

[10] ——, "Fixed-time path-following VFO control design for a unicycle-like mobile robot with constrained control inputs," in *23rd IFAC World Congress*, 2026, (accepté).

Acknowledgments

This doctoral dissertation summarizes four years of work and research, however, the PhD study itself was more than that to me... It was a journey toward growth – both scientific and personal. At this point, I would like to express my gratefulness to all those who made this growth possible.

First and foremost, I thank my family. I am grateful to my parents, brothers, and grandmother for their support in the challenges of everyday life. I thank my beloved Barbara for being with me and believing in me when I was plagued by doubt, and little Michał for his patience in waiting for Daddy to come home from work.

My thanks also go to the supervisors of this dissertation, Prof. Maciej Michałek and Prof. Michael Defoort. Like persistent guides, they showed me the paths that (perhaps) are worth following, while leaving space for my own ideas and creativity. Thank you for forming my research character and for ensuring that high scientific and ethical standards are maintained.

During this doctoral journey, I met many amazing people from various parts of the world who made this time truly unforgettable—for which I sincerely thank them. The support of numerous individuals made conducting this research significantly less challenging. In particular, Prof. Thierry Berger, Dr. Marcin Kiełczewski, Patryk Bartkowiak, and Arpit Joon made conducting the experimental tests much easier, while Joanna Gawęcka made everyday academic life more pleasant. I would like to thank all my friends whom I knew even before starting my doctoral studies and who supported me in various ways throughout the process, especially Grzegorz.

Last but not least, I would like to sincerely thank the person without whom I probably would not have undertaken this doctoral journey – Dr. Marta Drążkowska. Thank you for inspiring me to engage in scientific research, for introducing me to the world of science, and for your support, which made the beginning of this journey much easier.

I would like to thank my funder on the UPHF side, the Hauts-de-France region, which made these thesis works possible.

Thank you!

Podziękowania

Niniejsza rozprawa doktorska stanowi podsumowanie czterech lat pracy i badań, jednak same studia doktoranckie były dla mnie czymś więcej... Była to podróż ku rozwojowi – zarówno naukowemu jak i osobistemu. W tym miejscu pragnę wyrazić wdzięczność wszystkim osobom, które ten rozwój umożliwiły.

Przede wszystkim dziękuję mojej rodzinie. Rodzicom, Braciom i Babci składam wyrazy wdzięczności za ich wsparcie w wyzwaniach codzienności. Mojej ukochanej Barbarze dziękuję za obecność i wiarę we mnie gdy ja ulegałem zwątpieniu, a małemu Michałowi za cierpliwość w oczekiwaniu, aż tata wróci z pracy.

Dziękuję także promotorom niniejszej rozprawy, którymi byli prof. Maciej Michałek i prof. Michael Defoort. Niczym wytrwali przewodnicy wskazywali mi oni drogę którą (być może) warto podążyć, jednocześnie pozostawiając przestrzeń na realizację własnych pomysłów. Dziękuję za kształtowanie mojego badawczego charakteru oraz dbałość o zachowywanie wysokich standardów naukowo-etycznych.

W czasie tej doktoranckiej podróży poznałem wielu niezwykłych ludzi z różnych stron świata, którzy uczynili ten czas niezapomnianym – za co im szczerze dziękuję. Wsparcie licznych osób znacząco ułatwiło prowadzenie badań. Szczególnie prof. Thierry Berger, dr inż. Marcin Kiełczewski, mgr inż. Patryk Bartkowiak i mgr inż. Arpit Joon sprawili, że przeprowadzenie testów eksperymentalnych było dużo łatwiejsze, a pani Joanna Gawęcka uczyniła akademicką codzienność bardziej przyjazną. Dziękuję również wszystkim przyjaciołom, których znałem jeszcze przed rozpoczęciem doktoratu i którzy na różne sposoby wspierali mnie w jego trakcie, a w szczególności Grzegorzowi.

Na koniec chciałbym serdecznie podziękować osobie, bez której prawdopodobnie nie rozpocząłbym tej doktoranckiej podróży — dr inż. Marcie Drążkowskiej. Dziękuję za inspirację do podjęcia pracy naukowo-badawczej, wprowadzenie w świat nauki oraz wsparcie, dzięki któremu początek tej drogi był znacznie łatwiejszy.

Pragnę także podziękować podmiotowi finansującemu ze strony UPHF - regionowi Hauts-de-France - dzięki któremu realizacja tej pracy doktorskiej była możliwa.

Dziękuję!

Remerciements

Cette thèse de doctorat résume quatre années de travail et de recherche, toutefois, le doctorat a représenté pour moi bien plus que cela... Ce fut un cheminement vers le développement – à la fois scientifique et personnel. À ce stade, je souhaite exprimer ma profonde gratitude à toutes les personnes qui ont rendu cette évolution possible.

Avant tout, je remercie ma famille. Je suis reconnaissant envers mes parents, mes frères et ma grand-mère pour leur soutien face aux défis du quotidien. Je remercie ma chère Barbara d'avoir été à mes côtés et d'avoir cru en moi lorsque j'étais en proie au doute, ainsi que le petit Michał pour sa patience à attendre que son papa rentre du travail.

J'adresse également mes remerciements aux directeurs de cette thèse, le Prof. Maciej Michałek et le Prof. Michael Defoort. Tels des guides persévérants, ils m'ont montré des chemins (peut-être) dignes d'être suivis, tout en laissant de la place à mes propres idées et à ma créativité. Merci d'avoir contribué à façonner mon caractère de chercheur et de veiller au respect d'exigences scientifiques et éthiques élevées.

Au cours de ce parcours doctoral, j'ai rencontré de nombreuses personnes formidables venant de différentes régions du monde, qui ont rendu cette période véritablement inoubliable – je leur en suis sincèrement reconnaissant. Le soutien de nombreuses personnes a rendu la réalisation de ces travaux de recherche nettement moins difficile. En particulier, le Prof. Thierry Berger, le Dr. Marcin Kiełczewski, Patryk Bartkowiak et Arpit Joon ont grandement facilité la réalisation des essais expérimentaux, tandis que Joanna Gawęcka a rendu la vie académique quotidienne plus agréable. Je tiens également à remercier tous mes amis que je connaissais avant même de commencer mes études doctorales et qui m'ont soutenu de diverses manières tout au long de ce processus, en particulier Grzegorz.

Enfin, je souhaite exprimer mes sincères remerciements à la personne sans laquelle je n'aurais probablement pas entrepris ce parcours doctoral – la Dr. Marta Drążkowska. Merci de m'avoir inspiré à m'engager dans la recherche scientifique, de m'avoir introduit au monde de la science et pour votre soutien, qui a rendu le début de cette aventure beaucoup plus facile.

Finalement, je tiens à remercier mon financeur du côté UPHF, la région Hauts-de-France, qui a permis que ces travaux de thèse, soient possibles.

Merci beaucoup !

Table of contents

List of symbols

General notation

z	a symbol used in definitions, lemmas, etc.
$\boldsymbol{z}$	(bold lowercase letter) a vector
$\boldsymbol{Z}$	(bold uppercase letter) a matrix
$\lvert z \rvert$	absolute value of z
$\lVert \boldsymbol{z} \rVert$	Euclidean norm of the vector $\boldsymbol{z}$
$\angle(\boldsymbol{z}_1, \boldsymbol{z}_2)$	angle between vector $\boldsymbol{z}_1$ and vector $\boldsymbol{z}_2$
$\dot{z}$	time derivative of z
z_N	(subscript N) a value computed based on *nominal* control inputs (without considering input constraints)
z_i	(subscript i) value of z for the i-th vehicle
z_0	an initial value $z(0)$ of variable $z(t)$
$\hat{z}$	a value estimated, computed by an observer, or calculated based on a value estimated by an observer

Other notation

$\mathbf{0}$	vector of zeros
$\underline{\mathbf{1}}$	vector of ones
$\mathrm{Atan2}\,(\cdot,\cdot)$	four-quadrant inverse tangent function: $\mathbb{R} \times \mathbb{R} \to (-\pi, \pi]$
$\mathrm{Atan2c}\,(\cdot,\cdot)$	continuous version of the four-quadrant inverse tangent function: $\mathbb{R} \times \mathbb{R} \to \mathbb{R}$
a_{ij}	an element of adjacency matrix $\boldsymbol{\mathcal{A}}$
$\boldsymbol{\mathcal{A}}$	adjacency matrix associated with the communication topology
$d_{\mathcal{G}}(z_1, z_2)$	graph distance, that is, the number of edges between node z_1 and node z_2
d_x	displacement in the x-coordinate
d_y	displacement in the y-coordinate
$\boldsymbol{d}$	configuration displacement vector
$\bar{\boldsymbol{d}}$	positional displacement vector
$\mathcal{D}$	domain of acceptable positions in the path-following problem
$\mathcal{D}_e$	error space in path-following problem
e_θ	orientation error
$\bar{e}_\theta$	difference between the auxiliary orientation θ_a and the desired orientation θ_d
e_a	auxiliary orientation error

e_a^*	value of the auxiliary orientation error e_a at which u_{1N} reaches the maximum admissible value u_{1M}
e_F	positional error in path-following problem
e_x	error in the x-coordinate
e_x^*	analytically determined x-coordinate of the integral curve, expressed in error space
e_y	error in the y-coordinate
e_y^*	analytically determined y-coordinate of the integral curve, expressed in error space
$\breve{e}_y$	value of the y-coordinate at which the curvature of the motion along a given integral curve reaches its maximum value
$\boldsymbol{e}$	error vector
$\bar{\boldsymbol{e}}$	positional subvector of the error vector $\boldsymbol{e}$
$\bar{\boldsymbol{e}}^*$	vector of the analytically determined positional coordinates of the integral curve, expressed in error space
$\mathscr{E}$	set of edges
$\mathcal{E}$	set of admissible initial configuration errors
$\bar{\mathcal{E}}$	set of admissible initial positional errors
$f(\cdot)$	a function
$f_\theta(\cdot)$	function such that $\mathbb{R} \to (-\pi, \pi]$
f_p	base function defining the reference path
f_o	function that switches between the observation phase and the control phase
f_s	function that switches between the orientation phase and the pushing phase
F	function defining the reference path
F_x	partial derivative of the function F with respect to x
F_y	partial derivative of the function F with respect to y
∇F	gradient of the function F defined as a column vector
$\boldsymbol{g}_1$	first column of matrix $\boldsymbol{G}$
$\boldsymbol{g}_2(\theta)$	second column of matrix $\boldsymbol{G}$
$\bar{\boldsymbol{g}}_2(\theta)$	vector containing the second and third elements of the vector $\boldsymbol{g}_2(\theta)$
$\bar{\boldsymbol{g}}_{2d}$	vector $\bar{\boldsymbol{g}}_2(\theta)$ computed for the desired orientation θ_d, that is, $\bar{\boldsymbol{g}}_2(\theta_d)$
$\boldsymbol{G}$	matrix of vehicle kinematics
$\mathcal{G}$	graph of communication topology
h_θ	element of the convergence vector field associated with the orientation θ
h_x	element of the convergence vector field associated with the x coordinate
h_y	element of the convergence vector field associated with the y coordinate
$\boldsymbol{h}$	convergence vector field
$\bar{\boldsymbol{h}}$	positional subvector of the convergence vector field
$\boldsymbol{I}$	identity matrix
j	a neighbor of vehicle i in a multi-vehicle system
K_a	positive gain of the orientation process
K_o	positive gain of the observer
K_p	positive gain of the pushing process

ℓ_{ij}	an element of matrix $\boldsymbol{\mathcal{L}}$
$\boldsymbol{\mathcal{L}}$	*Laplacian matrix* (or *nonsymmetric Laplacian matrix*) associated with the communication topology
$\boldsymbol{\mathcal{L}}_p$	symmetric positive semi-definite matrix obtained from a *nonsymmetric Laplacian matrix*
$\boldsymbol{\mathcal{L}}_q$	block matrix formed from two *Laplacian matrices*
m_G	lower bound of the gradient of the function F
M_F	maximum admissible absolute value of the function F
M_G	upper bound of the gradient of function F
n	number of dimensions, for example, an n-dimensional space $\mathbb{R}^n$
n_v	number of vehicles in a multi-vehicle system
$\mathcal{N}_i$	set of neighbors of vehicle i
p^*	function related to the analytical derivation of the integral curve
P_1, P_2	powers used in definitions, lemmas, etc., such that $P_1 \in (0, 1)$ and $P_2 > 1$
$\boldsymbol{q}$	vector of vehicle configuration
$\bar{\boldsymbol{q}}$	positional subvector of the vehicle's configuration vector
$\boldsymbol{q}_c$	vector of consensus equilibrium states
$\bar{\boldsymbol{q}}_c$	positional subvector of the consensus equilibrium states vector
$\boldsymbol{q}_d$	vector of vehicle desired configuration
$\bar{\boldsymbol{q}}_d$	positional subvector of the vehicle's desired configuration vector
$\mathcal{Q}_e$	configuration space in the set-point stabilization problem
$r_{\mathcal{E}}$	the smallest admissible norm of positional error belonging to the set $\bar{\mathcal{E}}$
$R_{\mathcal{E}}$	the largest admissible norm of positional error belonging to the set $\bar{\mathcal{E}}$
$\boldsymbol{R}$	rotation matrix by the angle $-\pi/2$
$\mathbb{R}$	set of real numbers
$\mathbb{R}_+$	set of positive real numbers
s	scaling function
$\underline{s}$	the smallest value of the scaling function for a particular initial condition
$\underline{\underline{s}}$	the smallest value of the scaling function for all possible initial conditions belonging to the set $\mathcal{E}$
$\hat{\underline{\underline{s}}}$	(conservatively) estimated smallest value of the scaling function for all possible initial conditions belonging to the set $\mathcal{E}$
$\bar{s}_{\mathcal{D}}$	the smallest possible value of the scaling function for an initial condition belonging to the domain $\mathcal{D}$
$s_{\mathcal{D}}$	the smallest possible value of the scaling function in the domain $\mathcal{D}$
$\bar{s}$	the smallest value of the scaling function among the values generated by a vehicle in a multi-vehicle system at a given moment in time
$\bar{\underline{s}}$	the smallest value of the scaling function among the values generated by a vehicle in a multi-vehicle system
$\bar{s}_{iF_k}$	input of the k-th filter on the i-th vehicle in the filter-based approach
$\tilde{s}_{iF_k}$	output of the k-th filter on the i-th vehicle in the filter-based approach

S_d	set of points that define a reference path
$\mathcal{S}$	a dynamical system
t	time
t_s	a settling time
t_{sa}	settling time of the auxiliary orientation error
t_{sa}^*	time of movement with the maximum possible angular velocity
t_{sf}	settling time of the filter error
t_{sF}	settling time of the positional error e_F
t_{so}	settling time of the observation error
t_{sp}	settling time of the positional error
T	an upper bound of a settling time, depending on the initial condition
T_c	an upper bound of a settling time, independent on the initial condition
T_{ca}	upper bound of the auxiliary orientation error settling time
T_{ca}^*	movement time without saturation on the orienting control
T_{cF}	upper bound of the settling time of the error e_F
T_{co}	upper bound of the observation error settling time
T_{cp}	upper bound of the positional error settling time
u_1	angular velocity (and orienting control)
$u_{1\mathcal{E}}$	maximum possible value of the orienting control for initial conditions from the set $\mathcal{E}$
$\hat{u}_{1\mathcal{E}}$	(conservatively) estimated maximum possible value of the orienting control for initial conditions from the set $\mathcal{E}$
u_{1M}	maximum admissible absolute angular velocity
u_{1N}	nominal orienting control
u_2	longitudinal velocity (and pushing control)
$u_{2\mathcal{E}}$	maximum possible value of the pushing control for initial conditions from the set $\mathcal{E}$
u_{2d}	desired longitudinal velocity
u_{2M}	maximum permitted absolute longitudinal velocity
u_{2N}	nominal pushing control
$\boldsymbol{u}$	vector of control inputs
$\boldsymbol{u}_N$	vector of nominal control inputs
$\mathscr{U}$	set of admissible control inputs
$\boldsymbol{v}_1, \boldsymbol{v}_2$	auxiliary terms used in stability proofs
$\boldsymbol{v}_{\lambda i}$	eigenvector associated with the i-th eigenvalue of matrix $\boldsymbol{\mathcal{L}}$
v_d	absolute value of the desired longitudinal velocity
V	a Lyapunov function
$\mathcal{V}$	a set of admissible initial conditions used in definitions, lemmas, etc.
$\mathscr{V}$	set of nodes associated with the communication topology
w	auxiliary scalar term used in definitions, lemmas, etc.
$w_1, \ldots, w_{n_v}$	left-hand eigenvalues
$\boldsymbol{w}_0$	left zero unit eigenvector
$\bar{w}$	the largest left-hand eigenvalue
$\mathscr{W}$	diagonal matrix containing the left-hand eigenvalues

x	x-coordinate of the vehicle's guidance point
x_c	x-coordinate of the consensus equilibrium state
$\hat{x}_{ci}$	x-coordinate of the consensus equilibrium state estimated by the observer on the i-th vehicle
x_d	desired x-coordinate
y	y-coordinate of the vehicle's guidance point
y_c	y-coordinate of the consensus equilibrium state
$\hat{y}_{ci}$	y-coordinate of the consensus equilibrium state estimated by the observer on the i-th vehicle
y_d	desired y-coordinate
$\mathbb{Z}$	set of integers
α	angle between $\bar{\boldsymbol{h}}$ and $\bar{\boldsymbol{g}}_2(\theta)$
β_1, β_2	positive gains used in definitions, lemmas, etc.
γ	parameter used in definitions, lemmas, etc., to correlate powers P_1 and P_2
$\Gamma(\cdot)$	gamma function
δ_1, δ_2	powers in the orientation process, such that $\delta_1 \in (0,1)$ and $\delta_2 > 1$
$\bar{\delta}$	parameter used to correlate powers δ_1 and δ_2
ϵ	positive small vicinity of zero
ζ	non-zero parameter that modifies the slope of the function defining the reference path, such that $\zeta f_p = F$
$\bar{\eta}$	design coefficient related to the so-called *directing effect*
θ	vehicle's orientation angle in global coordinates
θ_ϵ	value of the orientation angle θ at the moment when the vehicle enters the vicinity ϵ of the desired point
θ_a	auxiliary orientation
$\theta_{a\epsilon}$	value of the auxiliary orientation θ_a at the moment when the vehicle enters the vicinity ϵ of the desired point
θ_c	orientation angle in the consensus equilibrium state
$\hat{\theta}_{ci}$	orientation angle in the consensus equilibrium state estimated by the observer on the i-th vehicle
θ_d	desired orientation
κ_1, κ_2	positive gains of the observer
κ	vehicle movement curvature
κ^*	analytically determined vehicle motion curvature
$\underline{\kappa}^*$	maximum absolute value of the analytically determined vehicle motion curvature for a particular initial condition
$\kappa_{\mathcal{E}}$	maximum absolute value of the analytically determined vehicle motion curvature for initial conditions belonging to the set $\mathcal{E}$
λ_2	second smallest eigenvalue of matrix $\boldsymbol{\mathcal{L}}$, known as the *algebraic connectivity* in the case of an undirected communication topology
λ_i	i-th eigenvalue of matrix $\boldsymbol{\mathcal{L}}$
μ_1, μ_2	powers in the pushing process, such that $\mu_1 \in (0,1)$ and $\mu_2 > 1$
$\bar{\mu}$	parameter used to correlate powers μ_1 and μ_2
$\xi_{\theta i}$	observation error associated with the orientation angle θ obtained by the i-th vehicle
ξ_{xi}	observation error associated with the x-coordinate obtained by the i-th vehicle

ξ_{yi}	observation error associated with the y-coordinate obtained by the i-th vehicle
$\boldsymbol{\xi}_i$	vector of the observation errors from the i-th vehicle
$\boldsymbol{\xi}_q$	vector of the vehicle's position combined with the displacement vector that defines the desired formation
ρ	function used in the pushing process to ensure *fixed-time stability*
ρ_0	positive gain used in ρ function
σ	decision variable that determines the vehicle's movement strategy (forward or backward)
τ, τ_x, τ_y	auxiliary time instants used in definitions, lemmas, etc.
ϕ_1, ϕ_2	auxiliary positive constant used in definitions, lemmas, etc.
χ_1, χ_2	powers of the observer, such that $\chi_1 \in (0, 1)$ and $\chi_2 > 1$
$\bar{\chi}$	parameter used to correlate powers χ_1 and χ_2
ψ	auxiliary positive constant used in definitions, lemmas, etc.

Introduction

Preface and motivation

This doctoral dissertation is an outcome of nearly four years of research conducted in collaboration between the Institute of Automatic Control and Robotics (IAR) at Poznan University of Technology (PUT) and Laboratory of Industrial and Human Automation Control, Mechanical Engineering and Computer Science (LAMIH) at Université Polytechnique Hauts-de-France (UPHF). The topics covered in this dissertation and the research objectives defined therein are closely related to the latest trends in the modern world, which are also reflected in the topics addressed by researchers in the field of robotics. The main areas covered in this dissertation can be characterized as follows:

- *Mobile robotics* – a field that has consistently captured the attention of researchers for many decades. It is a well-established area that still holds great potential for further development.
- *Multi-vehicle systems* – a well-known area, significant due to the fact that a fleet of coordinated vehicles can perform tasks that would be difficult or impossible for a single vehicle. As the popularity of robotization grows, the popularity of multi-vehicle systems is also on the rise.
- *Control input constraints* – one of the fundamental constraints faced by researchers in the field of mobile robotics, as in practice it stems directly from the robot's design and the physical limitations of the actuators used.
- *Time constraints* – an issue that has gained increasing attention in recent decades. Today, simply knowing that a task can be completed is often no longer sufficient, so researchers are increasingly asking themselves how long it will take to complete a given task.

Nowadays, time management has become particularly important. This fact has also influenced the topics undertaken by researchers, including those working in the field of robotics. In recent years, there has been a significant increase in the popularity of areas related to control systems under task execution time constraints. There are many factors behind this trend, however the most important one seems to be the fact that knowing the time required to complete a task can be useful from a practical point of view. In times of increasing automation and robotization, there is a need to synchronize many processes, and knowing the maximum time required to complete a given process can definitely help with this. From the perspective of mobile robotics and multi-vehicle systems, control algorithms that take time constraints into account can find practical application in tasks such as the spatiotemporal synchronization of a multi-vehicle system, tasks related to flexible transportation/delivery, monitoring tasks, or tasks related to safety issues, such as searching for a missing person.

However, algorithms that take time constraints into account will be practically useful if physical vehicle limitations, such as maximum velocities and related maximum control input values, are also considered during the design phase. Currently, the literature includes studies that consider vehicle velocity constraints, as well as studies that consider time constraints. However, there are still relatively small number of studies that address both of these constraints simultaneously, which served as the motivation for conducting research in this direction, whose results are presented in this doctoral dissertation.

Control problem, novelty, and contribution

The research objectives of this doctoral dissertation are formulated as follows:

1. Development of the Vector Field Orientation (VFO) control law for a nonholonomic mobile robot that guarantees satisfaction of the imposed time constraints in the presence of the control inputs limitations.
2. Adaptation of the proposed control law to a decentralized multi-vehicle system.
3. Formal stability analysis and numerical and experimental control performance verification for a single nonholonomic mobile robot and for a multi-vehicle system.

The research will be conducted in accordance with a three-stage research paradigm commonly used in robotics, which includes formal mathematical analysis, simulational validation, and laboratory-scale experimental tests using physical robots.

Based on the objectives outlined above, the following research hypothesis has been formulated:

> ***Hypothesis***
>
> The Vector Field Orientation (VFO) methodology enables the development of a control algorithm for a single nonholonomic mobile robot and its decentralized extension for a multi-robot system, that guarantees satisfaction of time constraints imposed on the execution of a selected motion task defined for nonholonomic mobile robots in the presence of control input constraints.

The main novelty of this study lies in the development of control laws within the VFO methodology for a single nonholonomic mobile robot that simultaneously takes into account control input constraints and task execution time constraints, as well as control algorithms for a distributed multi-vehicle system composed of nonholonomic vehicles, which also takes into account both control input constraints and task-execution time constraints. The contribution of this work also includes the extension of the VFO methodology to a version that considers time constraints in accordance with the *fixed-time stability* concept, as well as the application of the method for estimating an upper bound of the settling time for a specific set of admissible initial conditions. The dissertation explicitly addresses the limitations on control inputs in the form of maximum admissible absolute values of vehicle velocities and takes into account the presence of this constraint when estimating the upper bound of the settling time according to the *fixed-time stability* concept. Two control algorithms have been proposed for a single nonholonomic mobile robot to solve the

set-point control problem and path-following problem, as well as two algorithms for a distributed multi-vehicle system to solve the formation control problem.

Outline

The remainder of this dissertation consists of four chapters. Chapter 1 provides an overview of the current state of the art and preliminaries. It consists of three sections that discuss the concept of *fixed-time stability* (see Section 1.2), the control of nonholonomic systems (see Section 1.3), and the control of multi-vehicle systems (see Section 1.4).

Chapters 2 and 3 present the main results obtained during the PhD studies. Chapter 2 deals with the design of VFO control laws for a single nonholonomic mobile robot. It consists of four sections: the introduction (see Section 2.1), the design of a set-point stabilizer (see Section 2.2), the design of a control law for path-following problem (see Section 2.3), and a conclusion summarizing the presented results (see Section 2.4). Each of Sections 2.2 and 2.3 includes a formulation of the control problem (see Section 2.2.1 and 2.3.2), a synthesis of the VFO control law along with a formal stability proof (see Section 2.2.2 and 2.3.3), the results of numerical simulations (see Section 2.2.4 and 2.3.4) and experimental tests (see Section 2.2.5 and 2.3.5). Furthermore, Section 2.2.3 presents an *a priori* estimation method for an upper bound of the system error settling times for the set-point control problem, while Section 2.3.1 provides a definition of a reference nonparametric path for the path-following problem.

Chapter 3 addresses the VFO control algorithms for a distributed multi-vehicle system composed of nonholonomic vehicles. It consists of five sections containing: the introduction (see Section 3.1), the formulation of the control problem common to both control algorithms discussed (see Section 3.2), an observer-based formation algorithm (see Section 3.3), a consensus-based formation algorithm (see Section 3.4), and a conclusion summarizing the presented results (see Section 3.5). Section 3.3 presents the synthesis of distributed observers along with a formal stability proof (see Section 3.3.1), the synthesis of the VFO control algorithm (see Section 3.3.2), the results of numerical simulations (see Section 3.3.3), and a discussion of collision avoidance (see Section 3.3.4). Section 3.4, on the other hand, contains a synthesis of the VFO control algorithm along with a formal stability proof (see Section 3.4.1), a distributed estimation method for the smallest value of a scaling function required for the presented stability proof (see Section 3.4.2), the results of numerical simulations (see Section 3.4.3) and experimental tests (see Section 3.4.4).

Finally, Chapter 4 provides a summary of the results presented in this dissertation and discusses potential directions for future research.

The results presented in this doctoral dissertation have also been included in the following journal publications:

[J1] R. M. Sobański, M. M. Michałek, and M. Defoort,
"Fixed-time VFO control design for nonholonomic mobile robots with constrained control inputs,"
IEEE Transactions on Cybernetics, vol. 55, no. 7, pp. 3038-3050, 2025.

[J2] R. M. Sobański, M. M. Michałek, and M. Defoort,
"Predefined-time VFO control design for unicycle-like mobile robots,"

Nonlinear Dynamics, vol. 112, pp. 3591-3603, 2024.

and in the following conference papers:

[C1] R. M. Sobański, M. M. Michałek, and M. Defoort,
"Fixed-time path-following VFO control design for a unicycle-like mobile robot with constrained control inputs,"
in *23rd IFAC World Congress*, 2026, (accepted).

[C2] R. M. Sobański, M. Defoort, and M. M. Michałek,
"Observer-based fixed-time VFO control algorithm for leaderless multi-vehicle systems with directed communication topology,"
in *22nd Polish Control Conference*, 2026, (accepted).

[C3] R. M. Sobański, M. Defoort, and M. M. Michałek,
"Decentralized predefined-time leaderless consensus-formation VFO control for nonholonomic multi-agent systems,"
in *13th International Workshop on Robot Motion andControl (RoMoCo)*, 2024, pp. 136-141.

[C4] R. M. Sobański, M. M. Michałek, and M. Defoort,
"VFO control design for a mobile robot in the presence of time and input constraints,"
in *27th International Conference on Methods and Models in Automation and Robotics (MMAR)*, 2023, pp. 356-361.

[C5] M. M. Michałek, R. M. Sobański, and M. Defoort,
"Fixed-time VFO control for a unicycle,"
in *Prace Naukowe. Elektronika, Tom I,.* Warszawa: Oficyna Wydawnicza Politechniki Warszawskiej, 2022, vol. 197, pp. 191-200.

Chapter 1

Preliminaries and state of the art

1.1 Introduction

This chapter will present preliminaries and the current state of knowledge regarding the three main areas addressed in this dissertation, namely the concept of *fixed-time stability* (see Section 1.2), the control of nonholonomic systems (see Section 1.3), and the control of multi-vehicle systems (see Section 1.4). Finally, Section 1.5 will summarize the current state of knowledge and discuss its relation to the topic of this dissertation.

1.2 Fixed-time stability

This section will discuss the concept of *fixed-time stability*. First, formal definition of this concept will be recalled from the literature, along with important lemmas useful in the practical application, and then a review of the literature will be conducted to provide an overview of the current state of knowledge and some historical context.

1.2.1 Formal definition

First, let us define a connected set $\mathcal{V} \subseteq \mathbb{R}^n$ and a dynamical system:

$$\mathcal{S} : \dot{\boldsymbol{z}}(t, \boldsymbol{z}_0) = f\Big(\boldsymbol{z}(t, \boldsymbol{z}_0)\Big), \quad \boldsymbol{z}_0 \in \mathcal{V}, \tag{1.1}$$

with a solution $\boldsymbol{z}(t, \boldsymbol{z}_0)$ and an initial condition $\boldsymbol{z}_0$, where $f(\cdot) : \mathcal{V} \to \mathbb{R}^n$ is a continuous function, such that $f(0) = 0$.

Then, let us recall the definition of the *fixed-time stability* concept:

Definition 1 (cf. [22]) *The equilibrium point $\boldsymbol{z} = \mathbf{0}$ of a dynamical system $\mathcal{S}$, defined in* (1.1)*, is said to be:*

1. *Lyapunov stable: if for any $\phi_1 > 0$ there exists $\phi_2 > 0$ such that for any*

$$\|\boldsymbol{z}_0\| \leq \phi_2 \implies \forall t \geq 0 \quad \|\boldsymbol{z}(t, \boldsymbol{z}_0)\| \leq \phi_1.$$

2. *finite-time stable: if it is Lyapunov stable and there exists an upper bound $T(\boldsymbol{z}_0) \geq 0$ of the settling time $t_s(\boldsymbol{z}_0) \geq 0$ such that*

$$\forall t \geq t_s(\boldsymbol{z}_0) \quad \boldsymbol{z}(t, \boldsymbol{z}_0) = 0$$

and

$$t_s(\boldsymbol{z}_0) \leq T(\boldsymbol{z}_0) < \infty.$$

3. *fixed-time stable: if it is finite-time stable and there exists an upper bound* T_c *such that*

$$\sup_{\boldsymbol{z}_0 \in \mathcal{V}} T(\boldsymbol{z}_0) \leq T_c \leq \infty.$$

4. *nearly fixed-time stable: if it is Lyapunov stable and for any* $\psi > 0$ *there exists an upper bound* $0 \leq T_c < \infty$ *such that*

$$\forall \boldsymbol{z}_0 \in \mathcal{V} \; \forall t \geq T_c \quad \|\boldsymbol{z}(t, \boldsymbol{z}_0)\| \leq \psi.$$

Therefore, it can be observed that the *fixed-time stability* concept ensures convergence in finite time, similar to the concept of *finite-time stability*, and ensures the existence of an upper bound of the system errors settling time, which is independent of a particular initial condition, unlike the upper bound whose existence is ensured by the *finite-time stability* concept.

Let us now recall the lemma that allows one to verify whether the equilibrium point of the system is *fixed-time stable*.

Lemma 1 (cf. [103]) *The equilibrium point* $\boldsymbol{z} = \mathbf{0}$ *of a dynamical system* $\mathcal{S}$*, defined in* (1.1)*, is (nearly) fixed-time stable if there exists a continuous radially unbounded positive definite function* $V : \mathbb{R}^n \to \mathbb{R}_+ \cup \{0\}$ *such that any solution* $\boldsymbol{z}(t, \boldsymbol{z}_0)$ *of system* $\mathcal{S}$ *satisfies*

$$\dot{V}(\|\boldsymbol{z}\|) \leq -\beta_1 V^{P_1}(\|\boldsymbol{z}\|) - \beta_2 V^{P_2}(\|\boldsymbol{z}\|), \tag{1.2}$$

where $\beta_1 > 0$*,* $\beta_2 > 0$*,* $P_2 > 1$*, and* $0 < P_1 < 1$*.*

It can be noted that Lemma 1 uses the well-known Lyapunov method (see [59]).

Next, let us look at the problem of estimating the value of the upper bound T_c of the settling time. Several methods for such estimation are known in the literature (see, for example, [103, 143]), however, they usually lead to conservative results. To the best of our knowledge, the least conservative estimates are obtained using the method proposed in [101], which is formulated as follows.

Lemma 2 (cf. [101]) *If the equilibrium point* $\boldsymbol{z} = \mathbf{0}$ *of a dynamical system* $\mathcal{S}$*, defined in* (1.1)*, is (nearly) fixed-time stable and there exists a function* V *satisfying Lemma 1, with* $P_1 = 1 - \gamma$*,* $P_2 = 1 + \gamma$*,* $\gamma \in (0, 1)$*, then the upper bound* T_c *can be assessed as follows:*

$$\forall \boldsymbol{z}_0 \in \mathbb{R}^n \quad T_c = \frac{\pi}{2\gamma\sqrt{\beta_1 \beta_2}}. \tag{1.3}$$

However, this result introduces an additional restriction on the selection of powers P_1 and P_2, hence in [3] a solution was presented that generalizes the solution from [101] to the case of arbitrary selection of P_1 and P_2, consistent with the guidelines from Lemma 1.

Lemma 3 (cf. [3]) *If the equilibrium point* $\boldsymbol{z} = \mathbf{0}$ *of a dynamical system* $\mathcal{S}$*, defined in* (1.1)*, is (nearly) fixed-time stable and there exists a function* V *satisfying Lemma 1, then the upper bound* T_c *can be assessed as follows:*

$$\forall \boldsymbol{z}_0 \in \mathbb{R}^n \quad T_c = \frac{\Gamma\left(\dfrac{1 - P_1}{P_2 - P_1}\right) \Gamma\left(\dfrac{P_2 - 1}{P_2 - P_1}\right)}{\beta_1 (P_2 - P_1)} \left(\frac{\beta_1}{\beta_2}\right)^{\frac{1 - P_1}{P_2 - P_1}}, \tag{1.4}$$

where $\Gamma(\cdot)$ *is the gamma function defined as* $\Gamma(w) \triangleq \int_0^\infty e^{-t} t^{w-1} dt$*.*

It should be noted that the results presented in Lemma 2 and 3 apply to the global case, that is, the considered set of admissible initial conditions $\mathcal{V} = \mathbb{R}^n$. This approach is not necessarily interesting when additional constraints are imposed on the system, especially the constraints on the control inputs considered in this dissertation. Therefore, inspired by the results presented in [23], it is proposed to adapt the method proposed in [101] to a version that takes into account subsets of $\mathbb{R}^n$ for admissible initial conditions rather than the whole $\mathbb{R}^n$. Let us begin by recalling the following definition

Definition 2 (see [38]) *A continuous function $f(\cdot) : [0, z) \to [0, \infty)$ is said to belong to class $\mathcal{K}$ if it is strictly increasing and $f(0) = 0$.*

and then let us formulate the appropriate lemma.

Lemma 4 (see [119]) *If the equilibrium point $\boldsymbol{z} = \mathbf{0}$ of a dynamical system $\mathcal{S}$, defined in (1.1), is (nearly) fixed-time stable and there exist a $\mathcal{K}$-class function V satisfying Lemma 1, with $P_1 = 1 - \gamma$, $P_2 = 1 + \gamma$, $\gamma \in (0, 1)$, then the upper bound T_c can be assessed as follows:*

$$\forall \boldsymbol{z}_0 \in \mathcal{V} \quad T_c = \frac{1}{\gamma\sqrt{\beta_1\beta_2}} \arctan\left(\frac{\beta_2 V^{\gamma}(\bar{z})}{\sqrt{\beta_1\beta_2}}\right), \tag{1.5}$$

where $\beta_1 > 0$, $\beta_2 > 0$, and $\bar{z} = \sup_{\boldsymbol{z}_0 \in \mathcal{V}} \|\boldsymbol{z}_0\|$.

Proof. Based on Lemma 1, the equilibrium point $\boldsymbol{z} = \mathbf{0}$ of the dynamical system $\mathcal{S}$ is *fixed-time stable*, if there exists a continous radially unbounded positive definite function V, such that any solution $\boldsymbol{z}(t, \boldsymbol{z}_0)$ of system $\mathcal{S}$ satisfies:

$$\dot{V}(\|\boldsymbol{z}\|) \leq -\beta_1 V(\|\boldsymbol{z}\|)^{P_1} - \beta_2 V(\|\boldsymbol{z}\|)^{P_2}.$$

Then, based on the above inequality, it can be observed that:

$$\begin{aligned}
\forall \|\boldsymbol{z}\| \neq 0 \qquad & \frac{1}{-\beta_1 V^{P_1}(\|\boldsymbol{z}\|) - \beta_2 V^{P_2}(\|\boldsymbol{z}\|)} \frac{dV(\|\boldsymbol{z}\|)}{dt} \geq 1 \\
\implies & \int_0^{t_s} \frac{1}{-\beta_1 V^{P_1}(\|\boldsymbol{z}\|) - \beta_2 V^{P_2}(\|\boldsymbol{z}\|)} \frac{dV(\|\boldsymbol{z}\|)}{dt} \geq \int_0^{t_s} dt \\
\implies & \int_{V(\|\boldsymbol{z}_0\|)}^{V(\|\boldsymbol{z}(t_s)\|)} \frac{dV(\|\boldsymbol{z}\|)}{-\beta_1 V^{P_1}(\|\boldsymbol{z}\|) - \beta_2 V^{P_2}(\|\boldsymbol{z}\|)} \geq t_s \\
\implies & \int_{V(\|\boldsymbol{z}_0\|)}^{0} \frac{dV(\|\boldsymbol{z}\|)}{-\beta_1 V^{P_1}(\|\boldsymbol{z}\|) - \beta_2 V^{P_2}(\|\boldsymbol{z}\|)} \geq t_s
\end{aligned}$$

where T_c denotes the upper bound of the settling time t_s. Let us select $P_1 = 1 - \gamma$, $P_2 = 1 + \gamma$, $\gamma \in (0, 1)$, and then, by substituting $w \triangleq V^{\gamma}$, $\frac{dw}{dV} = \gamma V^{\gamma-1} \implies \frac{dw}{w} = \frac{\gamma dV}{V}$, one gets

$$\begin{aligned}
& \int_{V(\|\boldsymbol{z}_0\|)}^{0} \frac{dV(\|\boldsymbol{z}\|)}{-\beta_1 V^{P_1}(\|\boldsymbol{z}\|) - \beta_2 V^{P_2}(\|\boldsymbol{z}\|)} \\
= & \int_{V(\|\boldsymbol{z}_0\|)}^{0} \frac{dV(\|\boldsymbol{z}\|)}{-V(\|\boldsymbol{z}\|)\left(\beta_1 V^{-\gamma}(\|\boldsymbol{z}\|) + \beta_2 V^{\gamma}(\|\boldsymbol{z}\|)\right)}
\end{aligned}$$

$$
\begin{aligned}
&= -\frac{1}{\gamma}\int_{V^{\gamma}(\|\boldsymbol{z}_0\|)}^{0} \frac{dw}{w\left(\beta_1 w^{-1}+\beta_2 w\right)} \\
&= -\frac{1}{\gamma}\int_{V^{\gamma}(\|\boldsymbol{z}_0\|)}^{0} \frac{dw}{\beta_1+\beta_2 w^{2}} \\
&= \frac{1}{\gamma\sqrt{\beta_1\beta_2}} \arctan\left(\frac{\beta_2 V^{\gamma}(\|\boldsymbol{z}_0\|)}{\sqrt{\beta_1\beta_2}}\right)
\end{aligned}
$$

where the last line is the solution of the integral according to mathematical tables devoted to elementary integrals (see, for example, [32]). It should be noted that since V is a $\mathcal{K}$-class function, then $\forall \boldsymbol{z}_0 \in \mathcal{V} \quad V(\|\boldsymbol{z}_0\|) \leq V(\bar{z})$ holds, and thus one can write

$$
\forall \boldsymbol{z}_0 \in \mathcal{V} \quad \frac{1}{\gamma\sqrt{\beta_1\beta_2}} \arctan\left(\frac{\beta_2 V^{\gamma}(\|\boldsymbol{z}_0\|)}{\sqrt{\beta_1\beta_2}}\right) \leq \frac{1}{\gamma\sqrt{\beta_1\beta_2}} \arctan\left(\frac{\beta_2 V^{\gamma}(\bar{z})}{\sqrt{\beta_1\beta_2}}\right),
$$

and consequently

$$
\forall \boldsymbol{z}_0 \in \mathcal{V} \quad T_c = \frac{1}{\gamma\sqrt{\beta_1\beta_2}} \arctan\left(\frac{\beta_2 V^{\gamma}(\bar{z})}{\sqrt{\beta_1\beta_2}}\right).
$$

That concludes the proof. ■

Remark 1 *It should be noted that the result presented in Lemma 4 has previously appeared in the literature (see, for example, [23, 101]), however it has usually been used as an intermediate step toward developing a 'global' method, that is, the one valid for initial conditions belonging to the set $\mathbb{R}^n$, and to the best of our knowledge it has not yet been used in a 'local' sense as proposed in this dissertation.*

1.2.2 State of the art

The *fixed-time stability* concept postulates that the dynamical system's errors will converge to zero within a finite time, which is upper-bounded by a certain constant value independent of the particular initial condition. It was originally defined in 2012 in [103], which also proposed the first method for (conservative) estimation of the upper bound of the system's error settling time. In the following years, new propositions for estimating this upper bound were published (see, for example, [3, 101, 143]), some of which imposed additional restrictions on the choice of the powers P_1 and P_2 in (1.2). Ultimately, to the best of our knowledge, the least conservative results were obtained in [101] (cf. Lemma 2), which imposes an additional restriction on the choice of the powers, and in [3] (cf. Lemma 3), which can be regarded as a generalization of the results from [101] that removes the additional restriction. According to the original concept of *fixed-time stability*, a particular initial condition cannot affect the upper bound of the settling time, hence the estimation results commonly used in the literature apply to the global case, that is, they guarantee that the settling time will not exceed the estimated upper bound regardless of the value of the initial condition.

One can rightly point out the similarity between the *fixed-time stability* concept and the older *finite-time stability* concept (see, for example, [6, 90]). Basically, both

concepts guarantee that the dynamical system's errors will converge to zero in a finite time and will be upper-bounded by a constant value. The fundamental difference lies in the value of this upper bound, since in the case of the *finite-time stability* concept it depends on an initial condition, whereas in the case of the *fixed-time stability* it does not depend on a particular initial condition.

The literature also discusses the concept of *predefined-time stability*, which can be treated as a special case of the *fixed-time stability* concept. For both of these concepts, the upper bound of the settling time is independent of a particular initial condition, however, in the case of the *predefined-time stability*, this upper bound is taken as a parameter selected by a designer. *Predefined-time stability* was considered, for example, in [40, 41, 123].

The *fixed-time stability* concept remains an active field of research, and to date, apart from works in which the authors have explored new methods for estimating the upper bound on the settling time (see, for example, [3,101,143]), there are also studies devoted to the development of control algorithms that guarantee the convergence of system errors within a fixed time. Various control strategies have been developed, including fixed-time sliding-mode controllers (see, for example, [15,51,89,142]), stabilizers (see, for example, [5,34,105,140]), multi-agent system formation controllers (see, for example, [2, 17, 18, 56, 136]), as well as adaptive controllers (see, for example, [62]) and fuzzy controllers (see, for example, [122]), to name a few. This dissertation focuses on the design of control laws for a single nonholonomic mobile robots and for a multi-vehicle system composed of nonholonomic mobile vehicles. The fundamental novelty and contribution of the achieved results will be compared with existing works in the following sections of this chapter.

Remark 2 *It is worth noting that the literature also presents an alternative approach of fixed-time stability, which is based on the homogeneity theory instead of using the Lyapunov method (see, for example, [4, 104, 124]).*

1.3 Control of nonholonomic systems

This section will focus on the control of nonholonomic systems, which include the vehicles considered in this dissertation. First, Section 1.3.1 will provide an overview of the most important literature. Then, Section 1.3.2 will describe the kinematic model of a unicycle-like mobile robot, and finally, Section 1.3.3 will introduce the Vector Field Orientation (VFO) design methodology.

1.3.1 State of the art

A nonholonomic system is a system with nonintegrable constraints imposed on their velocities (see [8, 35]), which means that the system cannot move freely in some directions. One of the fundamental example of a nonholonomic system is a wheel rolling without slipping on a flat surface. Movement in the direction of rolling is possible, however, instantaneous movement perpendicular to the direction of rolling is impossible. Therefore, the significant number of wheeled vehicles belong to the class of nonholonomic systems – including the unicycle-like vehicles that are considered in this dissertation.

The control of nonholonomic vehicles is widely discussed in the literature. The three fundamental tasks defined for this type of vehicle are trajectory tracking, path-following, and set-point stabilization, where the last of these is the most challenging. The reason for this comes from the work [10] of Roger W. Brockett, who pointed out that there is no continuously differentiable state-feedback stabilizer that would guarantee asymptotic stabilization of the equilibrium point for these systems. This issue was also addressed, for example, in [137]. Consequently, the literature distinguishes three classes of approaches that allow the stabilization of nonholonomic vehicles at a desired configuration (see, for example, [43, 87]):

- *Discontinuous stabilizers* – in which the control signals are discontinuous functions of states (see, for example, [7]),
- *Continuous time-dependent stabilizers* – in which the feedback depends on both the state and the time (see, for example, [106]),
- *Hybrid stabilizers* – which combine the properties of the two other classes (see, for example, [121]).

The class of discontinuous stabilizers also includes control laws designed according to the Vector Field Orientation (VFO) methodology (see [73]), which is used in this dissertation and will be discussed in more details later.

Considering the issue of control of nonholonomic vehicles, one must also take into account the practical limitations of vehicles. Physical vehicles cannot reach arbitrary velocities, as they are restricted by the capabilities of their actuators, among other factors. These velocity limitations should be taken into account in the control design process, as they are related to the maximum admissible absolute values of the control signals. The issue of designing control laws for nonholonomic vehicles, taking into account control input constraints, is widely discussed in the literature (see, for example, [16, 31, 37, 39, 49, 97]). Generally, two main approaches to this problem can be distinguished: taking input constraints into account during the controller design phase, or designing the *nominal* controller without considering input constraints and then ensuring that they are met through a post-processing phase. An example of the first approach is the use of the Model Predictive Control (MPC) methodology, which is well-known in the literature (see, for example, [11]), and treating the control input constraints as an additional constraint in the formulation of the optimization problem. The second approach, in some sense, increases the designer's freedom, as it reduces the number of factors that must be taken into account during the design of the control law. The aforementioned post-processing can be performed, for example, by using a so-called *scaling procedure*, which rescales the *nominal* control signals to ensure that the imposed constraints are satisfied, while simultaneously preserving the direction and orientation of the *nominal* velocity vector (see, for example, [16, 73, 97]). The scaling procedure will be discussed in more details hereinafter.

The literature also includes works in which control laws for nonholonomic vehicles have been developed based on the concept of *fixed-time stability* (see, for example, [46, 98, 99, 133]). However, due to the fact that fixed-time controllers are typically characterized by relatively large amplitude of control signals for an initial condition, the problem of satisfying the imposed control input constraints appears particularly significant. Although there are some propositions in the literature for fixed-time control laws that take into account input constraints (see, for example, [30, 130, 131, 138]), only a few of them can be applied to nonholonomic vehicles (see, for example, [23]).

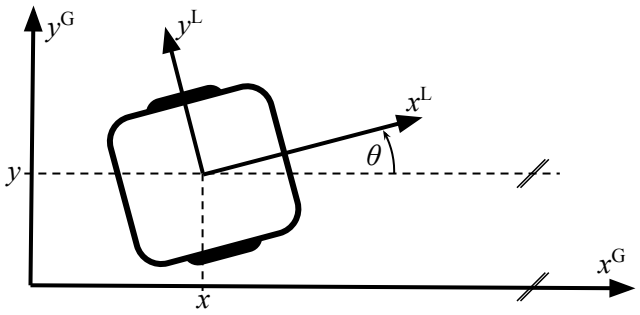

Figure 1.1 – Two-wheeled mobile robot of unicycle kinematics.

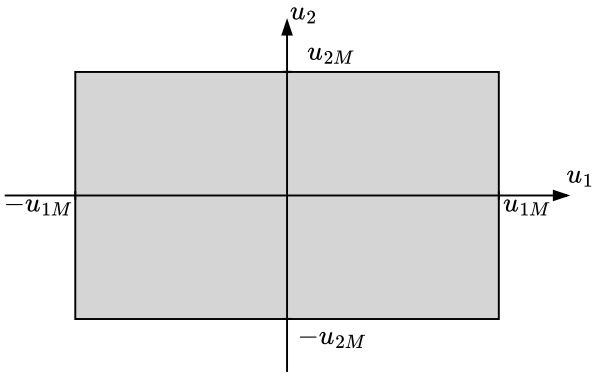

Figure 1.2 – Set $\mathscr{U}$ of admissible control inputs.

1.3.2 Unicycle model and input constraints

This work considers a kinematic model of a unicycle-like wheeled differentially driven mobile robot (see, for example, [12, 43]), which can be written as follows:

$$\dot{\boldsymbol{q}} \triangleq \boldsymbol{G}(\boldsymbol{q})\boldsymbol{u} = \begin{bmatrix} 1 & 0 \\ 0 & \cos\theta \\ 0 & \sin\theta \end{bmatrix} \begin{bmatrix} u_1 \\ u_2 \end{bmatrix} = \boldsymbol{g}_1 u_1 + \boldsymbol{g}_2(\theta) u_2 \tag{1.6}$$

where $\boldsymbol{q} = \begin{bmatrix} \theta & \bar{\boldsymbol{q}}^\top \end{bmatrix}^\top = \begin{bmatrix} \theta & x & y \end{bmatrix}^\top \in \mathbb{R}^3$ denotes the configuration vector containing the positional coordinates x and y of the vehicle's guidance point and the orientation angle θ expressed in the global frame. It should be noted that for the considered model the vehicle's guidance point is located in the center of the axis connecting the right and left wheels (see Fig. 1.1). Vector $\boldsymbol{u} = \begin{bmatrix} u_1 & u_2 \end{bmatrix}^\top \in \mathscr{U} \subset \mathbb{R}^2$ contains control inputs which denote the angular velocity u_1 and longitudinal velocity u_2 of the vehicle's guidance point, respectively. This dissertation considers control in the presence of control input constraints, that is, the values of the control inputs must belong to a bounded set $\mathscr{U} = \{\boldsymbol{u} : |u_1| \leq u_{1M}, |u_2| \leq u_{2M}\}$, where u_{1M} and u_{2M} are design parameters and denote the maximum admissible absolute values of angular velocity and longitudinal velocity, respectively (see Fig. 1.2).

A scaling procedure (see, for example, [16, 73, 97]) will be used to ensure that control inputs meet the imposed constraints. This method increases the designer's flexibility, as it allows to design a *nominal* control algorithm without paying attention to the imposed control input limitations, and then perform post-processing of the *nominal* (unconstrained) control inputs to obtain values that meet the imposed constraints. The key element of this procedure is a scaling function defined

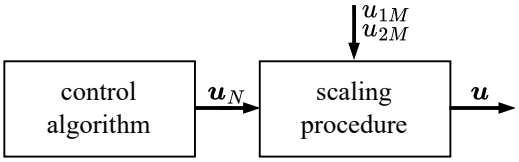

Figure 1.3 – Block diagram showing an example of the scaling procedure application.

as follows:

$$s(t) \triangleq \left(\max \left\{ 1, \frac{|u_{1N}(t)|}{u_{1M}}, \frac{|u_{2N}(t)|}{u_{2M}} \right\} \right)^{-1} \in (0,1), \tag{1.7}$$

where $\begin{bmatrix} u_{1N}(t) & u_{2N}(t) \end{bmatrix}^\top = \boldsymbol{u}_N(t) \in \mathbb{R}^2$ denotes the vector of *nominal* control signals (that is, those that do not take into account the imposed constraints). A post-processing involves scaling the vector of the *nominal* control inputs by the scaling function, that is: $\boldsymbol{u}(t) = \boldsymbol{u}_N(t)s(t) \in \mathscr{U}$ (see Fig. 1.3).

1.3.3 Vector Field Orientation design methodology

The Vector Field Orientation (VFO) (see [73]) is a control design methodology for a certain subclass of dynamical systems, which includes unicycle-like mobile robots (1.6). The methodology is geometric in nature, and each of its components has a simple and intuitive interpretation. The key component is the so-called *convergence vector field*, which for system (1.6) is defined as follows:

$$\boldsymbol{h}(\boldsymbol{e}) \triangleq \begin{bmatrix} h_\theta(\boldsymbol{e}) \\ \bar{\boldsymbol{h}}(\boldsymbol{e}) \end{bmatrix} = \begin{bmatrix} h_\theta(\boldsymbol{e}) \\ h_x(\boldsymbol{e}) \\ h_y(\boldsymbol{e}) \end{bmatrix} \in \mathbb{R}^3, \tag{1.8}$$

where $\boldsymbol{e}\left(\boldsymbol{q}(t), \boldsymbol{q}_d(\cdot), \cdot\right)$ denotes a vector of system errors that depends on the configuration vector $\boldsymbol{q}(t)$ and a desired configuration vector $\boldsymbol{q}_d(\cdot)$. The convergence vector field for each point $\boldsymbol{e} \in \mathbb{R}^3$ in the error space indicates the direction to the goal, that is, to obtain $\boldsymbol{e} = \boldsymbol{0}$. However, to ensure that the goal can be achieved, it is essential to ensure that the configuration velocity $\dot{\boldsymbol{q}}(t) \overset{(1.6)}{=} \boldsymbol{G}(\boldsymbol{q}(t))\boldsymbol{u}(t)$ converges to the field $\boldsymbol{h}(\boldsymbol{e}(t))$, that is, $[\boldsymbol{G}(\boldsymbol{q}(t))\boldsymbol{u}(t) - \boldsymbol{h}(\boldsymbol{e}(t))] \xrightarrow{t \to \tau} 0$, where $0 < \tau < \infty$ is a convergence horizon. By taking $\boldsymbol{G}(\boldsymbol{q}(t))\boldsymbol{u}(t) - \boldsymbol{h}(\boldsymbol{e}(t)) = \boldsymbol{0}$, it is possible to directly determine $\boldsymbol{u}(t)$ as follows:

$$\begin{aligned} \boldsymbol{G}(\boldsymbol{q})\boldsymbol{u} &= \boldsymbol{h}(\boldsymbol{e}) \\ \boldsymbol{G}^\top(\boldsymbol{q})\boldsymbol{G}(\boldsymbol{q})\boldsymbol{u} &= \boldsymbol{G}^\top(\boldsymbol{q})\boldsymbol{h}(\boldsymbol{e}), \end{aligned}$$

where $\boldsymbol{G}^\top(\boldsymbol{q})\boldsymbol{G}(\boldsymbol{q}) = 1$, which leads to the basic form of the VFO control law defined as follows:

$$\boldsymbol{u} = \begin{bmatrix} u_1 \\ u_2 \end{bmatrix} = \boldsymbol{G}^\top(\boldsymbol{q})\boldsymbol{h}(\boldsymbol{e}) = \begin{bmatrix} h_\theta(\boldsymbol{e}) \\ h_x(\boldsymbol{e})\cos\theta + h_y(\boldsymbol{e})\sin\theta \end{bmatrix} = \begin{bmatrix} h_\theta(\boldsymbol{e}) \\ \bar{\boldsymbol{h}}^\top(\boldsymbol{e})\bar{\boldsymbol{g}}_2(\theta) \end{bmatrix}, \tag{1.9}$$

with $\bar{\boldsymbol{g}}_2(\theta) \triangleq \begin{bmatrix} \cos\theta & \sin\theta \end{bmatrix}^\top$. In geometric interpretation, u_1 is called *orienting* control, as it directly affects the change in the orientation of the field $\boldsymbol{g}_2(\theta)$, while u_2 is *pushing* control, as it is responsible for pushing the robot along the field $\bar{\boldsymbol{h}}$.

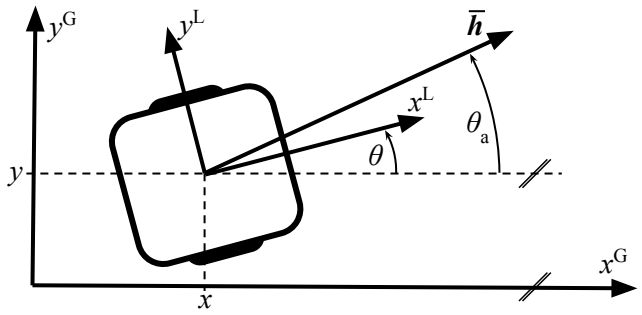

Figure 1.4 – Two-wheeled unicycle-like mobile robot with the convergence vector field and with the auxiliary orientation angle θ_a denoted.

Let us now introduce an another characteristic component of the VFO methodology, namely the so-called *auxiliary orientation* θ_a, which is the orientation of the positional subvector $\bar{\boldsymbol{h}}$ of the convergence vector field $\boldsymbol{h}$, expressed in the global frame (see Fig. 1.4), and it is defined as follows:

$$\theta_a \triangleq \begin{cases} \operatorname{Atan2c}\left(\sigma h_y(\boldsymbol{e}), \sigma h_x(\boldsymbol{e})\right) & \text{if } \left\|\bar{\boldsymbol{h}}\right\| \neq 0 \\ 0 & \text{otherwise} \end{cases} . \tag{1.10}$$

The operator $\operatorname{Atan2c}(\cdot,\cdot) : \mathbb{R} \times \mathbb{R} \to \mathbb{R}$ is a continuous version of the four-quadrant inverse tangent function $\operatorname{Atan2}(\cdot,\cdot) : \mathbb{R} \times \mathbb{R} \to (-\pi, \pi]$, while $\sigma \in \{-1, 1\}$ determines the robot's motion strategy, that is, forward motion if $\sigma = 1$ or backward motion if $\sigma = -1$.

Until now, control laws formulated according to the VFO methodology have been used to solve fundamental motion tasks, that is set-point control, trajectory tracking, and path following, for the unicycle-like mobile robot (see, for example, [73,81]) and for the car-like mobile robot (see, for example, [28, 70, 75]). Usually, the choice of task determines the definition of the convergence vector field (1.8), while the general structure of the control law (1.9) remains unchanged. The literature also includes works that consider other tasks, such as moving through waypoints (see, for example, [24, 72]), movement in the presence of skid-slip phenomena (see, for example, [63, 65, 80]), obstacle avoidance (see, for example, [44, 45]), and movement with a bounded curvature of motion (see [25–27]), to name a few.

However, mobile robots with unicycle and car-like kinematics are not the only dynamic systems for which control laws have been designed using the VFO methodology. The literature includes, for example, VFO control algorithms dedicated to nonholonomic manipulators (see [68, 76]), for three-dimensional chained systems (see [69]), for N-trailer vehicles (see, for example, [33, 64, 67, 83]), for visual servoing (see, for example, [79,86]), as well as for vehicles moving in 3D space (see, for example, [47, 48, 84]). The VFO methodology has also been successfully used to develop driver assistance systems (see, for example, [29, 66, 82]).

Most of the VFO control algorithms currently available in the literature focus on the asymptotic convergence of control errors toward zero, with the exception of [71] and [74], which consider convergence within a finite time, according to the concept of *finite-time stability*. This doctoral dissertation, along with the related works [85, 115–120], expands existing applications of VFO methodology by introducing control algorithms developed in accordance with the concepts of *fixed-time stability*

and *predefined-time stability*, dedicated to nonholonomic unicycle-type mobile robots and multi-vehicle systems composed of nonholonomic mobile robots.

1.4 Control of multi-vehicle systems

This section will address the problem of control of multi-vehicle systems. First, in Section 1.4.1, an overview of the most important literature will be provided. Next, in Section 1.4.2 terms related to the communication topology will be introduced, and finally, in Section 1.4.3, the consensus mechanism that can be used to perform the formation task will be discussed.

1.4.1 State of the art

The term *multi-agent system* is broad and multidisciplinary, since depending on the definition of *agent*, it can be applied to many different scientific disciplines, covering fields such as robotics, computer science, artificial intelligence, and even social sciences, economics, and many others. Although the *agent* can be defined in many different ways, it will always have several characteristic features, such as (see [13]):

- *autonomy* – an agent should have at least partial autonomy, that is, the ability to make decisions,
- *perception* – an agent should be able to interact with its environment,
- *communication* – an agent should be able to communicate with other agents,
- *computations* – an agent must be capable of performing at least basic calculations or basic data processing.

This dissertation considers a system composed of agents that are nonholonomic vehicles, hence it will be referred to as a (nonholonomic) multi-vehicle system. Furthermore, the considered system is *decentralized*, which means that there is no single unit that knows everything about the entire system and generates information for all vehicles. It is also *distributed*, which means that each vehicle has access only to a part of the information about the system and, based on this 'local' information, works toward solving the 'global' problem facing the entire system.

The control of multi-vehicle systems is a well-established field in the literature (see, for example, [13, 94, 96, 109]). The discussion should be started with the observation that such systems can successfully undertake tasks that would be very difficult or even impossible for a single vehicle, such as: transporting large or heavy objects that a single robot cannot safely lift or move, or simultaneously real-time monitoring of a wide area, for example during a search-and-rescue operation, to name a few. There are many factors that can characterize a multi-vehicle system, the most important of which appear to be the ability of vehicles to communicate with others. Without communication, there is no multi-vehicle system. The ability to communicate is therefore the feature that distinguishes a group of vehicles operating independently from vehicles cooperating within a multi-vehicle system. The primary task defined for a multi-vehicle system is a creation of formations, which can serve as the initial stage of further actions undertaken by the system.

Similar to the case of single nonholonomic mobile robots (see Section 1.3.1), the literature contains studies on the control of nonholonomic multi-vehicle systems (see, for example, [14, 55, 102, 128, 132]), as well as studies in which the control

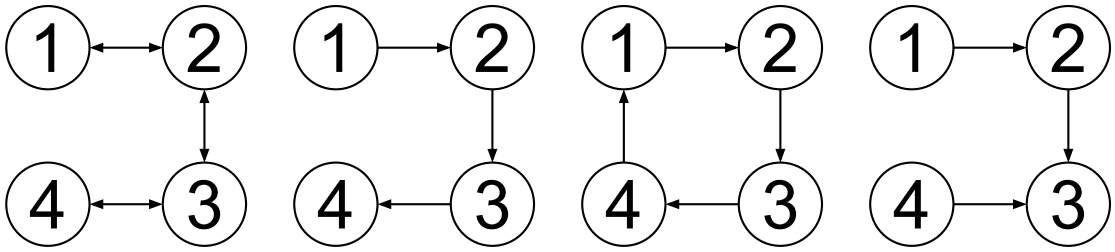

Figure 1.5 – Four example graphs of communication network.

design takes into account certain constraints imposed on the control inputs (see, for example, [93, 100, 113]). Naturally, the literature also includes propositions for control algorithms developed based on the *fixed-time stability* concept (see, for example, [2, 17, 18, 56, 136]). This dissertation proposes a fixed-time control algorithm for a multi-vehicle system composed of nonholonomic vehicles that takes into account imposed control input constraints. Although the literature contains approaches proposing fixed-time control algorithms and algorithms that consider control input limitations, the number of solutions that simultaneously: consider a nonholonomic vehicle model, utilize the concept of *fixed-time stability*, and take into account control input constraints is still relatively limited. Further discussion on this issue will be presented in the section devoted to the consensus mechanism, which will be used in this dissertation to perform the formation task.

1.4.2 Communication topologies

The theoretical background in this section follows [109]. A communication network in a multi-vehicle system is described by a graph $\mathcal{G} = \{\mathscr{V}, \mathscr{E}\}$, where $\mathscr{V} = \{1, 2, \ldots, n_v\}$ is a set of nodes and $\mathscr{E} \subseteq \mathscr{V} \times \mathscr{V}$ is a set of edges containing ordered pairs of nodes. For a directed graph, the pair $(i, j) \in \mathscr{E}$, where $i \in \mathscr{V}$, $j \in \mathscr{V}$, and $i \neq j$, means that vehicle j can receive information from vehicle i, but vehicle i is not necessarily able to receive information from vehicle j. In the case of an undirected graph, the existence of the pair $(i, j) \in \mathscr{E}$ guarantees that the pair $(j, i) \in \mathscr{E}$ also exists. Moreover, if $(i, j) \in \mathscr{E}$ then vehicle j is called a neighbor of vehicle i. The set of neighbors of vehicle i is denoted as $\mathcal{N}_i$.

Let us introduce the adjacency matrix $\boldsymbol{\mathcal{A}} = [a_{ij}] \in \mathbb{R}^{n_v \times n_v}$, with $a_{ij} > 0$ if $(j, i) \in \mathscr{E}$ and $a_{ij} = 0$ if $(j, i) \notin \mathscr{E}$, while $a_{ii} = 0$. The values of a_{ij} correspond to the weights of the edges, however, if the weights are not usefull, it is usually assumed that $a_{ij} \in \{0, 1\}$. It is worth noting that for an undirected graph, $a_{ij} = a_{ji}$, and thus matrix $\boldsymbol{\mathcal{A}}$ is symmetrical.

Let us define the matrix $\boldsymbol{\mathcal{L}} = [\ell_{ij}] \in \mathbb{R}^{n_v \times n_v}$ such that $\ell_{ij} = -a_{ij}$ for $i \neq j$ and $\ell_{ii} = \sum_{j=1}^{n_v} a_{ij}$. For an undirected graph, the matrix $\boldsymbol{\mathcal{L}}$ is symmetrical and it is called the *Laplacian matrix*, while for a directed graph, it is called the *nonsymmetrical Laplacian matrix* or *directed Laplacian matrix*. Furthermore, matrix $\boldsymbol{\mathcal{L}}$ is characterized by a zero row sum.

Four examples of communication topology graphs are shown in Fig. 1.5, for which the adjacency matrices $\boldsymbol{\mathcal{A}}$ and Laplacian matrices $\boldsymbol{\mathcal{L}}$ can be written as follows:

- for the graph in Fig. 1.5a:

$$\boldsymbol{\mathcal{A}} = \begin{bmatrix} 0 & 1 & 0 & 0 \\ 1 & 0 & 1 & 0 \\ 0 & 1 & 0 & 1 \\ 0 & 0 & 1 & 0 \end{bmatrix}, \qquad \boldsymbol{\mathcal{L}} = \begin{bmatrix} 1 & -1 & 0 & 0 \\ -1 & 2 & -1 & 0 \\ 0 & -1 & 2 & -1 \\ 0 & 0 & -1 & 1 \end{bmatrix} \tag{1.11}$$

- for the graph in Fig. 1.5b:

$$\boldsymbol{\mathcal{A}} = \begin{bmatrix} 0 & 0 & 0 & 0 \\ 1 & 0 & 0 & 0 \\ 0 & 1 & 0 & 0 \\ 0 & 0 & 1 & 0 \end{bmatrix}, \qquad \boldsymbol{\mathcal{L}} = \begin{bmatrix} 0 & 0 & 0 & 0 \\ -1 & 1 & 0 & 0 \\ 0 & -1 & 1 & 0 \\ 0 & 0 & -1 & 1 \end{bmatrix}, \tag{1.12}$$

- for the graph in Fig. 1.5c:

$$\boldsymbol{\mathcal{A}} = \begin{bmatrix} 0 & 0 & 0 & 1 \\ 1 & 0 & 0 & 0 \\ 0 & 1 & 0 & 0 \\ 0 & 0 & 1 & 0 \end{bmatrix}, \qquad \boldsymbol{\mathcal{L}} = \begin{bmatrix} 1 & 0 & 0 & -1 \\ -1 & 1 & 0 & 0 \\ 0 & -1 & 1 & 0 \\ 0 & 0 & -1 & 1 \end{bmatrix}, \tag{1.13}$$

- for the graph in Fig. 1.5d:

$$\boldsymbol{\mathcal{A}} = \begin{bmatrix} 0 & 0 & 0 & 0 \\ 1 & 0 & 0 & 0 \\ 0 & 1 & 0 & 1 \\ 0 & 0 & 0 & 0 \end{bmatrix}, \qquad \boldsymbol{\mathcal{L}} = \begin{bmatrix} 0 & 0 & 0 & 0 \\ -1 & 1 & 0 & 0 \\ 0 & -1 & 2 & -1 \\ 0 & 0 & 0 & 0 \end{bmatrix}. \tag{1.14}$$

It should be noted that the graph in Fig. 1.5a describe an undirected communication topology, and therefore the matrices $\boldsymbol{\mathcal{A}}$ and $\boldsymbol{\mathcal{L}}$ in (1.11) are symmetrical. On the other hand, the graphs in Figs. 1.5b-1.5d describe directed communication topologies, and thus the associated matrices $\boldsymbol{\mathcal{A}}$ and $\boldsymbol{\mathcal{L}}$ in equations (1.12)-(1.14) are nonsymmetrical.

1.4.3 Consensus problem

The theoretical framework in this section is based on [109], as the consensus problem is well known in the literature (see, for example, [9, 19, 52, 60, 91, 95, 126]). A multi-vehicle system reaches *consensus* if there is a variable of interest to the system and the vehicles agree on its common value. The shared variable of interest is called the *information state*, while the algorithm for negotiating its common value is known as the *consensus algorithm*. The agreed common value of the information state is called the *consensus equilibrium state*.

To achieve consensus, it must be possible to exchange information between vehicles in a multi-vehicle system, that is, the graph $\mathcal{G}$ describing the communication topology must contain a *directed spanning tree*, which means that there must be a vehicle that has a direct communication path to every other vehicle (see, for example, the graphs shown in Figs. 1.5a-1.5c). It is also worth noting that the value of the consensus equilibrium state is affected only by the information states of those vehicles that have a direct communication path to every other vehicle. It can therefore be concluded that if the graph is *strongly connected*, that is, if each vehicle has

a direct communication path to every other vehicle (see, for example, the graphs shown in Figs. 1.5a and 1.5c), then the information state of each vehicle affects the value of the consensus equilibrium state. It should also be noted that if the graph $\mathcal{G}$ is undirected and has a directed spanning tree, then it is always strongly connected.

Various consensus algorithms can be found in the literature, among which the most popular basic algorithm is defined as follows (see, for example, [95, 109]):

$$\dot{z}_i(t) = -\sum_{j \in \mathcal{N}_i} a_{ij} \left(z_i(t) - z_j(t) \right), \quad i \in \mathcal{V}, \tag{1.15}$$

where z_i denotes the information state of vehicle i, and $\boldsymbol{z} = \begin{bmatrix} z_1 & z_2 & \dots & z_n \end{bmatrix}^\top$, while a_{ij} denotes the appropriate value from the adjacency matrix $\boldsymbol{\mathcal{A}}$. Consensus is achieved when $\boldsymbol{z}(t) \to z_c \underline{\mathbf{1}}$, where $\underline{\mathbf{1}}$ is the $n_v \times 1$ column vector of ones, with n_v denoting the number of vehicles in a multi-vehicle system, and z_c is the value of the consensus equilibrium state. It can be easily seen that in the case of algorithm (1.15), consensus is reached when the value of the information state of each vehicle is the same. Note that (1.15) can be written in a matrix form as follows:

$$\dot{\boldsymbol{z}}(t) = \begin{bmatrix} -\sum_{j \in \mathcal{N}_1} a_{1j} \left(z_1(t) - z_j(t) \right) \\ -\sum_{j \in \mathcal{N}_2} a_{2j} \left(z_2(t) - z_j(t) \right) \\ \vdots \\ -\sum_{j \in \mathcal{N}_n} a_{nj} \left(z_n(t) - z_j(t) \right) \end{bmatrix} = \begin{bmatrix} -\sum_{j=1}^{n_v} \ell_{1j} z_j(t) \\ -\sum_{j=1}^{n_v} \ell_{2j} z_j(t) \\ \vdots \\ -\sum_{j=1}^{n_v} \ell_{nj} z_j(t) \end{bmatrix} = -\boldsymbol{\mathcal{L}} \boldsymbol{z}(t). \tag{1.16}$$

The literature on consensus algorithms typically considers relatively simple system dynamics, modeling them as a single-integrator (see, for example, [53,110,127]), that is,

$$\dot{z}_{1i}(t) = u_i(t), \quad i \in \mathcal{V},$$

or a double-integrator (see, for example, [21, 61, 129]), that is,

$$\dot{z}_{1i}(t) = z_{2i}(t), \quad \dot{z}_{2i}(t) = u_i(t), \quad i \in \mathcal{V},$$

where $z_{1i} \in \mathbb{R}^m$ is the information state, $z_{2i} \in \mathbb{R}^m$ is the time derivative of the information state, while $u_i \in \mathbb{R}^m$ is the control input, associated with the i-th vehicle. The popularity of such models may be related to their mathematical simplicity and the simplicity of stability analysis for consensus algorithms. In the case of the single-integrator model, the control input directly affects the change of the value of the information state, whereas the double-integrator model additionally considers a certain dynamics of the speed of changes in the value of the information state. Despite the popularity of such models, many real-world multi-vehicle systems are characterized by kinematic constraints that often cannot be properly described using simple linear models. Hence, the literature includes studies that consider nonholonomic vehicle models (see, for example, [36,88,139]) or model them in chained form (see, for example, [20,92,108,112]). The literature also includes works that consider the consensus problem for nonholonomic vehicles while taking into account control input constraints (see, for example, [54]), as well as those presenting fixed-time consensus algorithms for nonholonomic vehicles (see, for example, [42, 111, 112, 127]). Currently there are only a few approaches that propose fixed-time consensus algorithms for nonholonomic vehicles while simultaneously taking into account control input constraints. However, these approaches typically do not directly consider the

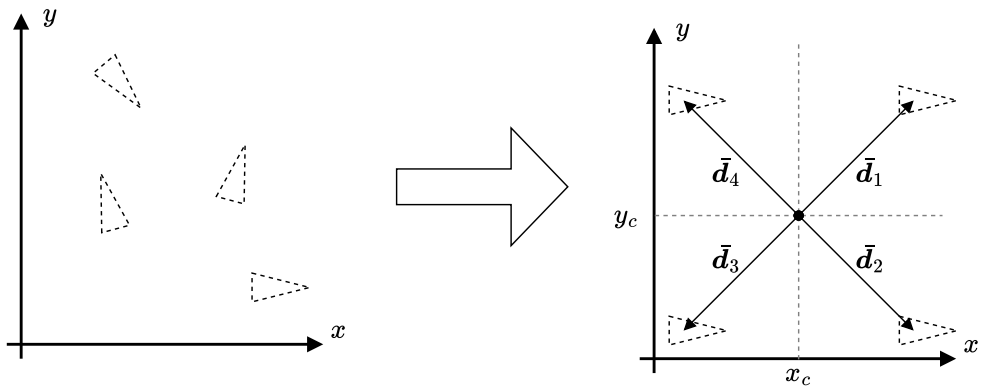

Figure 1.6 – Example of a desired formation for a multi-vehicle system consisting of 4 vehicles, where $\bar{\boldsymbol{d}}_1$, $\bar{\boldsymbol{d}}_2$, $\bar{\boldsymbol{d}}_3$, and $\bar{\boldsymbol{d}}_4$ represent the displacement vectors of the vehicles' guidance points from the *a priori* unknown consensus equilibrium point (x_c, y_c). The vehicles are denoted by dashed triangles.

model of a nonholonomic vehicle but simplify it, for example, to a single-integrator model (see [53]).

This dissertation considers the problem of creating formations by a multi-vehicle system, and the consensus mechanism can be successfully used to accomplish this task. In such a case, certain displacements are usually defined such that, when consensus is reached, the information states of individual vehicles remain in a certain relation to the consensus equilibrium state and are not necessarily equal to it (cf. [109]). To create a formation on the XY plane, it can be done as follows:

$$\dot{\boldsymbol{z}}_i(t) = -\sum_{j\in\mathcal{N}_i} a_{ij}\Big(\boldsymbol{z}_i(t) - \bar{\boldsymbol{d}}_i - \boldsymbol{z}_j(t) + \bar{\boldsymbol{d}}_j\Big), \quad i \in \mathcal{V}, \tag{1.17}$$

where the information state $\boldsymbol{z}_i \triangleq \begin{bmatrix} x_i & y_i \end{bmatrix}^\top \in \mathbb{R}^2$ of the i-th vehicle can be interpreted as the positional coordinates (x_i, y_i) of the vehicle's guidance point, and $\bar{\boldsymbol{d}}_i \in \mathbb{R}^2$ denotes the displacement vector of the vehicles' guidance point from the consensus equilibrium point. Thus, it can be noted that the vector $\bar{\boldsymbol{d}}_i$ defines the position of the i-th robot in the formation (see Fig. 1.6).

1.5 Conclusions

This chapter provides preliminaries and literature review on the *fixed-time stability* concept, the control of nonholonomic systems, and the control of multi-vehicle systems. The objective of this dissertation is to develop control laws for a single nonholonomic mobile robot and for a multi-vehicle system composed of nonholonomic vehicles, based on the concept of *fixed-time stability*. Based on Sections 1.3 and 1.4, it can be concluded that fixed-time control algorithms for such systems currently exist in the literature. However, unlike most approaches in the literature, the purpose of this doctoral dissertation is to design fixed-time control laws while simultaneously taking into account control input constraints. This is a gap in the current state of knowledge that this doctoral dissertation will attempt to fill.

The following chapters will present the control design for a single unicycle-like mobile robot and the control design for a distributed multi-vehicle system, both based on the VFO methodology.

Chapter 2

Control design for a single unicycle-like mobile robot

2.1 Introduction

This chapter presents two control law designs for a single nonholonomic mobile robot, whose kinematic model is discussed in Section 1.3.2. It is organized as follows: Section 2.2 presents the set-point fixed-time VFO control law, then Section 2.3 discusses the path-following fixed-time VFO control law, and finally, Section 2.4 provides a summary including the discussion of the presented control methods.

2.2 Set-point control

First, let us take a look at the problem of set-point fixed-time control. The design of a control law within the VFO methodology that solves this problem while taking into account the control input constraints will be carried out in two stages: first, a *nominal* control law will be defined that ensures a solution to this problem without considering the control input constraints, and then, in a post-processing process that uses the scaling procedure introduced in Section 1.3.2, a VFO control law will be obtained that meets the imposed control input constraints. A method for *a priori* estimation of the upper bound of the settling time in the presence of control input constraints will also be presented, as well as the results of numerical simulations from the Matlab-Simulink environment and experimental tests performed using a physical robot. The results presented in this Sections were originally published in [119].

2.2.1 Control problem formulation

Let us define the vector of configuration errors as follows:

$$\boldsymbol{e}(t) = \begin{bmatrix} e_\theta(t) \\ \bar{\boldsymbol{e}}(t) \end{bmatrix} = \begin{bmatrix} e_\theta(t) \\ e_x(t) \\ e_y(t) \end{bmatrix} = \begin{bmatrix} f_\theta\big(\theta_d - \theta(t)\big) \\ x_d - x(t) \\ y_d - y(t) \end{bmatrix} \in \mathcal{Q}_e, \tag{2.1}$$

where $\mathcal{Q}_e \in (-\pi, \pi] \times \mathbb{R}^2$ denotes the configuration error space, while $\begin{bmatrix} \theta_d & x_d & y_d \end{bmatrix}^\top \triangleq \boldsymbol{q}_d$ is the vector of the desired configuration which is constant. Note that the orien-

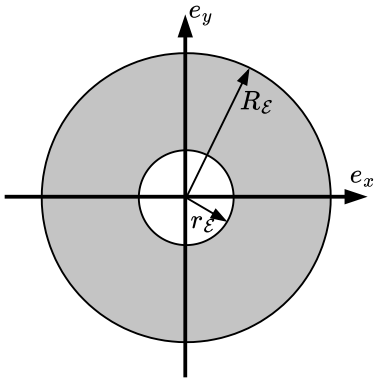

Figure 2.1 – Set $\bar{\mathcal{E}}$ of admissible values of the norm of positional error.

tation error is considered in the sense of modulo 2π, hence the function $f_\theta : \mathbb{R} \to (-\pi, \pi]$ is introduced.

Since this dissertation deals with the control in the presence of control input constraints and task-execution time constraints, let us define a set $\mathcal{E}$ of admissible initial conditions:

$$\mathcal{E} \triangleq (-\pi, \pi] \times \bar{\mathcal{E}}, \qquad \bar{\mathcal{E}} \triangleq \{\bar{\boldsymbol{e}}_0 : 0 < r_\mathcal{E} \leq \|\bar{\boldsymbol{e}}_0\| \leq R_\mathcal{E}\}, \tag{2.2}$$

where $\bar{\boldsymbol{e}}_0 \triangleq \bar{\boldsymbol{e}}(0) \in \mathbb{R}^2$, while $r_\mathcal{E}$ and $R_\mathcal{E}$ denote the smallest and the largest admissible values of the norm of the positional error, respectively (see Fig. 2.1). They are determined by a designer, and their values influence the degree of conservatism in the estimation of the upper bound of the settling time, which will be discussed in more details later.

Finally, let us formulate the control problem as follows:

Problem 1 *For system* (1.6)*, find a feedback control law* $\boldsymbol{u}(\boldsymbol{e})$ *which, for any initial configuration error* $\boldsymbol{e}_0 \in \mathcal{E}$*, guarantees that the solution* $\boldsymbol{e}(t, \boldsymbol{e}_0)$ *of the closed-loop system dynamics* $\dot{\boldsymbol{e}} = -\boldsymbol{G}(\boldsymbol{q})\boldsymbol{u}(\boldsymbol{e})$ *satisfies:*

- $\forall t \geq 0 \quad \|\boldsymbol{e}(t, \boldsymbol{e}_0)\| < \infty$,
- $\forall t \geq 0 \quad \boldsymbol{u}(\boldsymbol{e}(t, \boldsymbol{e}_0)) \in \mathscr{U}$,
- $\forall t \geq t_s(\boldsymbol{e}_0) \quad \|\bar{\boldsymbol{e}}(t, \boldsymbol{e}_0)\| \leq \epsilon$,
- $\forall t \geq t_s(\boldsymbol{e}_0) \quad e_\theta(t, \boldsymbol{e}_0) = \theta_\epsilon$,
- $\sup_{\boldsymbol{e}_0 \in \mathcal{E}} t_s(\boldsymbol{e}_0) \leq T_c < \infty$,

where $\epsilon \in [0, r_\mathcal{E})$ *denotes a small (or zero) constant chosen by the designer,* θ_ϵ *is a constant whose value is related to* ϵ*, while the term* T_c *is the upper bound of the settling time* t_s*.*

It should be noted that if $\epsilon > 0$ is chosen, the above problem becomes a problem of convergence to a vicinity of zero, and in that case one can consider *nearly fixed-time stability* (cf. Definition 1). The choice of $\epsilon > 0$ is mainly motivated by practical implementation issues, since achieving an exact zero value may be difficult due to numerical inaccuracies. However, if $\epsilon = 0$ is chosen, one can consider the convergence of the system errors to zero and the *fixed-time stability* of the equilibrium point $\boldsymbol{e} = \boldsymbol{0}$. The control law that solves Problem 1 will be developed according to the conceptual scheme of the control system shown in Fig. 2.2.

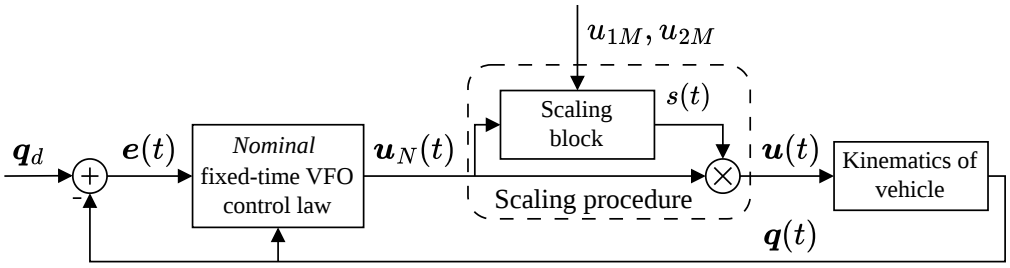

Figure 2.2 – Scheme of the control system for the set-point stabilization control problem.

2.2.2 Set-point fixed-time VFO control law

According to the VFO methodology discussed in Section 1.3.3, let us begin by defining the convergence vector field:

$$\boldsymbol{h} = \begin{bmatrix} h_\theta \\ \bar{\boldsymbol{h}} \end{bmatrix} \triangleq \begin{bmatrix} K_a \left(|e_a|^{\delta_1} + |e_a|^{\delta_2} \right) \operatorname{sign}(e_a) + \dot{\theta}_{aN} \\ K_p \left(\bar{\boldsymbol{e}} - \bar{\eta}\sigma \|\bar{\boldsymbol{e}}\| \bar{\boldsymbol{g}}_{2d} \right) \end{bmatrix}, \tag{2.3}$$

where $K_a > 0$ and $K_p > 0$ are design coefficients, $\bar{\boldsymbol{g}}_{2d} \triangleq \bar{\boldsymbol{g}}_2(\theta_d) = \begin{bmatrix} \cos\theta_d & \sin\theta_d \end{bmatrix}^\top$, while $\bar{\eta} \in (0.5, 1)$ is related to the so-called *directing effect*, that is, the length of the final stage consists of the nearly straight-line movement towards the desired point – the higher the $\bar{\eta}$ is, the longer the final stage is.

The decision variable $\sigma \in \{-1, 1\}$, introduced in Section 1.3.3, can be chosen arbitrarily by the designer, or its value can be related to the initial error such that

$$\sigma \triangleq \operatorname{sgn}\Big(e_x(0) \cos\theta_d + e_y(0) \sin\theta_d \Big). \tag{2.4}$$

Please note that $\operatorname{sign}(\cdot)$ and $\operatorname{sgn}(\cdot)$ are functions defined as follows:

$$\operatorname{sign}(z) \triangleq \begin{cases} 1 & \text{if} \quad z > 0 \\ 0 & \text{if} \quad z = 0 \\ -1 & \text{if} \quad z < 0 \end{cases}, \qquad \operatorname{sgn}(z) \triangleq \begin{cases} 1 & \text{if} \quad z \geq 0 \\ -1 & \text{if} \quad z < 0 \end{cases}, \tag{2.5}$$

while the powers δ_1 and δ_2 are chosen such that

$$\delta_1 \triangleq 1 - \bar{\delta}, \qquad \delta_2 \triangleq 1 + \bar{\delta}, \qquad \bar{\delta} \in (0, 1). \tag{2.6}$$

Remark 3 *It should be noted that the choice of powers proposed in* (2.6) *is primarily motivated by the intention to use the 'local' method for estimating the upper bound of the settling time proposed in Lemma 4. If one is not interested in the 'local' method and prefers to consider the global case, one may choose the powers as proposed in Lemma 1 and use Lemma 3 to estimate the upper bound of the settling time.*

The term e_a denotes the auxiliary orientation error and it is defined as follows:

$$e_a(t) \triangleq \theta_a(t) - \theta(t), \tag{2.7}$$

where θ_a is the auxiliary orientation introduced in (1.10).

Assumption 1 *For the purpose of applying the 'local' method for estimating the upper bound of the settling time formulated in Lemma 4, let us assume that* $e_a(0) \in (-\pi, \pi]$.

Taking into account considerations related to the practical implementation of the proposed control law, let us modify the definition (1.10) as follows:

$$\theta_a\left(\bar{\boldsymbol{h}}(\bar{\boldsymbol{e}})\right) \triangleq \begin{cases} \operatorname{Atan2c}\left(\sigma h_y(\bar{\boldsymbol{e}}), \sigma h_x(\bar{\boldsymbol{e}})\right) & \text{if } \|\bar{\boldsymbol{e}}(t)\| > \epsilon \\ \theta_{a\epsilon} & \text{otherwise} \end{cases}, \tag{2.8}$$

where ϵ denotes the small neighbourhood of zero chosen by the designer, while $\theta_{a\epsilon} = \lim_{\|\bar{\boldsymbol{e}}\| \to \epsilon} \theta_a\left(\bar{\boldsymbol{h}}(\bar{\boldsymbol{e}})\right)$, and the term $\operatorname{Atan2c}(\cdot,\cdot) : \mathbb{R} \times \mathbb{R} \to \mathbb{R}$ is a continuous version of the four-quadrant inverse tangent function $\operatorname{Atan2}(\cdot,\cdot) : \mathbb{R} \times \mathbb{R} \to (-\pi, \pi]$. Based on (2.3), it can be observed that $\left\|\bar{\boldsymbol{h}}\right\| \to 0$ only if $\|\bar{\boldsymbol{e}}\| \to 0$.

Let us define the *nominal* time derivative $\dot{\theta}_{aN}$ of the auxiliary orientation θ_a used in (2.3):

$$\dot{\theta}_{aN}\left(\bar{\boldsymbol{h}}(\bar{\boldsymbol{e}})\right) \triangleq \begin{cases} \frac{\dot{h}_{yN} h_x - \dot{h}_{xN} h_y}{\|\bar{\boldsymbol{h}}\|^2} & \text{if } \|\bar{\boldsymbol{e}}(t)\| > \epsilon \\ 0 & \text{otherwise} \end{cases}, \tag{2.9}$$

where the *nominal* time derivative $\dot{\bar{\boldsymbol{h}}}_N$ of the positional subvector $\bar{\boldsymbol{h}}$ of the convergence vector field $\boldsymbol{h}$ can be computed as

$$\dot{\bar{\boldsymbol{h}}}_N = \begin{bmatrix} \dot{h}_{xN} \\ \dot{h}_{yN} \end{bmatrix} = K_p \left(\dot{\bar{\boldsymbol{e}}}_N - \bar{\eta}\sigma \frac{\bar{\boldsymbol{e}}^\top \dot{\bar{\boldsymbol{e}}}_N}{\|\bar{\boldsymbol{e}}\|} \bar{\boldsymbol{g}}_{2d} \right), \tag{2.10}$$

where

$$\dot{\bar{\boldsymbol{e}}}_N = -\dot{\bar{\boldsymbol{q}}}_N = -u_{2N} \bar{\boldsymbol{g}}_{2d} \tag{2.11}$$

is the time derivative of the positional error. Please note that the subscript N indicates that the value has been computed based on *nominal* (unconstrained) control law $\boldsymbol{u}_N \in \mathbb{R}^2$, which is defined as follows:

$$\boldsymbol{u}_N = \begin{bmatrix} u_{1N} \\ u_{2N} \end{bmatrix} \triangleq \begin{bmatrix} h_\theta \\ f_s \rho \bar{\boldsymbol{h}}^\top \bar{\boldsymbol{g}}_2(\theta) \end{bmatrix} = \begin{bmatrix} K_a \left(|e_a|^{\delta_1} + |e_a|^{\delta_2} \right) \operatorname{sign}(e_a) + \dot{\theta}_{aN} \\ f_s \rho \left\| \bar{\boldsymbol{h}} \right\| \cos\alpha \end{bmatrix}, \tag{2.12}$$

with h_θ defined in (2.3), while $\alpha \triangleq \angle\left(\bar{\boldsymbol{h}}, \bar{\boldsymbol{g}}_2(\theta)\right)$ and

$$\rho \triangleq \begin{cases} \rho_0 \left(\|\bar{\boldsymbol{e}}\|^{\mu_1} + \|\bar{\boldsymbol{e}}\|^{\mu_2} \right) \left\| \bar{\boldsymbol{h}} \right\|^{-1} & \text{if } \|\bar{\boldsymbol{e}}(t)\| > \epsilon \\ 0 & \text{otherwise} \end{cases}, \tag{2.13}$$

where ρ_0 is a positive design coefficient, and the powers μ_1, μ_2 are defined as follows:

$$\mu_1 \triangleq 1 - \bar{\mu}, \qquad \mu_2 \triangleq 1 + \bar{\mu}, \qquad \bar{\mu} \in (0, 1). \tag{2.14}$$

Remark 4 (cf. Remark 3) *It should be noted that the choice of powers proposed in* (2.14) *is primarily motivated by the intention to use the 'local' method for estimating the upper bound of the settling time proposed in Lemma 4. If one is not interested in the 'local' method and prefers to consider the global case, one may choose the powers as proposed in Lemma 1 and use Lemma 3 to estimate the upper bound of the settling time.*

Comparing (2.12) with (1.9), it can be seen that the function ρ does not appear in the general definition (1.9), however, it was introduced in (2.12) to ensure *fixed-time stability* of the closed-loop dynamics, as will be shown later. Please also see [71], where the function ρ was used in a way that ensures finite-time stability.

The function

$$f_s(t) \triangleq \begin{cases} 0 & \text{if} \quad t < t_{sa} \\ 1 & \text{if} \quad t \geq t_{sa} \end{cases} \tag{2.15}$$

is introduced to enable scheduling of the *pre-orientation* process and the *motion* process and thus enables an *a priori* estimation of the upper bound of the settling time t_{sa} of the auxiliary orientation error e_a, which will be discussed in more details later. If one is not interested in *a priori* estimation, one can simply choose $\forall t \geq 0$ $f_s(t) = 1$.

Finally, let us formulate the following theorem:

Theorem 1 *For system* (1.6)*, the application of the nominal fixed-time VFO control law* $\boldsymbol{u}_N(t)$ *defined in* (2.12) *with scaling function* $s(t)$ *introduced in* (1.7) *leads to the control law*

$$\boldsymbol{u} = \begin{bmatrix} u_1 \\ u_2 \end{bmatrix} \triangleq s\boldsymbol{u}_N = \begin{bmatrix} sK_a \left(|e_a|^{\delta_1} + |e_a|^{\delta_2} \right) \operatorname{sign}(e_a) + s\dot{\theta}_{aN} \\ sf_s\rho \left\| \bar{\boldsymbol{h}} \right\| \cos\alpha \end{bmatrix} \in \mathscr{U}, \tag{2.16}$$

which solves Problem 1 and ensures fixed-time stability of the equilibrium point $\boldsymbol{e} = \boldsymbol{0}$ *of the closed-loop dynamics.*

Proof. Stability proof will be shown separately for the equilibrium point of the auxiliary orientation error dynamics and for the equilibrium point of the positional error dynamics. Then, the convergence of the orientation error will be shown. For a notational convenience, the proof will be carried out for $\epsilon = 0$, however, this does not affect the generality of the results.

Auxiliary orientation error: First, let us analyze the stability of the equilibrium point of the auxiliary orientation error dynamics. The time derivative of the auxiliary orientation error e_a defined in (2.7) can be derived as follows:

$$\dot{e}_a \overset{(2.7)}{=} \dot{\theta}_a - \dot{\theta} \overset{(1.6)}{=} \dot{\theta}_a - u_1 \overset{(2.16)}{=} \dot{\theta}_a - sK_a \left(|e_a|^{\delta_1} + |e_a|^{\delta_2} \right) \operatorname{sign}(e_a) - s\dot{\theta}_{aN}. \tag{2.17}$$

One can observe that

$$s\dot{\bar{\boldsymbol{e}}}_N \overset{(2.11)}{=} -s\dot{\bar{\boldsymbol{q}}}_N \overset{(1.6)}{=} -su_{2N}\bar{\boldsymbol{g}}_2(\theta) \overset{(2.16)}{=} -u_2\bar{\boldsymbol{g}}_2(\theta) \triangleq \dot{\bar{\boldsymbol{e}}} \tag{2.18}$$

and

$$\begin{aligned} s\dot{\bar{\boldsymbol{h}}}_N = \begin{bmatrix} s\dot{h}_{xN} \\ s\dot{h}_{yN} \end{bmatrix} &\overset{(2.19)}{=} sK_p \left(\dot{\bar{\boldsymbol{e}}}_N - \bar{\eta}\sigma \frac{\bar{\boldsymbol{e}}^\top \dot{\bar{\boldsymbol{e}}}_N}{\|\bar{\boldsymbol{e}}\|} \bar{\boldsymbol{g}}_{2d} \right) \\ &\overset{(2.18)}{=} K_p \left(\dot{\bar{\boldsymbol{e}}} - \bar{\eta}\sigma \frac{\bar{\boldsymbol{e}}^\top \dot{\bar{\boldsymbol{e}}}}{\|\bar{\boldsymbol{e}}\|} \bar{\boldsymbol{g}}_{2d} \right) \triangleq \begin{bmatrix} \dot{h}_x \\ \dot{h}_y \end{bmatrix} = \dot{\bar{\boldsymbol{h}}}, \end{aligned} \tag{2.19}$$

which leads to

$$\forall \|\bar{\boldsymbol{e}}(t)\| > \epsilon \quad s\dot{\theta}_{aN} \overset{(2.9)}{=} \frac{s\dot{h}_{yN} h_x(\bar{\boldsymbol{e}}) - s\dot{h}_{xN} h_y(\bar{\boldsymbol{e}})}{\left\| \bar{\boldsymbol{h}}(\bar{\boldsymbol{e}}) \right\|^2}$$

$$\overset{(2.19)}{=} \frac{\dot{h}_y h_x(\bar{\boldsymbol{e}}) - \dot{h}_x h_y(\bar{\boldsymbol{e}})}{\left\|\bar{\boldsymbol{h}}(\bar{\boldsymbol{e}})\right\|^2} \triangleq \dot{\theta}_a. \tag{2.20}$$

Furthermore, for $\|\bar{\boldsymbol{e}}(t)\| \leq \epsilon$, one obtains $s\dot{\theta}_{aN} = \dot{\theta}_a = 0$. Then, substituting (2.20) into (2.17), one gets:

$$\begin{aligned}\dot{e}_a &\overset{(2.20)}{=} \dot{\theta}_a - sK_a\left(|e_a|^{\delta_1} + |e_a|^{\delta_2}\right)\operatorname{sign}(e_a) - \dot{\theta}_a \\ &= -sK_a\left(|e_a|^{\delta_1} + |e_a|^{\delta_2}\right)\operatorname{sign}(e_a),\end{aligned} \tag{2.21}$$

and one can conclude that the $e_a = 0$ is the equilibrium point of the auxiliary orientation error dynamics (2.21).

Let us now use the Lyapunov's method and choose a positive definite function $V_a \triangleq \frac{1}{2}e_a^2$, whose time derivative can be determined as follows:

$$\begin{aligned}\dot{V}_a = e_a\dot{e}_a &\overset{(2.21)}{=} -e_a sK_a\left(|e_a|^{\delta_1} + |e_a|^{\delta_2}\right)\operatorname{sign}(e_a) = -sK_a\left(|e_a|^{\delta_1+1} + |e_a|^{\delta_2+1}\right) \\ &= -sK_a\sqrt{2}^{\delta_1+1}V_a^{(\delta_1+1)/2} - sK_a\sqrt{2}^{\delta_2+1}V_a^{(\delta_2+1)/2}.\end{aligned} \tag{2.22}$$

Next, by comparing the obtained result with (1.2) from Lemma 1, it can be concluded that the equilibrium point $e_a = 0$ is *fixed-time stable*. However, it should be noted that $s(\boldsymbol{e}(t)) \in (0, 1]$ in (2.22), hence it is bounded but not constant. Then, using Lemma 4 to compute the upper bound of the settling time would not lead to a time-independent upper bound. Note that considerations regarding the stability of the equilibrium point of the auxiliary orientation error dynamics occur for $\forall t < t_{sa}$, which means that $f_s(t) \overset{(2.15)}{=} 0$ and thus $u_{2N}(t) \overset{(2.12)}{=} 0 \implies \dot{\bar{\boldsymbol{e}}}_N \overset{(2.11)}{=} 0 \implies \dot{\bar{\boldsymbol{h}}}_N \overset{(2.10)}{=} \mathbf{0} \implies \dot{\theta}_{aN} \overset{(2.9)}{=} 0$. Therefore, one can write

$$\forall t < t_{sa} \quad s(t) \overset{(1.7)}{=} \left(\max\left\{1, \frac{|u_{1N}(t)|}{u_{1M}}\right\}\right)^{-1} \in (0, 1), \tag{2.23}$$

and thus one can observe that for $\forall t < t_{sa}$ the scaling function acts as a classical saturation function, that is:

$$\forall t < t_{sa} \quad s(t) \overset{(1.7)}{=} \begin{cases} 1 & \text{if } |u_{1N}(t)| < u_{1M} \\ \frac{u_{1M}}{|u_{1N}(t)|} & \text{otherwise} \end{cases}, \tag{2.24}$$

which leads to

$$\forall t < t_{sa} \quad u_1(t) \overset{(2.16)}{=} \begin{cases} K_a\left(|e_a|^{\delta_1} + |e_a|^{\delta_2}\right)\operatorname{sign}(e_a) & \text{if } |u_{1N}(t)| < u_{1M} \\ u_{1M}\operatorname{sign}(e_a) & \text{otherwise} \end{cases}. \tag{2.25}$$

Let us now introduce the term

$$e_a^* \triangleq e_a : u_{1N}(e_a) = u_{1M}, \tag{2.26}$$

which denotes the non-negative value of the auxiliary orientation error for which u_{1N} reaches its maximum admissible value u_{1M}. The value e_a^* can be obtained as the solution of

$$K_a\left((e_a^*)^{\delta_1} + (e_a^*)^{\delta_2}\right) = u_{1M}. \tag{2.27}$$

Then, the dynamics of the auxiliary orientation error, defined in (2.17), can be rewritten as follows:

$$\forall t < t_{sa} \quad \dot{e}_a(t) = \begin{cases} -K_a \left(|e_a(t)|^{\delta_1} + |e_a(t)|^{\delta_2}\right) \text{sign}(e_a(t)) & \text{if } e_a(t) < e_a^* \\ -u_{1M} \text{sign}(e_a(t)) & \text{otherwise} \end{cases} . \quad (2.28)$$

One concludes that the time interval $[0, t_{sa}]$ can be divided into two ranges depending on the value of $e_a(t)$. Based on the above considerations and the stability analysis, it can be shown that there exists a time instant t_{sa}^* such that $\forall t \in (0, t_{sa}^*)\ |e_a(t)| > e_a^*$ and $\forall t \geq t_{sa}^*\ |e_a(t)| \leq e_a^*$. The value t_{sa}^* can be determined as follows:

$$t_{sa}^* \triangleq \begin{cases} \frac{\pi - e_a^*}{u_{1M}} & \text{if } e_a^* < \pi \\ 0 & \text{otherwise} \end{cases} . \quad (2.29)$$

Thus, t_{sa}^* can be interpreted as the time instant for which $|u_{1N}|$ is equal to the maximum permissible value and also as the time needed to change the value of the auxiliary orientation error e_a from π (which, according to Assumption 1, is the largest admissible initial value of e_a) to e_a^*. Moreover $e_a^* > \pi$ means that for the given design coefficients, the control input will not be saturated at any time instant (assuming no disturbance).

Let us now consider convergence from e_a^* to 0. Comparing Lemma 4 and (2.22) with $s = 1$, one can define the upper bound of this settling time as

$$T_{ca}^* = \frac{1}{K_a \bar{\delta}} \arctan\left(\sqrt{2}^{\bar{\delta}} V_a^{\bar{\delta}/2}(e_a^*)\right), \quad (2.30)$$

while the total upper bound of the settling time t_{sa} of the auxiliary orientation error e_a can be expressed as:

$$T_{ca} = t_{sa}^* + T_{ca}^*. \quad (2.31)$$

In this way, the upper bound T_{ca} is determined without using the value of $s\Big(\boldsymbol{e}(t)\Big)$ that occurs in (2.22). It should be noted that this result can be obtained thanks to the appropriate scheduling of the *pre-orientation* process and the *motion* process achieved by using the function f_s defined in (2.15).

Positional error: Let us now consider the stability of the equilibrium point of positional error dynamics defined as follows:

$$\begin{aligned} \dot{\bar{\boldsymbol{e}}} &\overset{(2.18)}{=} -u_2 \bar{\boldsymbol{g}}_2(\theta) \overset{(2.16)}{=} -s f_s \rho \left\|\bar{\boldsymbol{h}}\right\| \cos\alpha\ \bar{\boldsymbol{g}}_2(\theta) \\ &\overset{(2.13)}{=} -s f_s \rho_0 \left(\|\bar{\boldsymbol{e}}\|^{\mu_1} + \|\bar{\boldsymbol{e}}\|^{\mu_2}\right) \cos\alpha\ \bar{\boldsymbol{g}}_2(\theta). \end{aligned} \quad (2.32)$$

A convergence of the positional error occurs during the *motion* process, that is, for $t \geq t_{sa}$, which means that $f_s(t) \overset{(2.15)}{=} 1$. Therefore, (2.32) can be rewritten as follows:

$$\forall t \geq t_{sa} \quad \dot{\bar{\boldsymbol{e}}} = -s\rho_0 \left(\|\bar{\boldsymbol{e}}\|^{\mu_1} + \|\bar{\boldsymbol{e}}\|^{\mu_2}\right) \cos\alpha\ \bar{\boldsymbol{g}}_2(\theta). \quad (2.33)$$

Based on (2.33), one can conclude that $\bar{\boldsymbol{e}} = \boldsymbol{0}$ is the equilibrium point of the positional error dynamics. It should also be noted that $\forall t < t_{sa}\ f_s(t) \overset{(2.15)}{=} 0 \implies u_2(t) \overset{(2.16)}{=} 0 \implies \dot{\bar{\boldsymbol{e}}} \overset{(2.32)}{=} 0$. For further analysis, let us rewrite (2.32) again:

$$\dot{\bar{\boldsymbol{e}}} = -u_2 \bar{\boldsymbol{g}}_2(\theta) + s\rho\bar{\boldsymbol{h}} - s\rho\bar{\boldsymbol{h}}$$

$$\begin{aligned}
&\overset{(2.3)}{=} -u_2\bar{\boldsymbol{g}}_2(\theta) + s\rho\bar{\boldsymbol{h}} - s\rho(K_p\bar{\boldsymbol{e}} \underbrace{-K_p\bar{\eta}\sigma\|\bar{\boldsymbol{e}}\|\bar{\boldsymbol{g}}_{2d}}_{\triangleq \boldsymbol{v}_1})\\
&= -u_2\bar{\boldsymbol{g}}_2(\theta) + s\rho\bar{\boldsymbol{h}} - s\rho(K_p\bar{\boldsymbol{e}} + \boldsymbol{v}_1)\\
&\overset{(2.16)}{=} -su_{2N}\bar{\boldsymbol{g}}_2(\theta) + s\rho\bar{\boldsymbol{h}} - s\rho K_p\bar{\boldsymbol{e}} - s\rho\boldsymbol{v}_1\\
&= s\rho \underbrace{\left(\bar{\boldsymbol{h}} - \frac{1}{\rho}u_{2N}\bar{\boldsymbol{g}}_2(\theta)\right)}_{\triangleq \boldsymbol{v}_2} - s\rho K_p\bar{\boldsymbol{e}} - s\rho\boldsymbol{v}_1\\
&= s\rho\boldsymbol{v}_2 - s\rho K_p\bar{\boldsymbol{e}} - s\rho\boldsymbol{v}_1. \qquad (2.34)
\end{aligned}$$

Let us introduce a few additional terms that will be useful in the further analysis:

$$\begin{aligned}
\|\boldsymbol{v}_2\| =& \left\|\bar{\boldsymbol{h}} - \frac{1}{\rho}u_{2N}\bar{\boldsymbol{g}}_2(\theta)\right\| \overset{(2.12)}{=} \left\|\bar{\boldsymbol{h}} - \left\|\bar{\boldsymbol{h}}\right\|\cos\alpha\bar{\boldsymbol{g}}_2(\theta)\right\|\\
=& \left\|\bar{\boldsymbol{h}}\right\| \left\| \frac{\bar{\boldsymbol{h}}}{\left\|\bar{\boldsymbol{h}}\right\|} - \cos\alpha\bar{\boldsymbol{g}}_2(\theta)\right\| = \left\|\bar{\boldsymbol{h}}\right\| \left\| \begin{bmatrix} \frac{h_x}{\left\|\bar{\boldsymbol{h}}\right\|} - \cos\alpha\cos\theta \\ \frac{h_y}{\left\|\bar{\boldsymbol{h}}\right\|} - \cos\alpha\sin\theta \end{bmatrix}\right\|\\
=& \left\|\bar{\boldsymbol{h}}\right\| \left(\left(\frac{h_x}{\left\|\bar{\boldsymbol{h}}\right\|} - \cos\alpha\cos\theta \right)^2 + \left(\frac{h_y}{\left\|\bar{\boldsymbol{h}}\right\|} - \cos\alpha\sin\theta \right)^2 \right)^{\frac{1}{2}}\\
=& \left\|\bar{\boldsymbol{h}}\right\| \left(\frac{h_x^2}{\left\|\bar{\boldsymbol{h}}\right\|^2} - \frac{2h_x}{\left\|\bar{\boldsymbol{h}}\right\|}\cos\alpha\cos\theta + \cos^2\alpha\cos^2\theta \right.\\
&\left. + \frac{h_y^2}{\left\|\bar{\boldsymbol{h}}\right\|^2} - \frac{2h_y}{\left\|\bar{\boldsymbol{h}}\right\|}\cos\alpha\sin\theta + \cos^2\alpha\sin^2\theta \right)^{\frac{1}{2}}\\
=& \left\|\bar{\boldsymbol{h}}\right\| \left(\underbrace{(h_x^2 + h_y^2)}_{=\left\|\bar{\boldsymbol{h}}\right\|^2} \frac{1}{\left\|\bar{\boldsymbol{h}}\right\|^2} - 2\cos\alpha \underbrace{\frac{h_x\cos\theta + h_y\sin\theta}{\left\|\bar{\boldsymbol{h}}\right\|}}_{=\cos\alpha} \right.\\
&\left. + \cos^2\alpha \underbrace{(\sin^2\theta + \cos^2\theta)}_{=1} \right)^{\frac{1}{2}}\\
=& \left\|\bar{\boldsymbol{h}}\right\| \sqrt{1 - 2\cos^2\alpha + \cos^2\alpha} = \left\|\bar{\boldsymbol{h}}\right\| \sqrt{1 - \cos^2\alpha}. \qquad (2.35)
\end{aligned}$$

It should be noted that:

$$\forall t \geq t_{sa} \quad e_a = 0 \implies \theta = \theta_a \implies \tan\theta \overset{(1.10)}{=} \frac{\sigma h_y}{\sigma h_x}, \qquad (2.36)$$

so it can be concluded that:

$$\forall t \geq t_{sa} \quad \cos\theta = \frac{\sigma h_x}{\left\|\bar{\boldsymbol{h}}\right\|}, \qquad \forall t \geq t_{sa} \quad \sin\theta = \frac{\sigma h_y}{\left\|\bar{\boldsymbol{h}}\right\|}. \qquad (2.37)$$

It can be observed that:

$$\alpha \triangleq \angle\left(\bar{\boldsymbol{h}}, \bar{\boldsymbol{g}}_2(\theta)\right) \implies \cos\alpha = \frac{\bar{\boldsymbol{h}}^\top\bar{\boldsymbol{g}}_2(\theta)}{\left\|\bar{\boldsymbol{h}}\right\|\left\|\bar{\boldsymbol{g}}_2(\theta)\right\|} = \frac{h_x\cos\theta + h_y\sin\theta}{\left\|\bar{\boldsymbol{h}}\right\|}, \qquad (2.38)$$

where $\|\bar{\boldsymbol{g}}_2(\theta)\| = \sqrt{\cos^2\theta + \sin^2\theta} = 1$. Therefore, applying (2.37) to (2.38) yields

$$\forall t \geq t_{sa} \quad \cos\alpha \overset{(2.37)}{=} \frac{\sigma h_x^2 + \sigma h_y^2}{\left\|\bar{\boldsymbol{h}}\right\|^2} = \frac{\sigma\left\|\bar{\boldsymbol{h}}\right\|^2}{\left\|\bar{\boldsymbol{h}}\right\|^2} = \sigma. \tag{2.39}$$

It should be noted that $\forall t \geq t_{sa}\ \cos^2\alpha \overset{(2.39)}{=} \sigma^2 \overset{(2.4)}{=} 1 \implies \|\boldsymbol{v}_2\| \overset{(2.35)}{=} 0$. Next, the term $\left\|\bar{\boldsymbol{h}}\right\|$ can be upper bounded as follows:

$$\begin{aligned}\left\|\bar{\boldsymbol{h}}\right\| &\overset{(2.3)}{=} \left\|(K_p\bar{\boldsymbol{e}} - K_p\bar{\eta}\sigma\|\bar{\boldsymbol{e}}\|\bar{\boldsymbol{g}}_{2d})\right\| \\ &\leq \left\|K_p\bar{\boldsymbol{e}}\right\| + \left\|-K_p\bar{\eta}\sigma\|\bar{\boldsymbol{e}}\|\bar{\boldsymbol{g}}_{2d}\right\| \\ &= K_p\|\bar{\boldsymbol{e}}\| + K_p\bar{\eta}\|\bar{\boldsymbol{e}}\|\|\bar{\boldsymbol{g}}_{2d}\| \\ &= K_p(1+\bar{\eta})\|\bar{\boldsymbol{e}}\|, \end{aligned} \tag{2.40}$$

where $|\sigma| = 1$ and $\|\bar{\boldsymbol{g}}_{2d}\| = \sqrt{\cos^2\theta_d + \sin^2\theta_d} = 1$.

Finally, let us use the Lyapunov method and choose a positive definite function $V_p(\|\bar{\boldsymbol{e}}\|) \triangleq \frac{1}{2}\|\bar{\boldsymbol{e}}\|^2 = \frac{1}{2}\bar{\boldsymbol{e}}^\top\bar{\boldsymbol{e}}$. Its time derivative can be assessed as follows:

$$\begin{aligned}\forall t \geq t_{sa} \quad \dot{V}_p &= \bar{\boldsymbol{e}}^\top\dot{\bar{\boldsymbol{e}}} \overset{(2.34)}{=} \bar{\boldsymbol{e}}^\top\left(s\rho\boldsymbol{v}_2 - s\rho K_p\bar{\boldsymbol{e}} - s\rho\boldsymbol{v}_1\right) \\ &= s\rho\bar{\boldsymbol{e}}^\top\boldsymbol{v}_2 - s\rho K_p\|\bar{\boldsymbol{e}}\|^2 - s\rho\bar{\boldsymbol{e}}^\top\boldsymbol{v}_1 \\ &= -s\rho\left(K_p\|\bar{\boldsymbol{e}}\|^2 - \bar{\boldsymbol{e}}^\top\boldsymbol{v}_2 + \bar{\boldsymbol{e}}^\top\boldsymbol{v}_1\right) \\ &= -s\rho\Big(K_p\|\bar{\boldsymbol{e}}\|^2 - \|\bar{\boldsymbol{e}}\|\|\boldsymbol{v}_2\|\cos\big(\angle(\bar{\boldsymbol{e}},\boldsymbol{v}_2)\big) + \|\bar{\boldsymbol{e}}\|\|\boldsymbol{v}_1\|\cos\big(\angle(\bar{\boldsymbol{e}},\boldsymbol{v}_1)\big)\Big) \\ &\leq -s\rho\Big(K_p\|\bar{\boldsymbol{e}}\|^2 - \underbrace{\|\bar{\boldsymbol{e}}\|\|\boldsymbol{v}_2\|}_{\overset{(2.35)}{=}0} - \|\bar{\boldsymbol{e}}\|\|\boldsymbol{v}_1\|\Big) \\ &\overset{(2.34)}{=} -s\rho\Big(K_p\|\bar{\boldsymbol{e}}\|^2 - \|\bar{\boldsymbol{e}}\|\Big\|-K_p\bar{\eta}\sigma\|\bar{\boldsymbol{e}}\|\bar{\boldsymbol{g}}_2(\theta)\Big\|\Big) \\ &= -s\rho\Big(K_p\|\bar{\boldsymbol{e}}\|^2 - K_p\bar{\eta}\|\bar{\boldsymbol{e}}\|^2\underbrace{\|\bar{\boldsymbol{g}}_2(\theta)\|}_{=1}\Big) \\ &= -s\rho\|\bar{\boldsymbol{e}}\|^2K_p(1-\bar{\eta}) \\ &\overset{(2.13)}{=} -\frac{sK_p(1-\bar{\eta})\rho_0}{\left\|\bar{\boldsymbol{h}}\right\|}\|\bar{\boldsymbol{e}}\|^2\left(\|\bar{\boldsymbol{e}}\|^{\mu_1} + \|\bar{\boldsymbol{e}}\|^{\mu_2}\right) \\ &\overset{(2.40)}{\leq} -\frac{sK_p(1-\bar{\eta})\rho_0}{K_p(1+\bar{\eta})\|\bar{\boldsymbol{e}}\|}\|\bar{\boldsymbol{e}}\|^2\left(\|\bar{\boldsymbol{e}}\|^{\mu_1} + \|\bar{\boldsymbol{e}}\|^{\mu_2}\right) \\ &= -s\rho_0\frac{1-\bar{\eta}}{1+\bar{\eta}}\left(\|\bar{\boldsymbol{e}}\|^{\mu_1+1} + \|\bar{\boldsymbol{e}}\|^{\mu_2+1}\right) \\ &= -s\rho_0\frac{1-\bar{\eta}}{1+\bar{\eta}}\left(\sqrt{2}^{\mu_1+1}V_p^{(\mu_1+1)/2} + \sqrt{2}^{\mu_2+1}V_p^{(\mu_2+1)/2}\right). \end{aligned} \tag{2.41}$$

Comparing (2.41) with (1.2) from Lemma 1, it can be concluded that the equilibrium point $\bar{\boldsymbol{e}} = \boldsymbol{0}$ of the positional error dynamics is *fixed-time stable*. However, it should be noted that (2.41) contains $s\big(\boldsymbol{e}(t)\big) \in (0,1]$, which is bounded but not constant. This means that (2.41) cannot be used to determine the time-independent upper

bound of the positional error $\bar{\boldsymbol{e}}$ settling time t_{sp} according to the method presented in Lemma 4. Let us therefore introduce two additional terms:

$$\underline{s}(\boldsymbol{e}_0) \triangleq \inf_{t\geq 0}\ s(\boldsymbol{e}(t,\boldsymbol{e}_0)), \qquad \underline{\underline{s}} \triangleq \inf_{\boldsymbol{e}_0\in\mathcal{E}}\ \underline{s}(\boldsymbol{e}_0) = \inf_{\boldsymbol{e}_0\in\mathcal{E}}\inf_{t\geq 0}\ s(\boldsymbol{e}(t,\boldsymbol{e}_0)), \tag{2.42}$$

that are independent of time. Note that none of the values s, $\underline{s}$, and $\underline{\underline{s}}$ are known *a priori*, however, the values $\underline{s}$ and $\underline{\underline{s}}$ can be estimated *a priori* under certain conditions, which will be discussed in more details later. Now, (2.41) can be rewritten as follows:

$$\begin{aligned}\forall t\geq t_{sa}\quad \dot{V}_p &\overset{(2.42)}{\leq} -\underline{s}\rho_0\frac{1-\bar{\eta}}{1+\bar{\eta}}\left(\sqrt{2}^{\mu_1+1}V_p^{(\mu_1+1)/2}+\sqrt{2}^{\mu_2+1}V_p^{(\mu_2+1)/2}\right)\\ &\overset{(2.42)}{\leq} -\underline{\underline{s}}\rho_0\frac{1-\bar{\eta}}{1+\bar{\eta}}\left(\sqrt{2}^{\mu_1+1}V_p^{(\mu_1+1)/2}+\sqrt{2}^{\mu_2+1}V_p^{(\mu_2+1)/2}\right).\end{aligned} \tag{2.43}$$

By comparing (2.43) with the result obtained with (1.5) from Lemma 4, it can be seen that the upper bound of the positional error $\bar{\boldsymbol{e}}$ settling time t_{sp} can be expressed as follows:

$$\forall\bar{\boldsymbol{e}}_0\in\mathcal{E}\quad T_{cp}=\frac{(1+\bar{\eta})\arctan\left(\sqrt{2}^{\bar{\mu}}V_p^{\bar{\mu}/2}(R_{\mathcal{E}})\right)}{\underline{\underline{s}}(1-\bar{\eta})\bar{\mu}\rho_0}, \tag{2.44}$$

where $R_{\mathcal{E}}$ is defined in (2.2) and denotes the highest admissible initial value of the norm of the positional error.

Please note that since the *pre-orientation* and *motion* processes are scheduled and occur one after the other, the total settling time should be understood as the sum of the auxiliary orientation error settling time and the positional error settling time, that is, $t_s = t_{sa}+t_{sp}$. Thus, a total upper bound of the settling time t_s can be determined (conservatively) as the sum of the upper bounds (2.31) and (2.44), that is:

$$T_c \triangleq T_{ca}+T_{cp}. \tag{2.45}$$

Orientation error: Let us also take a look at the convergence of orientation error e_θ, which is defined as follows:

$$\forall t\geq t_{sa}\quad e_\theta \overset{(2.1)}{=} f_\theta(\theta_d-\theta) \overset{(2.7)}{=} f_\theta(\theta_d+e_a-\theta_a)=f_\theta(\theta_d-\theta_a)=f_\theta(-\bar{e}_\theta), \tag{2.46}$$

where $\bar{e}_\theta \triangleq \theta_a-\theta_d$.

Considerations regarding the convergence of orientation errors will be presented in the local frame, determined by the desired configuration $\boldsymbol{q}_d$, analogous to the analysis presented in [78]. Therefore, let us transform the positional error $\bar{\boldsymbol{e}}$:

$$\bar{\boldsymbol{e}}^L=\begin{bmatrix}e_x^L\\ e_y^L\end{bmatrix}=\begin{bmatrix}\cos\theta_d & \sin\theta_d\\ -\sin\theta_d & \cos\theta_d\end{bmatrix}\begin{bmatrix}e_x\\ e_y\end{bmatrix}=\begin{bmatrix}e_x\cos\theta_d+e_y\sin\theta_d\\ -e_x\sin\theta_d+e_y\cos\theta_d\end{bmatrix}, \tag{2.47}$$

and the positional subvector $\bar{\boldsymbol{h}}$ of the convergence vector field $\boldsymbol{h}$:

$$\begin{aligned}\bar{\boldsymbol{h}}^L=\begin{bmatrix}h_x^L\\ h_y^L\end{bmatrix}&=\begin{bmatrix}\cos\theta_d & \sin\theta_d\\ -\sin\theta_d & \cos\theta_d\end{bmatrix}\begin{bmatrix}h_x\\ h_y\end{bmatrix}=\begin{bmatrix}h_x\cos\theta_d+h_y\sin\theta_d\\ -h_x\sin\theta_d+h_y\cos\theta_d\end{bmatrix}\\ &\overset{(2.3)}{=} K_p\begin{bmatrix}(e_x-\bar{\eta}\sigma\|\bar{\boldsymbol{e}}\|\cos\theta_d)\cos\theta_d+(e_y-\bar{\eta}\sigma\|\bar{\boldsymbol{e}}\|\sin\theta_d)\sin\theta_d\\ -(e_x-\bar{\eta}\sigma\|\bar{\boldsymbol{e}}\|\cos\theta_d)\sin\theta_d+(e_y-\bar{\eta}\sigma\|\bar{\boldsymbol{e}}\|\sin\theta_d)\cos\theta_d\end{bmatrix}\end{aligned} \tag{2.48}$$

$$= K_p \begin{bmatrix} e_x \cos\theta_d - \bar{\eta}\sigma\|\bar{\boldsymbol{e}}\| \cos^2\theta_d + e_y \sin\theta_d - \bar{\eta}\sigma\|\bar{\boldsymbol{e}}\| \sin^2\theta_d \\ -e_x \sin\theta_d + \bar{\eta}\sigma\|\bar{\boldsymbol{e}}\| \cos\theta_d \sin\theta_d + e_y \cos\theta_d - \bar{\eta}\sigma\|\bar{\boldsymbol{e}}\| \sin\theta_d \cos\theta_d \end{bmatrix}$$
$$= K_p \begin{bmatrix} e_x \cos\theta_d + e_y \sin\theta_d - \bar{\eta}\sigma\|\bar{\boldsymbol{e}}\| \\ -e_x \sin\theta_d + e_y \cos\theta_d \end{bmatrix} \overset{(2.47)}{=} K_p \begin{bmatrix} e_x^L - \bar{\eta}\sigma\|\bar{\boldsymbol{e}}\| \\ e_y^L \end{bmatrix} \tag{2.49}$$

to the local frame. Next, let us recall the positional error dynamics

$$\dot{\bar{\boldsymbol{e}}} \overset{(2.34)}{=} s\rho \left(\bar{\boldsymbol{h}} - \frac{1}{\rho} u_{2N} \bar{\boldsymbol{g}}_2(\theta) \right) - s\rho K_p \bar{\boldsymbol{e}} + s\rho K_p \bar{\eta}\sigma\|\bar{\boldsymbol{e}}\| \bar{\boldsymbol{g}}_{2d} \tag{2.50}$$

to examine the behavior of the positional error in the local frame. It should be noted that $\forall t \geq t_{sa} \;\; \cos\alpha \overset{(2.39)}{=} \sigma$ and $\forall t \geq t_{sa} \;\; f_s(t) \overset{(2.15)}{=} 1$. Therefore, one can observe that:

$$\begin{aligned} \forall t \geq t_{sa} \quad \bar{\boldsymbol{h}} - \frac{1}{\rho} u_{2N} \bar{\boldsymbol{g}}_2(\theta) &\overset{(2.12)}{=} \bar{\boldsymbol{h}} - f_s \left\| \bar{\boldsymbol{h}} \right\| \cos\alpha \; \bar{\boldsymbol{g}}_2(\theta) \overset{(2.39)}{=} \bar{\boldsymbol{h}} - \sigma \left\| \bar{\boldsymbol{h}} \right\| \bar{\boldsymbol{g}}_2(\theta) \\ &= \begin{bmatrix} h_x \\ h_y \end{bmatrix} - \sigma \left\| \bar{\boldsymbol{h}} \right\| \begin{bmatrix} \cos\theta \\ \sin\theta \end{bmatrix} \overset{(2.37)}{=} \begin{bmatrix} h_x - \sigma^2 h_x \\ h_y - \sigma^2 h_y \end{bmatrix} \\ &= \begin{bmatrix} h_x - h_x \\ h_y - h_y \end{bmatrix} = \boldsymbol{0}, \end{aligned} \tag{2.51}$$

since $\sigma^2 = 1$. Thus, one can conclude that

$$\forall t \geq t_{sa} \quad \dot{\bar{\boldsymbol{e}}} \overset{(2.34)}{=} (-K_p \bar{\boldsymbol{e}} + K_p \bar{\eta}\sigma\|\bar{\boldsymbol{e}}\| \bar{\boldsymbol{g}}_{2d}) s\rho \overset{(2.3)}{=} -\bar{\boldsymbol{h}} s\rho. \tag{2.52}$$

Now, let us transfer $\dot{\bar{\boldsymbol{e}}}$ to the local frame:

$$\begin{aligned} \dot{\bar{\boldsymbol{e}}}^L = \begin{bmatrix} \dot{e}_x^L \\ \dot{e}_y^L \end{bmatrix} &= \begin{bmatrix} \cos\theta_d & \sin\theta_d \\ -\sin\theta_d & \cos\theta_d \end{bmatrix} \begin{bmatrix} \dot{e}_x \\ \dot{e}_y \end{bmatrix} = \begin{bmatrix} \dot{e}_x \cos\theta_d + \dot{e}_y \sin\theta_d \\ -\dot{e}_x \sin\theta_d + \dot{e}_y \cos\theta_d \end{bmatrix} \\ &\overset{(2.52)}{=} -s\rho \begin{bmatrix} h_x \cos\theta_d + h_y \sin\theta_d \\ -h_x \sin\theta_d + h_y \cos\theta_d \end{bmatrix} \overset{(2.48)}{=} -s\rho \begin{bmatrix} h_x^L \\ h_y^L \end{bmatrix} \\ &\overset{(2.49)}{=} s\rho K_p \begin{bmatrix} -e_x^L + \bar{\eta}\sigma\|\bar{\boldsymbol{e}}\| \\ -e_y^L \end{bmatrix}. \end{aligned} \tag{2.53}$$

Next, it should be noted that

$$\sigma \overset{(2.4)}{=} \operatorname{sgn}\Big(e_x(0) \cos\theta_d + e_y(0) \sin\theta_d \Big) \overset{(2.47)}{=} \operatorname{sgn}\Big(e_x^L(0) \Big) \tag{2.54}$$

and consequently, one can write:

$$\dot{e}_x^L \overset{(2.53)}{=} s\rho K_p \left(-e_x^L + \bar{\eta} \operatorname{sgn}\Big(e_x^L(0) \Big) \|\bar{\boldsymbol{e}}\| \right) \tag{2.55}$$

$$\dot{e}_y^L \overset{(2.53)}{=} s\rho K_p \left(-e_y^L \right), \tag{2.56}$$

where $s \in (0, 1]$, $\rho > 0$, $K_p > 0$, and $\bar{\eta} > 0$. Based on (2.55) and (2.55) one can conclude that e_y^L converges to zero independently of e_x^L. Moreover, one can observe that e_y^L reaches zero faster than e_x^L, that is:

$$e_x^L(t) \xrightarrow{t \to \tau_x} 0, \qquad e_y^L(t) \xrightarrow{t \to \tau_y} 0, \qquad \tau_y < \tau_x \leq T_c, \tag{2.57}$$

and, based on (2.49) it can be concluded that:

$$h_x^L(t) \xrightarrow{t\to\tau_x} 0, \qquad h_y^L(t) \xrightarrow{t\to\tau_y} 0, \qquad \tau_y < \tau_x \leq T_c. \tag{2.58}$$

Let us now use (2.58) to demonstrate the convergence of the orientation error e_θ. Let us begin by defining the auxiliary orientation in the local frame:

$$\theta_a^L \triangleq \text{Atan2c}\left(h_y^L, h_x^L\right). \tag{2.59}$$

Next, it can be observed that:

$$\begin{aligned}\tan\theta_a^L = \frac{h_y^L}{h_x^L} &\overset{(2.49)}{=} \frac{h_y\cos\theta_d - h_x\sin\theta_d}{h_y\sin\theta_d + h_x\cos\theta_d} = \frac{h_x\cos\theta_d\left(\frac{h_y}{h_x} - \frac{\sin\theta_d}{\cos\theta_d}\right)}{h_x\cos\theta_d\left(\frac{h_y\sin\theta_d}{h_x\cos\theta_d} + 1\right)} \\ &= \frac{\tan\theta_a - \tan\theta_d}{\tan\theta_a\tan\theta_d + 1} = \tan(\theta_a - \theta_d) = \tan\bar{e}_\theta,\end{aligned} \tag{2.60}$$

and consequently,

$$\tan\bar{e}_\theta(t) \overset{(2.60)}{=} \frac{h_y^L(t)}{h_x^L(t)} \xrightarrow{t\to\tau_y} 0 \implies \bar{e}_\theta(t) \xrightarrow{t\to\tau_y} k\pi,\ k\in\mathbb{Z} \tag{2.61}$$

occurs. However, (2.61) does not imply that $e_\theta = f_\theta(-\bar{e}_\theta)$ converges to zero, since it could also converge to π. Nevertheless, if it can be shown that $\text{sgn}(\cos\bar{e}_\theta)$ is positive, with $\text{sgn}(\cdot)$ defined in (2.5), this would mean that convergence to zero has been obtained. One can observe that:

$$\cos\bar{e}_\theta \overset{(2.46)}{=} \cos(\theta - \theta_d) = \cos\theta\cos\theta_d + \sin\theta\sin\theta_d = \bar{\boldsymbol{g}}_{2d}^\top\bar{\boldsymbol{g}}_2(\theta). \tag{2.62}$$

Then, let us write

$$\bar{\boldsymbol{g}}_2(\theta) \overset{(1.6)}{=} \frac{\dot{\boldsymbol{q}}}{u_2} = \frac{1}{u_2}\begin{bmatrix}\dot{x}\\ \dot{y}\end{bmatrix} \implies \bar{\boldsymbol{g}}_{2d}^\top\bar{\boldsymbol{g}}_2(\theta) = \frac{1}{u_2}\Big(\dot{x}\cos\theta_d + \dot{y}\sin\theta_d\Big) \tag{2.63}$$

and consequently, it can be concluded that:

$$\begin{aligned}\text{sgn}\Big(\bar{\boldsymbol{g}}_{2d}^\top\bar{\boldsymbol{g}}_2(\theta)\Big) &\overset{(2.63)}{=} \text{sgn}\left(\frac{1}{u_2}\Big(\dot{x}\cos\theta_d + \dot{y}\sin\theta_d\Big)\right) \\ &= \text{sgn}\left(\frac{1}{u_2}\right)\text{sgn}\Big(\dot{x}\cos\theta_d + \dot{y}\sin\theta_d\Big) \\ &= \text{sgn}\,(u_2)\,\text{sgn}\Big(\dot{x}\cos\theta_d + \dot{y}\sin\theta_d\Big) \\ &\overset{(1.6)}{=} \text{sgn}\,(u_2)\,\text{sgn}\Big(u_2\cos\theta\cos\theta_d + u_2\sin\theta\sin\theta_d\Big) \\ &\overset{(2.16)}{=} \text{sgn}\left(sf_s\rho\left\|\bar{\boldsymbol{h}}\right\|\cos\alpha\right)\text{sgn}\Big(sf_s\rho\left\|\bar{\boldsymbol{h}}\right\|\cos\alpha\cos\theta\cos\theta_d \\ &\quad + sf_s\rho\left\|\bar{\boldsymbol{h}}\right\|\cos\alpha\sin\theta\sin\theta_d\Big) \\ &= \text{sgn}\left(sf_s\rho\left\|\bar{\boldsymbol{h}}\right\|\cos\alpha\right)\text{sgn}\,(sf_s\rho)\,\text{sgn}\Big(\left\|\bar{\boldsymbol{h}}\right\|\cos\alpha\cos\theta\cos\theta_d \\ &\quad + \left\|\bar{\boldsymbol{h}}\right\|\cos\alpha\sin\theta\sin\theta_d\Big) \\ &= \text{sgn}\,(\cos\alpha)\,\text{sgn}\Big(\left\|\bar{\boldsymbol{h}}\right\|\cos\alpha\cos\theta\cos\theta_d\end{aligned}$$

$$+ \left\|\bar{\boldsymbol{h}}\right\| \cos\alpha \sin\theta \sin\theta_d\Big) \tag{2.64}$$

since $\forall t \geq 0\ \operatorname{sgn}\Big(s(t)\Big) = 1$, $\forall t \geq 0\ \operatorname{sgn}\Big(f_s(t)\Big) = 1$, $\forall t \geq 0\ \operatorname{sgn}\Big(\rho(t)\Big) = 1$, and $\forall t \geq 0\ \operatorname{sgn}\Big(\left\|\bar{\boldsymbol{h}}(t)\right\|\Big) = 1$. Let us continue the analysis for $t \geq t_{sa}$:

$$\begin{aligned}
\forall t \geq t_{sa} \quad \operatorname{sgn}\Big(\bar{\boldsymbol{g}}_{2d}^{\top}\bar{\boldsymbol{g}}_2(\theta)\Big) &\overset{(2.39)}{=} \operatorname{sgn}(\sigma)\operatorname{sgn}\Big(\left\|\bar{\boldsymbol{h}}\right\|\sigma\cos\theta\cos\theta_d + \left\|\bar{\boldsymbol{h}}\right\|\sigma\sin\theta\sin\theta_d\Big) \\
&\overset{(2.37)}{=} \sigma\operatorname{sgn}\Big(\left\|\bar{\boldsymbol{h}}\right\|\sigma\frac{\sigma h_x}{\left\|\bar{\boldsymbol{h}}\right\|}\cos\theta_d + \left\|\bar{\boldsymbol{h}}\right\|\sigma\frac{\sigma h_y}{\left\|\bar{\boldsymbol{h}}\right\|}\sin\theta_d\Big) \\
&= \sigma\operatorname{sgn}\Big(h_x\cos\theta_d + h_y\sin\theta_d\Big) \\
&\overset{(2.48)}{=} \sigma\operatorname{sgn}\Big(h_x^L\Big) \overset{(2.49)}{=} \sigma\operatorname{sgn}\Big(K_p e_x^L - K_p\bar{\eta}\sigma\|\bar{\boldsymbol{e}}\|\Big) \\
&= \sigma\operatorname{sgn}\Big(K_p e_x^L - K_p\bar{\eta}\sigma\sqrt{e_x^{L2}+e_y^{L2}}\Big) \\
&\overset{(2.54)}{=} \operatorname{sgn}\Big(e_x^L(0)\Big)\operatorname{sgn}\Big(K_p e_x^L - K_p\bar{\eta}\operatorname{sgn}\Big(e_x^L(0)\Big)\sqrt{e_x^{L2}+e_y^{L2}}\Big).
\end{aligned} \tag{2.65}$$

Next, using (2.58), which shows that e_y^L converges to zero faster than e_x^L, let us continue the analysis for $t \geq \tau_y > t_{sa}$:

$$\begin{aligned}
\forall t \geq \tau_y \quad \operatorname{sgn}\Big(\bar{\boldsymbol{g}}_{2d}^{\top}\bar{\boldsymbol{g}}_2(\theta)\Big) &= \operatorname{sgn}\Big(e_x^L(0)\Big)\operatorname{sgn}\Big(K_p e_x^L - K_p\bar{\eta}\operatorname{sgn}\Big(e_x^L(0)\Big)\sqrt{e_x^{L2}}\Big) \\
&= \operatorname{sgn}\Big(e_x^L(0)\Big)\operatorname{sgn}\Big(K_p e_x^L - K_p\bar{\eta}\operatorname{sgn}\Big(e_x^L(0)\Big)|e_x^L|\Big) \\
&= \operatorname{sgn}\Big(e_x^L(0)\Big)\operatorname{sgn}\Big(K_p\operatorname{sgn}\Big(e_x^L\Big)|e_x^L| - K_p\bar{\eta}\operatorname{sgn}\Big(e_x^L(0)\Big)|e_x^L|\Big).
\end{aligned} \tag{2.66}$$

Based on (2.55) it can be concluded that e_x^L does not change the initial sign, that is, $\forall t \geq 0\ \operatorname{sgn}\Big(e_x^L(0)\Big) = \operatorname{sgn}\Big(e_x^L(t)\Big)$. Thus, one can write:

$$\begin{aligned}
\forall t \geq \tau_y \quad \operatorname{sgn}\Big(\bar{\boldsymbol{g}}_{2d}^{\top}\bar{\boldsymbol{g}}_2(\theta)\Big) &= \operatorname{sgn}\Big(e_x^L\Big)\operatorname{sgn}\Big(K_p\operatorname{sgn}\Big(e_x^L\Big)|e_x^L| - K_p\bar{\eta}\operatorname{sgn}\Big(e_x^L\Big)|e_x^L|\Big) \\
&= \operatorname{sgn}^2\Big(e_x^L\Big)\operatorname{sgn}\Big(K_p|e_x^L|\Big)\operatorname{sgn}\Big(1-\bar{\eta}\Big) \\
&= \operatorname{sgn}\Big(1-\bar{\eta}\Big) = 1,
\end{aligned} \tag{2.67}$$

since $\bar{\eta} \in (0.5, 1)$. Therefore, it can be concluded that $\operatorname{sgn}\Big(\bar{\boldsymbol{g}}_{2d}^{\top}\bar{\boldsymbol{g}}_2(\theta)\Big) = \operatorname{sgn}(\cos\bar{e}_\theta) = 1$, and consequently

$$\bar{e}_\theta \xrightarrow{t\to T_c} 2k\pi,\ k \in \mathbb{Z} \implies e_\theta \overset{(2.46)}{=} f_\theta(-\bar{e}_\theta) \xrightarrow{t\to T_c} 0. \tag{2.68}$$

And that concludes the proof. ■

Remark 5 *It should be noted that the convergence analysis is performed for $\epsilon = 0$. If $\epsilon > 0$ is selected, then based on the above analysis, it can be concluded that $\|\bar{\boldsymbol{e}}(t)\| \to \epsilon$ as $t \to T_c$ and $\theta_a(t) \to \theta_{a\epsilon}$ as $t \to T_c$. Consequently, one gets $e_\theta(t) \to f_\theta(\theta_d - \theta_{a\epsilon})$ as $t \to T_c$, thus one can conclude that the value $f_\theta(\theta_d - \theta_{a\epsilon})$ corresponds to the value θ_ϵ introduced in Problem 1. Furthermore, it can be observed that $\epsilon = 0 \implies \theta_\epsilon = 0$.*

Remark 6 *An important issue that is typically studied when discussing control laws is robustness. However, a detailed analysis of this aspect goes beyond the scope of this dissertation. Nevertheless, since the proposed algorithm is based on the concept of fixed-time stability, one can qualitatively discuss about the robustness of control methods of this type. According to the results presented in [104, 105], the use of Implicit Lyapunov Function allows proving the robustness of the system against bounded external disturbances. Moreover, the structure of fixed-time stable system exhibits Input-to-State Stability properties, which means that error trajectories remain bounded in a given neighborhood of the equilibrium state, and the settling time remains bounded (see, for example, [58]).*

2.2.3 A priori estimation of the settling time upper bound

From a practical point of view, knowing *a priori* the upper bound of the task completion time is highly beneficial, as it, for example, simplifies or enables the scheduling of sequential processes. Therefore, in this section, the method of estimating *a priori* the upper bound of the settling time, defined in Section 2.2.2, will be presented.

Let us look again at the values of the upper bounds T_{ca} and T_{cp} defined in (2.31) and (2.44), respectively. One can observe that the upper bound T_{ca} of the settling time t_{sa} of the auxiliary orientation error e_a can be computed *a priori* based on (2.29), (2.30), and (2.30). Meanwhile, the problem with computing the upper bound T_{cp} of the settling time t_{sa} of the positional error $\bar{\boldsymbol{e}}$ *a priori* lies in the lack of *a priori* knowledge of the value $\underline{\underline{s}}$ appearing in (2.44). Let us therefore take a closer look at the definition of $\underline{\underline{s}}$:

$$\begin{aligned}
\underline{\underline{s}} &\overset{(2.42)}{=} \inf_{\boldsymbol{e}_0\in\mathcal{E}} \inf_{t\geq 0} \; s\Big(\boldsymbol{e}(t,\boldsymbol{e}_0)\Big) \\
&\overset{(1.7)}{=} \left(\max\left\{1, \frac{\sup\limits_{\boldsymbol{e}_0\in\mathcal{E}} \sup\limits_{t\geq 0}\Big|u_{1N}\Big(\boldsymbol{e}(t,\boldsymbol{e}_0)\Big)\Big|}{u_{1M}}, \frac{\sup\limits_{\boldsymbol{e}_0\in\mathcal{E}} \sup\limits_{t\geq 0}\Big|u_{2N}\Big(\boldsymbol{e}(t,\boldsymbol{e}_0)\Big)\Big|}{u_{2M}}\right\}\right)^{-1} \\
&= \left(\max\left\{1, \frac{u_{1\mathcal{E}}}{u_{1M}}, \frac{u_{2\mathcal{E}}}{u_{2M}}\right\}\right)^{-1} \in (0,1).
\end{aligned} \tag{2.69}$$

It can be concluded that the problem of *a priori* estimation of T_{cp} leads to *a priori* estimation of $\underline{\underline{s}}$, which means that it is necessary to know *a priori* the values $u_{1\mathcal{E}}$ and $u_{2\mathcal{E}}$, which denote the largest absolute values of *nominal* angular velocity u_{1N} and *nominal* longitudinal velocity u_{2N}, respectively, for all initial conditions belonging to the set $\mathcal{E}$. It should be noted that since T_{cp} is related to the convergence of the positional error, and this only occurs for $t \geq t_{sa}$, the following analysis will focus on the case where $t \geq t_{sa} \implies f_s(t) = 1$. Let us now recall the definition of nominal control inputs:

$$\forall t \geq t_{sa} \quad \boldsymbol{u}_N = \begin{bmatrix} u_{1N} \\ u_{2N} \end{bmatrix} \overset{(2.12)}{=} \begin{bmatrix} K_a\left(|e_a|^{\delta_1} + |e_a|^{\delta_2}\right)\operatorname{sign}(e_a) + \dot{\theta}_{aN} \\ \rho_0\left(\|\bar{\boldsymbol{e}}\|^{\mu_1} + \|\bar{\boldsymbol{e}}\|^{\mu_2}\right)\cos\alpha \end{bmatrix}.$$

First, let us consider the pushing control u_{2N}. Based on the stability analysis from Section 2.2.2, it can be concluded that $\sup_{t\geq 0}\|\bar{\boldsymbol{e}}(t)\| = \|\bar{\boldsymbol{e}}_0\|$, and furthermore, based on (2.2), it can be seen that $\sup_{\boldsymbol{e}_0\in\mathcal{E}}\|\bar{\boldsymbol{e}}_0\| = R_{\mathcal{E}}$. Moreover, it should be noted

that $\sup_{t\geq 0}\cos\alpha(t)=1$. Therefore, it can be concluded that

$$\forall t\geq t_{sa}\quad u_{2\mathcal{E}}=\sup_{t\geq 0}\sup_{\boldsymbol{e}_0\in\mathcal{E}}\left|u_{2N}\left(\bar{\boldsymbol{e}}(t,\bar{\boldsymbol{e}}_0)\right)\right|=\rho_0\left(R_{\mathcal{E}}^{\mu_1}+R_{\mathcal{E}}^{\mu_2}\right). \tag{2.70}$$

Now let us take a look at orienting control u_{1N}. Direct determination of $u_{1\mathcal{E}}$ may be challenging, therefore it is proposed to estimate $\hat{u}_{1\mathcal{E}}$ such that $u_{1\mathcal{E}}\leq\hat{u}_{1\mathcal{E}}$. Let us recall the equation describing the motion curvature of the robot:

$$\kappa(t)=\frac{u_{1N}(t)}{u_{2N}(t)}\implies u_{1N}(t)=\kappa(t)u_{2N}(t)\implies u_{1\mathcal{E}}\leq\underbrace{\kappa_{\mathcal{E}}u_{2\mathcal{E}}}_{\triangleq\hat{u}_{1\mathcal{E}}}, \tag{2.71}$$

where $\kappa_{\mathcal{E}}\triangleq\sup_{t\geq 0}\sup_{\boldsymbol{e}_0\in\mathcal{E}}|\kappa(t,\boldsymbol{e}_0)|$ denotes the highest possible absolute value of the motion curvature κ for all initial conditions belonging to the set $\mathcal{E}$, while $u_{2\mathcal{E}}$ is defined in (2.70). To determine $\kappa_{\mathcal{E}}$, the so-called *integral curves* will be used, that is, an analytical solution to the closed-loop dynamics, which for the VFO design methodology were presented in [27]. It should be noted that, although this dissertation and [27] address different control problems, the *integral curves* obtained in [27] can be used in this dissertation, since the positional subvector $\bar{\boldsymbol{h}}$ of the convergence vector field $\boldsymbol{h}$ is defined in the analogous way in this dissertation and in [27]. Therefore, let us recall from [27] the definition of the parameterized integral curve:

$$e_x^*\left(e_y^*,p^*(\bar{\boldsymbol{e}}_0)\right)\triangleq\frac{\sigma|e_y^*|}{2}\left(\left(\frac{e_y^*}{p^*(\bar{\boldsymbol{e}}_0)}\right)^{\bar{\eta}}-\left(\frac{e_y^*}{p^*(\bar{\boldsymbol{e}}_0)}\right)^{-\bar{\eta}}\right), \tag{2.72}$$

where $\sigma\in\{-1,1\}$ and $\bar{\eta}\in(0.5,1)$ are introduced in Section 2.2.2, while $\begin{bmatrix}e_x^* & e_y^*\end{bmatrix}^\top\triangleq\bar{\boldsymbol{e}}^*$ denotes a vector of positional coordinates determined analytically and expressed in the error space. The parameter p^* is defined as follows:

$$\forall e_{y0}\neq 0\quad p^*(\bar{\boldsymbol{e}}_0)\triangleq e_{y0}\exp\left(\frac{1}{\bar{\eta}}\left|\operatorname{arsinh}\left(\frac{e_{x0}}{e_{y0}}\right)\right|\right), \tag{2.73}$$

where $\begin{bmatrix}e_{x0} & e_{y0}\end{bmatrix}^\top=\begin{bmatrix}e_x(0) & e_y(0)\end{bmatrix}^\top=\bar{\boldsymbol{e}}_0$ is the vector of initial condition error. It should be noted that $\forall e_{y0}\neq 0\ |p^*(\bar{\boldsymbol{e}}_0)|\in(0,\infty)$, while in the case of $e_{y0}=0$, the integral curve (2.72) will be a line $e_y^*=0$. Note that the vehicle will move along the analytically determined integral curve only if, at the moment of starting the movement, the auxiliary orientation error e_a is zero and remains zero until the end of the movement. By introducing the function f_s in (2.15) and scheduling the *pre-orientation* process and the *motion* process, it has been ensured that the above condition is met, and thus it can be stated that: $\forall t\geq t_{sa}\ e_a(t)=0\implies\bar{\boldsymbol{e}}^*\equiv\bar{\boldsymbol{e}}$.

Next, let us recall from [27] the definition of the motion curvature at point (e_x^*,e_y^*):

$$\kappa^*\left(e_y^*,p^*(\bar{\boldsymbol{e}}_0)\right)\triangleq\frac{e_y^*\left(\bar{\eta}\sigma+\bar{\eta}^2e_x^*\|\bar{\boldsymbol{e}}^*\|^{-1}\right)}{\sigma\|\bar{\boldsymbol{e}}^*\|^2\left(1+\bar{\eta}^2+2\sigma\bar{\eta}e_x^*\|\bar{\boldsymbol{e}}^*\|^{-1}\right)^{3/2}}, \tag{2.74}$$

with e_x^* and p^* defined in (2.72) and (2.73), respectively. Let us also recall the method for analytically determining the largest absolute value of the motion curvature along a given integral curve:

$$\underline{\kappa}^*(\bar{\boldsymbol{e}}_0)\triangleq\sup_{0\leq e_y^*\leq|e_{y0}|}\left|\kappa^*\left(e_y^*,p^*(\bar{\boldsymbol{e}}_0)\right)\right|=\frac{|\kappa^*(\breve{e}_y,1)|}{|p^*(\bar{\boldsymbol{e}}_0)|}, \tag{2.75}$$

where $\breve{e}_y = e_y^*$ such that $\kappa^*\left(e_y^*, p^*(\bar{\boldsymbol{e}}_0)\right) = \underline{\kappa}^*(\bar{\boldsymbol{e}}_0)$ denotes the value of e_y^* for which the absolute value of the motion curvature reaches its maximum on a given integral curve. The term $\breve{e}_y$ can be determined analytically as follows:

$$\breve{e}_y(\bar{\eta}) \triangleq \left(p_1(\bar{\eta}) - \frac{-6\bar{\eta}^3 + \bar{\eta}^2 + 2\bar{\eta} + 3}{(6\bar{\eta}+3)(\bar{\eta}+1)^2} + p_2(\bar{\eta})\right)^{\frac{1}{2\bar{\eta}}}, \tag{2.76}$$

where

$$p_1(\bar{\eta}) = \left(\frac{4}{3}p_6(\bar{\eta}) - p_3(\bar{\eta})\right)^{\frac{1}{3}}, \tag{2.77}$$

$$p_2(\bar{\eta}) = \frac{4\bar{\eta}^2\left(18\bar{\eta}^4 + 3\bar{\eta}^3 - 17\bar{\eta}^2 - 11\bar{\eta} + 7\right)}{9\left(\bar{\eta}+1\right)^4\left(2\bar{\eta}+1\right)^2 p_1(\bar{\eta})}, \tag{2.78}$$

$$p_3(\bar{\eta}) = \frac{p_4^3(\bar{\eta})}{27(2\bar{\eta}+1)^4(\bar{\eta}+1)^9} + p_7(\bar{\eta}) - p_5(\bar{\eta}), \tag{2.79}$$

$$p_4(\bar{\eta}) = -6\bar{\eta}^4 - 5\bar{\eta}^3 + 3\bar{\eta}^2 + 5\bar{\eta} + 3, \tag{2.80}$$

$$p_5(\bar{\eta}) = \frac{(-6\bar{\eta}^4 + 5\bar{\eta}^3 + 3\bar{\eta}^2 - 5\bar{\eta} + 3)p_4(\bar{\eta})}{6(2\bar{\eta}+1)^2(\bar{\eta}+1)^6}, \tag{2.81}$$

$$p_6(\bar{\eta}) = \left(\frac{\bar{\eta}^6(\bar{\eta}-1)^3(-36\bar{\eta}^4 + 33\bar{\eta}^2 - 29)}{(2\bar{\eta}+1)^4(\bar{\eta}+1)^9}\right)^{\frac{1}{2}}, \tag{2.82}$$

$$p_7(\bar{\eta}) = \frac{(2\bar{\eta}-1)(\bar{\eta}-1)^3}{(4\bar{\eta}+2)(\bar{\eta}+1)^3}, \tag{2.83}$$

come from [27]. Next, it can be observed that the largest absolute value of motion curvature for all the initial conditions from the set $\mathcal{E}$ can be expressed as

$$\kappa_{\mathcal{E}} = \sup_{\boldsymbol{e}_0 \in \mathcal{E}} \underline{\kappa}^*(\bar{\boldsymbol{e}}_0) \overset{(2.75)}{=} \sup_{\boldsymbol{e}_0 \in \mathcal{E}} \frac{|\kappa^*(\breve{e}_y, 1)|}{|p^*(\bar{\boldsymbol{e}}_0)|} = \frac{|\kappa^*(\breve{e}_y, 1)|}{\inf\limits_{\boldsymbol{e}_0 \in \mathcal{E}} |p^*(\bar{\boldsymbol{e}}_0)|}, \tag{2.84}$$

since only the parameter $p^*(\bar{\boldsymbol{e}}_0)$ depends on the initial condition $\boldsymbol{e}_0$. Therefore, it can be noted that:

$$\forall e_{y0} \neq 0 \quad |p^*(\bar{\boldsymbol{e}}_0)| \overset{(2.73)}{=} \underbrace{|e_{y0}|}_{>0} \underbrace{\left|\exp\underbrace{\left(\frac{1}{\bar{\eta}}\left|\operatorname{arsinh}\left(\frac{e_{x0}}{e_{y0}}\right)\right|\right)}_{\geq 0}\right|}_{\geq 1}. \tag{2.85}$$

It can be concluded that $|p^*|$ will take the smallest value when e_{x0} is zero and $|e_{y0}|$ takes the smallest non-zero value, such that

$$\|\bar{\boldsymbol{e}}_0\| = \sqrt{e_{x0}^2 + e_{y0}^2} = \sqrt{0^2 + e_{y0}^2} = |e_{y0}| \in \bar{\mathcal{E}} \implies |e_{y0}| \overset{(2.2)}{=} r_{\mathcal{E}}, \tag{2.86}$$

and consequently:

$$\inf_{\boldsymbol{e}_0 \in \mathcal{E}} |p^*(e_{x0}, e_{y0})| = |p^*(0, r_{\mathcal{E}})| \overset{(2.85)}{=} r_{\mathcal{E}} \implies \kappa_{\mathcal{E}} \overset{(2.84)}{=} \frac{|\kappa^*(\breve{e}_y, 1)|}{r_{\mathcal{E}}}, \tag{2.87}$$

with $r_{\mathcal{E}}$, κ^*, and $\breve{e}_y$, defined in (2.2), (2.74), and (2.76), respectively. Thus, the maximum possible value of $|u_{2N}|$ is determined, and the maximum possible value of

$|u_{1N}|$ is (conservatively) estimated based on (2.71) with (2.70) and (2.87). Therefore, the smallest value of the scaling function s for all initial conditions belonging to the set $\mathcal{E}$ of admissible initial conditions can be (conservatively) estimated as follows:

$$\hat{\underline{s}} \triangleq \left(\max\left\{1, \frac{\hat{u}_{1\mathcal{E}}}{u_{1M}}, \frac{u_{2\mathcal{E}}}{u_{2M}}\right\}\right)^{-1} \in (0,1). \tag{2.88}$$

However, in some cases, the estimation (2.88) with (2.71) may be too conservative for practical applications. Considering (2.69), it can be concluded that the use of a conservative estimated $\hat{u}_{1\mathcal{E}}$ can be avoided if it is ensured that

$$\frac{\hat{u}_{1\mathcal{E}}}{u_{1M}} \leq \frac{u_{2\mathcal{E}}}{u_{2M}} \implies \frac{\kappa_{\mathcal{E}} u_{2\mathcal{E}}}{u_{1M}} \leq \frac{u_{2\mathcal{E}}}{u_{2M}} \implies \kappa_{\mathcal{E}} u_{2M} \leq u_{1M} \implies u_{2M} \leq \frac{u_{1M}}{\kappa_{\mathcal{E}}}. \tag{2.89}$$

Therefore, substituting $u_{1\mathcal{E}} = \kappa_{\mathcal{E}} u_{2\mathcal{E}}$ and $u_{1M} = \kappa_{\mathcal{E}} u_{2M}$ into (2.69), one obtains

$$\begin{aligned} \underline{s} &\overset{(2.69)}{=} \left(\max\left\{1, \frac{\kappa_{\mathcal{E}} u_{2\mathcal{E}}}{\kappa_{\mathcal{E}} u_{2M}}, \frac{u_{2\mathcal{E}}}{u_{2M}}\right\}\right)^{-1} = \left(\max\left\{1, \frac{u_{2\mathcal{E}}}{u_{2M}}, \frac{u_{2\mathcal{E}}}{u_{2M}}\right\}\right)^{-1} \\ &= \left(\max\left\{1, \frac{u_{2\mathcal{E}}}{u_{2M}}\right\}\right)^{-1} \in (0,1), \end{aligned} \tag{2.90}$$

thus avoiding the use of the conservative estimated $\hat{u}_{1\mathcal{E}}$.

Finally, by substituting (2.90) or (2.88) into (2.44), the upper bound T_{cp} of the positional error settling time can be computed *a priori*.

Remark 7 *Since an application of the proposed method for* a priori *estimation requires performing several steps in the proper order, a summary with step-by-step instructions is provided below.*

First, let us take a look at the upper bound T_{ca} of the auxiliary orientation error settling time:

1. *Solve* (2.27) *with respect to e_a^* (it may require the use of a numerical solver).*
2. *Compute t_{sa}^* using* (2.29) *and e_a^*.*
3. *Compute T_{ca}^* using* (2.30) *and e_a^*.*
4. *Compute T_{ca} using t_{sa}^* and T_{ca}^*, based on* (2.31).

Then let us consider the a priori *estimation of the upper bound T_{cp} of the positional error settling time:*

1. *Compute $u_{2\mathcal{E}}$ using* (2.70).
2. *Compute $\breve{e}_y$ using* (2.76).
3. *Compute $e_x^*(\breve{e}_y, 1)$ using* (2.72), *with $e_y^* = \breve{e}_y$ and $p^* = 1$.*
4. *Compute κ^* using $e_x^*(\breve{e}_y, 1)$ and* (2.74), *with $e_y^* = \breve{e}_y$ and $p^* = 1$.*
5. *Compute $\kappa_{\mathcal{E}}$ using* (2.87) *and κ^*.*
6. *Using $\kappa_{\mathcal{E}}$ check if the postulate* (2.89) *is met:*
   - *a) if yes:*
     - *i. compute $\underline{s}$ using* (2.90) *and $u_{2\mathcal{E}}$.*
     - *ii. compute T_{cp} using* (2.44) *and $\underline{s}$.*
   - *b) if not:*
     - *i. compute $\hat{u}_{1\mathcal{E}}$ using $u_{2\mathcal{E}}$, $\kappa_{\mathcal{E}}$, and* (2.71).
     - *ii. compute $\hat{\underline{s}}$ using* (2.88), *$\hat{u}_{1\mathcal{E}}$, and $u_{2\mathcal{E}}$.*
     - *iii. compute T_{cp} using* (2.44) *and taking $\underline{s} = \hat{\underline{s}}$.*

2.2.4 Results of numerical simulations

Numerical simulations of the control law proposed in Section 2.2.2 were performed in the Matlab-Simulink environment. A variable-step solver with a maximum step size of 10^{-3} s was used. The set $\bar{\mathcal{E}}$ defined in (2.2) is determined by two circles with radius $R_{\mathcal{E}} = 2$ m and $r_{\mathcal{E}} = 1$ m, while $\epsilon = 10^{-10}$ m. The controller coefficients selected for the simulation were as follows: $K_p = 1$, $K_a = 2$, $\bar{\eta} = 0.82$, $\bar{\delta} = 0.1$, $\bar{\mu} = 0.2$, and σ is selected according to (2.4). Simulations have been carried out for 100 different initial positions of the robot, while, for simplicity, the initial orientation was set to $\frac{\pi}{2}$, and the desired configuration $\boldsymbol{q}_d = \mathbf{0}$.

Remark 8 *The choice of controller parameters was guided by an experience gained from previous use of the VFO controlles, according to which the gain K_a of the orientation process should be greater than the gain K_p of the pushing process. Therefore, the selection $K_a = 2K_p$ was proposed. On the other hand, the value $\bar{\eta}$ was selected based on [26], which showed that for $\bar{\eta} = 0.82$ a maximum arc-length derivative of the motion curvature reaches a lower value than for other values of $\bar{\eta}$ (for more details, see [26]).*

The obtained results are presented in Fig. 2.3. One can observe that, for each case, the positional errors (see Figs. 2.3a and 2.3b), the orientation error (see Fig. 2.3c), and the auxiliary orientation error (see Fig. 2.3d) converged towards zero in fixed time. Furthermore, the control signals satisfied the imposed constraints, that is, $\forall t \ |u_1(t)| \leq u_{1M}$ and $\forall t \ |u_2(t)| \leq u_{2M}$, where $u_{1M} = 3$ rad/s and $u_{2M} = 0.5$ m/s (see Figs. 2.3e and 2.3f). Fig. 2.3 also clearly shows the change from the *pre-orientation* stage to the *motion* stage, that is, the change in the value of the f_s defined in (2.15) from 0 to 1 (which is particularly visible in Fig. 2.3f, since $f_s = 0 \implies u_2 = 0$). One can also notice that for each considered case, the desired configuration $\boldsymbol{q}_d = \mathbf{0}$ has been achieved (see Fig. 2.3g). It can be observed that, thanks to the use of the VFO methodology, the robot's trajectories are free of oscillations, and no chattering effect appears in the control signals.

It is also worthwhile to look at the settling times: the upper bounds of the auxiliary orientation error settling time and the positional error settling time calculated according to (2.31) and (2.44), respectively, with the use of the *a priori* estimation method presented in Section 2.2.3, are $T_{ca} = 4.65$ s and $T_{cp} = 422.20$ s, whereas the actual settling times, which can be read from Figs. 2.3a, 2.3b, and 2.3d are no greater than 12 s for the norm of the positional error $\|\bar{\boldsymbol{e}}\|$ and no greater than 4.5 s for the auxiliary orientation error e_a.

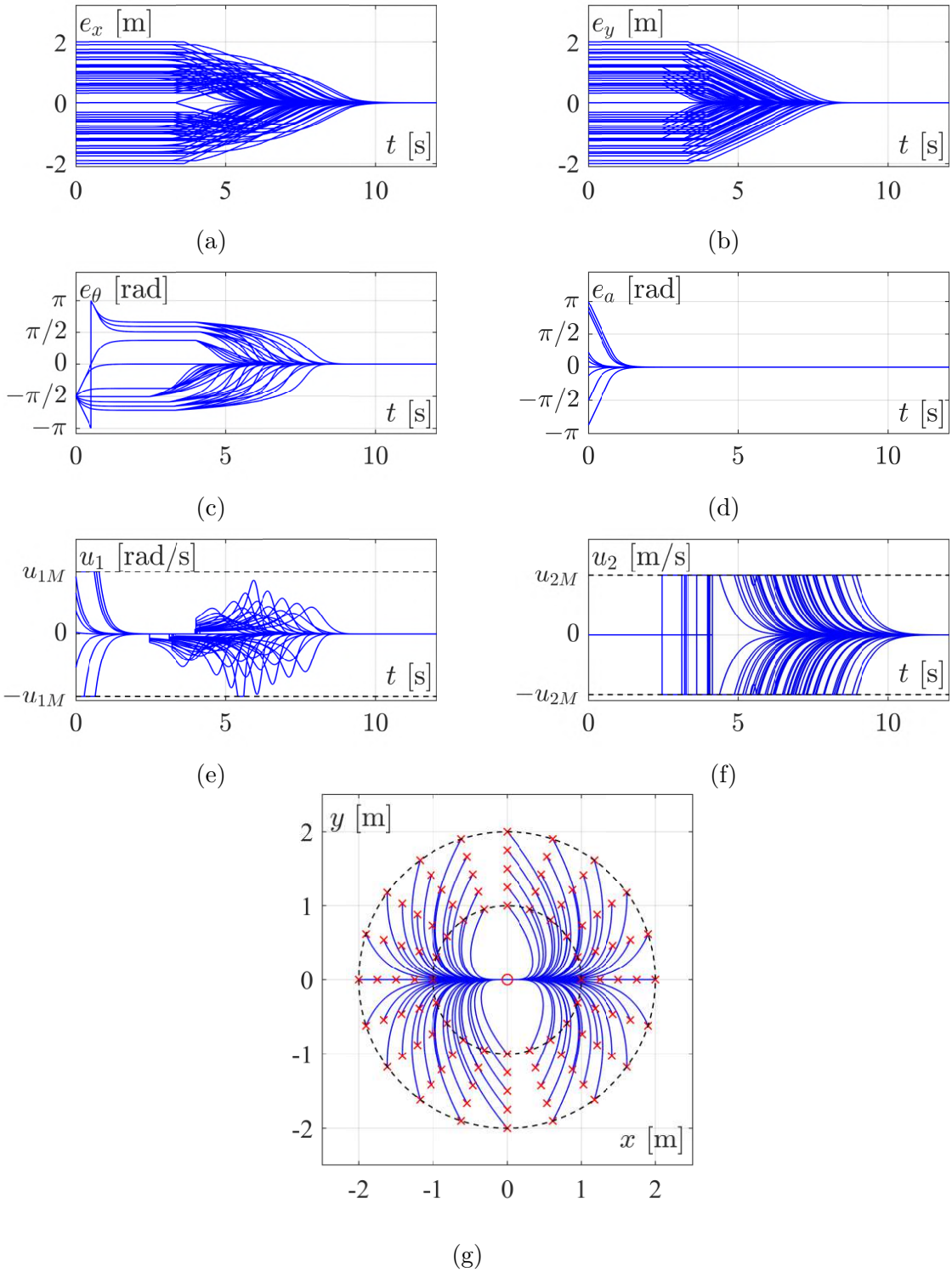

Figure 2.3 – Set of numerical simulation results for the fixed-time set-point control problem for 100 different initial positions (marked with red crosses) with $\theta(0) = \pi/2$ and $\boldsymbol{q}_d = \mathbf{0}$ (marked with red circle), where $u_{1M} = 3$ rad/s and $u_{2M} = 0.5$ m/s.

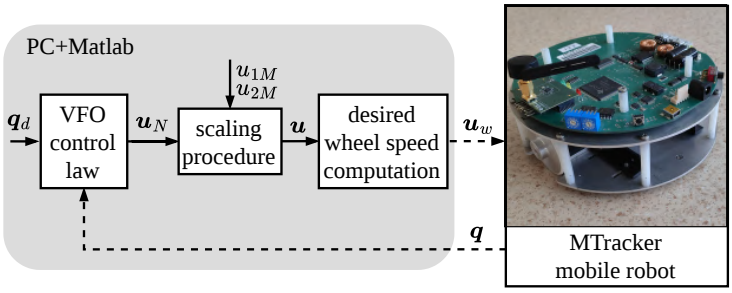

Figure 2.4 – Block scheme of the fast-prototyping system with the mTracker mobile robot. The communication link between the PC and the robot is provided via Bluetooth (dashed lines in the scheme).

2.2.5 Results of experimental tests

The experimental tests have been carried out using the mTracker mobile robot, which was designed and built at the Institute of Automatic Control and Robotics at the Poznań University of Technology. It is a two-wheeled differentially driven robot of unicycle-like kinematics, and is relatively small in size, common for robots designed to perform hardware experiments on a laboratory scale: the wheels' radius r_w is equal to 25 mm, while the wheels' base b_w is equal to 145 mm. There are several ways to work with the mTracker robot, depending on the robot version. The robot used to conduct this experiment allows for cooperation with Matlab in such a way that the control law is implemented on a PC computer in the Matlab environment and the vector $\boldsymbol{u}_k$ of desired wheel speeds, which includes the desired speeds for the right and left wheel, is sent to the robot via Bluetooth interface (cf. Fig. 2.4). This vector is determined based on the control signals u_1 and u_2 as follows:

$$\boldsymbol{u}_k = \frac{1}{r_w} \begin{bmatrix} b_w/2 & 1 \\ -b_w/2 & 1 \end{bmatrix} \begin{bmatrix} u_1 \\ u_2 \end{bmatrix}, \tag{2.91}$$

where r_w denotes the wheel radius and b_w means the wheel base. The robot has an internal PI wheel speed controllers on board, thus it is well suited for testing control algorithms that consider only the kinematic model. In response, the robot sends the configuration vector $\boldsymbol{q}$ computed using odometry (cf. Fig. 2.4). The average operating frequency in such a configuration is 30 Hz.

Remark 9 *It should be noted that, although velocity scaling is performed in the robot platform velocity space (cf. Fig. 2.4), the parameters u_{1M} and u_{2M} should be selected so that the maximum wheel velocity limitations are respected. These limitations are determined by the maximum rotational speed of the motors. Consequently, after substituting u_{1M} and u_{2M} into* (2.91) *in place of u_1 and u_2, the resulting components of $\boldsymbol{u}_k$ must be feasible for the robot drives.*

The test was conducted for five different cases with different initial configurations:

- $\boldsymbol{q}_0 = \begin{bmatrix} 0 & -2 & -2 \end{bmatrix}^\top$ for case I,
- $\boldsymbol{q}_0 = \begin{bmatrix} -\frac{\pi}{2} & 2 & 2 \end{bmatrix}^\top$ for case II,
- $\boldsymbol{q}_0 = \begin{bmatrix} 0 & 1.5 & -2 \end{bmatrix}^\top$ for case III,

- $\boldsymbol{q}_0 = \begin{bmatrix} \pi & 0 & 2.75 \end{bmatrix}^\top$ for case IV,
- $\boldsymbol{q}_0 = \begin{bmatrix} \frac{\pi}{2} & -2.7 & 0.3 \end{bmatrix}^\top$ for case V,

while $\boldsymbol{q}_d = \boldsymbol{0}$. The set $\mathcal{E}$ was defined by $R_{\mathcal{E}} = 3$ m and $r_{\mathcal{E}} = 2.5$ m, while $\epsilon = 0.003$ m, and $u_{1M} = 3$ rad/s and $u_{2M} = 0.5$ m/s. The control design parameters were chosen the same as in Section 2.2.4, that is: $K_p = 1$, $K_a = 2$, $\bar{\eta} = 0.82$, $\bar{\delta} = 0.1$, $\bar{\mu} = 0.2$, and σ was selected according to (2.4).

The obtained results are presented in Fig. 2.5. Based on Figs. 2.5a and 2.5b, it can be seen that the positional errors converged towards vicinity ϵ of zero zero within a fixed time not exceeding 10 s, while the auxiliary orientation errors shown in Fig. 2.5d converged towards vicinity of zero within a time not exceeding 2 s. Practical convergence of the orientation error is also achieved (see Fig. 2.5c), and the desired configuration is reached in each case (see Fig. 2.5g). Figure 2.5g also shows the *directing effect* associated with the coefficient $\bar{\eta}$: the final stage of each robot's motion is nearly linear, as the orientation error converged towards vicinity of zero faster than the positional error. One can also see in Figs. 2.5e and 2.5f that the control signals satisfy the imposed constraints. Once again, similar to the simulation results, one can see that the robot motion trajectories are without oscillations, and the control signals are free of chattering.

The *a priori* (conservatively) estimated upper bounds of the settling times for the considered set $\mathcal{E}$ are: $T_{ca} = 4.65$ s and $T_{cp} = 555.74$ s, thus one can conclude that the task execution time constraints are also satisfied.

Remark 10 *Although a robustness of the proposed algorithm has not been formally analyzed, the results of experimental tests obtained with a physical robot seem satisfactory, despite the presence of various types of disturbances like the measurement noise, model uncertainty, non-ideal regulation of the wheels' speeds, and communication delays between Matlab and the robot's on-board controller. It evidences the existence of some level of robustness in the proposed closed-loop system.*

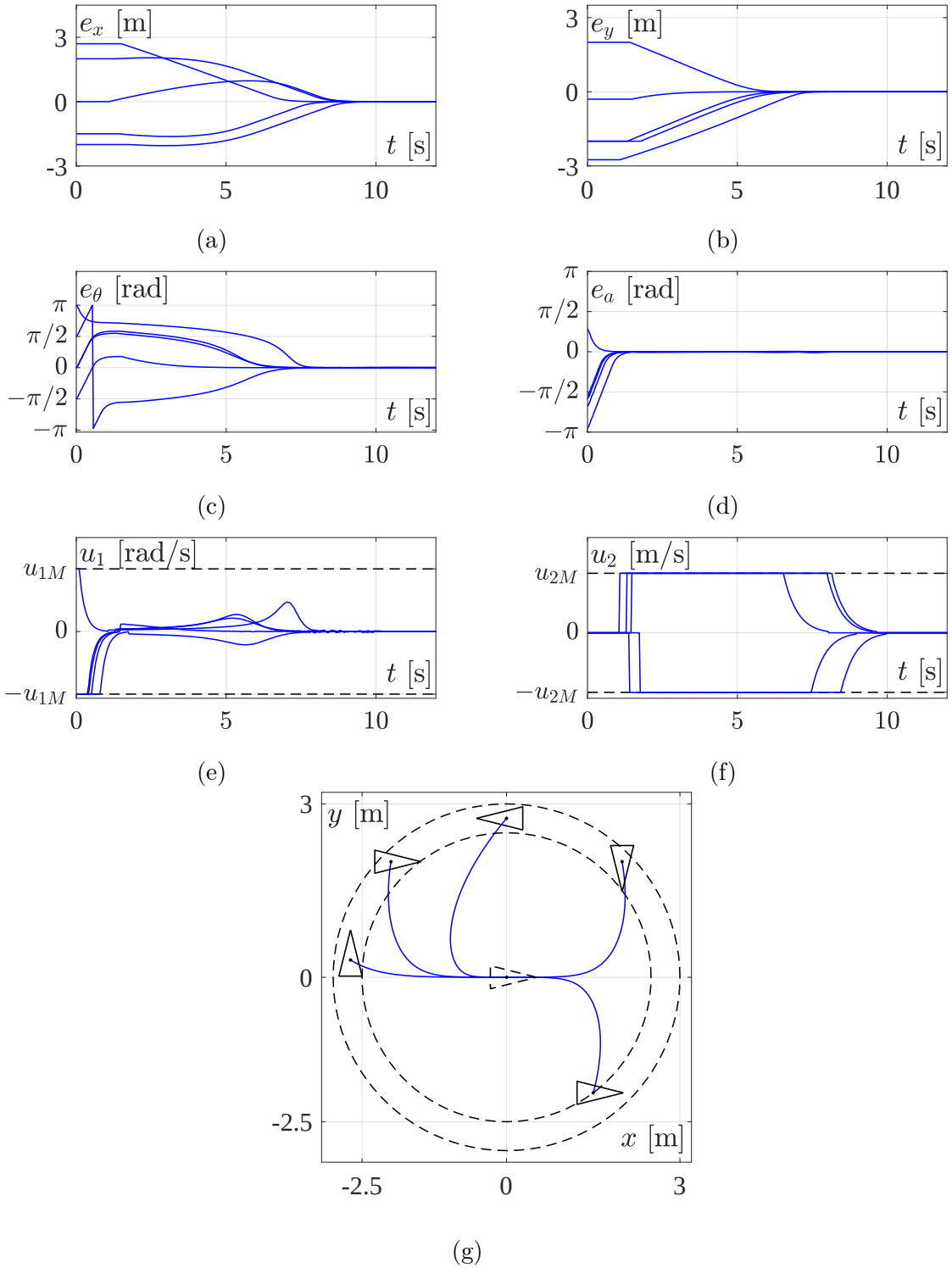

Figure 2.5 – Experimental results for the fixed-time set-point control problem for 5 different initial configurations (marked with solid triangles) with $\boldsymbol{q}_d = \mathbf{0}$ (marked with dashed triangle), while $u_{1M} = 3$ rad/s and $u_{2M} = 0.5$ m/s.

2.3 Path-following control

This section will address the problem of following a non-parametric path. First, the definition of a reference path will be presented. Next, the control problem will be formulated, and finally, the VFO control law will be defined in two steps: first in a *nominal* form (which does not satisfy the imposed control input constraints) and then in a form that meets the imposed control input limitations, obtained using the scaling procedure introduced in Section 1.3.2. Finally, the results of numerical simulations obtained in the Matlab-Simulink environment and experimental tests performed using a physical mobile robot will be presented. Please note that the results presented in this Sections were originally presented in [120].

2.3.1 Reference path definition

In order to deal with the path-following control problem, let us begin with a definition of a positional reference path. Following the method presented in [81,134,135], let us introduce a set $S_d \subset \mathbb{R}^2$ of points $\bar{\boldsymbol{q}}_d = \begin{bmatrix} x_d & y_d \end{bmatrix}^\top \in \mathbb{R}^2$ such that

$$S_d \triangleq \{\bar{\boldsymbol{q}}_d : F(\bar{\boldsymbol{q}}_d) \triangleq \zeta f_p(\bar{\boldsymbol{q}}_d) = 0\}, \tag{2.92}$$

where $\zeta \in \mathbb{R}\backslash\{0\}$ and the scalar function f_p are selected by a designer. The reference path is a zero-level curve of some function $F : \mathbb{R}^2 \to \mathbb{R}$ such that $F(\bar{\boldsymbol{q}}) = 0 \iff \bar{\boldsymbol{q}} \in S_d$ and $\forall \bar{\boldsymbol{q}} \notin S_d \; F(\bar{\boldsymbol{q}}) \neq 0$, while $\bar{\boldsymbol{q}} = \begin{bmatrix} x & y \end{bmatrix}^\top$ is defined in Section 1.3.2. The sign of ζ determines the desired motion direction along a reference path in a global frame, that is, the clockwise/counter-clockwise or the right/left direction. Let us also define the reference orientation as follows:

$$\theta_d(\bar{\boldsymbol{q}}) \triangleq \operatorname{Atan2}\left(\sigma F_x(\bar{\boldsymbol{q}}), -\sigma F_y(\bar{\boldsymbol{q}})\right) \in (-\pi, \pi], \tag{2.93}$$

where F_x and F_y denote the partial derivatives of the function F with respect to $\bar{\boldsymbol{q}}$ and will be defined later, while σ was introduced in Section 1.3.3 and determines the motion strategy, that is, forward motion for $\sigma = 1$ or backward motion for $\sigma = -1$.

Now, let us formulate some important assumptions:

Assumption 2 *The function F is locally bounded:*

$$\forall \bar{\boldsymbol{q}} \in \mathcal{D} \subseteq \mathbb{R}^2 \quad |F(\bar{\boldsymbol{q}})| \leq M_F, \quad 0 < M_F < \infty.$$

Assumption 3 *There exist bounded partial derivatives for the function F:*

$$F_x = \frac{\partial F(\bar{\boldsymbol{q}})}{\partial x}, \quad F_y = \frac{\partial F(\bar{\boldsymbol{q}})}{\partial y}, \quad F_{xx} = \frac{\partial^2 F(\bar{\boldsymbol{q}})}{\partial^2 x}, \quad F_{yy} = \frac{\partial^2 F(\bar{\boldsymbol{q}})}{\partial^2 y}, \quad F_{xy} = \frac{\partial^2 F(\bar{\boldsymbol{q}})}{\partial x \partial y},$$

for $\bar{\boldsymbol{q}} \in \mathcal{D} \subseteq \mathbb{R}^2$.

Assumption 4 *The norm of the gradient of the function F is bounded and non-zero in domain $\mathcal{D}$, that is:*

$$\forall \bar{\boldsymbol{q}} \in \mathcal{D} \quad \|\nabla F(\bar{\boldsymbol{q}})\| \in [m_G, M_G], \quad 0 < m_G \leq M_G < \infty.$$

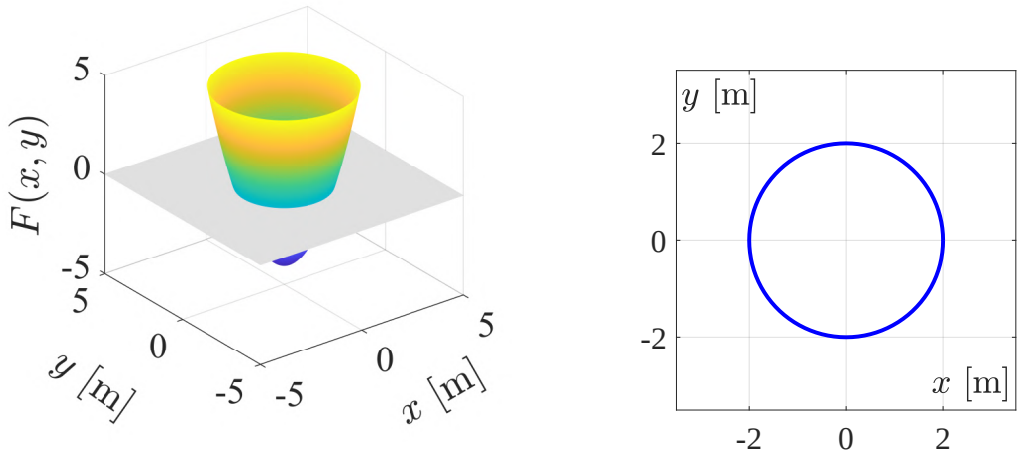

(a) (b)

Figure 2.6 – Example reference path with a shape of a circle with a radius of 2 m obtained as a zero-level set of the function $F(x, y) = x^2 + y^2 - 4$.

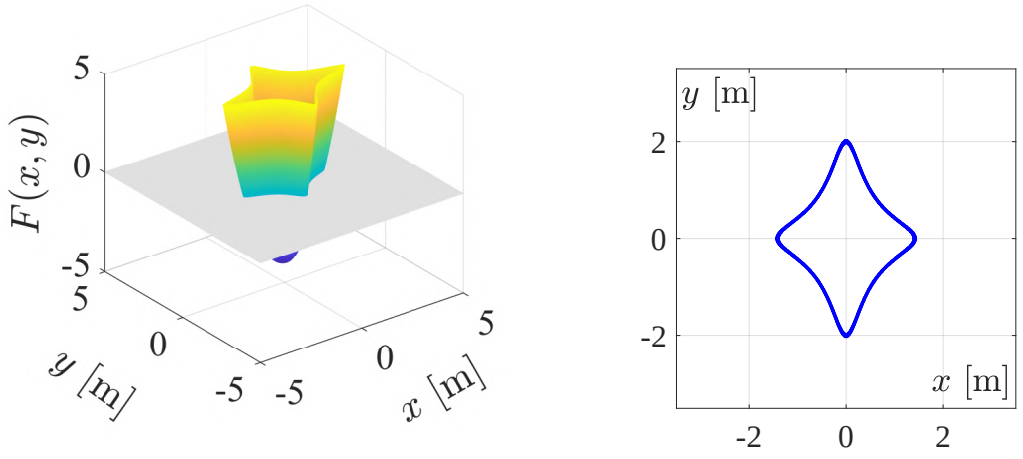

(a) (b)

Figure 2.7 – Example of a cross-shaped reference path obtained as a zero-level set of the function $F(x, y) = 2x^2 + 10x^2y^2 + y^2 - 4$.

Assumption 5 *The reference longitudinal velocity u_{2d} along the reference path is constant.*

Based on the above assumptions, one can observe that the path-following control problem is defined in some domain $\mathcal{D} \subseteq \mathbb{R}^2$ and the reference path should be designed such that Assumptions 2-4 are met. Figure 2.6 shows an example of a path obtained using this generator with $F(x, y) = x^2 + y^2 - 4$ (see Fig. 2.6a), which corresponds to a reference path in the shape of a circle with a radius of 2 m (see Fig. 2.6b), while Fig. 2.7 presents an another example of a cross-shaped reference path (see Fig. 2.7b) obtained using the function $F(x, y) = 2x^2 + 10x^2y^2 + y^2 - 4$ (see Fig. 2.7a).

Remark 11 *Based on the examples shown in Figs. 2.6 and 2.7, it can be concluded*

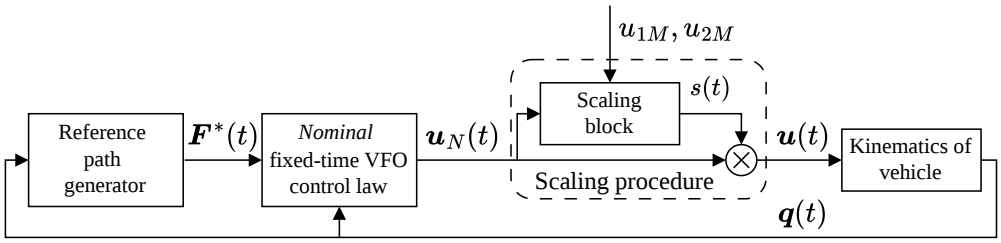

Figure 2.8 – Block scheme of the control system for the path following control problem, where $\boldsymbol{F}^*(\bar{\boldsymbol{q}}) \triangleq \begin{bmatrix} F(\bar{\boldsymbol{q}}) & F_x(\bar{\boldsymbol{q}}) & F_y(\bar{\boldsymbol{q}}) & F_{xx}(\bar{\boldsymbol{q}}) & F_{yy}(\bar{\boldsymbol{q}}) & F_{xy}(\bar{\boldsymbol{q}}) \end{bmatrix}$.

that Assumptions 2-4 are not very restrictive and can certainly be met in practical application.

2.3.2 Control problem formulation

First, let us define the error vector as follows:

$$\boldsymbol{e}_{PF} = \begin{bmatrix} e_\theta \\ e_F \end{bmatrix} = \begin{bmatrix} f_\theta(\theta_d - \theta) \\ e_F \end{bmatrix} \triangleq \begin{bmatrix} f_\theta(\theta_d - \theta) \\ F(\bar{\boldsymbol{q}}) \end{bmatrix} \in \mathcal{D}_e, \tag{2.94}$$

where $f_\theta(\cdot) : \mathbb{R} \to (-\pi, \pi]$, since the orientation error is considered in the sense of modulo 2π, and $\mathcal{D}_e = (-\pi, \pi] \times \mathcal{D}$, while $\bar{\boldsymbol{q}} \triangleq \begin{bmatrix} x & y \end{bmatrix}^\top$ was introduced in Section 1.3.2. The control problem can be formulated as follows:

Problem 2 *For system* (1.6)*, find a feedback control law* $\boldsymbol{u}(\boldsymbol{e}_{PF})$ *which guarantees that:*

- $\forall t \geq 0 \quad \|\boldsymbol{e}_{PF}(t, \boldsymbol{e}_{PF0})\| < \infty$,
- $\forall t \geq 0 \quad \boldsymbol{u}(\boldsymbol{e}_{PF}) \in \mathscr{U}$,
- $\forall t \geq t_s(\boldsymbol{e}_{PF0}) \quad \boldsymbol{e}_{PF}(t, \boldsymbol{e}_{PF0}) = \boldsymbol{0}$,
- $\sup\limits_{\boldsymbol{e}_{PF0} \in \mathcal{D}_e} t_s(\boldsymbol{e}_{PF0}) \leq T_c, \quad T_c < \infty$,

where T_c *means the upper bound of the settling time* $t_s(\boldsymbol{e}_{PF0})$*, while* $\boldsymbol{e}_{PF0} \triangleq \boldsymbol{e}_{PF}(0)$.

It should be noted that Problem 2 corresponds to the fixed-time path-following control problem, in which the robot should reach the reference path in a fixed time t_s, which is upper bounded by a constant T_c, and then follow the reference path (that is, $\forall t \geq t_s \ \boldsymbol{e}_{PF}(t) = \boldsymbol{0}$), with a constant reference longitudinal velocity u_{2d}. The control law that solves Problem 2 will be developed according to the conceptual scheme of the control system shown in Fig. 2.8.

2.3.3 Path-following fixed-time VFO control law

According to the VFO design methodology presented in Section 1.3.3 and inspired by [81], let us define the convergence vector field $\boldsymbol{h}$ for the fixed-time path-following control problem as follows:

$$\boldsymbol{h} = \begin{bmatrix} h_\theta \\ \bar{\boldsymbol{h}} \end{bmatrix} \triangleq \begin{bmatrix} K_a \left(|e_a|^{\delta_1} + |e_a|^{\delta_2} \right) \operatorname{sign}(e_a) + \dot{\theta}_{aN} \\ \left(v_d \boldsymbol{R} + K_p \big(|F(\bar{\boldsymbol{q}})|^{\mu_1} + |F(\bar{\boldsymbol{q}})|^{\mu_2} \big) \operatorname{sign}\big(F(\bar{\boldsymbol{q}})\big) \boldsymbol{I} \right) \dfrac{-\nabla \boldsymbol{F}(\bar{\boldsymbol{q}})}{\left\| \nabla \boldsymbol{F}(\bar{\boldsymbol{q}}) \right\|} \end{bmatrix}, \quad (2.95)$$

where $\bar{\boldsymbol{h}} \triangleq \begin{bmatrix} h_x & h_y \end{bmatrix}^\top$. The terms K_a and K_p are positive design coefficients, while

$$\boldsymbol{R} \triangleq \begin{bmatrix} 0 & 1 \\ -1 & 0 \end{bmatrix}, \qquad \boldsymbol{I} \triangleq \begin{bmatrix} 1 & 0 \\ 0 & 1 \end{bmatrix}$$

are a rotation matrix of angle $\frac{-\pi}{2}$ and an identity matrix, respectively. The term $v_d = |u_{2d}| > 0$ denotes an absolute value of the reference longitudinal velocity (cf. Assumption 5), while $\nabla \boldsymbol{F} \triangleq \begin{bmatrix} F_x & F_y \end{bmatrix}^\top$ means the gradient of function F (intentionally defined as a column vector), where F, F_x, and F_y are introduced in Section 2.3.1. The powers δ_1, δ_2, μ_1, and μ_2 are defined in (2.6) and (2.14) such that:

$$\delta_1 \overset{(2.6)}{=} 1 - \bar{\delta}, \quad \delta_2 \overset{(2.6)}{=} 1 + \bar{\delta}, \quad \mu_1 \overset{(2.14)}{=} 1 - \bar{\mu}, \quad \mu_2 \overset{(2.14)}{=} 1 + \bar{\mu}, \quad \bar{\delta}, \bar{\mu} \in (0, 1), \quad (2.96)$$

where

$$e_a(t) \overset{(2.7)}{=} \theta_a(t) - \theta(t)$$

is the auxiliary orientation error defined in (2.7).

Remark 12 *It should be noted that h_θ in the first row of* (2.95) *is defined similarly to h_θ in* (2.3)*. Meanwhile, the second row is selected analogously to the one in [81], and one can distinguish a component $v_d\boldsymbol{R}$ ensuring motion with a constant velocity along the reference path and a component ensuring reaching the reference path in a fixed time. It should also be noted that these components are orthogonal.*

Remark 13 *Please note that Assumption 1, according to which $e_a(0) \in (-\pi, \pi]$, also applies to the path-following fixed-time VFO control law.*

Remark 14 (cf. Remarks 3 and 4) *It should be noted that the choice of powers proposed in* (2.96) *is primarily motivated by the intention to use the 'local' method for estimating the upper bound of the settling time proposed in Lemma 4. If one is not interested in the 'local' method and prefers to consider the global case, one may choose the powers as proposed in Lemma 1 and use Lemma 3 to estimate the upper bound of the settling time.*

The term θ_a denotes the auxiliary orientation and is defined in (1.10). However, based on (2.95), one can observe that in this case $\forall t \geq 0 \ \left\| \bar{\boldsymbol{h}}(t) \right\| \neq 0$, sine

$$\forall t \geq 0 \quad v_d \boldsymbol{R} \frac{-\nabla \boldsymbol{F}\big(\bar{\boldsymbol{q}}(t)\big)}{\left\| \nabla \boldsymbol{F}\big(\bar{\boldsymbol{q}}(t)\big) \right\|} \neq 0.$$

Therefore, one can write

$$\theta_a \overset{(1.10)}{=} \operatorname{Atan2c}(\sigma h_y, \sigma h_x) \in \mathbb{R}, \tag{2.97}$$

where $\operatorname{Atan2c}(\cdot,\cdot) : \mathbb{R}\times\mathbb{R} \to \mathbb{R}$ is a continuous version of the four-quadrant inverse tangent function $\operatorname{Atan2}(\cdot,\cdot) : \mathbb{R}\times\mathbb{R} \to (-\pi, \pi]$, while σ is a decision parameter defined in Section 1.3.3. The time derivative of the auxiliary orientation θ_a, computed for the nominal case (that is, the case without control input constraints), can be derived in a manner similar to (2.9), that is:

$$\dot{\theta}_{aN} \overset{(2.9)}{=} \frac{\dot{h}_{yN}h_x - \dot{h}_{xN}h_y}{\left\|\bar{\boldsymbol{h}}\right\|^2} \quad \text{for} \quad \left\|\bar{\boldsymbol{h}}\right\| \neq 0, \tag{2.98}$$

where $\begin{bmatrix}\dot{h}_{xN} & \dot{h}_{yN}\end{bmatrix}^\top = \dot{\bar{\boldsymbol{h}}}_N$ is the time derivative of the positional subvector $\bar{\boldsymbol{h}}$ of the convergence vector field $\boldsymbol{h}$, which in the nominal case can be computed as follows:

$$\dot{\bar{\boldsymbol{h}}}_N = K_p \underline{\dot{F}}_N \tilde{\boldsymbol{F}} + v_d \boldsymbol{R} \dot{\tilde{\boldsymbol{F}}}_N + K_p \underline{F} \dot{\tilde{\boldsymbol{F}}}_N, \tag{2.99}$$

where

$$\underline{F} \triangleq (|F|^{\mu_1} + |F|^{\mu_2}) \operatorname{sign}(F) \tag{2.100}$$

and

$$\tilde{\boldsymbol{F}} \triangleq \frac{-\nabla \boldsymbol{F}}{\|\nabla \boldsymbol{F}\|}. \tag{2.101}$$

Next, it should be noted that the time derivative of function F in the nominal case can be expressed as follows:

$$\dot{F}_N\big(\bar{\boldsymbol{q}}(t)\big) = \frac{dF}{d\bar{\boldsymbol{q}}}\frac{d\bar{\boldsymbol{q}}}{dt} = (F_x \dot{x}_N + F_y \dot{y}_N) \overset{(1.6)}{=} u_{2N}\left(F_x \cos\theta + F_y \sin\theta\right), \tag{2.102}$$

and consequently the time derivative of (2.100) can be expressed as:

$$\begin{aligned}\underline{\dot{F}}_N &= \dot{F}_N\left(\mu_1 |F|^{\mu_1 - 1} + \mu_2 |F|^{\mu_2 - 1}\right) \\ &\overset{(2.102)}{=} u_{2N} \underbrace{\left(F_x \cos\theta + F_y \sin\theta\right)\left(\mu_1 |F|^{\mu_1 - 1} + \mu_2 |F|^{\mu_2 - 1}\right)}_{\triangleq \underline{F}_u}.\end{aligned} \tag{2.103}$$

The time derivative of (2.101) can be derived as:

$$\dot{\tilde{\boldsymbol{F}}}_N = u_{2N} \underbrace{\begin{bmatrix} F_y\Big((F_x F_{xy} - F_y F_{xx})\cos\theta + (F_x F_{yy} - F_y F_{xy})\sin\theta\Big) \\ F_x\Big((F_y F_{xx} - F_x F_{xy})\cos\theta + (F_y F_{xy} - F_x F_{yy})\sin\theta\Big) \end{bmatrix} \|\nabla \boldsymbol{F}\|^{-3}}_{\triangleq \tilde{\boldsymbol{F}}_u}. \tag{2.104}$$

Thus, one can observe that (2.99) can be rewritten as follows:

$$\dot{\bar{\boldsymbol{h}}}_N \overset{(2.99)}{=} u_{2N}\Big(K_p \underline{F}_u \tilde{\boldsymbol{F}} + v_d \boldsymbol{R} \tilde{\boldsymbol{F}}_u + K_p \underline{F} \tilde{\boldsymbol{F}}_u\Big). \tag{2.105}$$

Finally, according to the VFO design methodology presented in Section 1.3.3, the nominal control law can be formulated as in (1.9), that is:

$$\boldsymbol{u}_N = \begin{bmatrix} u_{1N} \\ u_{2N} \end{bmatrix} \overset{(1.9)}{=} \begin{bmatrix} h_\theta \\ \bar{\boldsymbol{h}}^\top \bar{\boldsymbol{g}}_2(\theta) \end{bmatrix} = \begin{bmatrix} h_\theta \\ \left\|\bar{\boldsymbol{h}}\right\| \cos\alpha \end{bmatrix} \in \mathbb{R}^2, \tag{2.106}$$

with h_θ and $\bar{\boldsymbol{h}}$ defined in (2.95), while $\bar{\boldsymbol{g}}_2(\theta) \triangleq \begin{bmatrix}\cos\theta & \sin\theta\end{bmatrix}^\top$ (cf. Section 1.3.2) and $\alpha \triangleq \angle\left(\bar{\boldsymbol{h}}, \bar{\boldsymbol{g}}_2(\theta)\right)$ (cf. Section 1.3.3). Next, let us formulate the following theorem.

Theorem 2 *For kinematics* (1.6)*, applying the nominal fixed-time VFO control law* $\boldsymbol{u}_N(t)$ *defined in* (2.106) *with scaling function* $s(t)$ *introduced in* (1.7) *leads to the control law*

$$\begin{aligned}\boldsymbol{u} = \begin{bmatrix} u_1 \\ u_2 \end{bmatrix} &\triangleq \begin{bmatrix} su_{1N} \\ su_{2N} \end{bmatrix} \overset{(2.106)}{=} \begin{bmatrix} sh_\theta \\ s\left\|\bar{\boldsymbol{h}}\right\| \cos\alpha \end{bmatrix} \\ &= \begin{bmatrix} sK_a\left(|e_a|^{\delta_1} + |e_a|^{\delta_2}\right)\operatorname{sign}(e_a) + s\dot{\theta}_{aN} \\ s\left\|\left(v_d\boldsymbol{R} + K_p(|F|^{\mu_1} + |F|^{\mu_2})\operatorname{sign}(F)\boldsymbol{I}\right)\dfrac{-\nabla\boldsymbol{F}}{\|\nabla\boldsymbol{F}\|}\right\| \cos\alpha \end{bmatrix} \in \mathscr{U} \end{aligned} \tag{2.107}$$

which solves Problem 2 and ensures fixed-time stability of the equilibrium point of the closed-loop dynamics.

Proof. The stability will be separately analyzed for the equilibrium point of auxiliary orientation error e_a dynamics and for the equilibrium point of the positional error dynamics. Moreover, a convergence of the orientation error e_θ will be shown as well.

Auxiliary orientation error: First, it should be noted that the following relations hold:

$$\begin{aligned} s\dot{\bar{\boldsymbol{h}}}_N = \begin{bmatrix} s\dot{h}_{xN} \\ s\dot{h}_{yN} \end{bmatrix} &\overset{(2.105)}{=} \left(K_p\underline{F}_u\tilde{\boldsymbol{F}} + v_d\boldsymbol{R}\tilde{\boldsymbol{F}}_u + K_p\underline{F}\tilde{\boldsymbol{F}}_u\right)su_{2N} \\ &\overset{(2.107)}{=} \left(K_p\underline{F}_u\tilde{\boldsymbol{F}} + v_d\boldsymbol{R}\tilde{\boldsymbol{F}}_u + K_p\underline{F}\tilde{\boldsymbol{F}}_u\right)u_2 = \dot{\bar{\boldsymbol{h}}} = \begin{bmatrix} \dot{h}_x \\ \dot{h}_y \end{bmatrix}, \end{aligned} \tag{2.108}$$

and consequently

$$s\dot{\theta}_{aN} \overset{(2.98)}{=} \frac{s\dot{h}_{yN}h_x - s\dot{h}_{xN}h_y}{\left\|\bar{\boldsymbol{h}}\right\|^2} \overset{(2.108)}{=} \frac{\dot{h}_y h_x - \dot{h}_x h_y}{\left\|\bar{\boldsymbol{h}}\right\|^2} = \dot{\theta}_a. \tag{2.109}$$

Next, let us look at the auxiliary orientation error dynamics:

$$\begin{aligned} \dot{e}_a = \dot{\theta}_a - \dot{\theta} &\overset{(1.6)}{=} \dot{\theta}_a - u_1 \overset{(2.107)}{=} \dot{\theta}_a - sh_\theta \\ &\overset{(2.95)}{=} \dot{\theta}_a - sK_a\left(|e_a|^{\delta_1} + |e_a|^{\delta_2}\right)\operatorname{sign}(e_a) - s\dot{\theta}_{aN} \\ &\overset{(2.95)}{=} \dot{\theta}_a - sK_a\left(|e_a|^{\delta_1} + |e_a|^{\delta_2}\right)\operatorname{sign}(e_a) - \dot{\theta}_a \\ &= -sK_a\left(|e_a|^{\delta_1} + |e_a|^{\delta_2}\right)\operatorname{sign}(e_a). \end{aligned} \tag{2.110}$$

One can conclude that $e_a = 0$ is the equilibrium point of the auxiliary orientation error dynamics. In order to check the *fixed-time stability* of this equilibrium point, let us use the positive definite function $V_a = \frac{1}{2}e_a^2$, whose time derivative can be assessed as follows:

$$\begin{aligned} \dot{V}_a = e_a\dot{e}_a &\overset{(2.110)}{=} -e_a sK_a\left(|e_a|^{\delta_1} + |e_a|^{\delta_2}\right)\operatorname{sign}(e_a) = -sK_a\left(|e_a|^{\delta_1+1} + |e_a|^{\delta_2+1}\right) \\ &= -sK_a\sqrt{2}^{\delta_1+1}V_a^{(\delta_1+1)/2} - sK_a\sqrt{2}^{\delta_2+1}V_a^{(\delta_2+1)/2}. \end{aligned} \tag{2.111}$$

Comparing (2.111) with (1.2) from Lemma 1, it can be concluded that the equilibrium point $e_a = 0$ is *fixed-time stable*. However, it should be noted that the function

$s\Big(\boldsymbol{e}_{PF}(t)\Big) \in (0,1]$ that appears in (2.111) is bounded but not constant. For this reason, the upper bound of the settling time, computed according to (1.5), will not yield a time-independant value. To deal with this, let us introduce an additional term in a similar manner as in (2.42):

$$s_{\mathcal{D}} = \inf_{\boldsymbol{e}_{PF0}\in\mathcal{D}_e} \underline{s}(\boldsymbol{e}_{PF0}) \triangleq \inf_{\boldsymbol{e}_{PF0}\in\mathcal{D}_e} \Big(\inf_{t\geq 0} s\Big(\boldsymbol{e}_{PF}(t,\boldsymbol{e}_{PF0})\Big)\Big) \in (0,1], \tag{2.112}$$

which denotes the smallest possible value of function $s\Big(\boldsymbol{e}_{PF}(t,\boldsymbol{e}_{PF0})\Big)$ for all initial conditions belonging to the set $\mathcal{D}_e$, defined in Section 2.3.2. Note that $s_{\mathcal{D}}$ is independent of time and of initial condition, in contrast to $s\left(\boldsymbol{e}_{PF}(t,\boldsymbol{e}_{PF0})\right)$. Then, (2.111) can be rewritten as follows:

$$\dot{V}_a \overset{(2.111)}{\leq} -s_{\mathcal{D}}K_a\sqrt{2}^{\delta_1+1}V_a^{(\delta_1+1)/2} - s_{\mathcal{D}}K_a\sqrt{2}^{\delta_2+1}V_a^{(\delta_2+1)/2}, \tag{2.113}$$

and by comparing this result with (1.5), and taking into account Assumption 1, one can obtain

$$T_{ca} \overset{(1.5)}{=} \frac{\arctan\Big(\sqrt{2}^{\bar{\delta}}V_a^{\bar{\delta}/2}(\pi)\Big)}{\bar{\delta}s_{\mathcal{D}}K_a}, \tag{2.114}$$

which is the upper bound of the auxiliary orientation error e_a settling time t_{sa}.

Remark 15 *One may notice a certain similarity between the above analysis and the analysis for the auxiliary orientation error presented in Section 2.2.2. This is due to the fact that for both the set-point and path-following VFO control laws, the form of h_θ is defined in a similar way (compare* (2.3) *with* (2.95)*), resulting in a similar behavior of the dynamics $\dot{e}_a$ (compare* (2.21) *with* (2.110)*).*

Positional error: Let us begin with showing that

$$s\dot{F}_N \overset{(2.102)}{=} (F_x\cos\theta + F_y\sin\theta)\, su_{2N} \overset{(2.107)}{=} (F_x\cos\theta + F_y\sin\theta)\, u_2 = \dot{F}. \tag{2.115}$$

Next, let us consider the dynamics of e_F, which can be expressed as follows:

$$\begin{aligned}
\dot{e}_F &\overset{(2.94)}{=} \dot{F} \overset{(2.115)}{=} u_2\,(F_x\cos\theta + F_y\sin\theta)\\
&\overset{(2.107)}{=} s\|\bar{\boldsymbol{h}}\|\cos\alpha\,(F_x\cos\theta + F_y\sin\theta)\\
&\overset{(2.7)}{=} s\|\bar{\boldsymbol{h}}\|\cos\alpha\Big(F_x\cos(\theta_a - e_a) + F_y\sin(\theta_a - e_a)\Big)\\
&= s\|\bar{\boldsymbol{h}}\|\cos\alpha\Big((F_x\cos\theta_a + F_y\sin\theta_a)\cos e_a\\
&\quad + (F_x\sin\theta_a - F_y\cos\theta_a)\sin e_a\Big).
\end{aligned} \tag{2.116}$$

One can observe that the following relations hold:

$$\cos\alpha \overset{(2.38)}{=} \frac{h_x\cos\theta + h_y\sin\theta}{\left\|\bar{\boldsymbol{h}}\right\|}, \quad \cos\theta_a \overset{(2.97)}{=} \frac{\sigma h_x}{\left\|\bar{\boldsymbol{h}}\right\|}, \quad \sin\theta_a \overset{(2.97)}{=} \frac{\sigma h_y}{\left\|\bar{\boldsymbol{h}}\right\|}, \tag{2.117}$$

and, consequently:

$$\cos e_a \overset{(2.7)}{=} \cos(\theta_a - \theta) = \cos\theta_a\cos\theta + \sin\theta_a\sin\theta \overset{(2.117)}{=} \frac{\sigma(h_x\cos\theta + h_y\sin\theta)}{\left\|\bar{\boldsymbol{h}}\right\|}$$

$$\overset{(2.117)}{=} \sigma \cos\alpha. \tag{2.118}$$

Therefore, it should be noted that (2.116) can be rewritten as follows:

$$\dot{e}_F \overset{(2.116)}{=} s\left(F_x h_x + F_y h_y\right)\cos^2 e_a + s\left(F_x h_y - F_y h_x\right)\sin e_a \cos e_a. \tag{2.119}$$

Then, based on (2.95), it can be observed that:

$$F_x h_x + F_y h_y = -K_p \|\nabla \boldsymbol{F}\| \left(|F|^{\mu_1} + |F|^{\mu_2}\right)\operatorname{sign}(F), \tag{2.120}$$

and

$$F_x h_y - F_y h_x = v_d \|\nabla \boldsymbol{F}\|, \tag{2.121}$$

hence one obtains:

$$\dot{e}_F \overset{(2.119)}{=} -sK_p \|\nabla \boldsymbol{F}\| \left(|F|^{\mu_1} + |F|^{\mu_2}\right)\operatorname{sign}(F)\cos^2 e_a + sv_d \|\nabla \boldsymbol{F}\| \sin e_a \cos e_a. \tag{2.122}$$

One can observe that under Assumptions 2 and 4, the right-hand side of (2.122) is bounded and the finite-time-escape effect is avoided. Furthermore, it should be noted that $\forall t \geq t_{sa}\ e_a(t) = 0 \implies \forall t \geq t_{sa}\ \sin e_a(t) = 0$ and $\forall t \geq t_{sa}\ \cos e_a(t) = 1$, therefore, (2.122) can be reduced to the following form:

$$\forall t \geq t_{sa} \quad \dot{e}_F(t) \overset{(2.122)}{=} -sK_p \|\nabla \boldsymbol{F}\| \left(|F|^{\mu_1} + |F|^{\mu_2}\right)\operatorname{sign}(F). \tag{2.123}$$

Therefore, one can conclude that $F \overset{(2.94)}{=} e_F = 0$ is the equilibrium point of (2.123) under Assumption 4. Now, let us use the Lyapunov's method to analyze the stability of this equilibrium point. The function $V_F = \frac{1}{2}e_F^2 \overset{(2.94)}{=} \frac{1}{2}F^2$ is chosen, and its time derivative can be assessed as follows:

$$\begin{aligned} \forall t \geq t_{sa} \quad \dot{V}_F = F\dot{F} &\overset{(2.123)}{=} -FsK_p \|\nabla \boldsymbol{F}\| \left(|F|^{\mu_1} + |F|^{\mu_2}\right)\operatorname{sign}(F) \\ &= -sK_p \|\nabla \boldsymbol{F}\| \left(|F|^{\mu_1+1} + |F|^{\mu_2+1}\right). \end{aligned} \tag{2.124}$$

Based on Assumption 4, one can observe that:

$$\begin{aligned} \forall t \geq t_{sa} \quad \dot{V}_F &\overset{(2.124)}{\leq} -sK_p m_G \left(|F|^{\mu_1+1} + |F|^{\mu_2+1}\right) \\ &= -sK_p m_G \sqrt{2}^{\mu_1+1} V_F^{(\mu_1+1)/2} - sK_p m_G \sqrt{2}^{\mu_2+1} V_F^{(\mu_2+1)/2}, \end{aligned} \tag{2.125}$$

By comparing (2.125) with (1.2) from Lemma 1 one can conclude that the equilibrium point $F = 0$ is fixed-time stable. It should be noted once again that the function $s\Big(\boldsymbol{e}_{PF}(t, \boldsymbol{e}_{PF0})\Big) \in (0, 1]$ that appears in (2.125) is bounded but not constant, thus let us use (2.112) to obtain:

$$\forall t \geq t_{sa} \quad \dot{V}_F \overset{(2.125)}{\leq} -s_{\mathcal{D}} K_p m_G \sqrt{2}^{\mu_1+1} V_F^{(\mu_1+1)/2} - s_{\mathcal{D}} K_p m_G \sqrt{2}^{\mu_2+1} V_F^{(\mu_2+1)/2}. \tag{2.126}$$

Now, upon Lemma 4 and Assumption 2, one can obtain:

$$T_{cF} \overset{(1.5)}{=} \frac{\arctan\left(\sqrt{2}^{\bar{\mu}} V_F^{\bar{\mu}/2}(M_F)\right)}{\bar{\mu} s_{\mathcal{D}} K_p m_G}. \tag{2.127}$$

Note that, since (2.127) is valid only for $t \geq t_{sa}$ and $t_{sa} \leq T_{ca}$, then the total upper bound of the settling time can be computed (conservatively) as

$$T_c = T_{ca} + T_{cF}. \tag{2.128}$$

Remark 16 *It should be noted that the upper bound* (2.128) *cannot be calculated without knowing* $s_{\mathcal{D}}$ *introduced in* (2.112)*, whose value is unknown, and no method has yet been developed to estimate it. However,* $\underline{s}$ *can be used instead of* $s_{\mathcal{D}}$*, whose value can be obtained* a posteriori*, allowing the upper bound* (2.128) *to be determined* a posteriori *as well, for a particular initial robot's configuration.*

Orientation error: Now let us consider a convergence of the orientation error e_θ. One can observe that

$$\theta(t) \xrightarrow{t\to T_{ca}} \theta_a(t) \implies \forall t \geq T_{ca} \quad \theta(t) \overset{(2.97)}{=} \operatorname{Atan2c}\left(\sigma h_y, \sigma h_x\right), \tag{2.129}$$

and, moreover, it should be noted that

$$\forall t \geq T_c \quad \bar{\boldsymbol{h}} \overset{(2.95)}{=} \begin{bmatrix} h_x \\ h_y \end{bmatrix} = -\frac{v_d \boldsymbol{R} \nabla \boldsymbol{F}}{\|\nabla \boldsymbol{F}\|} = \begin{bmatrix} 0 & 1 \\ -1 & 0 \end{bmatrix} \begin{bmatrix} -\frac{v_d F_x}{\|\nabla \boldsymbol{F}\|} \\ -\frac{v_d F_y}{\|\nabla \boldsymbol{F}\|} \end{bmatrix} = \begin{bmatrix} -\frac{v_d F_y}{\|\nabla \boldsymbol{F}\|} \\ \frac{v_d F_x}{\|\nabla \boldsymbol{F}\|} \end{bmatrix} \tag{2.130}$$

Next, substituting (2.130) into (2.129) yields:

$$\forall t \geq T_c \quad \theta(t) = \operatorname{Atan2c}\left(\sigma \frac{v_d F_x}{\|\nabla \boldsymbol{F}\|}, -\sigma \frac{v_d F_y}{\|\nabla \boldsymbol{F}\|}\right). \tag{2.131}$$

Since the term $v_d / \|\nabla \boldsymbol{F}\|$ is positive, one can obtain that

$$\begin{aligned} \forall t \geq T_c \quad \theta(t) &= \operatorname{Atan2c}\left(\sigma F_x, -\sigma F_y\right) = \operatorname{Atan2}\left(\sigma F_x, -\sigma F_y\right) + 2k\pi \\ &\overset{(2.93)}{=} \theta_d + 2k\pi, \quad k \in \mathbb{Z}. \end{aligned} \tag{2.132}$$

Consequently, it can be concluded that $e_\theta(t) \overset{(2.94)}{=} f_\theta\Big(\theta_d(t) - \theta(t)\Big) \to 0$ as $t \to T_c$. This concludes the proof. ■

2.3.4 Results of numerical simulations

The proposed control law was tested via numerical simulations, carried out in the Matlab-Simulink environment. A fixed-step solver with a step size of 10^{-2} s was selected. Two cases are considered, which differed in the function defining the reference path:

- case I:
  $f_p(\bar{\boldsymbol{q}}) = x^2 + y^2 - 0.4$, with $\mathcal{D}$ such that $M_F = 0.1$ and $m_G = 0.4$,
- case II:
  $f_p(\bar{\boldsymbol{q}}) = 2x^2 + 10x^2y^2 + y^2 - 0.25$, with $\mathcal{D}$ such that $M_F = 0.45$ and $m_G = 1$.

for which Assumptions 2-4 are met for selected domains $\mathcal{D}$. The controller coefficients were as follows: $K_a = 2$, $K_p = 1$, $\bar{\delta} = 0.1$, $\bar{\mu} = 0.2$, $\sigma = 1$, $v_d = 0.1$ m/s, and $\zeta = 1$. The maximum admissible absolute values for the control signals were selected as follows: $u_{1M} = 3$ rad/s and $u_{2M} = 0.5$ m/s. The results obtained for cases I and II are shown in Figs. 2.10 and 2.11, respectively.

It can be observed that, for both cases, the function F (see Figs. 2.10a and 2.11a), the auxiliary orientation error (see Figs. 2.10d and 2.11d), and the orientation error (see Figs. 2.10c and 2.11c) converge towards zero, while the control signals (see Figs. 2.10e-2.10f and 2.11e-2.11f) satisfy the imposed constraints. Furthermore, the robot reaches the desired path in a fixed time (see Figs. 2.12g and 2.13g) and then follows it with a constant longitudinal velocity $u_2 = v_d$ (see Figs. 2.10f and 2.11f). Moreover, one can see that the robot's motion to the desired path is characterized by the lack of oscillations. The upper bounds of the settling times, computed according to (2.114), and (2.127), with using $\underline{s}$ (see Remark 16), are as follows:

- $T_{ca} = 6.76$ s and $T_{cp} = 11.29$ s for case I (with $M_F = 0.1$ and $m_G = 0.4$),
- $T_{ca} = 15.92$ s and $T_{cp} = 13.34$ s for case II (with $M_F = 0.45$ and $m_G = 1$).

One can observe that the system errors converge in a time shorter than the computed upper bounds.

2.3.5 Results of experimental tests

The experimental tests were performed using the mTracker mobile robot, which was discussed in Section 2.2.5. The fast-prototyping setup was prepared according to the scheme shown in Fig. 2.9, with the reference path generator that generates reference signal $\boldsymbol{F}^*$ in accordance with the reference path definition provided in Section 2.3.1, and the VFO control law presented in Section 2.3.3. It should be noted that communication between the robot and a PC computer was carried out via a Bluetooth interface, and the robot's current configuration $\boldsymbol{q}$ was determined based on the odometry. It should be noted that a vector of desired wheel speeds is sent to the robot, which is calculated based on the control signals u_1 and u_2 as follows:

$$\boldsymbol{u}_k \overset{(2.91)}{=} \frac{1}{r_w} \begin{bmatrix} b_w/2 & 1 \\ -b_w/2 & 1 \end{bmatrix} \begin{bmatrix} u_1 \\ u_2 \end{bmatrix}, \tag{2.133}$$

where r_w denotes the wheel radius and b_w means the wheel base (cf. Section 2.2.5). The average operating frequency of this scheme was 30 Hz.

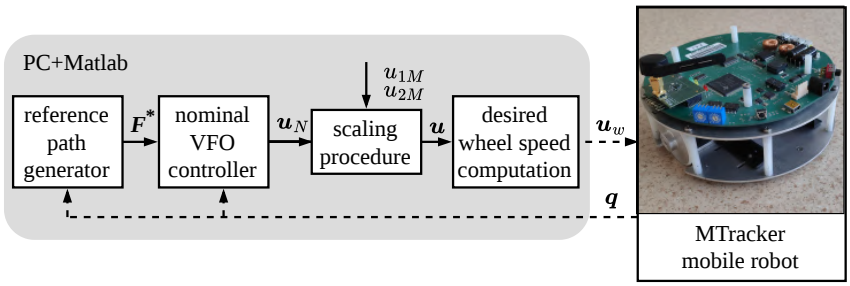

Figure 2.9 – Block scheme of the fast-prototyping system with the mTracker mobile robot. The communication link between the PC and the robot is provided via Bluetooth (dashed lines in the scheme), while $\boldsymbol{F}^* = \begin{bmatrix} F & F_x & F_y & F_{xx} & F_{yy} & F_{xy} \end{bmatrix}$.

Remark 17 (cf. Remark 9) *It should be noted that, although velocity scaling is performed in the robot platform velocity space (cf. Fig. 2.9), the parameters u_{1M} and u_{2M} should be selected so that the maximum wheel velocity limitations are respected. These limitations are determined by the maximum rotational speed of the motors. Consequently, after substituting u_{1M} and u_{2M} into* (2.133) *in place of u_1 and u_2, the resulting components of $\boldsymbol{u}_k$ must be feasible for the robot drives.*

Similarly to Section 2.3.4, two scenarios are considered that differ in the definition of the function determining the reference path:

- case I:
  $f_p(\bar{\boldsymbol{q}}) = x^2 + y^2 - 0.4$, with $\mathcal{D}$ such that $M_F = 0.1$ and $m_G = 0.4$,
- case II:
  $f_p(\bar{\boldsymbol{q}}) = 2x^2 + 10x^2y^2 + y^2 - 0.25$, with $\mathcal{D}$ such that $M_F = 0.45$ and $m_G = 1$.

for which Assumptions 2-4 are fulfilled for selected domains $\mathcal{D}$. The controller coefficients were as follows: $K_a = 2$, $K_p = 1$, $\bar{\delta} = 0.1$, $\bar{\mu} = 0.2$, $\sigma = 1$, $v_d = 0.1$ m/s, and $\zeta = 1$. The maximum admissible absolute values of the control inputs were selected as follows: $u_{1M} = 3$ rad/s and $u_{2M} = 0.5$ m/s. The results obtained for cases I and II are shown in Figs. 2.12 and 2.13, respectively. Figs. 2.12a and 2.13a show that the positional error $e_F \triangleq F$ converges towards zero for both cases, as well as the orientation error e_θ presented in Figs. 2.12c and 2.13c, and the auxiliary orientation error e_a shown in Figs. 2.12d and 2.13d. Based on Figs. 2.12e-2.12f and Figs. 2.13e-2.13f, one can see that the control signals satisfy the imposed constraints. Furthermore, one can observe that the robot reaches and follows the desired reference path (see Figs. 2.12g and 2.13g) with the desired velocity (see Figs. 2.12f and 2.12f).

Working with a real physical system, one encounters various types of disturbances like the measurement noise, model uncertainty, non-ideal regulation of the wheels' speeds, and communication delays between Matlab and the robot's on-board controller, the impact of which on control performance can be observed, for example, in Figs. 2.12a or 2.13e.

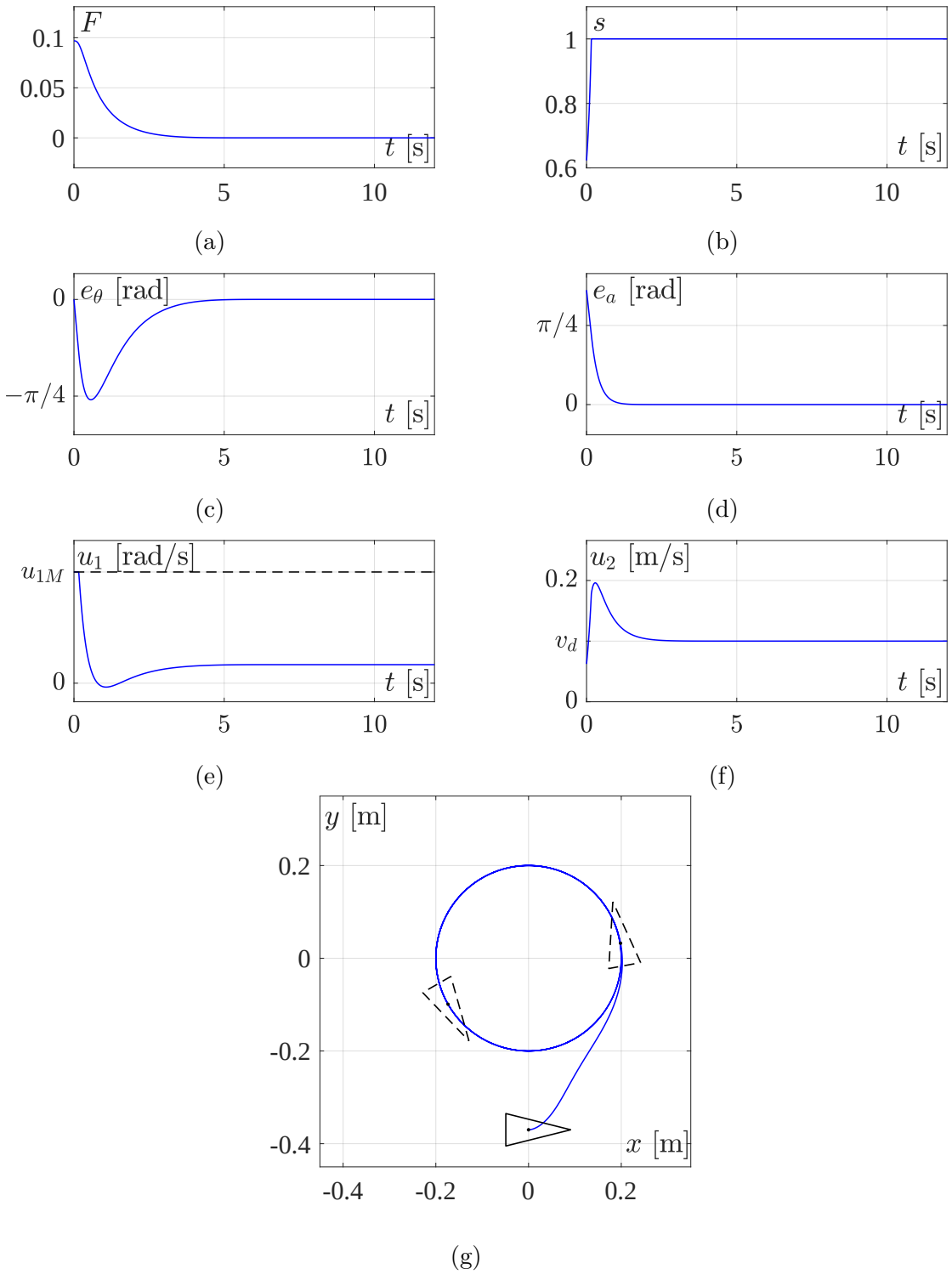

Figure 2.10 – Results of numerical simulations for the fixed-time path-following control problem for $f_p(\bar{\boldsymbol{q}}) = x^2 + y^2 - 0.4$ and $v_d = 0.1$ m/s, while $u_{1M} = 3$ rad/s and $u_{2M} = 0.5$ m/s. The initial configuration of the robot is marked by a solid triangle.

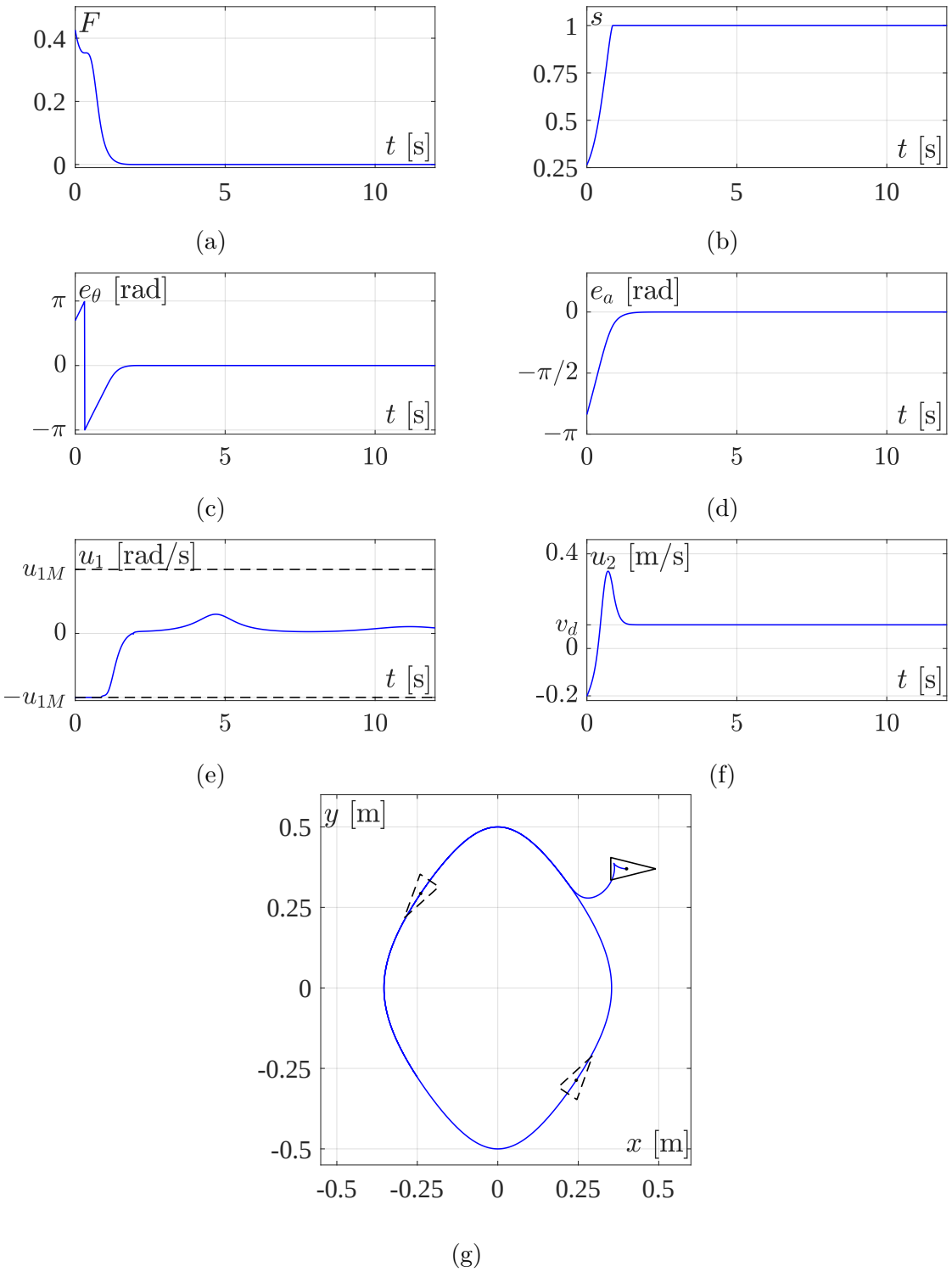

Figure 2.11 – Results of numerical simulations for the fixed-time path-following control problem for $f_p(\bar{\boldsymbol{q}}) = 2x^2 + 10x^2y^2 + y^2 - 0.25$ and $v_d = 0.1$ m/s, while $u_{1M} = 3$ rad/s and $u_{2M} = 0.5$ m/s. The initial configuration of the robot is marked by a solid triangle.

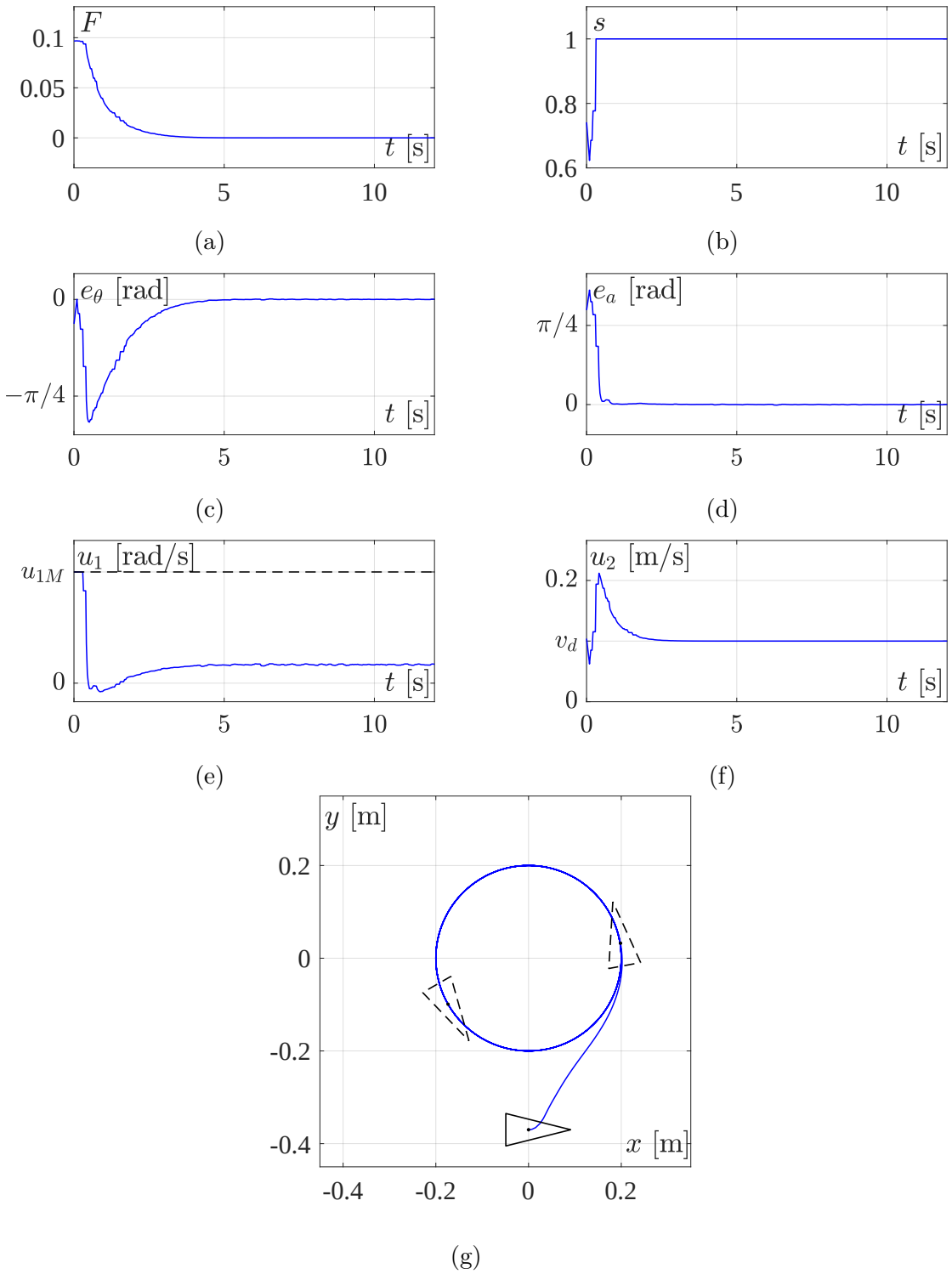

Figure 2.12 – Results of experimental tests with mTracker mobile robot for the fixed-time path-following control problem for $f_p(\bar{\boldsymbol{q}}) = x^2 + y^2 - 0.4$ and $v_d = 0.1$ m/s, while $u_{1M} = 3$ rad/s and $u_{2M} = 0.5$ m/s. The initial configuration of the robot is marked by a solid triangle.

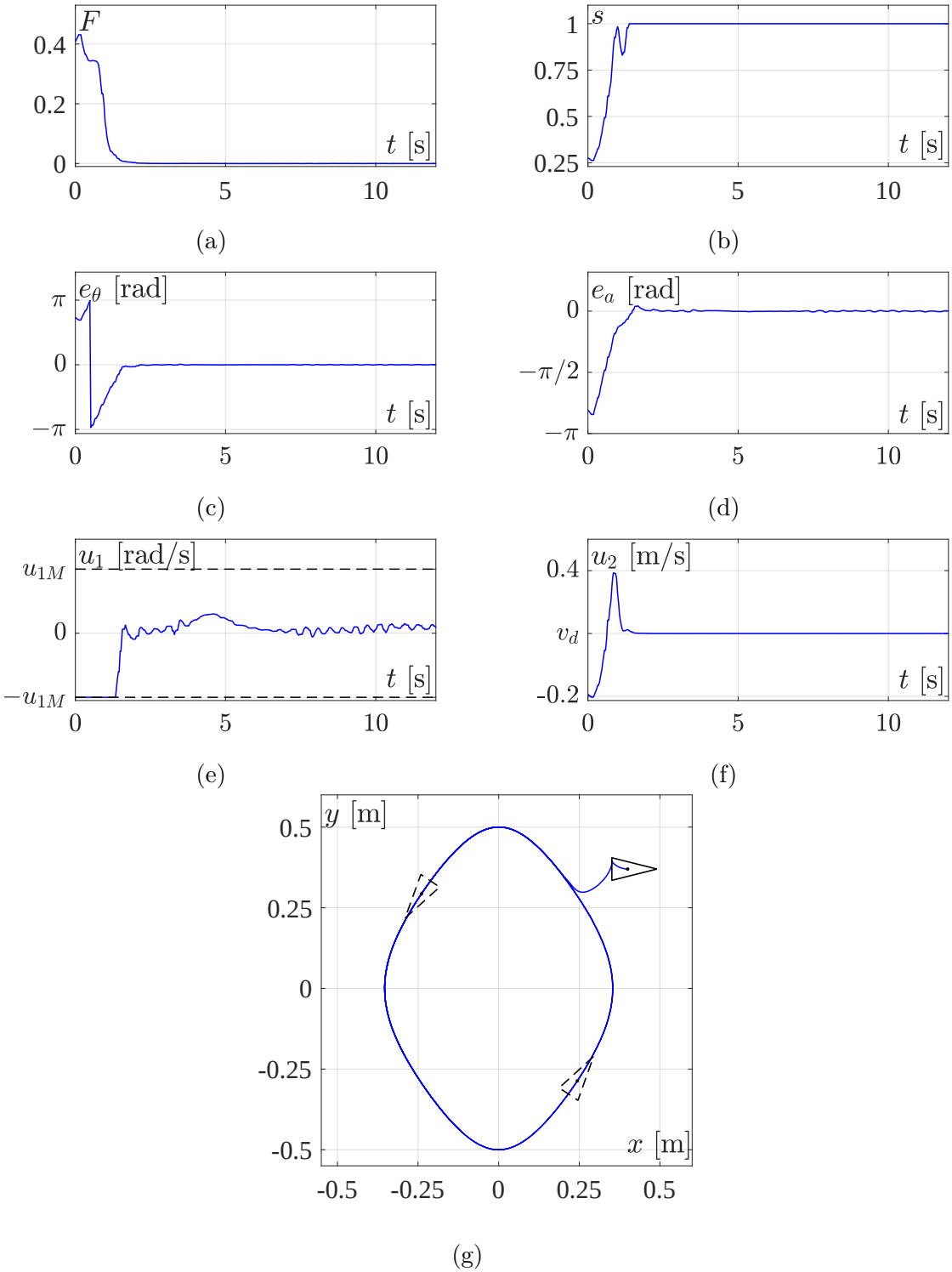

Figure 2.13 – Results of experimental tests with mTracker mobile robot for $f_p(\bar{\boldsymbol{q}}) = 2x^2 + 10x^2y^2 + y^2 - 0.25$ and $v_d = 0.1$ m/s, while $u_{1M} = 3$ rad/s and $u_{2M} = 0.5$ m/s. The initial configuration of the robot is marked by a solid triangle.

2.4 Conclusions

This chapter presents the fixed-time VFO control laws for the set-point control problem and for the problem of following a non-parameterized path. The proposed control laws ensure satisfaction of the imposed control input constraints and guarantee that the system errors converge to zero within a fixed time. The theoretical results obtained have been validated by numerical simulations and experimental tests.

Unlike works currently available in the literature, the proposed algorithms simultaneously consider the control input constraints and the task execution time constraints, using computationally simple algorithms that do not require significant computational power – unlike, for example, the work [23], in which the simultaneous consideration of these constraints requires solving an optimization problem online. Furthermore, the VFO methodology is characterized by non-oscillatory transient states and the absence of chattering, unlike classical sliding-mode methods, whose use is often associated with chattering and which are frequently employed in the design of fixed-time control algorithms (see, for example, [15, 89]). The proposed algorithms explicitly determine the maximum admissible absolute values of the control inputs, which, in the case of the unicycle model, correspond to the maximum admissible absolute values of the vehicle's velocities. These constraints were also explicitly taken into account in the method used to estimate the upper bound of the system error settling time.

The proposed algorithms use a 'local' method for estimating the upper bound of the system error settling times (see Lemma 4), that is, the one that takes into account a particular set of admissible initial conditions, which is a subset of $\mathbb{R}^n$. Although this 'local' method has appeared in the literature (see, for example, [101] or [23]), it has typically served as an intermediate step in deriving a global method (see Lemma 2), and to the best of our knowledge, the 'local' estimation of the upper bound has received limited attention in the literature. However, when considering the task execution time constraints and the control input constraints simultaneously, such an approach seems appropriate, since it is easy to see that in the case presented in this dissertation, for $\bar{z} \to \infty$, with $\bar{z}$ denoting the largest possible value of the norm of the initial condition within the considered set of admissible initial conditions (cf. Lemma 4), one obtains $\underline{\underline{s}} \to 0 \implies T_{cp} \to \infty$ based on (2.42) and (2.44).

This chapter also proposes a method for *a priori* estimation of $\underline{\underline{s}}$ in the case of a set-point control problem, which subsequently allows *a priori* estimation of the upper bounds. A method for estimating the upper bound of settling times in the case of a path-following problem has not yet been developed, so these values can only be calculated *a posteriori*.

Therefore, it can be concluded that the first objective defined for this dissertation has been achieved, that is the fixed-time control laws for a single nonholonomic mobile robot has been developed. The next chapter will present a solution to the second objective, namely, the adaptation of the developed control laws for nonholonomic distributed multi-vehicle systems.

Chapter 3

Control design for a distributed multi-vehicle system

3.1 Introduction

In this chapter, the focus will be on the second objective formulated in this dissertation, namely the designing of control algorithms within the VFO methodology for a distributed multi-vehicle system, taking into account control input constraints and task execution time constraints. The problem of creating formation is considered, and two approaches will be proposed to solve this problem using the VFO methodology. First, in Section 3.2 the control problem is formulated. Next, in Section 3.3, the observer-based approach will be presented, in which the set-point fixed-time VFO control law discussed before in Section 2.2.2 can be successfully applied to control a multi-vehicle system. In Section 3.4, a consensus-based approach will be discussed, which also relies on the algorithm presented in Section 2.2.2. However, it includes significant modifications that enable single-stage control (compared to the three-stage control in the observer-based approach). Finally, in Section 3.5 the obtained results will be summarized. For all proposed algorithms, a formal stability analysis as well as validation results are provided.

3.2 Control problem formulation

We are interested in the problem of formation creation by a nonholonomic multi-vehicle system, that is, one that consists of n_v vehicles with the unicycle kinematics defined as follows:

$$\dot{\boldsymbol{q}}_i \overset{(1.6)}{=} \boldsymbol{G}(\boldsymbol{q}_i)\boldsymbol{u}_i = \begin{bmatrix} 1 & 0 \\ 0 & \cos\theta_i \\ 0 & \sin\theta_i \end{bmatrix} \begin{bmatrix} u_{1i} \\ u_{2i} \end{bmatrix} = \boldsymbol{g}_1 u_{1i} + \boldsymbol{g}_2(\theta_i) u_{2i}, \tag{3.1}$$

where the subscript $i \in \mathcal{V} \triangleq \{1, 2, \ldots, n_v\}$ indicates the i-th vehicle, while $\mathcal{V}$ is the node set introduced in Section 1.4.2.

The desired formation is determined using a displacement vector

$$\bar{\boldsymbol{d}}_i \triangleq \begin{bmatrix} d_{xi} \\ d_{yi} \end{bmatrix} \tag{3.2}$$

that defines, in a global frame, the relative displacement of each robot's desired position from the consensus equilibrium point $\bar{\boldsymbol{q}}_c \triangleq \begin{bmatrix} x_c & y_c \end{bmatrix}^\top$ (cf. Fig. 1.6). Note that the value of the consensus equilibrium point $\bar{\boldsymbol{q}}_c$ is unknown *a priori*.

Let us formulate the control problem as follows:

Problem 3 *For each nonholonomic vehicle $i \in \mathscr{V} \triangleq \{1, 2, \ldots, n_v\}$ whose kinematics are described by* (3.1) *and which belongs to a distributed multi-vehicle system, find feedback control law $\boldsymbol{u}_i$, which guarantees that the configuration $\boldsymbol{q}_i = \begin{bmatrix} \theta_{di} & \bar{\boldsymbol{q}}_i^\top \end{bmatrix}^\top$ of each vehicle will converge to the desired position $\bar{\boldsymbol{q}}_{di} \triangleq \bar{\boldsymbol{q}}_c + \bar{\boldsymbol{d}}_i$ and desired orientation θ_{di} in a fixed time and, as a result, vehicles will create a formation around the* a priori *unknown consensus equilibrium point $\bar{\boldsymbol{q}}_c$, that is:*

- $\forall i \in \mathscr{V}\ \forall t \geq 0 \quad \|\bar{\boldsymbol{q}}_{di} - \bar{\boldsymbol{q}}_i(t)\| \leq \infty$,
- $\forall i \in \mathscr{V}\ \forall t \geq 0 \quad \boldsymbol{u}_i(t) \in \mathscr{U}$,
- $\forall i \in \mathscr{V}\ \forall t \geq t_{si} \quad \|\bar{\boldsymbol{q}}_{di} - \bar{\boldsymbol{q}}_i(t)\| \leq \epsilon$,
- $\forall i \in \mathscr{V}\ \forall t \geq t_{si} \quad f_\theta\big(\theta_{di} - \theta_i(t)\big) = \theta_\epsilon$,
- $\sup\limits_{\boldsymbol{e}_{0i} \in \mathbb{R}^3} \sup\limits_{i \in \mathscr{V}} t_{si}(\boldsymbol{e}_{0i}) \leq T_c < \infty$,

where $\epsilon \geq 0$ is a small (or zero) constant chosen by a designer, θ_ϵ is a constant whose value is related to ϵ, while $\boldsymbol{e}_{0i}$ means the initial value of the error vector for the i-th vehicle, $f_\theta(\cdot)$ is a function such that $\mathbb{R} \to (-\pi, \pi]$, $\mathscr{U}$ denotes the set of admissible control inputs defined in Section 1.3.2. The term t_{si} denotes a settling time of the i-th vehicle, while T_c is an upper bound of the settling times t_{si} for all $i \in \mathscr{V}$.

Remark 18 *It should be noted that the set $\mathscr{U}$ of admissible control inputs, defined in Section 1.3.2, is taken to be the same for each vehicle. This choice was made solely to simplify the notation, without compromising the validity of the reasoning presented in this chapter. One may select, in general, different maximum admissible absolute values for control inputs, and thus define different sets $\mathscr{U}_i$ for different vehicles.*

Remark 19 *Note that in Problem 3, the set $\mathcal{E}$ of admissible initial errors, which was present in Problem 1 (see Fig. 2.1), has not been defined. The main motivation for introducing this set lies in the intention to use a less conservative, 'local' estimation of the upper bound of settling times. Since no method has yet been developed for some of the algorithms considered in this chapter to estimate the upper bounds* a priori, *and such estimation is possible only* a posteriori, *it was decided to present considerations regarding the global case, that is, the initial error values belong to $\mathbb{R}^n$.*

Before the algorithms solving Problem 3 will be presented, let us introduce a few lemmas that will be important for stability analysis in the following sections.

Lemma 5 (cf. [114]) *Any square $m \times m$ matrix $\boldsymbol{M}$ can be represented as the sum of a symmetric matrix $\boldsymbol{M}_{sym}$ and a skew-symmetric matrix $\boldsymbol{M}_{skew}$, such that:*

$$\boldsymbol{M} = \boldsymbol{M}_{sym} + \boldsymbol{M}_{skew} = \frac{\boldsymbol{M} + \boldsymbol{M}^\top}{2} + \frac{\boldsymbol{M} - \boldsymbol{M}^\top}{2}. \tag{3.3}$$

Furthermore, the quadratic function associated with a skew-symmetric matrix is always zero, that is $\boldsymbol{z}^\top \boldsymbol{M}_{skew} \boldsymbol{z} = 0$, where $\boldsymbol{z} \in \mathbb{R}^m$.

Lemma 6 (cf. [141, 143]) *Let $z_1, z_2, \ldots, z_n \geq 0$, $0 < P_1 < 1$, and $P_2 > 1$. Then:*

$$\left(\sum_{i=1}^{n_v} z_i\right)^{P_1} \leq \sum_{i=1}^{n_v} (z_i)^{P_1}, \tag{3.4}$$

$$n_v{}^{1-P_2} \left(\sum_{i=1}^{n_v} z_i\right)^{P_2} \leq \sum_{i=1}^{n_v} (z_i)^{P_2} \leq \left(\sum_{i=1}^{n_v} z_i\right)^{P_2}. \tag{3.5}$$

Lemma 7 (cf. [107]) *Let $z_1, z_2, \ldots, z_n \geq 0$, $a > 0$, $b > 0$, $0 < P_1 < 1$, and $P_2 \geq 1$. Then:*

$$\left(\sum_{i=1}^{n_v} (z_i)^a + \sum_{i=1}^{n_v} (z_i)^b\right)^{P_1} \leq \left(\sum_{i=1}^{n_v} (z_i)^a\right)^{P_1} + \left(\sum_{i=1}^{n_v} (z_i)^b\right)^{P_1}, \tag{3.6}$$

$$\left(\sum_{i=1}^{n_v} (z_i)^a + \sum_{i=1}^{n_v} (z_i)^b\right)^{P_2} \leq 2^{P_2-1} \left(\sum_{i=1}^{n_v} (z_i)^a\right)^{P_2} + 2^{P_2-1} \left(\sum_{i=1}^{n_v} (z_i)^b\right)^{P_2}. \tag{3.7}$$

Lemma 8 (cf. [125]) *Let $a > 0$, $b > 0$, $r_1 > 1$, and $r_2 = r_1/(r_1 - 1)$. Then, based on the Young's inequality, the following inequality holds:*

$$ab \leq \frac{1}{r_1} a^{r_1} + \frac{1}{r_2} b^{r_2}. \tag{3.8}$$

Lemma 9 *Let $\boldsymbol{z}$ be a vector, $\boldsymbol{\mathcal{L}}$ be the Laplacian matrix of the connected graph $\mathcal{G}$ describing the undirected communication topology of a multi-vehicle system consisting of n_v vehicles, and $\lambda_2 > 0$ be the second smallest eigenvalue of $\boldsymbol{\mathcal{L}}$. Then the following inequality holds:*

$$\boldsymbol{z}^\top \boldsymbol{\mathcal{L}}\boldsymbol{\mathcal{L}}\boldsymbol{z} \geq \lambda_2 \boldsymbol{z}^\top \boldsymbol{\mathcal{L}}\boldsymbol{z}. \tag{3.9}$$

Proof. Let λ_i, $i \in \mathcal{V} \triangleq \{1, 2, \ldots, n_v\}$ be an eigenvalue of $\boldsymbol{\mathcal{L}}$ and $\boldsymbol{v}_{\lambda i}$ be a corresponding eigenvector, such that $\boldsymbol{v}_{\lambda i}^\top \boldsymbol{v}_{\lambda i} = 1$, while $\boldsymbol{v}_{\lambda i}^\top \boldsymbol{v}_{\lambda j} = 0$ for $i \neq j$, $j \in \mathcal{V}$ (since the eigenvectors of a symmetric matrix are ortogonal). Let $\boldsymbol{z}$ be a vector. One can observe that

$$\boldsymbol{\mathcal{L}}\boldsymbol{v}_{\lambda i} = \lambda_i \boldsymbol{v}_{\lambda i} \tag{3.10}$$

and that vector $\boldsymbol{z}$ can be written as follows:

$$\boldsymbol{z} = \sum_{i \in \mathcal{V}} c_i \boldsymbol{v}_{\lambda i}, \quad c_i \triangleq \boldsymbol{v}_{\lambda i}^\top \boldsymbol{z}. \tag{3.11}$$

Then, it should be noted that:

$$\begin{aligned} \boldsymbol{z}^\top \boldsymbol{\mathcal{L}}\boldsymbol{z} &\overset{(3.11)}{=} \left(\sum_{i \in \mathcal{V}} c_i \boldsymbol{v}_{\lambda i}\right)^\top \boldsymbol{\mathcal{L}} \sum_{i \in \mathcal{V}} c_i \boldsymbol{v}_{\lambda i} = \left(\sum_{i \in \mathcal{V}} c_i \boldsymbol{v}_{\lambda i}\right)^\top \sum_{i \in \mathcal{V}} c_i \boldsymbol{\mathcal{L}}\boldsymbol{v}_{\lambda i} \\ &\overset{(3.10)}{=} \left(\sum_{i \in \mathcal{V}} c_i \boldsymbol{v}_{\lambda i}\right)^\top \sum_{i \in \mathcal{V}} c_i \lambda_i \boldsymbol{v}_{\lambda i} = \sum_{i \in \mathcal{V}} \lambda_i c_i^2 \boldsymbol{v}_{\lambda i}^\top \boldsymbol{v}_{\lambda i} = \sum_{i \in \mathcal{V}} \lambda_i c_i^2 \end{aligned} \tag{3.12}$$

and:

$$\boldsymbol{z}^\top \boldsymbol{\mathcal{L}}\boldsymbol{\mathcal{L}}\boldsymbol{z} = (\boldsymbol{\mathcal{L}}\boldsymbol{z})^\top \boldsymbol{\mathcal{L}}\boldsymbol{z} \overset{(3.11)}{=} \left(\boldsymbol{\mathcal{L}} \sum_{i \in \mathcal{V}} c_i \boldsymbol{v}_{\lambda i}\right)^\top \boldsymbol{\mathcal{L}} \sum_{i \in \mathcal{V}} c_i \boldsymbol{v}_{\lambda i} = \left(\sum_{i \in \mathcal{V}} c_i \boldsymbol{\mathcal{L}}\boldsymbol{v}_{\lambda i}\right)^\top \sum_{i \in \mathcal{V}} c_i \boldsymbol{\mathcal{L}}\boldsymbol{v}_{\lambda i}$$

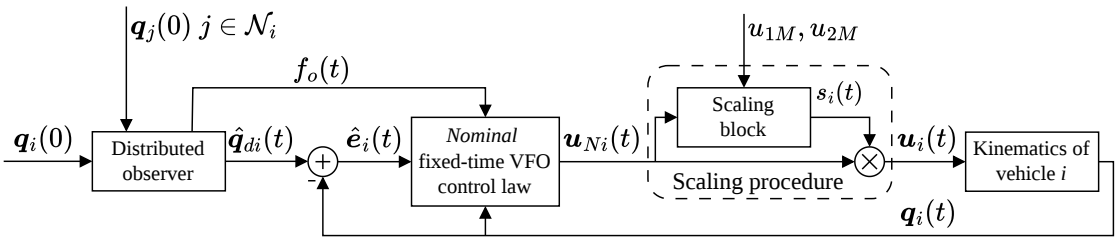

Figure 3.1 – Overview of the control system with the proposed observer-based control algorithm for the i-th vehicle.

$$\overset{(3.10)}{=} \left(\sum_{i\in\mathcal{V}} c_i\lambda_i\boldsymbol{v}_{\lambda i}\right)^{\top} \sum_{i\in\mathcal{V}} c_i\lambda_i\boldsymbol{v}_{\lambda i} = \sum_{i\in\mathcal{V}} \lambda_i^2 c_i^2 \boldsymbol{v}_{\lambda i}^{\top}\boldsymbol{v}_{\lambda i} = \sum_{i\in\mathcal{V}} \lambda_i^2 c_i^2. \tag{3.13}$$

Please note that matrix L is symmetric, since the graph $\mathcal{G}$ is connected and the communication topology is undirected. Furthermore, it can be seen that (see [96])

$$0 = \lambda_1 < \lambda_2 \leq \ldots \leq \lambda_{n_v}, \tag{3.14}$$

and based on this, it can be concluded that

$$\forall i \in \mathcal{V} \quad \lambda_i^2 \geq \lambda_i\lambda_2. \tag{3.15}$$

Therefore, it should be noted that

$$\boldsymbol{z}^{\top}\boldsymbol{\mathcal{L}}\boldsymbol{\mathcal{L}}\boldsymbol{z} \overset{(3.13)}{=} \sum_{i\in\mathcal{V}} \lambda_i^2 c_i^2 \overset{(3.15)}{\geq} \sum_{i\in\mathcal{V}} \lambda_i\lambda_2 c_i^2 = \lambda_2 \sum_{i\in\mathcal{V}} \lambda_i c_i^2 \overset{(3.12)}{=} \lambda_2 \boldsymbol{z}^{\top}\boldsymbol{\mathcal{L}}\boldsymbol{z}. \tag{3.16}$$

That concludes the proof. ■

The following sections will present two different approaches that solve Problem 3.

3.3 Observer-based formation control

The first proposed algorithm involves the use of distributed observers to estimate the consensus equilibrium state $\boldsymbol{q}_c \triangleq \left[\theta_c\ \bar{\boldsymbol{q}}_c^{\top}\right]^{\top}$ in a decentralized way. Then, the desired configuration

$$\boldsymbol{q}_{di} \triangleq \begin{bmatrix}\theta_d \\ \bar{\boldsymbol{q}}_{di}\end{bmatrix} = \begin{bmatrix}\theta_c \\ \bar{\boldsymbol{q}}_c + \boldsymbol{d}_i\end{bmatrix}$$

for each vehicle will be determined, and the set-point fixed-time VFO control law, introduced in Section 2.2.2, will be applied. An overview of the proposed algorithm is shown in Fig. 3.1. Note that the results presented in this section were originally presented in [115] and [116].

3.3.1 Distributed observer

Distributed fixed-time observers can be used to estimate the consensus equilibrium state $\boldsymbol{q}_c$. Let us formulate the appropriate theorem:

Theorem 3 *For each vehicle $i \in \mathcal{V} \triangleq \{1, 2, \ldots, n_v\}$, belonging to a multi-vehicle system whose communication topology is described by a connected graph $\mathcal{G}$, the distributed fixed-time observer*

$$\dot{\hat{\boldsymbol{q}}}_{ci} = \begin{bmatrix} \dot{\hat{\theta}}_{ci} \\ \dot{\hat{x}}_{ci} \\ \dot{\hat{y}}_{ci} \end{bmatrix} \triangleq \begin{bmatrix} -K_o \left(\kappa_1 |\xi_{\theta i}|^{\chi_1} + \kappa_2 |\xi_{\theta i}|^{\chi_2}\right) \operatorname{sign}\left(\xi_{\theta i}\right) \\ -K_o \left(\kappa_1 |\xi_{xi}|^{\chi_1} + \kappa_2 |\xi_{xi}|^{\chi_2}\right) \operatorname{sign}\left(\xi_{xi}\right) \\ -K_o \left(\kappa_1 |\xi_{yi}|^{\chi_1} + \kappa_2 |\xi_{yi}|^{\chi_2}\right) \operatorname{sign}\left(\xi_{yi}\right) \end{bmatrix}, \tag{3.17}$$

where $\hat{\boldsymbol{q}}_{ci} \triangleq \begin{bmatrix} \hat{\theta}_{ci} & \hat{x}_{ci} & \hat{y}_{ci} \end{bmatrix}^\top$ is the vector of consensus equilibrium state $\boldsymbol{q}_c$ computed by the i-th vehicle, and $\hat{\boldsymbol{q}}_{ci}(0) = \boldsymbol{q}_i(0)$. The terms K_o, κ_1, and κ_2 denote positive design coefficients, while the powers

$$\chi_1 \triangleq 1 - \bar{\chi}, \quad \chi_2 \triangleq 1 + \bar{\chi}, \tag{3.18}$$

where $\bar{\chi} \in (0, 1)$ is chosen by a designer, and

$$\boldsymbol{\xi}_i = \begin{bmatrix} \xi_{\theta i} \\ \xi_{xi} \\ \xi_{yi} \end{bmatrix} \triangleq \begin{bmatrix} \sum_{j \in \mathcal{N}_i} a_{ij} (\hat{\theta}_{ci} - \hat{\theta}_{cj}) \\ \sum_{j \in \mathcal{N}_i} a_{ij} (\hat{x}_{ci} - \hat{x}_{cj}) \\ \sum_{j \in \mathcal{N}_i} a_{ij} (\hat{y}_{ci} - \hat{y}_{cj}) \end{bmatrix}, \tag{3.19}$$

is the vector of the observation error, where a_{ij} are the elements of matrix $\boldsymbol{\mathcal{A}}$ defined in Section 1.4.2, guarantees that the consensus state $\boldsymbol{q}_c = \begin{bmatrix} \theta_c & x_c & y_c \end{bmatrix}^\top \in \mathbb{R}^3$ is a fixed-time stable equilibrium state with upper bound T_{co} of the settling time t_{so} of the observation error $\boldsymbol{\xi}_i$, that is: $\forall t \geq T_{co} \quad \boldsymbol{\xi}_i(t) = \mathbf{0} \implies \hat{\boldsymbol{q}}_{c1}(t) = \hat{\boldsymbol{q}}_{c2}(t) = \ldots = \hat{\boldsymbol{q}}_{cn}(t) = \boldsymbol{q}_c$.

Remark 20 *Please note that, to simplify the stability analysis, K_o, κ_1, κ_2, and $\bar{\chi}$ are taken to be the same for each vehicle.*

Proof. The proof will be presented separately for the undirected and directed communication topologies, and stability will be considered separately for each element of the error vector $\boldsymbol{\xi}_i$. Let us begin by considering the error $\xi_{\theta i}$ and noting that

$$\begin{aligned} \boldsymbol{\xi}_\theta \triangleq \begin{bmatrix} \xi_{\theta 1} \\ \xi_{\theta 2} \\ \vdots \\ \xi_{\theta n_v} \end{bmatrix} &\overset{(3.19)}{=} \begin{bmatrix} \sum_{j \in \mathcal{N}_1} a_{1j} (\hat{\theta}_{c1} - \hat{\theta}_{cj}) \\ \sum_{j \in \mathcal{N}_2} a_{2j} (\hat{\theta}_{c2} - \hat{\theta}_{cj}) \\ \vdots \\ \sum_{j \in \mathcal{N}_{n_v}} a_{n_v j} (\hat{\theta}_{cn_v} - \hat{\theta}_{cj}) \end{bmatrix} \\ &= \begin{bmatrix} \sum_{j=1}^{n_v} \ell_{1j} \hat{\theta}_{cj} \\ \sum_{j=1}^{n_v} \ell_{2j} \hat{\theta}_{cj} \\ \vdots \\ \sum_{j=1}^{n_v} \ell_{n_v j} \hat{\theta}_{cj} \end{bmatrix} = \boldsymbol{\mathcal{L}} \begin{bmatrix} \hat{\theta}_{c1} \\ \hat{\theta}_{c2} \\ \vdots \\ \hat{\theta}_{cn_v} \end{bmatrix} = \boldsymbol{\mathcal{L}} \hat{\boldsymbol{\theta}}_c, \end{aligned} \tag{3.20}$$

where $\hat{\boldsymbol{\theta}}_c \triangleq \begin{bmatrix} \hat{\theta}_{c1} & \hat{\theta}_{c2} & \ldots & \hat{\theta}_{cn_v} \end{bmatrix}^\top$.

Undirected communication topology: First, let us consider an undirected communication topology between the robots, associated with a connected graph $\mathcal{G}$, thus according to Section 1.4.2, the Laplacian matrix $\boldsymbol{\mathcal{L}}$ is symmetric.

Based on Lyapunov's method, the radially unbounded positive definite function

$$V_\theta \triangleq \frac{1}{n_v}\hat{\boldsymbol{\theta}}_c^\top \boldsymbol{\mathcal{L}}\hat{\boldsymbol{\theta}}_c \tag{3.21}$$

is chosen. Note that $V_\theta = 0 \iff \hat{\boldsymbol{\theta}}_c = \underline{\mathbf{1}}\theta_c$, since matrix $\boldsymbol{\mathcal{L}}$ has a zero rows sum, it can be observed that $\boldsymbol{\mathcal{L}}\hat{\boldsymbol{\theta}}_c = \mathbf{0} \iff \hat{\boldsymbol{\theta}}_c = \underline{\mathbf{1}}\theta_c$ where $\underline{\mathbf{1}} \triangleq \begin{bmatrix}1 & 1 & \dots & 1\end{bmatrix}^\top \in \mathbb{R}^n$ is the vector of ones. Next, the time derivative of (3.21) can be assessed as follows:

$$\begin{aligned}
\dot{V}_\theta &= \frac{2}{n_v}\hat{\boldsymbol{\theta}}_c^\top \boldsymbol{\mathcal{L}}\dot{\hat{\boldsymbol{\theta}}}_c \overset{(3.20)}{=} \frac{2}{n_v}\boldsymbol{\xi}_\theta^\top \dot{\hat{\boldsymbol{\theta}}}_c = \frac{2}{n_v}\sum_{i=1}^{n_v}\xi_{\theta i}\dot{\hat{\theta}}_{ci} \\
&\overset{(3.17)}{=} -\frac{2}{n_v}\sum_{i=1}^{n_v}\xi_{\theta i}K_o\left(\kappa_1|\xi_{\theta i}|^{\chi_1} + \kappa_2|\xi_{\theta i}|^{\chi_2}\right)\operatorname{sign}\left(\xi_{\theta i}\right) \\
&= -\frac{2K_o}{n_v}\sum_{i=1}^{n_v}\left(\kappa_1|\xi_{\theta i}|^{\chi_1+1} + \kappa_2|\xi_{\theta i}|^{\chi_2+1}\right) \\
&= -\frac{2K_o\kappa_1}{n_v}\sum_{i=1}^{n_v}|\xi_{\theta i}|^{\chi_1+1} - \frac{2K_o\kappa_2}{n_v}\sum_{i=1}^{n_v}|\xi_{\theta i}|^{\chi_2+1} \\
&\overset{(3.5)}{\leq} -2K_o\kappa_1\left(\frac{1}{n_v}\sum_{i=1}^{n_v}|\xi_{\theta i}|\right)^{\chi_1+1} - 2K_o\kappa_2\left(\frac{1}{n_v}\sum_{i=1}^{n_v}|\xi_{\theta i}|\right)^{\chi_2+1} \\
&\leq -2K_o\kappa_1\left(\frac{1}{n_v}\sqrt{\boldsymbol{\xi}_\theta^\top\boldsymbol{\xi}_\theta}\right)^{\chi_1+1} - 2K_o\kappa_2\left(\frac{1}{n_v}\sqrt{\boldsymbol{\xi}_\theta^\top\boldsymbol{\xi}_\theta}\right)^{\chi_2+1} \\
&= -2K_o\kappa_1\left(\frac{1}{{n_v}^2}\boldsymbol{\xi}_\theta^\top\boldsymbol{\xi}_\theta\right)^{\frac{\chi_1+1}{2}} - 2K_o\kappa_2\left(\frac{1}{{n_v}^2}\boldsymbol{\xi}_\theta^\top\boldsymbol{\xi}_\theta\right)^{\frac{\chi_2+1}{2}} \\
&\overset{(3.20)}{=} -2K_o\kappa_1\left(\frac{1}{{n_v}^2}\hat{\boldsymbol{\theta}}_c^\top\boldsymbol{\mathcal{L}}\boldsymbol{\mathcal{L}}\hat{\boldsymbol{\theta}}_c\right)^{\frac{\chi_1+1}{2}} - 2K_o\kappa_2\left(\frac{1}{{n_v}^2}\hat{\boldsymbol{\theta}}_c^\top\boldsymbol{\mathcal{L}}\boldsymbol{\mathcal{L}}\hat{\boldsymbol{\theta}}_c\right)^{\frac{\chi_2+1}{2}}.
\end{aligned} \tag{3.22}$$

Based on Lemma 9 one can observe that:

$$\begin{aligned}
\dot{V}_\theta &\overset{(3.9)}{\leq} -2K_o\kappa_1\left(\frac{\lambda_2(\boldsymbol{\mathcal{L}})}{{n_v}^2}\hat{\boldsymbol{\theta}}_c^\top\boldsymbol{\mathcal{L}}\hat{\boldsymbol{\theta}}_c\right)^{\frac{\chi_1+1}{2}} - 2K_o\kappa_2\left(\frac{\lambda_2(\boldsymbol{\mathcal{L}})}{{n_v}^2}\hat{\boldsymbol{\theta}}_c^\top\boldsymbol{\mathcal{L}}\hat{\boldsymbol{\theta}}_c\right)^{\frac{\chi_2+1}{2}} \\
&\overset{(3.18)}{=} -2K_o\kappa_1\left(\frac{\lambda_2(\boldsymbol{\mathcal{L}})}{{n_v}^2}\hat{\boldsymbol{\theta}}_c^\top\boldsymbol{\mathcal{L}}\hat{\boldsymbol{\theta}}_c\right)^{\frac{2-\bar{\chi}}{2}} - 2K_o\kappa_2\left(\frac{\lambda_2(\boldsymbol{\mathcal{L}})}{{n_v}^2}\hat{\boldsymbol{\theta}}_c^\top\boldsymbol{\mathcal{L}}\hat{\boldsymbol{\theta}}_c\right)^{\frac{2+\bar{\chi}}{2}} \\
&\overset{(3.21)}{=} -2K_o\kappa_1\left(\frac{\lambda_2(\boldsymbol{\mathcal{L}})}{n_v}V_\theta\right)^{1-\frac{\bar{\chi}}{2}} - 2K_o\kappa_2\left(\frac{\lambda_2(\boldsymbol{\mathcal{L}})}{n_v}V_\theta\right)^{1+\frac{\bar{\chi}}{2}},
\end{aligned} \tag{3.23}$$

where $\lambda_2(\boldsymbol{\mathcal{L}})$ is the second smallest eigenvalue of $\boldsymbol{\mathcal{L}}$. One can observe that $(1-\frac{\bar{\chi}}{2}) \in (0.5, 1)$ and $(1+\frac{\bar{\chi}}{2}) > 1$. Then, comparing (3.23) with (1.2) from Lemma 1, it can be concluded that the equilibrium point $\boldsymbol{\xi}_\theta = \mathbf{0}$ of the dynamics $\dot{\hat{\boldsymbol{\theta}}}_c$ is fixed-time stable. Next, by comparing (3.23) with (1.3), it can be observed that the upper bound T_{co} of the settling time t_{so} of the observation error can be expressed as follows:

$$T_{co} \overset{(1.3)}{=} \frac{n_v\pi}{2\bar{\chi}K_o\lambda_2(\boldsymbol{\mathcal{L}})\sqrt{\kappa_1\kappa_2}}. \tag{3.24}$$

Directed communication topology: Now, let us consider the directed communication topology. According to Section 1.4.2, $\boldsymbol{\mathcal{L}}$ is a nonsymmetric Laplacian matrix. First, let us define a symmetric positive semi-definite matrix

$$\boldsymbol{\mathcal{L}}_p \triangleq \mathscr{W}\boldsymbol{\mathcal{L}} + \boldsymbol{\mathcal{L}}^\top \mathscr{W}, \tag{3.25}$$

where $\mathscr{W} \triangleq \text{diag}\,(w_1, w_2, \ldots, w_n)$, while $\begin{bmatrix} w_1 & w_2 & \ldots & w_n \end{bmatrix}^\top \triangleq \boldsymbol{w}_0$ denotes the left zero unit eigenvector of $\boldsymbol{\mathcal{L}}$, that is $\boldsymbol{w}_0^\top \boldsymbol{\mathcal{L}} = \boldsymbol{0}$. Next, let us choose the radially unbounded positive definite function

$$V_\theta \triangleq \sum_{i=1}^{n_v} w_i \left(\frac{\kappa_1}{\chi_1 + 1} |\xi_{\theta i}|^{\chi_1 + 1} + \frac{\kappa_2}{\chi_2 + 1} |\xi_{\theta i}|^{\chi_2 + 1} \right), \tag{3.26}$$

whose time derivative can be determined as follows:

$$\begin{aligned} \dot{V}_\theta &= \sum_{i=1}^{n_v} \left(\kappa_1 |\xi_{\theta i}|^{\chi_1} + \kappa_2 |\xi_{\theta i}|^{\chi_2} \right) \text{sign}(\xi_{\theta i}) w_i \dot{\xi}_{\theta i} \\ &\overset{(3.17)}{=} -\frac{1}{K_o} \dot{\hat{\boldsymbol{\theta}}}_c^\top \mathscr{W} \dot{\boldsymbol{\xi}}_\theta \overset{(3.20)}{=} -\frac{1}{K_o} \dot{\hat{\boldsymbol{\theta}}}_c^\top \mathscr{W} \boldsymbol{\mathcal{L}} \dot{\hat{\boldsymbol{\theta}}}_c. \end{aligned} \tag{3.27}$$

Based on Lemma 5, one can observe that:

$$\dot{V}_\theta \overset{(3.27)}{=} -\frac{1}{2K_o} \dot{\hat{\boldsymbol{\theta}}}_c^\top \left(\mathscr{W}\boldsymbol{\mathcal{L}} + \boldsymbol{\mathcal{L}}^\top \mathscr{W} \right) \dot{\hat{\boldsymbol{\theta}}}_c \overset{(3.25)}{=} -\frac{1}{2K_o} \dot{\hat{\boldsymbol{\theta}}}_c^\top \boldsymbol{\mathcal{L}}_p \dot{\hat{\boldsymbol{\theta}}}_c \leq -\frac{k_1}{2K_o} \dot{\hat{\boldsymbol{\theta}}}_c^\top \dot{\hat{\boldsymbol{\theta}}}_c, \tag{3.28}$$

where $k_1 \triangleq \min_{\dot{\hat{\boldsymbol{\theta}}}_c \in \mathcal{R}} \dot{\hat{\boldsymbol{\theta}}}_c^\top \boldsymbol{\mathcal{L}}_p \dot{\hat{\boldsymbol{\theta}}}_c$, and $\mathcal{R} \triangleq \{\dot{\hat{\boldsymbol{\theta}}}_c : \dot{\hat{\boldsymbol{\theta}}}_c^\top \dot{\hat{\boldsymbol{\theta}}}_c = 1\}$. Next

$$\begin{aligned} \dot{V}_\theta &\overset{(3.28)}{\leq} -\frac{k_1}{2K_o} \dot{\hat{\boldsymbol{\theta}}}_c^\top \dot{\hat{\boldsymbol{\theta}}}_c = -\frac{k_1}{2K_o} \sum_{i=1}^{n_v} \dot{\hat{\theta}}_{ci}^2 \\ &\overset{(3.17)}{=} -\frac{k_1}{2K_o} \sum_{i=1}^{n_v} \Big(-K_o \left(\kappa_1 |\xi_{\theta i}|^{\chi_1} + \kappa_2 |\xi_{\theta i}|^{\chi_2} \right) \text{sign}(\xi_{\theta i}) \Big)^2 \\ &= -\frac{k_1}{2K_o} \sum_{i=1}^{n_v} K_o^2 \left(\kappa_1^2 |\xi_{\theta i}|^{2\chi_1} + 2\kappa_1\kappa_2 |\xi_{\theta i}|^{\chi_1 + \chi_2} + \kappa_2^2 |\xi_{\theta i}|^{2\chi_2} \right) \\ &= -\frac{k_1 K_o}{2} \left(\kappa_1^2 \sum_{i=1}^{n_v} |\xi_{\theta i}|^{2\chi_1} + 2\kappa_1\kappa_2 \sum_{i=1}^{n_v} |\xi_{\theta i}|^{\chi_1 + \chi_2} + \kappa_2^2 \sum_{i=1}^{n_v} |\xi_{\theta i}|^{2\chi_2} \right) \\ &\overset{(3.4)}{\leq} -\frac{k_1 K_o}{2} \left(\kappa_1^2 \left(\sum_{i=1}^{n_v} |\xi_{\theta i}| \right)^{2\chi_1} + 2\kappa_1\kappa_2 \sum_{i=1}^{n_v} |\xi_{\theta i}|^{\chi_1 + \chi_2} + \kappa_2^2 \sum_{i=1}^{n_v} |\xi_{\theta i}|^{2\chi_2} \right) \\ &\overset{(3.5)}{\leq} -\frac{k_1 K_o}{2} \left(\kappa_1^2 \left(\sum_{i=1}^{n_v} |\xi_{\theta i}| \right)^{2\chi_1} + 2\kappa_1\kappa_2 \left(\frac{1}{n_v} \right)^{\chi_1 + \chi_2 - 1} \left(\sum_{i=1}^{n_v} |\xi_{\theta i}| \right)^{\chi_1 + \chi_2} \right. \\ &\qquad \left. + \kappa_2^2 \left(\frac{1}{n_v} \right)^{2\chi_2 - 1} \left(\sum_{i=1}^{n_v} |\xi_{\theta i}| \right)^{2\chi_2} \right) \\ &\leq -\frac{k_1 k_2 K_o}{2} \left(\left(\sum_{i=1}^{n_v} |\xi_{\theta i}| \right)^{2\chi_1} + \left(\sum_{i=1}^{n_v} |\xi_{\theta i}| \right)^{\chi_1 + \chi_2} + \left(\sum_{i=1}^{n_v} |\xi_{\theta i}| \right)^{2\chi_2} \right), \end{aligned} \tag{3.29}$$

with $k_2 \triangleq \min \left\{ \kappa_1^2, 2\kappa_1\kappa_2 \left(\frac{1}{n_v} \right)^{\chi_1 + \chi_2 - 1}, \kappa_2^2 \left(\frac{1}{n_v} \right)^{2\chi_2 - 1} \right\}$.

Let us consider once again the function V_θ defined in (3.26):

$$\begin{aligned} V_\theta &\overset{(3.26)}{=} \sum_{i=1}^{n_v} w_i \left(\frac{\kappa_1}{\chi_1+1}|\xi_{\theta i}|^{\chi_1+1} + \frac{\kappa_2}{\chi_2+1}|\xi_{\theta i}|^{\chi_2+1} \right) \\ &\leq \bar{w} \sum_{i=1}^{n_v} \left(\frac{\kappa_1}{\chi_1+1}|\xi_{\theta i}|^{\chi_1+1} + \frac{\kappa_2}{\chi_2+1}|\xi_{\theta i}|^{\chi_2+1} \right), \end{aligned} \tag{3.30}$$

where $\bar{w} \triangleq \max\{w_1, w_2, \ldots, w_n\}$. Next, let us introduce the function

$$\begin{aligned} \bar{V}_\theta \triangleq & V_\theta^{\frac{2\chi_1}{\chi_1+1}} + V_\theta^{\frac{2\chi_2}{\chi_2+1}} \\ \overset{(3.30)}{\leq} & \left[\bar{w} \sum_{i=1}^{n_v} \left(\frac{\kappa_1}{\chi_1+1}|\xi_{\theta i}|^{\chi_1+1} + \frac{\kappa_2}{\chi_2+1}|\xi_{\theta i}|^{\chi_2+1} \right) \right]^{\frac{2\chi_1}{\chi_1+1}} \\ & + \left[\bar{w} \sum_{i=1}^{n_v} \left(\frac{\kappa_1}{\chi_1+1}|\xi_{\theta i}|^{\chi_1+1} + \frac{\kappa_2}{\chi_2+1}|\xi_{\theta i}|^{\chi_2+1} \right) \right]^{\frac{2\chi_2}{\chi_2+1}}. \end{aligned} \tag{3.31}$$

One can observe that $\frac{2\chi_1}{\chi_1+1} \in (0,1)$ and $\frac{2\chi_2}{\chi_2+1} > 1$. Then, based on Lemma 7, one can obtain:

$$\begin{aligned} \bar{V}_\theta \overset{(3.6)}{\leq} & \left[\bar{w} \sum_{i=1}^{n_v} \frac{\kappa_1}{\chi_1+1}|\xi_{\theta i}|^{\chi_1+1} \right]^{\frac{2\chi_1}{\chi_1+1}} + \left[\bar{w} \sum_{i=1}^{n_v} \frac{\kappa_2}{\chi_2+1}|\xi_{\theta i}|^{\chi_2+1} \right]^{\frac{2\chi_1}{\chi_1+1}} \\ & + \left[\bar{w} \sum_{i=1}^{n_v} \left(\frac{\kappa_1}{\chi_1+1}|\xi_{\theta i}|^{\chi_1+1} + \frac{\kappa_2}{\chi_2+1}|\xi_{\theta i}|^{\chi_2+1} \right) \right]^{\frac{2\chi_2}{\chi_2+1}} \\ \overset{(3.7)}{\leq} & \left[\bar{w} \sum_{i=1}^{n_v} \frac{\kappa_1}{\chi_1+1}|\xi_{\theta i}|^{\chi_1+1} \right]^{\frac{2\chi_1}{\chi_1+1}} + \left[\bar{w} \sum_{i=1}^{n_v} \frac{\kappa_2}{\chi_2+1}|\xi_{\theta i}|^{\chi_2+1} \right]^{\frac{2\chi_1}{\chi_1+1}} \\ & + 2^{\frac{\chi_2-1}{\chi_2+1}} \left[\bar{w} \sum_{i=1}^{n_v} \frac{\kappa_1}{\chi_1+1}|\xi_{\theta i}|^{\chi_1+1} \right]^{\frac{2\chi_2}{\chi_2+1}} + 2^{\frac{\chi_2-1}{\chi_2+1}} \left[\bar{w} \sum_{i=1}^{n_v} \frac{\kappa_2}{\chi_2+1}|\xi_{\theta i}|^{\chi_2+1} \right]^{\frac{2\chi_2}{\chi_2+1}} \\ = & \left[\frac{\bar{w}\kappa_1}{\chi_1+1} \sum_{i=1}^{n_v} |\xi_{\theta i}|^{\chi_1+1} \right]^{\frac{2\chi_1}{\chi_1+1}} + \left[\frac{\bar{w}\kappa_2}{\chi_2+1} \sum_{i=1}^{n_v} |\xi_{\theta i}|^{\chi_2+1} \right]^{\frac{2\chi_1}{\chi_1+1}} \\ & + 2^{\frac{\chi_2-1}{\chi_2+1}} \left[\frac{\bar{w}\kappa_1}{\chi_1+1} \sum_{i=1}^{n_v} |\xi_{\theta i}|^{\chi_1+1} \right]^{\frac{2\chi_2}{\chi_2+1}} + 2^{\frac{\chi_2-1}{\chi_2+1}} \left[\frac{\bar{w}\kappa_2}{\chi_2+1} \sum_{i=1}^{n_v} |\xi_{\theta i}|^{\chi_2+1} \right]^{\frac{2\chi_2}{\chi_2+1}} \\ \overset{(3.4)}{\leq} & \left[\frac{\bar{w}\kappa_1}{\chi_1+1} \left(\sum_{i=1}^{n_v} |\xi_{\theta i}| \right)^{\chi_1+1} \right]^{\frac{2\chi_1}{\chi_1+1}} + \left[\frac{\bar{w}\kappa_2}{\chi_2+1} \left(\sum_{i=1}^{n_v} |\xi_{\theta i}| \right)^{\chi_2+1} \right]^{\frac{2\chi_1}{\chi_1+1}} \\ & + 2^{\frac{\chi_2-1}{\chi_2+1}} \left[\frac{\bar{w}\kappa_1}{\chi_1+1} \sum_{i=1}^{n_v} |\xi_{\theta i}|^{\chi_1+1} \right]^{\frac{2\chi_2}{\chi_2+1}} + 2^{\frac{\chi_2-1}{\chi_2+1}} \left[\frac{\bar{w}\kappa_2}{\chi_2+1} \sum_{i=1}^{n_v} |\xi_{\theta i}|^{\chi_2+1} \right]^{\frac{2\chi_2}{\chi_2+1}} \\ \overset{(3.5)}{\leq} & \left[\frac{\bar{w}\kappa_1}{\chi_1+1} \left(\sum_{i=1}^{n_v} |\xi_{\theta i}| \right)^{\chi_1+1} \right]^{\frac{2\chi_1}{\chi_1+1}} + \left[\frac{\bar{w}\kappa_2}{\chi_2+1} \left(\sum_{i=1}^{n_v} |\xi_{\theta i}| \right)^{\chi_2+1} \right]^{\frac{2\chi_1}{\chi_1+1}} \\ & + 2^{\frac{\chi_2-1}{\chi_2+1}} \left[\frac{\bar{w}\kappa_1}{\chi_1+1} \left(\sum_{i=1}^{n_v} |\xi_{\theta i}| \right)^{\chi_1+1} \right]^{\frac{2\chi_2}{\chi_2+1}} + 2^{\frac{\chi_2-1}{\chi_2+1}} \left[\frac{\bar{w}\kappa_2}{\chi_2+1} \left(\sum_{i=1}^{n_v} |\xi_{\theta i}| \right)^{\chi_2+1} \right]^{\frac{2\chi_2}{\chi_2+1}} \end{aligned}$$

$$
\begin{aligned}
&= \left(\frac{\bar{w}\kappa_1}{\chi_1+1}\right)^{\frac{2\chi_1}{\chi_1+1}} \left(\sum_{i=1}^{n_v}|\xi_{\theta i}|\right)^{2\chi_1} + \left(\frac{\bar{w}\kappa_2}{\chi_2+1}\right)^{\frac{2\chi_1}{\chi_1+1}} \left(\sum_{i=1}^{n_v}|\xi_{\theta i}|\right)^{\frac{2\chi_1(\chi_2+1)}{\chi_1+1}} \\
&\quad + 2^{\frac{\chi_2-1}{\chi_2+1}} \left(\frac{\bar{w}\kappa_1}{\chi_1+1}\right)^{\frac{2\chi_2}{\chi_2+1}} \left(\sum_{i=1}^{n_v}|\xi_{\theta i}|\right)^{\frac{2\chi_2(\chi_1+1)}{\chi_2+1}} \\
&\quad + 2^{\frac{\chi_2-1}{\chi_2+1}} \left(\frac{\bar{w}\kappa_2}{\chi_2+1}\right)^{\frac{2\chi_2}{\chi_2+1}} \left(\sum_{i=1}^{n_v}|\xi_{\theta i}|\right)^{2\chi_2}. \qquad (3.32)
\end{aligned}
$$

Based on Lemma 8, let us derive the following inequalities:

$$
\begin{aligned}
\left(\sum_{i=1}^{n_v}|\xi_{\theta i}|\right)^{\frac{2\chi_1(\chi_2+1)}{\chi_1+1}} &= \left(\sum_{i=1}^{n_v}|\xi_{\theta i}|\right)^{\frac{2\chi_1(1-\chi_1)}{\chi_1+1}} \left(\sum_{i=1}^{n_v}|\xi_{\theta i}|\right)^{\frac{2\chi_1(\chi_1+\chi_2)}{\chi_1+1}} \\
&\le \frac{1-\chi_1}{\chi_1+1}\left(\sum_{i=1}^{n_v}|\xi_{\theta i}|\right)^{2\chi_1} + \frac{2\chi_1}{\chi_1+1}\left(\sum_{i=1}^{n_v}|\xi_{\theta i}|\right)^{\chi_1+\chi_2} \qquad (3.33)
\end{aligned}
$$

and

$$
\begin{aligned}
\left(\sum_{i=1}^{n_v}|\xi_{\theta i}|\right)^{\frac{2\chi_2(\chi_1+1)}{\chi_2+1}} &= \left(\sum_{i=1}^{n_v}|\xi_{\theta i}|\right)^{\frac{2\chi_1(\chi_2-1)}{\chi_2+1}} \left(\sum_{i=1}^{n_v}|\xi_{\theta i}|\right)^{\frac{2(\chi_1+\chi_2)}{\chi_2+1}} \\
&\le \frac{\chi_2-1}{\chi_2+1}\left(\sum_{i=1}^{n_v}|\xi_{\theta i}|\right)^{2\chi_1} + \frac{2}{\chi_2+1}\left(\sum_{i=1}^{n_v}|\xi_{\theta i}|\right)^{\chi_1+\chi_2}. \qquad (3.34)
\end{aligned}
$$

Then, substituting the above inequalities into (3.32), one obtains:

$$
\begin{aligned}
\bar{V}_\theta &\overset{(3.33)}{\le} \left(\frac{\bar{w}\kappa_1}{\chi_1+1}\right)^{\frac{2\chi_1}{\chi_1+1}} \left(\sum_{i=1}^{n_v}|\xi_{\theta i}|\right)^{2\chi_1} \\
&\quad + \left(\frac{\bar{w}\kappa_2}{\chi_2+1}\right)^{\frac{2\chi_1}{\chi_1+1}} \left[\frac{1-\chi_1}{\chi_1+1}\left(\sum_{i=1}^{n_v}|\xi_{\theta i}|\right)^{2\chi_1} + \frac{2\chi_1}{\chi_1+1}\left(\sum_{i=1}^{n_v}|\xi_{\theta i}|\right)^{\chi_1+\chi_2}\right] \\
&\quad + 2^{\frac{\chi_2-1}{\chi_2+1}} \left(\frac{\bar{w}\kappa_1}{\chi_1+1}\right)^{\frac{2\chi_2}{\chi_2+1}} \left(\sum_{i=1}^{n_v}|\xi_{\theta i}|\right)^{\frac{2\chi_2(\chi_1+1)}{\chi_2+1}} \\
&\quad + 2^{\frac{\chi_2-1}{\chi_2+1}} \left(\frac{\bar{w}\kappa_2}{\chi_2+1}\right)^{\frac{2\chi_2}{\chi_2+1}} \left(\sum_{i=1}^{n_v}|\xi_{\theta i}|\right)^{2\chi_2} \\
&\overset{(3.34)}{\le} \left(\frac{\bar{w}\kappa_1}{\chi_1+1}\right)^{\frac{2\chi_1}{\chi_1+1}} \left(\sum_{i=1}^{n_v}|\xi_{\theta i}|\right)^{2\chi_1} \\
&\quad + \left(\frac{\bar{w}\kappa_2}{\chi_2+1}\right)^{\frac{2\chi_1}{\chi_1+1}} \left[\frac{1-\chi_1}{\chi_1+1}\left(\sum_{i=1}^{n_v}|\xi_{\theta i}|\right)^{2\chi_1} + \frac{2\chi_1}{\chi_1+1}\left(\sum_{i=1}^{n_v}|\xi_{\theta i}|\right)^{\chi_1+\chi_2}\right] \\
&\quad + 2^{\frac{\chi_2-1}{\chi_2+1}} \left(\frac{\bar{w}\kappa_1}{\chi_1+1}\right)^{\frac{2\chi_2}{\chi_2+1}} \left[\frac{\chi_2-1}{\chi_2+1}\left(\sum_{i=1}^{n_v}|\xi_{\theta i}|\right)^{2\chi_1} + \frac{2}{\chi_2+1}\left(\sum_{i=1}^{n_v}|\xi_{\theta i}|\right)^{\chi_1+\chi_2}\right] \\
&\quad + 2^{\frac{\chi_2-1}{\chi_2+1}} \left(\frac{\bar{w}\kappa_2}{\chi_2+1}\right)^{\frac{2\chi_2}{\chi_2+1}} \left(\sum_{i=1}^{n_v}|\xi_{\theta i}|\right)^{2\chi_2}
\end{aligned}
$$

$$
\begin{aligned}
&= \underbrace{2^{\frac{\chi_2-1}{\chi_2+1}}\left(\frac{\bar{w}\kappa_2}{\chi_2+1}\right)^{\frac{2\chi_2}{\chi_2+1}}}_{\triangleq k_{31}}\left(\sum_{i=1}^{n_v}|\xi_{\theta i}|\right)^{2\chi_2} \\
&\quad + \underbrace{\left[\frac{2\chi_1}{\chi_1+1}\left(\frac{\bar{w}\kappa_2}{\chi_2+1}\right)^{\frac{2\chi_1}{\chi_1+1}} + \frac{2}{\chi_2+1}2^{\frac{\chi_2-1}{\chi_2+1}}\left(\frac{\bar{w}\kappa_1}{\chi_1+1}\right)^{\frac{2\chi_2}{\chi_2+1}}\right]}_{\triangleq k_{32}}\left(\sum_{i=1}^{n_v}|\xi_{\theta i}|\right)^{\chi_1+\chi_2} \\
&\quad + \underbrace{\left[\left(\frac{\bar{w}\kappa_1}{\chi_1+1}\right)^{\frac{2\chi_1}{\chi_1+1}} + \frac{1-\chi_1}{\chi_1+1}\left(\frac{\bar{w}\kappa_2}{\chi_2+1}\right)^{\frac{2\chi_1}{\chi_1+1}} + \frac{\chi_2-1}{\chi_2+1}2^{\frac{\chi_2-1}{\chi_2+1}}\left(\frac{\bar{w}\kappa_1}{\chi_1+1}\right)^{\frac{2\chi_2}{\chi_2+1}}\right]}_{\triangleq k_{33}} \\
&\quad \times \left(\sum_{i=1}^{n_v}|\xi_{\theta i}|\right)^{2\chi_1} \\
&= k_{31}\left(\sum_{i=1}^{n_v}|\xi_{\theta i}|\right)^{2\chi_2} + k_{32}\left(\sum_{i=1}^{n_v}|\xi_{\theta i}|\right)^{\chi_1+\chi_2} + k_{33}\left(\sum_{i=1}^{n_v}|\xi_{\theta i}|\right)^{2\chi_1} \\
&\leq k_3\left[\left(\sum_{i=1}^{n_v}|\xi_{\theta i}|\right)^{2\chi_2} + \left(\sum_{i=1}^{n_v}|\xi_{\theta i}|\right)^{\chi_1+\chi_2} + \left(\sum_{i=1}^{n_v}|\xi_{\theta i}|\right)^{2\chi_1}\right], \qquad (3.35)
\end{aligned}
$$

where $k_3 \triangleq \max\{k_{31}, k_{32}, k_{33}\} > 0$.

Now let us substitute (3.35) into (3.29), which results in

$$
\begin{aligned}
\dot{V}_\theta &\overset{(3.35)}{\leq} -\frac{k_1k_2K_o}{2k_3}\bar{V}_\theta \overset{(3.31)}{=} -\frac{k_1k_2K_o}{2k_3}\left(V_\theta^{\frac{2\chi_1}{\chi_1+1}} + V_\theta^{\frac{2\chi_2}{\chi_2+1}}\right) \\
&\overset{(3.18)}{=} -\frac{k_1k_2K_o}{2k_3}\left(V_\theta^{\frac{2(1-\bar{\chi})}{(1-\bar{\chi})+1}} + V_\theta^{\frac{2(1+\bar{\chi})}{(1+\bar{\chi})+1}}\right) \\
&= -\frac{k_1k_2K_o}{2k_3}\left(V_\theta^{\frac{2-2\bar{\chi}}{2-\bar{\chi}}} + V_\theta^{\frac{2+2\bar{\chi}}{2+\bar{\chi}}}\right). \qquad (3.36)
\end{aligned}
$$

One can observe that $\frac{2-2\bar{\chi}}{2-\bar{\chi}} \in (0,1)$ and $\frac{2+2\bar{\chi}}{2+\bar{\chi}} > 1$. Comparing (3.36) with (1.2) from Lemma 1, it can be concluded that the equilibrium point $\boldsymbol{\xi}_\theta = \mathbf{0}$ of the dynamics $\dot{\tilde{\boldsymbol{\theta}}}_c$ is fixed-time stable. Furthermore, comparing (3.36) with (1.4), the upper bound of the settling time can be determined as follows:

$$
T_{co} \overset{(1.4)}{=} \frac{k_3\left(4-\bar{\chi}^2\right)\Gamma\left(\frac{2+\bar{\chi}}{4}\right)\Gamma\left(\frac{2-\bar{\chi}}{4}\right)}{2k_1k_2K_o\bar{\chi}}, \qquad (3.37)
$$

where $\Gamma(\cdot)$ is the gamma function defined as $\Gamma(z) \triangleq \int_0^\infty e^{-t}t^{z-1}dt$. Hence, the analysis for $\boldsymbol{\xi}_\theta = \mathbf{0}$ is complete. It should be noted that stability proofs for $\boldsymbol{\xi}_x = \mathbf{0}$ and $\boldsymbol{\xi}_y = \mathbf{0}$ can be obtained in a analogous manner, since the dynamics $\dot{\hat{x}}_{ci}$ and $\dot{\hat{y}}_{ci}$ are defined analogously to $\dot{\hat{\theta}}_{ci}$ (cf. (3.17)),thus, they will be omitted here. ■

Remark 21 *An undirected communication topology is a special case of a directed communication topology, therefore the stability proof developed for directed communication topology will also be valid for undirected communication topology. However, it should also be noted that in the case of undirected communication topology, matrix*

$\mathcal{L}$ is symmetric, which results in a significantly simpler analysis, and thus may lead to a less conservative upper bound of the settling time.

Based on Theorem 3, it can be seen that after time $t_{so} \leq T_{co}$, the consensus equilibrium state $\boldsymbol{q}_c$ is known and thus the desired configuration $\boldsymbol{q}_{di} = \boldsymbol{q}_c + \boldsymbol{d}_i$ for each vehicle $i \in \mathcal{V}$ belonging to the multi-vehicle system is known.

3.3.2 Fixed-time VFO control algorithm

Let us now define the control law which guarantees that each vehicle will reach its desired configuration, that is, $\boldsymbol{q}_i(t) \to \boldsymbol{q}_{di}$. For this purpose, let us recall the set-point fixed-time VFO control law introduced in Section 2.2.2, as it is easily seen that for $t \geq t_{so}$, the task of creating a formation by a multi-vehicle system corresponds to the task of stabilization at a point for multiple vehicles simultaneously. Let us begin by defining the vector of error. It should be noted that, in this case, the desired configuration is unknown a priori and is estimated by the observers, thus the error should be expressed as

$$\hat{\boldsymbol{e}}_i(t) = \begin{bmatrix} \hat{e}_{\theta i}(t) \\ \hat{\boldsymbol{e}}_i(t) \end{bmatrix} = \begin{bmatrix} \hat{e}_{\theta i}(t) \\ \hat{e}_{xi}(t) \\ \hat{e}_{yi}(t) \end{bmatrix} \triangleq \begin{bmatrix} f_\theta\big(\hat{\theta}_{di}(t) - \theta_i(t)\big) \\ \hat{x}_{di}(t) - x_i(t) \\ \hat{y}_{di}(t) - y_i(t) \end{bmatrix}, \tag{3.38}$$

with $\begin{bmatrix} \hat{\theta}_{di} & \hat{x}_{di} & \hat{y}_{di} \end{bmatrix}^\top = \hat{\boldsymbol{q}}_{di} = \hat{\boldsymbol{q}}_{ci} + \boldsymbol{d}_i$, where $\hat{\boldsymbol{q}}_{ci}$ denotes the vector of the consensus equilibrium state estimated by the distributed observer of the i-th vehicle. It can therefore be concluded that $\forall i \in \mathcal{V}\ \forall t \geq t_{so}\ \hat{\boldsymbol{q}}_{ci}(t) = \boldsymbol{q}_c \implies \hat{\boldsymbol{q}}_{di}(t) = \boldsymbol{q}_{di} \implies \hat{\boldsymbol{e}}_i(t) = \boldsymbol{e}_i(t)$.

Then, let us recall the convergence vector field defined in (2.3):

$$\forall i \in \mathcal{V} \quad \hat{\boldsymbol{h}}_i = \begin{bmatrix} h_{\theta i} \\ \hat{\boldsymbol{h}}_i \end{bmatrix} \overset{(2.3)}{=} \begin{bmatrix} K_{ai}\left(|e_{ai}|^{\delta_{1i}} + |e_{ai}|^{\delta_{2i}}\right)\operatorname{sign}(e_{ai}) + \dot{\theta}_{aNi} \\ K_{pi}\left(\hat{\boldsymbol{e}}_i - \bar{\eta}_i \sigma_i \left\|\hat{\boldsymbol{e}}_i\right\| \bar{\boldsymbol{g}}_{2di}\right) \end{bmatrix}, \tag{3.39}$$

where K_{ai} and K_{pi} are positive design coefficients, $\bar{\boldsymbol{g}}_{2di} \triangleq \bar{\boldsymbol{g}}_2(\theta_{di}) = \begin{bmatrix} \cos\theta_{di} & \sin\theta_{di} \end{bmatrix}^\top$, $\sigma_i \in \{-1, 1\}$, $\bar{\eta}_i \in (0.5, 1)$ is related to the so-called *directing effect*, while the powers $\delta_{1i} \in (0, 1)$ and $\delta_{2i} > 1$ are defined as in (2.6). The term e_{ai} denotes the auxiliary orientation error of the i-th vehicle and is defined in (2.7), while $\dot{\theta}_{aNi}$ stands for the *nominal* time derivative of the auxiliary orientation θ_{ai} and is defined in (2.9). Please note that Assumption 1 also remains valid.

Analogously to Section 2.2.2, let us first formulate the nominal control law:

$$\boldsymbol{u}_{Ni} = \begin{bmatrix} u_{1Ni} \\ u_{2Ni} \end{bmatrix} \overset{(2.12)}{=} \begin{bmatrix} f_o K_{ai}\left(|e_{ai}|^{\delta_{1i}} + |e_{ai}|^{\delta_{2i}}\right)\operatorname{sign}(e_{ai}) + f_o \dot{\theta}_{aNi} \\ f_o f_{si} \hat{\rho}_i \left\|\hat{\boldsymbol{h}}_i\right\| \cos\alpha_i \end{bmatrix} \in \mathbb{R}^2, \tag{3.40}$$

with f_{si} defined for the i-th vehicle as in (2.15), that is

$$f_{si}(t) \overset{(2.15)}{=} \begin{cases} 0 & \text{if} \quad t < t_{sai} \\ 1 & \text{if} \quad t \geq t_{sai} \end{cases}, \tag{3.41}$$

where t_{sai} denotes the settling time of the auxiliary orientation error e_{ai} for the i-th vehicle, while

$$f_o(t) \triangleq \begin{cases} 0 & \text{if} \quad t < t_{so} \\ 1 & \text{if} \quad t \geq t_{so} \end{cases}, \tag{3.42}$$

and

$$\hat{\rho}_i \overset{(2.13)}{=} \begin{cases} \rho_{0i} \left(\left\| \hat{\tilde{\boldsymbol{e}}}_i \right\|^{\mu_{1i}} + \left\| \hat{\tilde{\boldsymbol{e}}}_i \right\|^{\mu_{2i}} \right) \left\| \hat{\boldsymbol{h}}_i \right\|^{-1} & \text{if } \left\| \hat{\tilde{\boldsymbol{e}}}_i(t) \right\| > \epsilon \\ 0 & \text{otherwise} \end{cases}, \tag{3.43}$$

where ρ_{0i} is a positive coefficient, while the powers μ_{1i} and μ_{2i} are defined as in (2.14). Note that ϵ is a small constant chosen by the designer and its value is the same for each vehicle to ensure similar control performance. The control law that satisifies the imposed control input constraints is obtained as a result of post-processing, that is, as a result of scaling the nominal control law $\boldsymbol{u}_{Ni}$ by a scaling function

$$s_i(t) \overset{(1.7)}{=} \left(\max \left\{ 1, \frac{|u_{1Ni}(t)|}{u_{1M}}, \frac{|u_{2Ni}(t)|}{u_{2M}} \right\} \right)^{-1} \in (0, 1), \tag{3.44}$$

where u_{1M} and u_{2M} denote the maximum permissible absolute angular and longitudinal velocities, respectively (cf. Section 1.3.2).

Remark 22 *In* (3.44)*, choosing the same constraints u_{1M} and u_{2M} for every vehicle was proposed. It should be noted that selecting different values of u_{1Mi} and u_{2Mi} for different vehicles will only result in changes in the maximum possible absolute velocities of individual vehicles and will not have a significant impact on the stability analysis or the control performance of the multi-vehicle system.*

Let us now formulate the appropriate theorem:

Theorem 4 (cf. Theorem 1) *For each vehicle $i \in \mathcal{V}$ with kinematics* (3.1)*, belonging to a distributed multi-vehicle system whose communication topology is described by a connected graph $\mathcal{G}$, application of the nominal VFO control law $\boldsymbol{u}_{Ni}(t)$ defined in* (3.40) *with the scaling function $s_i(t)$ introduced in* (3.44) *leads to the control law*

$$\boldsymbol{u}_i \triangleq s_i \boldsymbol{u}_{Ni} = \begin{bmatrix} s_i f_o K_{ai} \left(|e_{ai}|^{\delta_{1i}} + |e_{ai}|^{\delta_{2i}} \right) \operatorname{sign}(e_{ai}) + s_i f_o \dot{\theta}_{aNi} \\ s_i f_o f_{si} \hat{\rho}_i \left\| \hat{\boldsymbol{h}}_i \right\| \cos \alpha_i \end{bmatrix} \in \mathscr{U}, \tag{3.45}$$

which solves Problem 3 and ensures fixed-time stability of the equilibrium point of the closed-loop dynamics.

Proof. Please note that the proof can be provided in a similar manner to the proof presented for Theorem 1, thus it will be omitted here. ■

Remark 23 *Please note that the control algorithm presented in Section 3.3 operates in the three stages, and the transitions between the particular stages are scheduled by the functions* (3.41) *and* (3.42) *as follows:*

- *observation stage, in which the observation errors converge:*

$$\forall i \in \mathcal{V} \quad 0 \leq t < t_{so} < t_{sai} \implies f_{si}(t) \overset{(3.41)}{=} 0 \text{ and } f_o(t) \overset{(3.42)}{=} 0,$$

- *pre-orientation stage, in which the auxiliary orientation errors converge:*

$$\forall i \in \mathcal{V} \quad 0 < t_{so} \leq t < t_{sai} \implies f_{si}(t) \overset{(3.41)}{=} 0 \text{ and } f_o(t) \overset{(3.42)}{=} 1,$$

- *motion stage, in which the orientation and positional errors converge:*

$$\forall i \in \mathcal{V} \quad 0 < t_{so} < t_{sai} \leq t \implies f_{si}(t) \overset{(3.41)}{=} 1 \text{ and } f_o(t) \overset{(3.42)}{=} 1.$$

It should be noted that the only purpose of separating the pre-orientation stage from the motion stage is to enable the calculation of upper bounds of settling times a priori using the method presented in Section 2.2.3. If one is not interested in a priori estimation of these upper bounds, one may set $\forall i \in \mathcal{V}\ \forall t \geq 0\ f_{si}(t) = 1$ *and thereby include the pre-orientation stage in the motion stage.*

3.3.3 Results of numerical simulations

Numerical simulations were performed in the Matlab-Simulink environment, according to the scheme presented in Fig. 3.1. A fixed-step solver with a step size of 10^{-3} s was selected. The following observer parameters were selected: $K_o = \kappa_1 = \kappa_2 = 1$, and $\bar{\chi} = 0.2$, while the controller parameters were the same for each vehicle: $\forall i \in \mathcal{V}\ K_{pi} = 1$, $K_{ai} = 2$, $\rho_{0i} = 1$ $\bar{\eta}_i = 0.82$, and $\bar{\mu}_i = \bar{\delta}_i = 0.2$. Furthermore, σ_i were selected according to (2.4), while $\epsilon = 10^{-10}$ m, $u_{1M} = 3$ rad/s, and $u_{2M} = 0.5$ m/s.

A scenario with 5 vehicles was considered, with a directed communication topology described by graph $\mathcal{G}$ presented in Fig. 3.2 and by the following matrices:

$$\boldsymbol{\mathcal{A}} = \begin{bmatrix} 0 & 1 & 0 & 0 & 0 \\ 0 & 0 & 1 & 0 & 0 \\ 0 & 0 & 0 & 1 & 0 \\ 0 & 0 & 0 & 0 & 1 \\ 1 & 0 & 0 & 0 & 0 \end{bmatrix}, \quad \boldsymbol{\mathcal{L}} = \begin{bmatrix} 1 & -1 & 0 & 0 & 0 \\ 0 & 1 & -1 & 0 & 0 \\ 0 & 0 & 1 & -1 & 0 \\ 0 & 0 & 0 & 1 & -1 \\ -1 & 0 & 0 & 0 & 1 \end{bmatrix}.$$

The initial configurations of the vehicles were as follows:

$$\boldsymbol{q}_1(0) = \begin{bmatrix} 0 \\ 4 \\ 3 \end{bmatrix}, \ \boldsymbol{q}_2(0) = \begin{bmatrix} 0 \\ 4 \\ 4 \end{bmatrix}, \ \boldsymbol{q}_3(0) = \begin{bmatrix} \frac{\pi}{2} \\ -3 \\ 5 \end{bmatrix}, \ \boldsymbol{q}_4(0) = \begin{bmatrix} \pi \\ -3.5 \\ 0 \end{bmatrix}, \ \boldsymbol{q}_5(0) = \begin{bmatrix} -\frac{\pi}{2} \\ 3 \\ -3 \end{bmatrix}.$$

The obtained results are presented in Figs. 3.3 and 3.4. It can be seen that the observation errors shown in Figs. 3.3a–3.3c converge toward zero, and the settling time was 3.98 s, while the upper bound T_{co}, computed based on (3.37), is 33.77 s. Furthermore, it can be observed that the positional errors (see Figs. 3.4a and 3.4b), and the orientation error (see Fig. 3.4d) converge towards the vicinity of zero within a fixed time, while the auxiliary orientation error (see Fig. 3.4c), converge towards within a fixed time as well. Moreover, the control inputs satisfy the imposed constraints (see Figs. 3.4e and 3.4f) and each vehicle reaches its desired configuration with the prescribed accuracy (see Fig. 3.4g). It is worth noting the non-oscillatory and chattering-free nature of the control signals shown in Figs. 3.4e and 3.4f, as well as the oscillation-free trajectories of the vehicles visible in Fig. 3.4g.

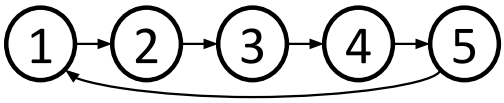

Figure 3.2 – Graph of the undirected communication topology used in simulations.

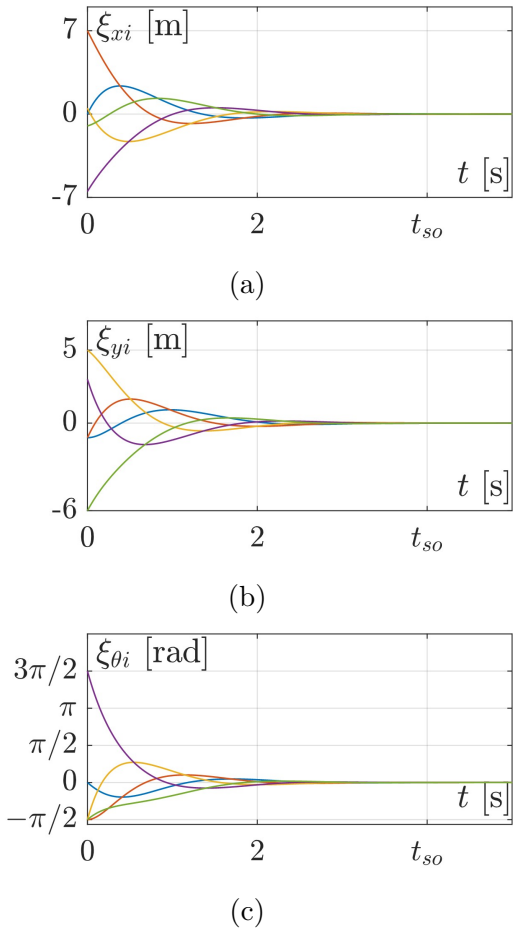

Figure 3.3 – Observation errors of distributed fixed-time observers, where $t_{so} = 3.98$ s denotes the observation error settling time.

Remark 24 *It should be noted that the results presented in Fig. 3.4 mainly concern the controller originally presented in Section 2.2.2, whereas the main contribution of this section is the proposition to use the distributed fixed-time observers, whose operation is shown in Fig. 3.3. However, it should be noted that the observers use only information about the initial configurations and operate before the vehicles start moving. Therefore, this section will not present experimental results, as they would mainly concern the control algorithm already discussed in Section 2.2.2 and not the observers, which are a novelty in this section.*

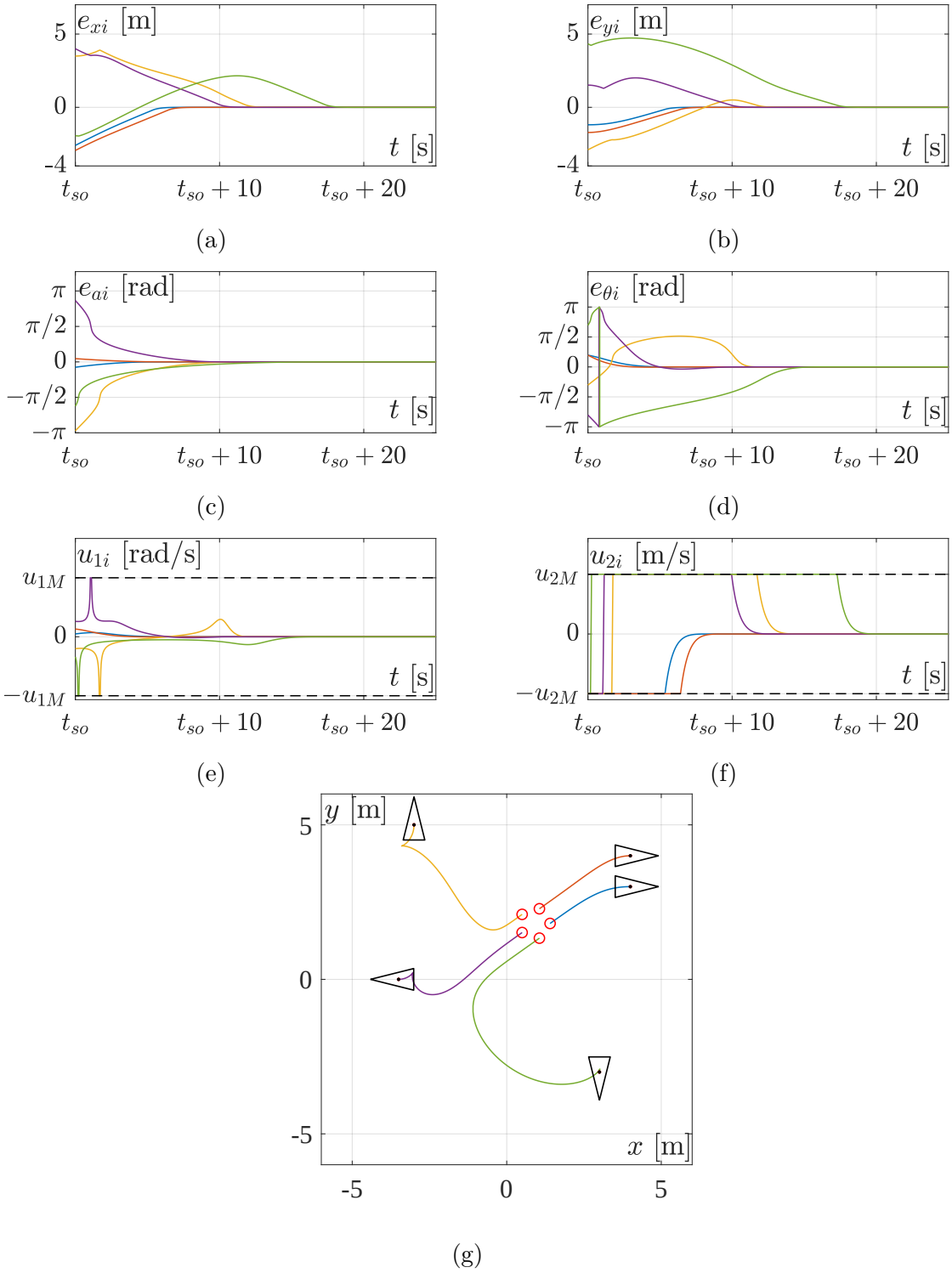

Figure 3.4 – Results of a numerical simulation for the observer-based formation control algorithm, where the solid triangles indicate the initial robot configurations, and the red circles represent the desired configurations determined by the observer, while $t_{so} = 3.98$ s is the observation error settling time, $u_{1M} = 3$ rad/s, and $u_{2M} = 0.5$ m/s.

3.3.4 Discussion on collision avoidance

An important aspect that is often discussed when considering multi-vehicle systems is collision avoidance. Although this issue is beyond the scope of the dissertation, based on the results presented in earlier sections and available literature, the features of the VFO methodology can be used to develop a method for detecting collisions with static obstacles whose positions are known *a priori*. The idea is to use so-called integral curves to predict the robot motion path and then determine the possibility of collision with a static obstacle by comparing their positions.

First, let us recall the definition of a parameterized integral curve from [27], which was already used in Section 2.2.3:

$$e_{xi}^*\left(e_{yi}^*, p_i^*(\bar{\boldsymbol{e}}_{0i})\right) \overset{(2.72)}{=} \frac{\sigma_i |e_{yi}^*|}{2}\left(\left(\frac{e_{yi}^*}{p_i^*(\bar{\boldsymbol{e}}_{0i})}\right)^{\bar{\eta}_i} - \left(\frac{e_{yi}^*}{p_i^*(\bar{\boldsymbol{e}}_{0i})}\right)^{-\bar{\eta}_i}\right), \tag{3.46}$$

where $\begin{bmatrix} e_{xi}^* & e_{yi}^* \end{bmatrix}^\top \triangleq \bar{\boldsymbol{e}}_i^*$ is a vector of positional coordinates determined analytically and expressed in the error space for the i-th vehicle, while

$$\forall e_{y0i} \neq 0 \quad p_i^*(\bar{\boldsymbol{e}}_{0i}) \overset{(2.73)}{=} e_{y0i} \exp\left(\frac{1}{\bar{\eta}_i}\left|\operatorname{arsinh}\left(\frac{e_{x0i}}{e_{y0i}}\right)\right|\right). \tag{3.47}$$

The predicted motion path is determined by computing the value of e_{xi}^* for $e_{yi}^* \in (0, e_{y0i}]$ if $e_{y0i} > 0$, or for $e_{yi}^* \in [e_{y0i}, 0)$ if $e_{y0i} < 0$. It is assumed that the static obstacle is enclosed within a circle. The radius of this circle is defined as the sum of the smallest radius of a circle enclosing the obstacle and the smallest radius of a circle enclosing the robot. The coordinates of the static obstacle are assumed to be known *a priori*, thus, the coordinates of the circle containing the obstacle are known as well. By comparing the positional coordinates of the predicted path with those of this circle, one can determine whether the path is collision-free, since no collision occurs if the predicted path remains outside the circle.

It should be noted that in (3.46) and (3.47) a design coefficient $\bar{\eta}_i \in (0.5, 1)$ is used, which is related to the so-called *directing effect* and influences the shape of the robots path (cf. Fig. 3.5). Therefore, if a collision is detected, the designer has a possibility to change the value of $\bar{\eta}_i$, which will cause a (slight) change in the predicted motion path and thus may lead to finding a collision-free path (cf. Fig. 3.6). It should be noted, as described in Section 2.2.3, that $\forall i \in \mathcal{V}\ \forall t \geq t_{sai} \quad \bar{\boldsymbol{e}}_i^* \equiv \bar{\boldsymbol{e}}_i$, therefore, thanks to the function f_{si} (3.41) which schedules the *pre-orientation* stage and the *motion* stage, the vehicle will follow the predicted path in nominal conditions, that is, in the absence of disturbances.

The performance of the proposed method was validated through numerical simulation in the Mathlab-Simulink environment with a fixed-step solver using a step size of 10^{-3} s. A multi-vehicle system consisting of four vehicles communicating via an undirected communication topology was considered. Five static obstacles were placed within the vehicles' operational space, which, for simplicity, were modeled as circles of different radii. The parameters of the controller and observers were chosen similarly to those in Section 3.3.3, with the exception of $\bar{\eta}_i$, whose values were determined using the proposed collision detection method. As can be seen in Fig. 3.7, a collision-free path was found for each vehicle, and the desired formation was established. The parameter values determined by the collision checking method

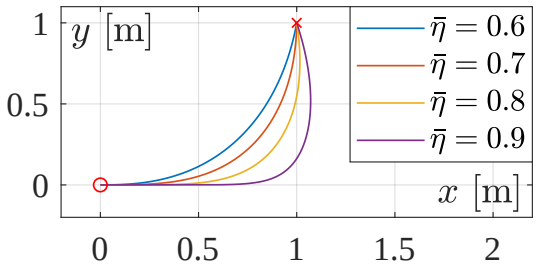

Figure 3.5 – Exemplary predicted robot motion paths for $\bar{\eta} \in \{0.6, 0.7, 0.8, 0.9\}$. The initial position is marked with a red cross, while the desired configuration, marked with a red circle, is $\boldsymbol{q}_d = \mathbf{0}$.

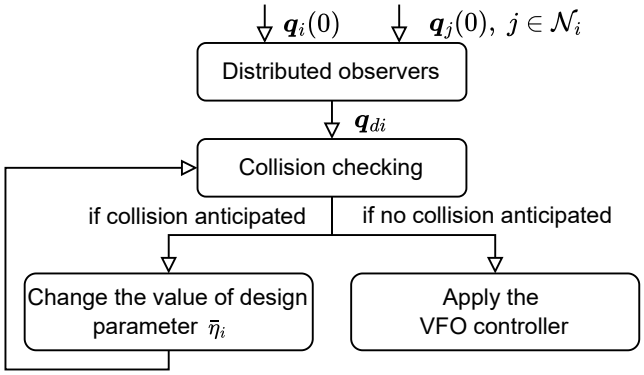

Figure 3.6 – Overview of the proposed observer-based algorithm for the i-th vehicle, with collision checking algorithm.

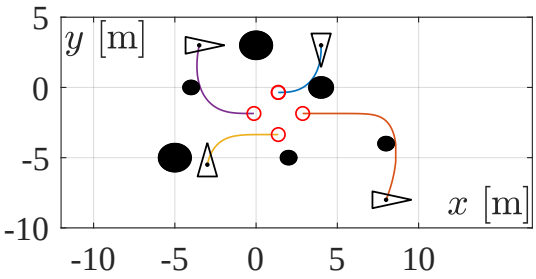

Figure 3.7 – Exemplary results of collision checking in a case where collision-free paths are found. The black circles indicate obstacles, the red circles represent the desired positions for each vehicle determined by the distributed observer, and the solid triangles indicate the initial configurations of the vehicles.

were as follows:

$$\bar{\eta}_1 = 0.64, \quad \bar{\eta}_2 = 0.9, \quad \bar{\eta}_3 = 0.82, \quad \bar{\eta}_4 = 0.72.$$

Remark 25 *It should be noted that the proposed method always allows one to verify whether a path is collision-free, but does not always guarantee collision avoidance. That is why it is called a collision detection method rather than a collision avoidance method. Furthermore, the proposed method is effective only in cases when vehicles move along paths predicted based on the knowledge of integral curves, that is, when*

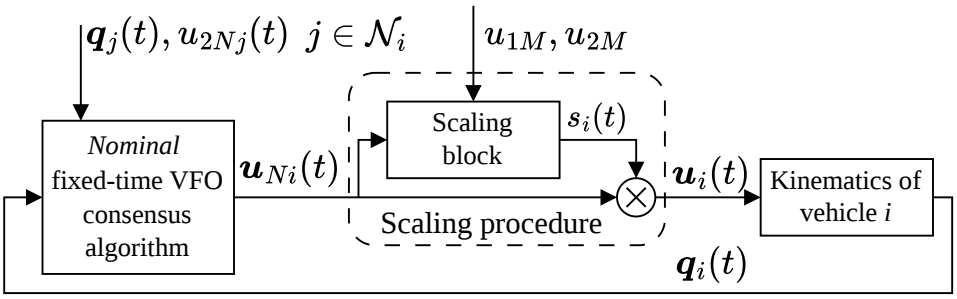

Figure 3.8 – Scheme of the control system for the consensus-based formation control approach for the i-th vehicle.

the auxiliary orientation error e_{ai} is zero at the beginning of the movement and remains zero until the end of the movement.

3.4 Consensus-based formation control

The second proposed algorithm involves the direct use of the consensus mechanism to appropriately define system errors, and then formulate a control law within the VFO design methodology, which will lead to the creation of a formation by the multi-vehicle system even though the consensus equilibrium state remains unknown. First, the design of a *nominal* control algorithm will be presented – that is, the one which does not meet the imposed control input constraints. Then, a scaling procedure that uses the scaling function s will be presented (see Section 1.3.2), yielding control inputs that satisfy the imposed constraints. This control algorithm will be developed according to the conceptual scheme of the control system shown in Fig. 3.8.

3.4.1 Distributed fixed-time VFO consensus algorithm

Let us define the vector of system errors for each vehicle $i \in \mathcal{V}$ as follows:

$$\boldsymbol{e}_i(t) = \begin{bmatrix} e_{\theta i}(t) \\ \bar{\boldsymbol{e}}_i(t) \end{bmatrix} = \begin{bmatrix} e_{\theta i}(t) \\ e_{xi}(t) \\ e_{yi}(t) \end{bmatrix} \triangleq \begin{bmatrix} f_\theta\big(\theta_d - \theta_i(t)\big) \\ -\sum_{j\in\mathcal{N}_i}\ a_{ij}\big(x_i(t) - d_{xi} - x_j(t) + d_{xj}\big) \\ -\sum_{j\in\mathcal{N}_i}\ a_{ij}\big(y_i(t) - d_{yi} - y_j(t) + d_{yj}\big) \end{bmatrix}, \tag{3.48}$$

where the desired orientation $\forall i \in \mathcal{V} \theta_{di} = \theta_d$ is the same for each vehicle and is selected by the designer, a_{ij} denotes the elements of adjacency matrix $\boldsymbol{\mathcal{A}}$ introduced in Section 1.4.2, while $\begin{bmatrix} d_{xi}\ d_{yi} \end{bmatrix}^\top \triangleq \boldsymbol{d}_i$.

Remark 26 *It should be noted that the designer may choose θ_d arbitrarily based on some prior knowledge of the environment, the task, or the robot configurations, or may use a tool to determine this value based on the initial orientations of the vehicles – for example, the observer presented in Section 3.3.1.*

Let us also define $\boldsymbol{d}_x \triangleq \begin{bmatrix} d_{x1}\ d_{x2}\ \dots\ d_{xn_v} \end{bmatrix}^\top$, $\boldsymbol{d}_y \triangleq \begin{bmatrix} d_{y1}\ d_{y2}\ \dots\ d_{yn_v} \end{bmatrix}^\top$, and $\bar{\boldsymbol{q}} \triangleq \begin{bmatrix} \boldsymbol{x}^\top\ \boldsymbol{y}^\top \end{bmatrix}^\top$, with $\boldsymbol{x} \triangleq \begin{bmatrix} x_1\ x_2\ \dots\ x_{n_v} \end{bmatrix}^\top$ and $\boldsymbol{y} \triangleq \begin{bmatrix} y_1\ y_2\ \dots\ y_{n_v} \end{bmatrix}^\top$. Then, one can

rewrite the positional error in a matrix form:

$$\bar{\boldsymbol{e}} \triangleq \begin{bmatrix}\boldsymbol{e}_x\\ \boldsymbol{e}_y\end{bmatrix} \triangleq \begin{bmatrix} e_{x1}\\ \vdots\\ e_{xn_v}\\ e_{y1}\\ \vdots\\ e_{yn_v}\end{bmatrix} \overset{(3.48)}{=} \begin{bmatrix} -\sum_{j\in\mathcal{N}_1}\ a_{1j}(x_1-d_{x1}-x_j+d_{xj})\\ \vdots\\ -\sum_{j\in\mathcal{N}_n}\ a_{n_vj}(x_{n_v}-d_{xn_v}-x_j+d_{xj})\\ -\sum_{j\in\mathcal{N}_1}\ a_{1j}(y_1-d_{y1}-y_j+d_{yj})\\ \vdots\\ -\sum_{j\in\mathcal{N}_n}\ a_{n_vj}(y_{n_v}-d_{yn_v}-y_j+d_{yj})\end{bmatrix}$$
$$= \begin{bmatrix} -\sum_{j=1}^{n_v}\ \ell_{1j}(x_j-d_{xj})\\ \vdots\\ -\sum_{j=1}^{n_v}\ \ell_{n_vj}(x_j-d_{xj})\\ -\sum_{j=1}^{n_v}\ \ell_{1j}(y_j-d_{yj})\\ \vdots\\ -\sum_{j=1}^{n_v}\ \ell_{n_vj}(y_j-d_{yj})\end{bmatrix} = \begin{bmatrix}-\boldsymbol{\mathcal{L}}(\boldsymbol{x}-\boldsymbol{d}_x)\\ -\boldsymbol{\mathcal{L}}(\boldsymbol{y}-\boldsymbol{d}_y)\end{bmatrix} = -\boldsymbol{\mathcal{L}}_q \underbrace{\left(\bar{\boldsymbol{q}}-\begin{bmatrix}\boldsymbol{d}_x\\ \boldsymbol{d}_y\end{bmatrix}\right)}_{\triangleq\boldsymbol{\xi}_q}, \tag{3.49}$$

where ℓ_{ij} is an element of matrix $\boldsymbol{\mathcal{L}}$ presented in Section 1.4.2, while

$$\boldsymbol{\mathcal{L}}_q \triangleq \begin{bmatrix}\boldsymbol{\mathcal{L}} & 0\\ 0 & \boldsymbol{\mathcal{L}}\end{bmatrix}. \tag{3.50}$$

Each agent will reach its desired configuration in the formation once the consensus is achieved, that is $\boldsymbol{\xi}_q \to \boldsymbol{\xi}_c$, where $\boldsymbol{\xi}_c \triangleq \begin{bmatrix}x_c\underline{\mathbf{1}} & y_c\underline{\mathbf{1}}\end{bmatrix}^\top$ is the consensus equilibrium state, which is constant but unknown *a priori*. Moreover, the time derivative of the positional error $\bar{\boldsymbol{e}}$ can be derived as

$$\dot{\bar{\boldsymbol{e}}}_N = -\boldsymbol{\mathcal{L}}_q\dot{\bar{\boldsymbol{q}}}_N = \begin{bmatrix}-\boldsymbol{\mathcal{L}}\dot{\boldsymbol{x}}_N\\ -\boldsymbol{\mathcal{L}}\dot{\boldsymbol{y}}_N\end{bmatrix} = \begin{bmatrix} -\sum_{j=1}^{n_v}\ell_{1j}\dot{x}_{Nj}\\ \vdots\\ -\sum_{j=1}^{n_v}\ell_{n_vj}\dot{x}_{Nj}\\ -\sum_{j=1}^{n_v}\ell_{1j}\dot{y}_{Nj}\\ \vdots\\ -\sum_{j=1}^{n_v}\ell_{n_vj}\dot{y}_{Nj}\end{bmatrix}$$
$$\overset{(1.6)}{=} \begin{bmatrix} -\sum_{j=1}^{n_v}\ell_{1j}u_{2Nj}\cos\theta_j\\ \vdots\\ -\sum_{j=1}^{n_v}\ell_{n_vj}u_{2Nj}\cos\theta_j\\ -\sum_{j=1}^{n_v}\ell_{1j}u_{2Nj}\sin\theta_j\\ \vdots\\ -\sum_{j=1}^{n_v}\ell_{n_vj}u_{2Nj}\sin\theta_j\end{bmatrix}. \tag{3.51}$$

It should be noted that the subscript N indicates that the particular value is obtained based on the nominal control input.

Next, according to the VFO design methodology, the convergence vector field for the i-th vehicle can be defined as follows:

$$\boldsymbol{h}_i = \begin{bmatrix}h_{\theta i}\\ h_{xi}\\ h_{yi}\end{bmatrix} = \begin{bmatrix}h_{\theta i}\\ \bar{\boldsymbol{h}}_i\end{bmatrix} \overset{(2.3)}{=} \begin{bmatrix}K_a\left(|e_{ai}|^{\delta_1}+|e_{ai}|^{\delta_2}\right)\operatorname{sign}(e_{ai})+\dot{\theta}_{aNi}\\ K_p\left(\bar{\boldsymbol{e}}_i-\bar{\eta}\sigma_i\|\bar{\boldsymbol{e}}_i\|\bar{\boldsymbol{g}}_{2d}\right)\end{bmatrix}, \tag{3.52}$$

where K_a and K_p are positive design coefficients, $\bar{\eta} \in (0,1)$, $\bar{\boldsymbol{g}}_{2d} \triangleq \bar{\boldsymbol{g}}_2(\theta_d) = \begin{bmatrix}\cos\theta_d & \sin\theta_d\end{bmatrix}^\top$, while σ_i and the powers δ_1, δ_2 are defined by analogy to (2.4) and (2.6), respectively, that is:

$$\sigma_i \overset{(2.4)}{=} \operatorname{sgn}\Big(e_{xi}(0)\cos\theta_d + e_{yi}(0)\sin\theta_d\Big) \in \{-1,1\},$$

and

$$\delta_1 \overset{(2.6)}{=} 1-\bar{\delta}, \qquad \delta_2 \overset{(2.6)}{=} 1+\bar{\delta}, \qquad \bar{\delta} \in (0,1).$$

The term

$$e_{ai}(t) \overset{(2.7)}{=} \theta_{ai}(t) - \theta_i(t) \tag{3.53}$$

denotes the auxiliary orientation error for i-th vehicle, while

$$\theta_{ai}\left(\bar{\boldsymbol{h}}_i(\bar{\boldsymbol{e}}_i)\right) \overset{(2.8)}{=} \begin{cases} \operatorname{Atan2c}\left(\sigma_i h_{yi}(\bar{\boldsymbol{e}}_i), \sigma_i h_{xi}(\bar{\boldsymbol{e}}_i)\right) & \text{if } \|\bar{\boldsymbol{e}}_i(t)\| > \epsilon \\ \theta_{a\epsilon i} & \text{otherwise} \end{cases} \tag{3.54}$$

means the auxiliary orientation of the i-ith vehicle, while $\operatorname{Atan2c}(\cdot,\cdot)$ is a continuous version of $\operatorname{Atan2}(\cdot,\cdot)$ and it was introduced in Section 2.2.2. The nominal time derivative $\dot{\theta}_{aNi}$ of the auxiliary orientation θ_{ai} for the i-th vehicle can be expressed as follows:

$$\dot{\theta}_{aNi}\left(\bar{\boldsymbol{h}}_i(\bar{\boldsymbol{e}}_i)\right) \overset{(2.9)}{=} \begin{cases} \dfrac{\dot{h}_{yNi}(\bar{\boldsymbol{e}}_i)h_{xi}(\bar{\boldsymbol{e}}_i) - \dot{h}_{xNi}(\bar{\boldsymbol{e}}_i)h_{yi}(\bar{\boldsymbol{e}}_i)}{\left\|\bar{\boldsymbol{h}}_i(\bar{\boldsymbol{e}}_i)\right\|^2} & \text{if } \|\bar{\boldsymbol{e}}_i(t)\| > \epsilon \\ 0 & \text{otherwise} \end{cases}, \tag{3.55}$$

where

$$\dot{\bar{\boldsymbol{h}}}_{Ni} = \begin{bmatrix}\dot{h}_{xNi} \\ \dot{h}_{yNi}\end{bmatrix} \overset{(2.10)}{=} K_p\left(\dot{\bar{\boldsymbol{e}}}_{Ni} - \bar{\eta}\sigma_i \frac{\bar{\boldsymbol{e}}_i^\top \dot{\bar{\boldsymbol{e}}}_{Ni}}{\|\bar{\boldsymbol{e}}_i\|}\bar{\boldsymbol{g}}_{2d}\right) \tag{3.56}$$

denotes the nominal time derivative of the positional subvector $\bar{\boldsymbol{h}}_i$ of the convergence vector field $\boldsymbol{h}_i$ for the i-th vehicle, while $\dot{\bar{\boldsymbol{e}}}_{Ni} = \begin{bmatrix}-\boldsymbol{\mathcal{L}}\dot{x}_{Ni} & -\boldsymbol{\mathcal{L}}\dot{y}_{Ni}\end{bmatrix}$.

Next, let us recall the definition of function

$$\rho_i(\bar{\boldsymbol{e}}_i) \overset{(2.13)}{=} \begin{cases} \rho_0\left(\|\bar{\boldsymbol{e}}_i\|^{\mu_1} + \|\bar{\boldsymbol{e}}_i\|^{\mu_2}\right)\left\|\bar{\boldsymbol{h}}_i(\bar{\boldsymbol{e}}_i)\right\|^{-1} & \text{if } \|\bar{\boldsymbol{e}}_i(t)\| > \epsilon \\ 0 & \text{otherwise} \end{cases}, \tag{3.57}$$

with $\rho_0 > 0$ and

$$\mu_1 \overset{(2.14)}{=} 1-\bar{\mu}, \qquad \mu_2 \overset{(2.14)}{=} 1+\bar{\mu}, \qquad \bar{\mu} \in (0,1),$$

and finally, let us define the nominal VFO control law for the i-th vehicle as follows:

$$\boldsymbol{u}_{Ni} = \begin{bmatrix}u_{1Ni} \\ u_{2Ni}\end{bmatrix} \triangleq \begin{bmatrix}h_{\theta i} \\ \rho_i \bar{\boldsymbol{h}}_i^\top \bar{\boldsymbol{g}}_2(\theta_i)\end{bmatrix} = \begin{bmatrix}K_a\left(|e_{ai}|^{\delta_1} + |e_{ai}|^{\delta_2}\right)\operatorname{sign}(e_{ai}) + \dot{\theta}_{aNi} \\ \rho_i \left\|\bar{\boldsymbol{h}}_i\right\| \cos\alpha_i\end{bmatrix}, \tag{3.58}$$

where $u_{1Ni} \in \mathbb{R}$ is called the *nominal orienting control*, while $u_{2Ni} \in \mathbb{R}$ is the *nominal pushing control*, while $\alpha_i \triangleq \angle\left(\bar{\boldsymbol{h}}_i, \bar{\boldsymbol{g}}_2(\theta_i)\right)$.

Remark 27 *Please note that for the purposes of the stability analysis that will be presented later, the values of the design coefficients K_p, K_a, $\bar{\eta}$, ρ_0, $\bar{\delta}$, and $\bar{\mu}$ are selected uniformly across all vehicles.*

Remark 28 *Note that* (3.52) *corresponds to* (2.3)*, while* (3.58) *is similar to* (2.12)*. This is consistent with the intuition that the problem of creating formation by a multi-vehicle system corresponds to the problem of set-point stabilization for a single vehicle. In the VFO methodology, changing the definition of the convergence vector field allows for a completion of various control problems. In this case, altering the definition of system errors, while keeping the convergence vector field unchanged, enables the resolution of the corresponding consensus control problem.*

Now, as in Section 2.2.2, the control law $\boldsymbol{u}_i \in \mathscr{U}$ that satisfies the imposed constraints will be obtained through post-processing, that is, by rescaling the nominal control law (3.58) with the scaling function

$$s_i(t) \overset{(1.7)}{=} \left(\max \left\{ 1, \frac{|u_{1Ni}(t)|}{u_{1M}}, \frac{|u_{2Ni}(t)|}{u_{2M}} \right\} \right)^{-1} \in (0,1). \tag{3.59}$$

Remark 29 (cf. Remark 22) *In* (3.59)*, choosing the same constraints u_{1M} and u_{2M} for every vehicle was proposed. It should be noted that selecting different values of u_{1Mi} and u_{2Mi} for different vehicles will only result in changes in the maximum possible absolute velocities of individual vehicles and will not have a significant impact on the stability analysis or the control performance of the multi-vehicle system.*

Let us formulate the appropriate theorem:

Theorem 5 *For a distributed multi-vehicle system consisting of n_v vehicles whose kinematics is given by* (1.6) *and the communication topology is undirected, applying the nominal control law $\boldsymbol{u}_i \in \mathbb{R}^2$ defined in* (3.58) *with the scaling function s_i introduced in* (3.59) *leads to a control law*

$$\forall i \in \mathscr{V} \quad \boldsymbol{u}_i \triangleq s_i \boldsymbol{u}_{Ni} \overset{(3.58)}{=} \begin{bmatrix} s_i K_a \left(|e_{ai}|^{\delta_1} + |e_{ai}|^{\delta_2} \right) \operatorname{sign}(e_{ai}) + s_i \dot{\theta}_{aNi} \\ s_i \rho_i \left\| \bar{\boldsymbol{h}}_i \right\| \cos \alpha_i \end{bmatrix} \in \mathscr{U}, \tag{3.60}$$

that satisfies the imposed control input constraints and solves Problem 3 in fixed time.

Proof. Stability proof will be presented separately for an equilibrium point of the auxiliary orientation error dynamics and for an equilibrium point of the positional error dynamics.

Auxiliary orientation error: Let us begin by looking at the dynamics of the auxiliary orientation error:

$$\begin{aligned} \dot{e}_{ai} &\overset{(3.53)}{=} \dot{\theta}_{ai} - \dot{\theta}_i \overset{(1.6)}{=} \dot{\theta}_{ai} - u_{1i} \\ &\overset{(3.60)}{=} -s_i K_a \left(|e_{ai}|^{\delta_1} + |e_{ai}|^{\delta_2} \right) \operatorname{sign}(e_{ai}) + \dot{\theta}_{ai} - s_i \dot{\theta}_{aNi}, \end{aligned} \tag{3.61}$$

where

$$\dot{\theta}_{ai}\left(\bar{\boldsymbol{h}}_i(\bar{\boldsymbol{e}}_i) \right) \overset{(3.55)}{=} \begin{cases} \dfrac{\dot{h}_{yi}(\bar{\boldsymbol{e}}_i) h_{xi}(\bar{\boldsymbol{e}}_i) - \dot{h}_{xi}(\bar{\boldsymbol{e}}_i) h_{yi}(\bar{\boldsymbol{e}}_i)}{\left\| \bar{\boldsymbol{h}}_i(\bar{\boldsymbol{e}}_i) \right\|^2} & \text{if } \|\bar{\boldsymbol{e}}_i(t)\| > \epsilon \\ 0 & \text{otherwise} \end{cases}, \tag{3.62}$$

means the time derivative of the auxiliary orientation θ_{ai} for the i-th vehicle, determined in the case of constrained control inputs, while

$$\dot{\bar{\boldsymbol{h}}}_i = \begin{bmatrix} \dot{h}_{xi} \\ \dot{h}_{yi} \end{bmatrix} \overset{(3.56)}{=} K_p \left(\dot{\bar{\boldsymbol{e}}}_i - \bar{\eta}\sigma_i \frac{\bar{\boldsymbol{e}}_i^\top \dot{\bar{\boldsymbol{e}}}_i}{\|\bar{\boldsymbol{e}}_i\|} \bar{\boldsymbol{g}}_{2d} \right) \tag{3.63}$$

denote the time derivative of the positional subvector $\bar{\boldsymbol{h}}_i$ of the convergence vector field, and

$$\begin{aligned} \dot{\bar{\boldsymbol{e}}}_i = \begin{bmatrix} \dot{e}_{xi} \\ \dot{e}_{yi} \end{bmatrix} &\overset{(3.51)}{=} \begin{bmatrix} -\sum_{j=1}^{n_v} \ell_{ij} \dot{x}_j \\ -\sum_{j=1}^{n_v} \ell_{ij} \dot{y}_j \end{bmatrix} \overset{(1.6)}{=} \begin{bmatrix} -\sum_{j=1}^{n_v} \ell_{ij} u_{2j} \cos\theta_j \\ -\sum_{j=1}^{n_v} \ell_{ij} u_{2j} \sin\theta_j \end{bmatrix} \\ &\overset{(3.60)}{=} \begin{bmatrix} -\sum_{j=1}^{n_v} \ell_{ij} s_j u_{2Nj} \cos\theta_j \\ -\sum_{j=1}^{n_v} \ell_{ij} s_j u_{2Nj} \sin\theta_j \end{bmatrix} = -\sum_{j=1}^{n_v} \ell_{ij} s_j u_{2Nj} \bar{\boldsymbol{g}}_2(\theta_j) \end{aligned} \tag{3.64}$$

is the time derivative of the positional error $\bar{\boldsymbol{e}}_i$, calculated using the constrained control signals. One can observe that, based on (3.63) and (3.64), the term $\dot{\theta}_{ai}$ from (3.62) can be rewritten as follows for $\|\bar{\boldsymbol{e}}_i\| > \epsilon$:

$$\begin{aligned} \dot{\theta}_{ai} &\overset{(3.62)}{=} \left(\dot{h}_{yi} h_{xi} - \dot{h}_{xi} h_{yi} \right) \left\| \bar{\boldsymbol{h}}_i \right\|^{-2} \\ &\overset{(3.63)}{=} K_p \left(\left(\dot{e}_{yi} - \bar{\eta}\sigma_i \frac{\bar{\boldsymbol{e}}_i^\top \dot{\bar{\boldsymbol{e}}}_i}{\|\bar{\boldsymbol{e}}_i\|} \sin\theta_d \right) h_{xi} - \left(\dot{e}_{xi} - \bar{\eta}\sigma_i \frac{\bar{\boldsymbol{e}}_i^\top \dot{\bar{\boldsymbol{e}}}_i}{\|\bar{\boldsymbol{e}}_i\|} \cos\theta_d \right) h_{yi} \right) \left\| \bar{\boldsymbol{h}}_i \right\|^{-2} \\ &= K_p \left(\dot{e}_{yi} h_{xi} - \bar{\eta}\sigma_i \frac{\bar{\boldsymbol{e}}_i^\top \dot{\bar{\boldsymbol{e}}}_i}{\|\bar{\boldsymbol{e}}_i\|} \sin\theta_d h_{xi} - \dot{e}_{xi} h_{yi} + \bar{\eta}\sigma_i \frac{\bar{\boldsymbol{e}}_i^\top \dot{\bar{\boldsymbol{e}}}_i}{\|\bar{\boldsymbol{e}}_i\|} \cos\theta_d h_{yi} \right) \left\| \bar{\boldsymbol{h}}_i \right\|^{-2} \\ &\overset{(3.64)}{=} K_p \left(-h_{xi} \sum_{j=1}^{n_v} \ell_{ij} s_j u_{2Nj} \sin\theta_j + \bar{\eta}\sigma_i \sin\theta_d h_{xi} \sum_{j=1}^{n_v} \ell_{ij} s_j u_{2Nj} \frac{\bar{\boldsymbol{e}}_i^\top \bar{\boldsymbol{g}}_2(\theta_j)}{\|\bar{\boldsymbol{e}}_i\|} \right. \\ &\quad \left. + h_{yi} \sum_{j=1}^{n_v} \ell_{ij} s_j u_{2Nj} \cos\theta_j - \bar{\eta}\sigma_i \cos\theta_d h_{yi} \sum_{j=1}^{n_v} \ell_{ij} s_j u_{2Nj} \frac{\bar{\boldsymbol{e}}_i^\top \bar{\boldsymbol{g}}_2(\theta_j)}{\|\bar{\boldsymbol{e}}_i\|} \right) \left\| \bar{\boldsymbol{h}}_i \right\|^{-2} \\ &= \sum_{j=1}^{n_v} s_j \ell_{ij} u_{2Nj} K_p \left\| \bar{\boldsymbol{h}}_i \right\|^{-2} \left(-h_{xi} \sin\theta_j + \bar{\eta}\sigma_i \sin\theta_d h_{xi} \frac{\bar{\boldsymbol{e}}_i^\top \bar{\boldsymbol{g}}_2(\theta_j)}{\|\bar{\boldsymbol{e}}_i\|} \right. \\ &\quad \left. + h_{yi} \cos\theta_j - \bar{\eta}\sigma_i \cos\theta_d h_{yi} \frac{\bar{\boldsymbol{e}}_i^\top \bar{\boldsymbol{g}}_2(\theta_j)}{\|\bar{\boldsymbol{e}}_i\|} \right) \\ &= \sum_{j=1}^{n_v} s_j \ell_{ij} \theta_{aj}^*, \end{aligned} \tag{3.65}$$

where

$$\begin{aligned} \theta_{aj}^* \triangleq u_{2Nj} K_p \left\| \bar{\boldsymbol{h}}_i \right\|^{-2} &\left(-h_{xi} \sin\theta_j + \bar{\eta}\sigma_i \sin\theta_d h_{xi} \frac{\bar{\boldsymbol{e}}_i^\top \bar{\boldsymbol{g}}_2(\theta_j)}{\|\bar{\boldsymbol{e}}_i\|} \right. \\ &\left. + h_{yi} \cos\theta_j - \bar{\eta}\sigma_i \cos\theta_d h_{yi} \frac{\bar{\boldsymbol{e}}_i^\top \bar{\boldsymbol{g}}_2(\theta_j)}{\|\bar{\boldsymbol{e}}_i\|} \right). \end{aligned} \tag{3.66}$$

Meanwhile, it should be noted that for the nominal case, one can obtain:

$$s_i \dot{\theta}_{aNi} \overset{(3.55)}{=} \begin{cases} s_i \dfrac{\dot{h}_{yNi} h_{xi} - \dot{h}_{xNi} h_{yi}}{\left\| \bar{\boldsymbol{h}}_i \right\|^2} & \text{if } \|\bar{\boldsymbol{e}}_i(t)\| > \epsilon \\ 0 & \text{otherwise} \end{cases}, \tag{3.67}$$

with

$$\dot{\bar{\boldsymbol{h}}}_{Ni} = \begin{bmatrix} \dot{h}_{xNi} \\ \dot{h}_{yNi} \end{bmatrix} \overset{(3.56)}{=} K_p \left(\dot{\bar{\boldsymbol{e}}}_{Ni} - \bar{\eta}\sigma_i \frac{\bar{\boldsymbol{e}}_i^\top \dot{\bar{\boldsymbol{e}}}_{Ni}}{\|\bar{\boldsymbol{e}}_i\|} \bar{\boldsymbol{g}}_{2d} \right), \tag{3.68}$$

while

$$\begin{aligned} \dot{\bar{\boldsymbol{e}}}_{Ni} = \begin{bmatrix} \dot{e}_{xNi} \\ \dot{e}_{yNi} \end{bmatrix} &\overset{(3.51)}{=} \begin{bmatrix} -\sum_{j=1}^{n_v} \ell_{ij} \dot{x}_{jN} \\ -\sum_{j=1}^{n_v} \ell_{ij} \dot{y}_{jN} \end{bmatrix} \overset{(1.6)}{=} \begin{bmatrix} -\sum_{j=1}^{n_v} \ell_{ij} u_{2Nj} \cos\theta_j \\ -\sum_{j=1}^{n_v} \ell_{ij} u_{2Nj} \sin\theta_j \end{bmatrix} \\ &= -\sum_{j=1}^{n_v} \ell_{ij} u_{2Nj} \bar{\boldsymbol{g}}_2(\theta_j). \end{aligned} \tag{3.69}$$

Next, based on (3.68) and (3.69), the term $s_i \dot{\theta}_{aNi}$ from (3.55) can be rewritten as follows for $\|\bar{\boldsymbol{e}}_i\| > \epsilon$:

$$\begin{aligned} s_i \dot{\theta}_{aNi} &\overset{(3.55)}{=} s_i \left(\dot{h}_{yNi} h_{xi} - \dot{h}_{xNi} h_{yi} \right) \left\| \bar{\boldsymbol{h}}_i \right\|^{-2} \\ &\overset{(3.68)}{=} s_i K_p \left(\left(\dot{e}_{yNi} - \bar{\eta}\sigma_i \frac{\bar{\boldsymbol{e}}_i^\top \dot{\bar{\boldsymbol{e}}}_{Ni}}{\|\bar{\boldsymbol{e}}_i\|} \sin\theta_d \right) h_{xi} \right. \\ &\quad \left. - \left(\dot{e}_{xNi} - \bar{\eta}\sigma_i \frac{\bar{\boldsymbol{e}}_i^\top \dot{\bar{\boldsymbol{e}}}_{Ni}}{\|\bar{\boldsymbol{e}}_i\|} \cos\theta_d \right) h_{yi} \right) \left\| \bar{\boldsymbol{h}}_i \right\|^{-2} \\ &\overset{(3.69)}{=} s_i K_p \left(-h_{xi} \sum_{j=1}^{n_v} \ell_{ij} u_{2Nj} \sin\theta_j + \bar{\eta}\sigma_i \sin\theta_d h_{xi} \sum_{j=1}^{n_v} \ell_{ij} u_{2Nj} \frac{\bar{\boldsymbol{e}}_i^\top \bar{\boldsymbol{g}}_2(\theta_j)}{\|\bar{\boldsymbol{e}}_i\|} \right. \\ &\quad \left. + h_{yi} \sum_{j=1}^{n_v} \ell_{ij} u_{2Nj} \cos\theta_j - \bar{\eta}\sigma_i \cos\theta_d h_{yi} \sum_{j=1}^{n_v} \ell_{ij} u_{2Nj} \frac{\bar{\boldsymbol{e}}_i^\top \bar{\boldsymbol{g}}_2(\theta_j)}{\|\bar{\boldsymbol{e}}_i\|} \right) \left\| \bar{\boldsymbol{h}}_i \right\|^{-2} \\ &= s_i \sum_{j=1}^{n_v} \ell_{ij} u_{2Nj} K_p \left\| \bar{\boldsymbol{h}}_i \right\|^{-2} \left(-h_{xi} \sin\theta_j + \bar{\eta}\sigma_i \sin\theta_d h_{xi} \frac{\bar{\boldsymbol{e}}_i^\top \bar{\boldsymbol{g}}_2(\theta_j)}{\|\bar{\boldsymbol{e}}_i\|} \right. \\ &\quad \left. + h_{yi} \cos\theta_j - \bar{\eta}\sigma_i \cos\theta_d h_{yi} \frac{\bar{\boldsymbol{e}}_i^\top \bar{\boldsymbol{g}}_2(\theta_j)}{\|\bar{\boldsymbol{e}}_i\|} \right) \\ &\overset{(3.65)}{=} s_i \sum_{j=1}^{n_v} \ell_{ij} \theta_{aj}^* = \sum_{j=1}^{n_v} s_i \ell_{ij} \theta_{aj}^*. \end{aligned} \tag{3.70}$$

Then, based on (3.65) and (3.70), one can observe that:

$$\dot{\theta}_{ai} - s_i \dot{\theta}_{aNi} = \sum_{j=1}^{n_v} s_j \ell_{ij} \theta_{aj}^* - \sum_{j=1}^{n_v} s_i \ell_{ij} \theta_{aj}^* = \sum_{j=1}^{n_v} (s_j - s_i) \ell_{ij} \theta_{aj}^*, \tag{3.71}$$

and (3.61) can be rewritten as follows:

$$\dot{e}_{ai} \overset{(3.61)}{=} -s_i K_a \left(|e_{ai}|^{\delta_1} + |e_{ai}|^{\delta_2} \right) \operatorname{sign}(e_{ai}) + \sum_{j=1}^{n_v} (s_j - s_i) \ell_{ij} \theta_{aj}^*. \tag{3.72}$$

Therefore, it should be noted that if $\forall j \in \mathcal{N}_i$ $s_j(t) \neq s_i(t)$, then $e_{ai} = 0$ is not an equilibrium point of the dynamics (3.72). However, it can be observed that the finite-time escape effect cannot occur since $s_i \in (0, 1]$, $s_j \in (0, 1]$, $(s_j - s_i) \in (-1, 1)$, ℓ_{ij} is a constant, and $\theta_{aj}^* < \infty$. Furthermore, if the difference between s_i and s_j is sufficiently small, the value of e_{ai} will converge to some small vicinity of zero, and the control performance will be satisfactory. Moreover, since the scaling function s

tends to become 1, ultimately $\forall i \in \mathscr{V}\ s_i = 1$ will be obtained, and thus $e_{ai} = 0$ will be the equilibrium point. However, if it is ensured in advance that $e_{ai} = 0$ is the equilibrium point of dynamics (3.72), the broadly understood control performance will be significantly better, that is, the transient states will be characterized by the absence of oscillations in the vehicle motion trajectories. Thus, let us formulate the following assumption:

Assumption 6 *After the time instant $0 \leq t_s^* < \infty$, the values of the scaling functions of each vehicle are equal, that is:*

$$\forall t \geq t_s^* \quad \forall i \in \mathscr{V}\ s_i(t) = \bar{s}(t). \tag{3.73}$$

Remark 30 *It should be noted that the next section will present a method which will ensure that Assumption 6 is satisfied in practical application.*

Next, one can observe that by applying Assumption 6 to (3.61) one can obtain:

$$\forall t \geq t_s^* \quad \dot{e}_{ai} = -\bar{s}K_a \left(|e_{ai}|^{\delta_1} + |e_{ai}|^{\delta_2}\right) \operatorname{sign}(e_{ai}), \tag{3.74}$$

which allows concluding that $e_{ai} = 0$ is the equilibrium point of the auxiliary orientation error dynamics $\forall t \geq t_s^*$. Furthermore, it should be noted that (3.74) corresponds to (2.21) and thus the rest of the stability analysis for the equilibrium point $e_{ai} = 0$ proceeds analogously to that shown in the proof for Theorem 1, hence the rest of the proof will be omitted here.

Positional error: Let us consider the dynamics of positional error:

$$\dot{\bar{\boldsymbol{e}}} \overset{(3.51)}{=} -\boldsymbol{\mathcal{L}}_q \dot{\bar{\boldsymbol{q}}} = -\boldsymbol{\mathcal{L}}_q \boldsymbol{u}_2^*(\bar{\boldsymbol{e}}), \tag{3.75}$$

where $\boldsymbol{u}_2^*(\bar{\boldsymbol{e}}) \triangleq \begin{bmatrix} u_{21}(\bar{\boldsymbol{e}}_1)\cos\theta_1 & \dots & u_{2n}(\bar{\boldsymbol{e}}_n)\cos\theta_n & u_{21}(\bar{\boldsymbol{e}}_1)\sin\theta_1 & \dots u_{2n}(\bar{\boldsymbol{e}}_n)\sin\theta_n \end{bmatrix}^\top$, with $\bar{\boldsymbol{e}}$ and $\bar{\boldsymbol{e}}_i$ defined in (3.49) and (3.48), respectively, while

$$\forall \|\bar{\boldsymbol{e}}_i\| > \epsilon \quad u_{2i} \overset{(3.60)}{=} s_i \rho_i \left\|\bar{\boldsymbol{h}}_i\right\| \cos\alpha_i \overset{(2.13)}{=} s_i \rho_0 \left(\|\bar{\boldsymbol{e}}_i\|^{\mu_1} + \|\bar{\boldsymbol{e}}_i\|^{\mu_2}\right) \cos\alpha_i. \tag{3.76}$$

Since $\boldsymbol{\mathcal{L}}$ has zero row sums, it follows that

$$\boldsymbol{\mathcal{L}}\underline{\mathbf{1}} = \mathbf{0},$$

where $\underline{\mathbf{1}}$ is the vector of ones. Hence, one can observe that

$$\dot{\bar{\boldsymbol{e}}} \overset{(3.75)}{=} \mathbf{0} \implies \boldsymbol{u}_2^*(\bar{\boldsymbol{e}}) = \begin{bmatrix} z_{ux}^* \underline{\mathbf{1}} \\ z_{uy}^* \underline{\mathbf{1}} \end{bmatrix},$$

which implies that the vehicles are moving in the same direction with the same longitudinal velocity, that is,

$$\boldsymbol{u}_2 \triangleq \begin{bmatrix} u_{21} \\ \vdots \\ u_{2n_v} \end{bmatrix} = z_u \underline{\mathbf{1}},$$

where z_{ux}^*, z_{uy}^*, and z_u are constant scalars. Based on (3.76), one can conclude that

$$\boldsymbol{u}_2 = z_u \underline{\mathbf{1}} \implies \begin{bmatrix} \boldsymbol{e}_x \\ \boldsymbol{e}_y \end{bmatrix} = \begin{bmatrix} z_x \underline{\mathbf{1}} \\ z_y \underline{\mathbf{1}} \end{bmatrix},$$

where z_x and z_y are constants. However, since matrix $\boldsymbol{\mathcal{L}}$ is symmetric and has zero row sums, its left null space is spanned by $\underline{\mathbf{1}}$. Thus, the equation

$$\begin{bmatrix} -\boldsymbol{\mathcal{L}}(\boldsymbol{x} - \boldsymbol{d}_x) \\ -\boldsymbol{\mathcal{L}}(\boldsymbol{y} - \boldsymbol{d}_y) \end{bmatrix} \overset{(3.49)}{=} \begin{bmatrix} \boldsymbol{e}_x \\ \boldsymbol{e}_y \end{bmatrix} = \begin{bmatrix} z_x \underline{\mathbf{1}} \\ z_y \underline{\mathbf{1}} \end{bmatrix},$$

has a solution only if

$$z_x = z_y = 0 \implies \begin{bmatrix} \boldsymbol{e}_x \\ \boldsymbol{e}_y \end{bmatrix} = \mathbf{0} \implies \boldsymbol{u}_2^* = \mathbf{0}.$$

Therefore, one can conclude that $\dot{\bar{\boldsymbol{e}}} \overset{(3.75)}{=} \mathbf{0} \iff \boldsymbol{u}_2^*(\bar{\boldsymbol{e}}) \overset{(3.76)}{=} \mathbf{0} \iff \bar{\boldsymbol{e}} \overset{(3.49)}{=} -\boldsymbol{\mathcal{L}}_q \boldsymbol{\xi}_q = \mathbf{0}$ and, since matrix $\boldsymbol{\mathcal{L}}$ has zero row sums, one can observe that:

$$\boldsymbol{\mathcal{L}}_q \boldsymbol{\xi}_q = \mathbf{0} \iff \boldsymbol{\xi}_q = \boldsymbol{\xi}_c = \begin{bmatrix} x_c \underline{\mathbf{1}} \\ y_c \underline{\mathbf{1}} \end{bmatrix}, \tag{3.77}$$

where x_c and y_c denote the coordinates of the consensus equilibrium state. Thus, it can be seen that the equilibrium point $\bar{\boldsymbol{e}} = \begin{bmatrix} \boldsymbol{e}_x & \boldsymbol{e}_y \end{bmatrix}^\top = \mathbf{0}$ of positional error dynamics corresponds to the consensus equilibrium state $\boldsymbol{\xi}_q = \boldsymbol{\xi}_c$, which means that positional error dynamics reach equilibrium if and only if consensus is achieved.

For the purposes of further analysis, let us recall several definitions originally derived in the proof for Theorem 1:

$$\dot{\bar{\boldsymbol{q}}}_i \overset{(2.34)}{=} -s_i \rho_i \boldsymbol{v}_{2i} + s_i \rho_i K_p \bar{\boldsymbol{e}}_i + s_i \rho_i \boldsymbol{v}_{1i}, \tag{3.78}$$

with

$$\boldsymbol{v}_{1i} \triangleq -K_p \bar{\eta} \sigma_i \|\bar{\boldsymbol{e}}_i\| \bar{\boldsymbol{g}}_{2d} \tag{3.79}$$

and

$$\boldsymbol{v}_{2i} \triangleq \bar{\boldsymbol{h}}_i - \frac{1}{\rho_i} u_{2Ni} \bar{\boldsymbol{g}}_2(\theta_i). \tag{3.80}$$

Moreover, it should be noted that:

$$\|\boldsymbol{v}_{2i}\| \overset{(2.35)}{=} \left\|\bar{\boldsymbol{h}}_i\right\| \sqrt{1 - \cos^2 \alpha_i}, \tag{3.81}$$

and

$$\left\|\bar{\boldsymbol{h}}_i\right\| \overset{(2.40)}{\leq} K_p (1 + \bar{\eta}) \|\bar{\boldsymbol{e}}_i\|. \tag{3.82}$$

Then, let us introduce the following positive definite function:

$$V_p \triangleq \frac{1}{2} \boldsymbol{\xi}_q^\top \boldsymbol{\mathcal{L}}_q \boldsymbol{\xi}_q \tag{3.83}$$

It should be noted that $V_p = 0 \iff \boldsymbol{\mathcal{L}}_q \boldsymbol{\xi}_q = \mathbf{0}$, since $\boldsymbol{\mathcal{L}}$ has zero row sums (cf. Section 1.4.2). The time derivative of (3.83) can be derived as follows:

$$\dot{V}_p = \boldsymbol{\xi}_q^\top \boldsymbol{\mathcal{L}}_q \dot{\boldsymbol{\xi}}_q \overset{(3.49)}{=} \boldsymbol{\xi}_q^\top \boldsymbol{\mathcal{L}}_q \dot{\bar{\boldsymbol{q}}} \overset{(3.49)}{=} -\bar{\boldsymbol{e}}^\top \dot{\bar{\boldsymbol{q}}} = -\sum_{i \in \mathscr{V}} \bar{\boldsymbol{e}}_i^\top \dot{\bar{\boldsymbol{q}}}_i$$

$$
\begin{aligned}
&\overset{(3.78)}{=} -\sum_{i\in\mathscr{V}} \bar{\boldsymbol{e}}_i^\top \left(-s_i\rho_i\boldsymbol{v}_{2i} + s_i\rho_i K_p\bar{\boldsymbol{e}}_i + s_i\rho_i\boldsymbol{v}_{1i}\right)\\
&= -\sum_{i\in\mathscr{V}} s_i\rho_i\left(-\bar{\boldsymbol{e}}_i^\top\boldsymbol{v}_{2i} + K_p\bar{\boldsymbol{e}}_i^\top\bar{\boldsymbol{e}}_i + \bar{\boldsymbol{e}}_i^\top\boldsymbol{v}_{1i}\right)\\
&= \sum_{i\in\mathscr{V}} s_i\rho_i\left(\bar{\boldsymbol{e}}_i^\top\boldsymbol{v}_{2i} - K_p\|\bar{\boldsymbol{e}}_i\|^2 - \bar{\boldsymbol{e}}_i^\top\boldsymbol{v}_{1i}\right)\\
&= \sum_{i\in\mathscr{V}} s_i\rho_i\Big(-K_p\|\bar{\boldsymbol{e}}_i\|^2 + \|\bar{\boldsymbol{e}}_i\|\|\boldsymbol{v}_{2i}\|\cos\big(\angle(\bar{\boldsymbol{e}}_i,\boldsymbol{v}_{2i})\big) - \|\bar{\boldsymbol{e}}_i\|\|\boldsymbol{v}_{1i}\|\cos\big(\angle(\bar{\boldsymbol{e}}_i,\boldsymbol{v}_{1i})\big)\Big)\\
&\le \sum_{i\in\mathscr{V}} s_i\rho_i\left(-K_p\|\bar{\boldsymbol{e}}_i\|^2 + \|\bar{\boldsymbol{e}}_i\|\|\boldsymbol{v}_{2i}\| + \|\bar{\boldsymbol{e}}_i\|\|\boldsymbol{v}_{1i}\|\right)\\
&\overset{(3.81)}{=} \sum_{i\in\mathscr{V}} s_i\rho_i\left(-K_p\|\bar{\boldsymbol{e}}_i\|^2 + \|\bar{\boldsymbol{e}}_i\|\left\|\bar{\boldsymbol{h}}_i\right\|\sqrt{1-\cos^2\alpha_i} + \|\bar{\boldsymbol{e}}_i\|\|\boldsymbol{v}_{1i}\|\right)\\
&= \sum_{i\in\mathscr{V}} s_i\rho_i\left(-K_p\|\bar{\boldsymbol{e}}_i\|^2 + \|\bar{\boldsymbol{e}}_i\|\left\|\bar{\boldsymbol{h}}_i\right\|\sqrt{1-\cos^2\alpha_i} + K_p\bar{\eta}\|\bar{\boldsymbol{e}}_i\|^2\right)\\
&\overset{(3.82)}{\le} \sum_{i\in\mathscr{V}} s_i\rho_i\left(-K_p\|\bar{\boldsymbol{e}}_i\|^2 + K_p(1+\bar{\eta})\|\bar{\boldsymbol{e}}_i\|^2\sqrt{1-\cos^2\alpha_i} + K_p\bar{\eta}\|\bar{\boldsymbol{e}}_i\|^2\right)\\
&= -\sum_{i\in\mathscr{V}} s_i\rho_i K_p\|\bar{\boldsymbol{e}}_i\|^2\left(1-(1+\bar{\eta})\sqrt{1-\cos^2\alpha_i} - \bar{\eta}\right)\\
&\overset{(3.57)}{=} -\sum_{i\in\mathscr{V}} s_i\frac{\rho_0}{\left\|\bar{\boldsymbol{h}}_i\right\|}\left(\|\bar{\boldsymbol{e}}_i\|^{\mu_1} + \|\bar{\boldsymbol{e}}_i\|^{\mu_2}\right)K_p\|\bar{\boldsymbol{e}}_i\|^2\left(1-\bar{\eta}-(1+\bar{\eta})\sqrt{1-\cos^2\alpha_i}\right)\\
&= -\sum_{i\in\mathscr{V}} s_i\frac{K_p\rho_0\|\bar{\boldsymbol{e}}_i\|}{\left\|\bar{\boldsymbol{h}}_i\right\|}\left(\|\bar{\boldsymbol{e}}_i\|^{\mu_1+1} + \|\bar{\boldsymbol{e}}_i\|^{\mu_2+1}\right)\left(1-\bar{\eta}-(1+\bar{\eta})\sqrt{1-\cos^2\alpha_i}\right)\\
&\overset{(3.82)}{\le} -\sum_{i\in\mathscr{V}} s_i\frac{K_p\rho_0\|\bar{\boldsymbol{e}}_i\|\left(1-\bar{\eta}-(1+\bar{\eta})\sqrt{1-\cos^2\alpha_i}\right)}{K_p(1+\bar{\eta})\|\bar{\boldsymbol{e}}_i\|}\left(\|\bar{\boldsymbol{e}}_i\|^{\mu_1+1} + \|\bar{\boldsymbol{e}}_i\|^{\mu_2+1}\right)\\
&= -\sum_{i\in\mathscr{V}} s_i\frac{\rho_0\left(1-\bar{\eta}-(1+\bar{\eta})\sqrt{1-\cos^2\alpha_i}\right)}{1+\bar{\eta}}\left(\|\bar{\boldsymbol{e}}_i\|^{\mu_1+1} + \|\bar{\boldsymbol{e}}_i\|^{\mu_2+1}\right). \qquad (3.84)
\end{aligned}
$$

It should be noted that $\forall t \ge t_{sai}\ \cos^2\alpha \overset{(2.39)}{=} 1$, where t_{sai} is the settling time of the auxiliary orientation error for the i-th vehicle. Thus, (3.84) can be rewritten as follows:

$$
\forall t \ge t_{sai}\quad \dot{V}_p \overset{(3.84)}{\le} -\sum_{i\in\mathscr{V}} s_i\rho_0\frac{1-\bar{\eta}}{1+\bar{\eta}}\left(\|\bar{\boldsymbol{e}}_i\|^{\mu_1+1} + \|\bar{\boldsymbol{e}}_i\|^{\mu_2+1}\right). \qquad (3.85)
$$

Next, an application of Assumption 6 to (3.85) leads to:

$$
\begin{aligned}
\forall t \ge t_{sai}\quad \dot{V}_p &\overset{(3.85)}{\le} -\sum_{i\in\mathscr{V}} \bar{s}\rho_0\frac{1-\bar{\eta}}{1+\bar{\eta}}\left(\|\bar{\boldsymbol{e}}_i\|^{\mu_1+1} + \|\bar{\boldsymbol{e}}_i\|^{\mu_2+1}\right)\\
&= -\bar{s}\rho_0\frac{1-\bar{\eta}}{1+\bar{\eta}}\sum_{i\in\mathscr{V}}\left(\|\bar{\boldsymbol{e}}_i\|^{\mu_1+1} + \|\bar{\boldsymbol{e}}_i\|^{\mu_2+1}\right)\\
&= -\bar{s}\rho_0\frac{1-\bar{\eta}}{1+\bar{\eta}}\left(\sum_{i\in\mathscr{V}}\|\bar{\boldsymbol{e}}_i\|^{\mu_1+1} + \sum_{i\in\mathscr{V}}\|\bar{\boldsymbol{e}}_i\|^{\mu_2+1}\right)\\
&= -\bar{s}\rho_0\frac{1-\bar{\eta}}{1+\bar{\eta}}\left(\sum_{i\in\mathscr{V}}\left(\|\bar{\boldsymbol{e}}_i\|^2\right)^{\frac{\mu_1+1}{2}} + \sum_{i\in\mathscr{V}}\left(\|\bar{\boldsymbol{e}}_i\|^2\right)^{\frac{\mu_2+1}{2}}\right)
\end{aligned}
$$

$$\begin{aligned}
&\overset{(3.4)}{\leq} -\bar{s}\rho_0\frac{1-\bar{\eta}}{1+\bar{\eta}}\left(\left(\sum_{i\in\mathscr{V}}\|\bar{\boldsymbol{e}}_i\|^2\right)^{\frac{\mu_1+1}{2}}+\sum_{i\in\mathscr{V}}\left(\|\bar{\boldsymbol{e}}_i\|^2\right)^{\frac{\mu_2+1}{2}}\right)\\
&\overset{(3.5)}{\leq} -\bar{s}\rho_0\frac{1-\bar{\eta}}{1+\bar{\eta}}\left(\left(\sum_{i\in\mathscr{V}}\|\bar{\boldsymbol{e}}_i\|^2\right)^{\frac{\mu_1+1}{2}}+n_v{}^{\frac{1-\mu_2}{2}}\left(\sum_{i\in\mathscr{V}}\|\bar{\boldsymbol{e}}_i\|^2\right)^{\frac{\mu_2+1}{2}}\right)\\
&= -\bar{s}\rho_0\frac{1-\bar{\eta}}{1+\bar{\eta}}\left(\left(\bar{\boldsymbol{e}}^\top\bar{\boldsymbol{e}}\right)^{\frac{\mu_1+1}{2}}+n_v{}^{\frac{1-\mu_2}{2}}\left(\bar{\boldsymbol{e}}^\top\bar{\boldsymbol{e}}\right)^{\frac{\mu_2+1}{2}}\right)\\
&\overset{(3.49)}{=} -\bar{s}\rho_0\frac{1-\bar{\eta}}{1+\bar{\eta}}\left(\left(\boldsymbol{\xi}_q^\top\boldsymbol{\mathcal{L}}_q\boldsymbol{\mathcal{L}}_q\boldsymbol{\xi}_q\right)^{\frac{\mu_1+1}{2}}+n_v{}^{\frac{1-\mu_2}{2}}\left(\boldsymbol{\xi}_q^\top\boldsymbol{\mathcal{L}}_q\boldsymbol{\mathcal{L}}_q\boldsymbol{\xi}_q\right)^{\frac{\mu_2+1}{2}}\right).
\end{aligned}\tag{3.86}$$

Then, based on (3.9) from Lemma 9, it can be observed that

$$\begin{aligned}
\forall t\geq t_{sai}\quad \dot{V}_p &\overset{(3.86)}{\leq} -\bar{s}\rho_0\frac{1-\bar{\eta}}{1+\bar{\eta}}\left(\left(\lambda_2\boldsymbol{\xi}_q^\top\boldsymbol{\mathcal{L}}_q\boldsymbol{\xi}_q\right)^{\frac{\mu_1+1}{2}}+n_v{}^{\frac{1-\mu_2}{2}}\left(\lambda_2\boldsymbol{\xi}_q^\top\boldsymbol{\mathcal{L}}_q\boldsymbol{\xi}_q\right)^{\frac{\mu_2+1}{2}}\right)\\
&\overset{(3.83)}{=} -\bar{s}\rho_0\frac{1-\bar{\eta}}{1+\bar{\eta}}\left(\left(2\lambda_2V_p\right)^{\frac{\mu_1+1}{2}}+n_v{}^{\frac{1-\mu_2}{2}}\left(2\lambda_2V_p\right)^{\frac{\mu_2+1}{2}}\right)
\end{aligned}\tag{3.87}$$

By comparing (3.87) with (1.2), one can conclude that the equilibrium point $\boldsymbol{\xi}_q=\boldsymbol{\xi}_c$ is fixed-time stable. However, it should be noted that $\bar{s}(t)\in(0,1]$ is bounded but time-varying, hence the upper bound T_{cp} computed with the use of it would not be a constant value. Therefore, let us introduce the term

$$\underline{\bar{s}}\triangleq\min_{i\in\mathscr{V}}\underline{s}_i(\boldsymbol{e}_{0i})\in(0,1],\tag{3.88}$$

with

$$\underline{s}_i(\boldsymbol{e}_{0i})\overset{(2.42)}{=}\inf_{t\geq0}\ s(\boldsymbol{e}_i(t,\boldsymbol{e}_{0i}))\in(0,1].\tag{3.89}$$

Then, one can obtain

$$\dot{V}_p\overset{(3.87)}{\leq} -\underline{\bar{s}}\rho_0\frac{1-\bar{\eta}}{1+\bar{\eta}}\left(\left(2\lambda_2V_p\right)^{\frac{\mu_1+1}{2}}+n_v{}^{\frac{1-\mu_2}{2}}\left(2\lambda_2V_p\right)^{\frac{\mu_2+1}{2}}\right).\tag{3.90}$$

Finally, based on (1.3), the upper bound of the settling time can be formulated as follows:

$$T_{cp}=\frac{\pi(1+\bar{\eta})}{2\underline{\bar{s}}\bar{\mu}(1-\bar{\eta})n_v{}^{(1-\mu_2)/4}}.\tag{3.91}$$

Remark 31 *It should be noted that the upper bound T_{cp} will be valid if the auxiliary orientation error has converged to zero. Therefore, the total upper bound of the settling time of system errors should be expressed as the sum:*

$$T_c\triangleq T_{ca}+T_{cp},\tag{3.92}$$

where T_{cp} can be computed based on (3.91)*, while T_{ca} based on* (2.31)*, under Assumptions 1 and 6.*

Orientation error: The convergence proof for the orientation error follows in a similar manner to the proof given for Theorem 1. The analysis will be performed for $\epsilon = 0$. First, based on (3.78) and (2.34) one can observe that

$$\forall t \geq t_{sai} \quad \dot{\bar{\boldsymbol{q}}}_i = \begin{bmatrix} \dot{x}_i \\ \dot{y}_i \end{bmatrix} \overset{(3.78)}{=} s_i \rho_i K_p (\bar{\boldsymbol{e}}_i + \bar{\eta} \sigma_i \|\bar{\boldsymbol{e}}_i\| \bar{\boldsymbol{g}}_{2d}) \overset{(3.52)}{=} s_i \rho_i \bar{\boldsymbol{h}}_i = s_i \rho_i \begin{bmatrix} h_{xi} \\ h_{yi} \end{bmatrix} \tag{3.93}$$

and, consequently,

$$\forall t \geq t_{sai} \quad \dot{\bar{\boldsymbol{e}}}_i = \begin{bmatrix} \dot{e}_{xi} \\ \dot{e}_{yi} \end{bmatrix} \overset{(3.64)}{=} \begin{bmatrix} -\sum_{j=1}^{n_v} \ell_{ij} \dot{x}_j \\ -\sum_{j=1}^{n_v} \ell_{ij} \dot{y}_j \end{bmatrix} \overset{(3.93)}{=} \begin{bmatrix} -\sum_{j=1}^{n_v} \ell_{ij} s_j \rho_j h_{xj} \\ -\sum_{j=1}^{n_v} \ell_{ij} s_j \rho_j h_{yj} \end{bmatrix}. \tag{3.94}$$

Next, let us consider a local frame determined by the desired configuration $\boldsymbol{q}_{di} = \begin{bmatrix} \theta_d & \bar{\boldsymbol{q}}_{di}^\top \end{bmatrix}^\top$. Note that the positional subvector $\bar{\boldsymbol{q}}_{di}$ is unknown *a priori*, while the desired orientation θ_d is the same for each vehicle. Let us transform the vector $\dot{\bar{\boldsymbol{e}}}_i = \begin{bmatrix} \dot{e}_{xi} & \dot{e}_{yi} \end{bmatrix}^\top$ into this local frame:

$$\begin{aligned} \forall t \geq t_{sai} \quad \dot{\boldsymbol{e}}_i^L &= \begin{bmatrix} \cos\theta_d & \sin\theta_d \\ -\sin\theta_d & \cos\theta_d \end{bmatrix} \begin{bmatrix} \dot{e}_{xi} \\ \dot{e}_{yi} \end{bmatrix} = \begin{bmatrix} \dot{e}_{xi}\cos\theta_d + \dot{e}_{yi}\sin\theta_d \\ -\dot{e}_{xi}\sin\theta_d + \dot{e}_{yi}\cos\theta_d \end{bmatrix} \\ &\overset{(3.94)}{=} \begin{bmatrix} -\sum_{j=1}^{n_v} \Big((h_{xj}\cos\theta_d + h_{yj}\sin\theta_d) \ell_{ij} s_j \rho_j \Big) \\ -\sum_{j=1}^{n_v} \Big((-h_{xj}\sin\theta_d + h_{yj}\cos\theta_d) \ell_{ij} s_j \rho_j \Big) \end{bmatrix} \\ &\overset{(2.48)}{=} \begin{bmatrix} -\sum_{j=1}^{n_v} h_{xj}^L \ell_{ij} s_j \rho_j \\ -\sum_{j=1}^{n_v} h_{yj}^L \ell_{ij} s_j \rho_j \end{bmatrix} \\ &\overset{(2.49)}{=} \begin{bmatrix} -\sum_{j=1}^{n_v} \Big(e_{xj}^L - \bar{\eta}\sigma_j \|\bar{\boldsymbol{e}}\| \Big) K_p \ell_{ij} s_j \rho_j \\ -\sum_{j=1}^{n_v} e_{yj}^L K_p \ell_{ij} s_j \rho_j \end{bmatrix}. \end{aligned} \tag{3.95}$$

Please note that (2.49) can be used since the convergence vector field is defined in the same way in Sections 2.2.2 and 3.4.1 (compare (3.52) with (2.3)). Therefore, one can conclude that e_{yi}^L converges to zero independently of e_{xi}^L. Furthermore, by analogy to (2.57) and (2.58), one can observe that

$$e_{xi}^L(t) \xrightarrow{t \to \tau_{xi}} 0, \qquad e_{yi}^L(t) \xrightarrow{t \to \tau_{yi}} 0, \qquad \tau_{yi} < \tau_{xi} \leq T_c, \tag{3.96}$$

and

$$h_{xi}^L(t) \xrightarrow{t \to \tau_{xi}} 0, \qquad h_{yi}^L(t) \xrightarrow{t \to \tau_{yi}} 0, \qquad \tau_{yi} < \tau_{xi} \leq T_c. \tag{3.97}$$

The rest of the analysis proceeds in an analogous manner to the proof of Theorem 1, that is, based on (2.60) and (2.61), one can conclude that

$$(\theta_d - \theta_i) \xrightarrow{t \to \tau_{yi}} k\pi, \ k \in \mathbb{Z}, \tag{3.98}$$

and then, thanks to (2.67), one can obtain

$$(\theta_d - \theta_i) \xrightarrow{t \to T_c} 2k\pi, \ k \in \mathbb{Z} \implies e_{\theta i} \overset{(3.48)}{=} f_\theta(\theta_d - \theta_i) \xrightarrow{t \to T_c} 0. \tag{3.99}$$

That concludes the proof. ■

3.4.2 Distributed consensus of the smallest common value of the scaling function

In this section, a method will be presented that allows for the fulfillment of Assumption 6. First, let us introduce a term called the *graph distance* $d_{\mathcal{G}}(z_1, z_2)$, which denotes the shortest communication path between nodes z_1 and z_2 (or, in other words, the smallest number of edges connecting nodes z_1 and z_2) for a connected graph $\mathcal{G}$. Based on Section 1.4.2, one can conclude that for $i \in \mathcal{V}$ and $j \in \mathcal{N}_i$, the graph distance $d_{\mathcal{G}}(i, j) = 1$. Furthermore, one can observe that

$$\max_{z_1, z_2 \in \{1,\ldots,n_v\}} d_{\mathcal{G}}(z_1, z_2) = n_v - 1,$$

without considering a particular graph $\mathcal{G}$. For the purposes of further analysis, let us now introduce the notation $j_1, j_2, \ldots$ to denote neighbors of neighbors, that is:

$$\begin{aligned}
d_{\mathcal{G}}(i, j) &= 1 \quad \text{for } j \in \mathcal{N}_i, \\
d_{\mathcal{G}}(i, j_1) &= 2 \quad \text{for } j_1 \in \mathcal{N}_j, \\
d_{\mathcal{G}}(i, j_2) &= 3 \quad \text{for } j_2 \in \mathcal{N}_{j_1}, \\
&\vdots \\
d_{\mathcal{G}}(i, j_{n_v-3}) &= n_v - 2 \quad \text{for } j_{n_v-3} \in \mathcal{N}_{j_{n_v-4}}, \\
d_{\mathcal{G}}(i, j_{n_v-2}) &= n_v - 1 \quad \text{for } j_{n_v-2} \in \mathcal{N}_{j_{n_v-3}}.
\end{aligned}$$

The proposed approach involves the use of finite-/fixed-time filters and the $\min(\cdot)$ function, as shown in the scheme presented in Fig. 3.9. The primary objective of using these filters is to reproduce the input signal at the filter output within a finite time. When the filters error, that is the difference between the input and output values of the filters converges to zero, the filters will act as memory blocks and will be used to prevent an algebraic loop. Let us now introduce the notation that will be used: the values at the filter input will be indicated with a bar (for example, $\bar{z}$), while the values at the filter output will be indicated with a tilde (for example, $\tilde{z}$). It should be noted that $\forall t \geq t_{sf}\ \tilde{z}(t) = \bar{z}(t)$, where $0 \leq t_{sf} < \infty$ denotes the settling time of the filters error.

Now let us prove that the use of the filter-based approach proposed in Fig. 3.9 will result in reaching a consensus on the smallest value $\bar{s}$ of the scaling functions generated by the distributed multi-vehicle system, that is

$$\forall t \geq t_{sf} \quad \bar{s}(t) = \min_{i \in \mathcal{V}} s_i(t). = \min\Big\{s_1(t), s_2(t), \ldots, s_{n_v}(t)\Big\}. \tag{3.100}$$

To maintain consistency with the previous analyses conducted in this dissertation, the focus is again placed on the continuous-time domain. The analysis will be performed for $t \geq t_{sf}$. According to the scheme in Fig. 3.9, the outputs of the first filters can be expressed as follows:

$$\begin{aligned}
\bar{s}_{iF_1} &= \min\{s_i, s_j\} \quad \forall j \in \mathcal{N}_i, \\
\bar{s}_{jF_1} &= \min\{s_i, s_j, s_{j_1}\} \quad \forall j \in \mathcal{N}_i\ \forall j_1 \in \mathcal{N}_j, \\
\bar{s}_{j_1F_1} &= \min\{s_j, s_{j_1}, s_{j_2}\} \quad \forall j \in \mathcal{N}_i\ \forall j_1 \in \mathcal{N}_j\ \forall j_2 \in \mathcal{N}_{j_1}, \\
\bar{s}_{j_2F_1} &= \min\{s_{j_1}, s_{j_2}, s_{j_3}\} \quad \forall j_1 \in \mathcal{N}_j\ \forall j_2 \in \mathcal{N}_{j_1}\ \forall j_3 \in \mathcal{N}_{j_2},
\end{aligned}$$

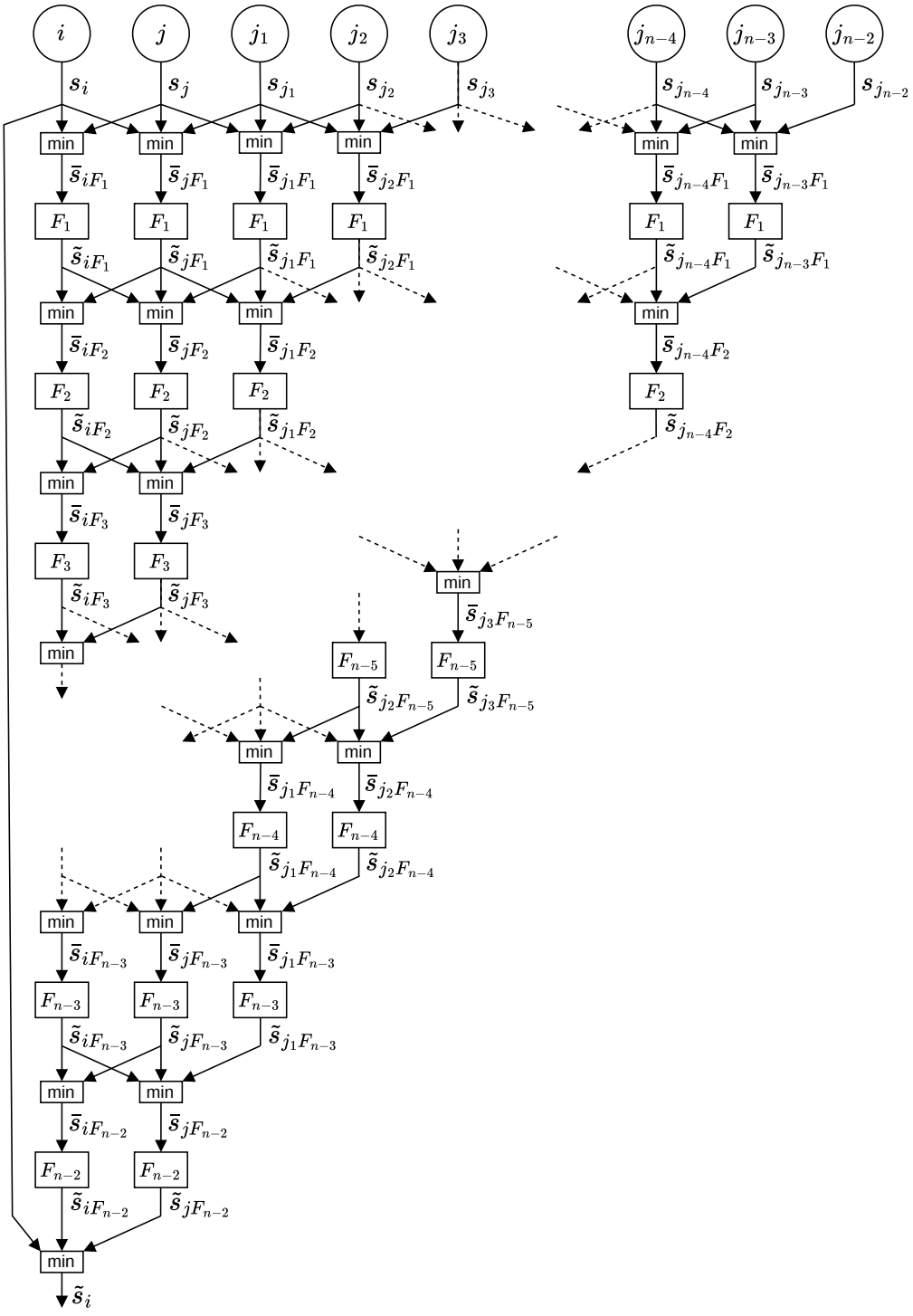

Figure 3.9 – Scheme of the filter-based approach for distributed consensus on the smallest value of the scaling function, where $\forall i \in \mathcal{V}\ \forall t \geq t_{sf}\ \tilde{s}_i(t) = \bar{s}(t)$.

$$\vdots$$
$$\bar{s}_{j_{n_v-3}F_1} = \min\{s_{j_{n_v-4}}, s_{j_{n_v-3}}, s_{j_{n_v-2}}\}$$
$$\forall j_{n_v-4} \in \mathcal{N}_{j_{n_v-5}}\ \forall j_{n_v-3} \in \mathcal{N}_{j_{n_v-4}}\ \forall j_{n_v-2} \in \mathcal{N}_{j_{n_v-3}}.$$

Then, after further filtering on vehicle i, for $t \geq t_{sf}$ one can obtain:

$$\begin{aligned}
\bar{s}_{iF_2} &= \min\{\bar{s}_{iF_1}, \bar{s}_{jF_1}\} \\
&= \min\Big\{\min\{s_i, s_j\}, \min\{s_i, s_j, s_{j_1}\}\Big\} \\
&= \min\{s_i, s_j, s_{j_1}\} \quad \forall j \in \mathcal{N}_i\ \forall j_1 \in \mathcal{N}_j \\
\bar{s}_{iF_3} &= \min\{\bar{s}_{iF_2}, \bar{s}_{jF_2}\} \\
&= \min\Big\{\min\{\bar{s}_{iF_1}, \bar{s}_{jF_1}\}, \min\{\bar{s}_{iF_1}, \bar{s}_{jF_1}, \bar{s}_{j_1F_1}\}\Big\} \\
&= \min\{\bar{s}_{iF_1}, \bar{s}_{jF_1}, \bar{s}_{j_1F_1}\} \\
&= \min\Big\{\min\{s_i, s_j\}, \min\{s_i, s_j, s_{j_1}\}, \min\{s_j, s_{j_1}, s_{j_2}\}\Big\} \\
&= \min\{s_i, s_j, s_{j_1}, s_{j_2}\} \quad \forall j \in \mathcal{N}_i\ \forall j_1 \in \mathcal{N}_j\ \forall j_2 \in \mathcal{N}_{j_1} \\
&\vdots \\
\bar{s}_{iF_{n_v-1}} = \bar{s} &= \min\{s_i, \bar{s}_{iF_{n_v-2}}, \bar{s}_{jF_{n_v-2}}\} = \ldots \qquad (3.101) \\
&= \min\{s_i, \bar{s}_{iF_1}, \bar{s}_{jF_1}, \bar{s}_{j_1F_1}, \ldots, \bar{s}_{j_{n_v-3}F_1}\} \\
&= \min\{s_i, s_j, s_{j_1}, s_{j_2}, \ldots, s_{j_{n_v-4}}, s_{j_{n_v-3}}, s_{j_{n_v-2}}\} \\
&\qquad \forall j \in \mathcal{N}_i\ \forall j_1 \in \mathcal{N}_j\ \forall j_2 \in \mathcal{N}_{j_1}\ \ldots\ \forall j_{n_v-2} \in \mathcal{N}_{j_{n_v-3}} \\
&= \min\{s_k\} \quad \forall k \in \mathcal{N}_i \cup \mathcal{N}_j \cup \mathcal{N}_{j_1} \cup \ldots \cup \mathcal{N}_{j_{n_v-3}} \qquad (3.102)
\end{aligned}$$

It should be noted that since the sets $\mathcal{N}_i, \mathcal{N}_j, \mathcal{N}_{j_1}, \ldots, \mathcal{N}_{j_{n_v-3}}$ contain unique indices, it can be written that

$$\mathcal{N}_i \cup \mathcal{N}_j \cup \mathcal{N}_{j_1} \cup \ldots \cup \mathcal{N}_{j_{n_v-3}} = \mathcal{V}, \qquad (3.103)$$

where $\mathcal{V} \triangleq \{1, 2, \ldots, n_v\}$ denotes the set of all nodes. Consequently, it can be concluded that:

$$\forall t \geq t_{sf} \quad \bar{s}(t) \overset{(3.102)}{=} \min_{k \in \mathcal{V}} s_k(t) = \min\Big\{s_1(t), s_2(t), \ldots, s_n(t)\Big\}. \qquad (3.104)$$

The term $\bar{s}$ obtained according to (3.104) is used to modify the scaling procedure, resulting in the control scheme in Fig. 3.10 (cf. Fig. 3.8).

One should also consider the output of the algorithm for $t < t_{sf}$. Based on (3.101), it can be observed that:

$$\forall t < t_{sf} \quad \bar{s}_{iF_{n_v-1}} = \tilde{s}_i = \min\Big\{s_i(t), \tilde{s}_{iF_{n_v-2}}(t), \tilde{s}_{jF_{n_v-2}}(t)\Big\} \in \Big(0, s_i(t)\Big], \qquad (3.105)$$

which ensures that the imposed control input constraints are met by vehicle i at all time instants, even for $t < t_{sf}$. It should be noted that $\tilde{s}_i(t)$ never exceeds $s_i(t)$, which is generated by the i-th vehicle and is the largest possible value of the scaling function that ensures satisfaction of the imposed control input constraints at a given time instant.

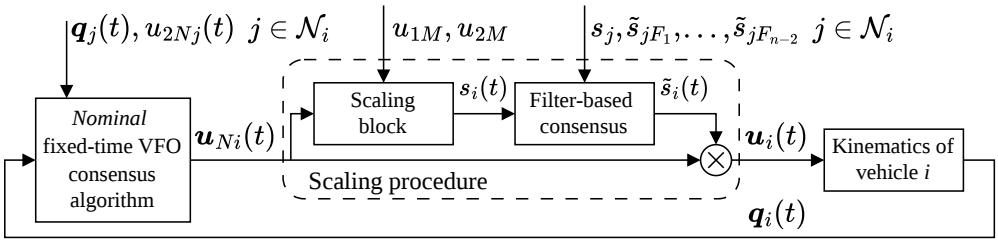

Figure 3.10 – Scheme of the control system for the i-th vehicle, belonging to a distributed multi-vehicle system, with the modified scaling procedure using a filter-based consensus, where $\forall i \in \mathcal{V}\ \forall t \geq t_{sf}\ \tilde{s}_i(t) = \bar{s}(t)$.

3.4.3 Results of numerical simulation

The numerical simulation was performed in the Matlab-Simulink environment. A fixed-step solver with a step size of 10^{-4} s was selected. The differentiator from [50] acts as a finite-time filter, which enables the reconstruction of the input signal within a finite time, according to the scheme discussed in Section 3.4.2.

The following controller coefficients were selected: $K_p = 1$, $K_a = 2$, $\bar{\eta} = 0.82$, $\rho_0 = 1$, $\bar{\delta} = \bar{\mu} = 0.1$, and σ_i was selected according to (2.4), while: $\epsilon = 10^{-10}$ m, $u_{1M} = 3$ rad/s, $u_{2M} = 0.5$ m/s, and $\theta_d = 0$ rad. A scenario involving 6 vehicles was considered, whose communication topology was undirected and was described by the graph $\mathcal{G}$ shown in Fig. 3.11 and by the following matrices:

$$\boldsymbol{\mathcal{A}} = \begin{bmatrix} 0 & 1 & 0 & 0 & 0 & 1 \\ 1 & 0 & 1 & 0 & 0 & 0 \\ 0 & 1 & 0 & 1 & 0 & 0 \\ 0 & 0 & 1 & 0 & 1 & 0 \\ 0 & 0 & 0 & 1 & 0 & 1 \\ 1 & 0 & 0 & 0 & 1 & 0 \end{bmatrix}, \quad \boldsymbol{\mathcal{L}} = \begin{bmatrix} 2 & -1 & 0 & 0 & 0 & -1 \\ -1 & 2 & -1 & 0 & 0 & 0 \\ 0 & -1 & 2 & -1 & 0 & 0 \\ 0 & 0 & -1 & 2 & -1 & 0 \\ 0 & 0 & 0 & -1 & 2 & -1 \\ -1 & 0 & 0 & 0 & -1 & 2 \end{bmatrix}.$$

The initial configurations for the vehicles were selected as follows:

$$\boldsymbol{q}_1(0) = \begin{bmatrix} \frac{\pi}{2} \\ 7 \\ 1 \end{bmatrix}, \quad \boldsymbol{q}_2(0) = \begin{bmatrix} 0 \\ 8 \\ 6 \end{bmatrix}, \quad \boldsymbol{q}_3(0) = \begin{bmatrix} -\frac{\pi}{2} \\ 1 \\ 8 \end{bmatrix},$$

$$\boldsymbol{q}_4(0) = \begin{bmatrix} 0 \\ -3.5 \\ 4 \end{bmatrix}, \quad \boldsymbol{q}_5(0) = \begin{bmatrix} \frac{\pi}{2} \\ -1 \\ -0.5 \end{bmatrix}, \quad \boldsymbol{q}_6(0) = \begin{bmatrix} 0 \\ 4 \\ -3 \end{bmatrix}.$$

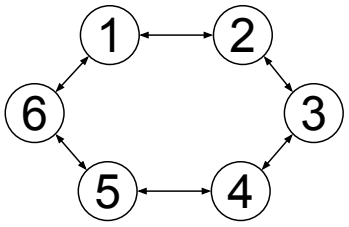

Figure 3.11 – Communication topology graph used in the simulation.

The obtained results are shown in Fig. 3.12. Based on Figs. 3.12a, 3.12b, and 3.12c, it can be seen that the norm of the positional error, auxiliary orientation error,

and orientation error, respectively, converge toward zero. One can observe that the control signals satisfy the imposed constraints (see Figs. 3.12e and 3.12f), and that the proposed filtering method for distributed consensus on the smallest value of the scaling function allows each vehicle to find and use the smallest common value (see Fig. 3.12d). Fig. 3.12g shows that each vehicle reached its desired position (which was unknown *a priori*) within the vicinity ϵ and that the trajectory of each vehicle was free of oscillations.

3.4.4 Results of experimental test

The experimental test was conducted using mTracker mobile robots equipped with the Intel NUC computers (see Fig. 3.13), and using the Robot Operating System (ROS) (see [1]). Each robot was equipped with a two low-level PI controllers to control wheel speeds and was capable to subscribe to ROS topics to read the desired speeds and publish odometer data to the appropriate ROS topic, according to the ROS philosophy. On the NUC computers, a control law and a method for finding the lowest value of the scaling function have been implemented. The vehicles exchange all necessary data with each other in accordance with the chosen communication topology via ROS topics. The system uses WiFi wireless communication.

A scenario with four vehicles was considered, using an undirected communication topology described by the graph $\mathcal{G}$ shown in Fig. 3.14 and by the following matrices:

$$\boldsymbol{\mathcal{A}} = \begin{bmatrix} 0 & 1 & 0 & 1 \\ 1 & 0 & 1 & 0 \\ 0 & 1 & 0 & 1 \\ 1 & 0 & 1 & 0 \end{bmatrix}, \quad \boldsymbol{\mathcal{L}} = \begin{bmatrix} 2 & -1 & 0 & -1 \\ -1 & 2 & -1 & 0 \\ 0 & -1 & 2 & -1 \\ -1 & 0 & -1 & 2 \end{bmatrix}.$$

The initial configurations for the vehicles were selected as follows:

$$\boldsymbol{q}_1(0) = \begin{bmatrix} 0 \\ 3 \\ -2 \end{bmatrix}, \quad \boldsymbol{q}_2(0) = \begin{bmatrix} 0 \\ 1 \\ 4 \end{bmatrix}, \quad \boldsymbol{q}_3(0) = \begin{bmatrix} 0 \\ -2 \\ 1 \end{bmatrix}, \quad \boldsymbol{q}_4(0) = \begin{bmatrix} 0 \\ -3 \\ -3 \end{bmatrix},$$

while the controllers coefficients were chosen as: $K_p = 1$, $K_a = 2$, $\bar{\eta} = 0.82$, $\rho_0 = 1$, $\bar{\mu} = 0.2$, $\bar{\delta} = 0.1$, and σ_i is selected based on (2.4). Other parameters were selected as follows: $\epsilon = 0.01$ m, $u_{1M} = 0.5$ rad/s, $u_{2M} = 0.1$ m/s, and $\theta_d = 0$ rad.

For experimental tests, the filters discussed in Section 3.4.2 were implemented as first-order low-pass filters. Although these filters do not guarantee convergence within a finite time, in the case of practical implementation in the discrete-time domain, one can reasonably consider a practical convergence to a neighborhood of zero, and thus, for a linear filter, one can expect that such convergence will occur after a time period corresponding to approximately five filter time constants. As can be concluded from results presented in Fig. 3.15, this approach seems practically acceptable for the practical implementation of the proposed algorithm on physical robots.

Remark 32 *It should be noted that the differentiator from [50] used in the simulations was not used in the experiments, as its discrete-time implementation does not guarantee convergence to zero within a finite time (see, for example, [57]). Indeed, in this case one may consider a certain practical convergence to the vicinity of zero*

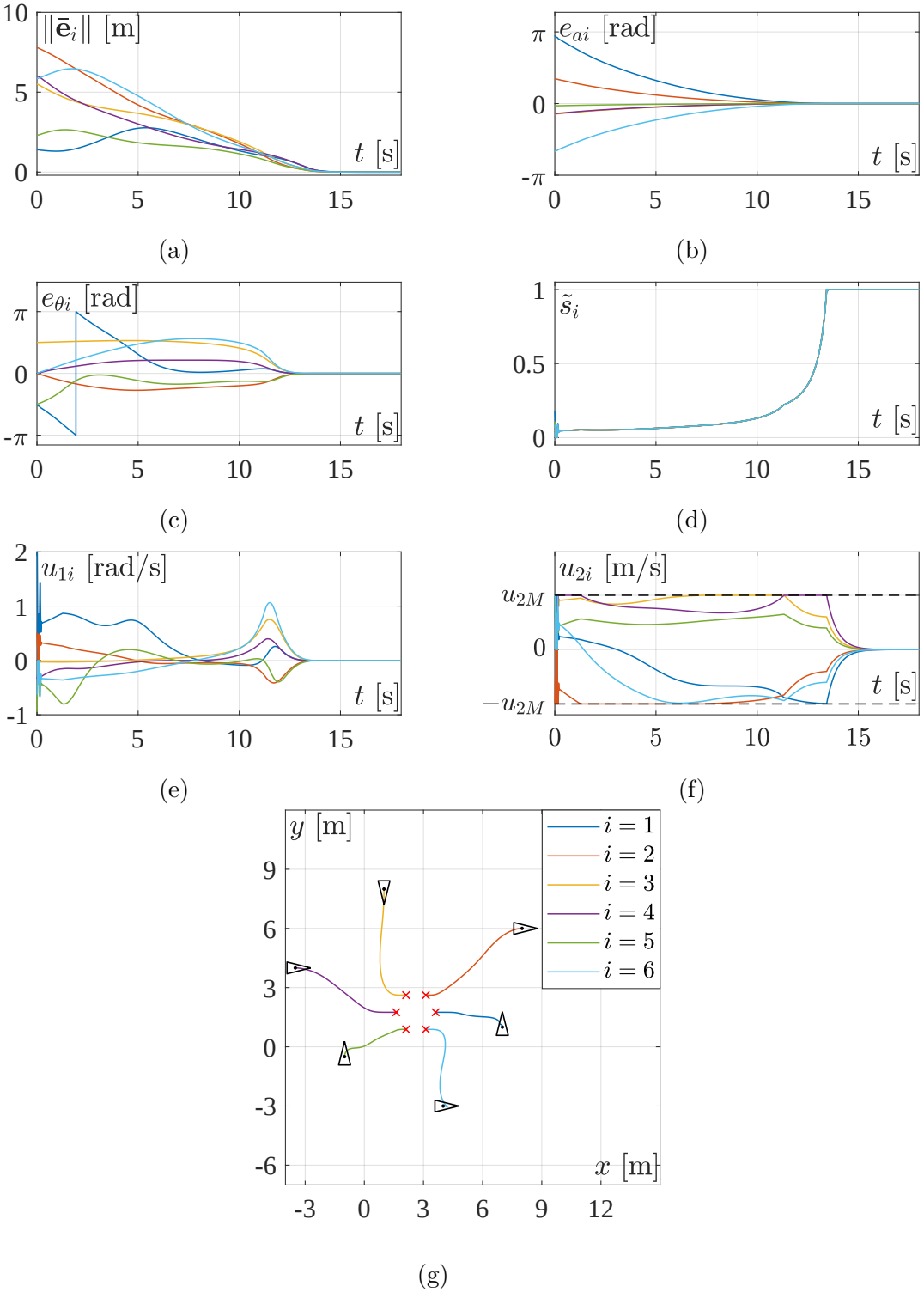

Figure 3.12 – Results of the numerical simulation for the consensus-based formation control algorithm for a multi-vehicle system with an undirected communication topology, where the initial configurations are marked with solid triangles and the desired positions with red crosses, while $\theta_d = 0$ rad, $u_{1M} = 3$ rad/s, and $u_{2M} = 0.5$ m/s. Note that each plot shows the waveforms for 6 robots, and the legend in Fig. 3.12g applies to all plots.

Figure 3.13 – The mTracker mobile robots, equipped with the Intel NUC computers, which were used to create a multi-vehicle system for the purpose of experimental tests.

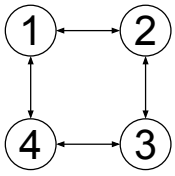

Figure 3.14 – Communication topology graph used in the experimental test.

in a finite time, nevertheless, its discrete-time implementation is characterized by an oscillatory response, which makes the use of this differentiator problematic for the considered purpose. Therefore, in the experimental tests, a discrete implementation of a linear filter was used, in which a practical convergence to the vicinity of zero in a finite time can also be considered, however, its response does not contain oscillations.

It can be observed in Figs. 3.15a and 3.15b that the norm of positional error and the auxiliary orientation error converged toward zero within a settling time not exceeding 60 s. The orientation error also converges toward the vicinity of zero (see Fig. 3.15c). It can be seen that the control inputs satisfy the imposed constraints (see Figs. 3.15e and 3.15f). In the final phase of motion, certain oscillations can be observed in the control signal waveforms, particularly evident in Fig. 3.15e, which result from, among other things, communication delays. These oscillations are also visible in Fig. 3.15b. It is also worth noting that the proposed method for finding the common lowest value of the scaling function remains effective in this case, allowing one to reduce the differences between the values used by individual vehicles (see Fig. 3.15d). Although the individual values of $\tilde{s}_i$ were not equal, the differences between them did not prevent the proposed algorithm from achieving the intended control objectives. Fig. 3.15g shows that the vehicles formed the desired formation (in a positional sense) with the assumed accuracy and their trajectories are characterized by the lack of oscillations. Note that the average operating frequency of the control system during the experimental test was 30 Hz.

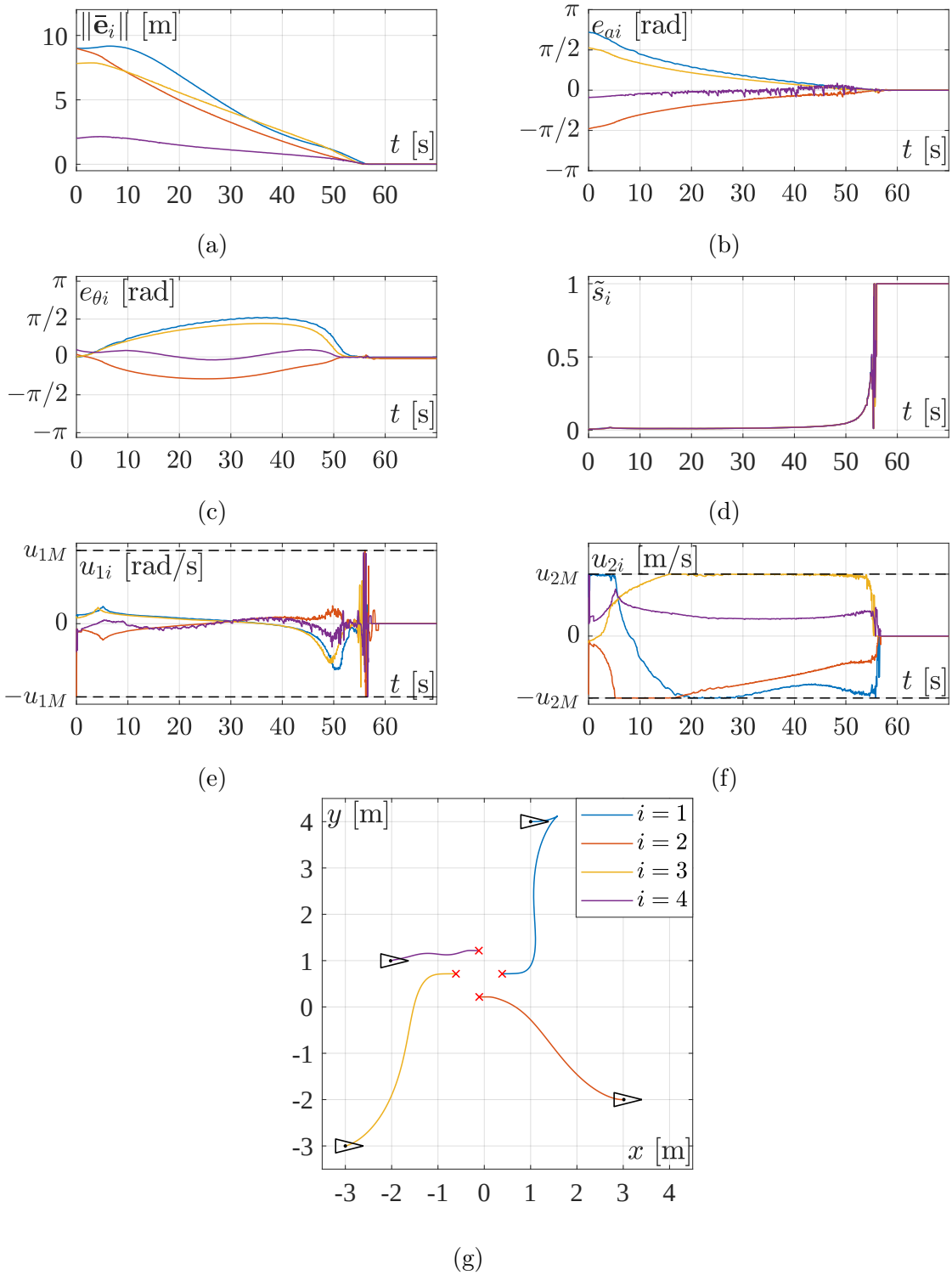

Figure 3.15 – Experimental results obtained using a multi-vehicle system consisting of four mTracker mobile robots equipped with Intel NUC computers, where the initial configurations are marked with solid triangles and the desired positions with red crosses, with $\theta_d = 0$ rad, $u_{1M} = 0.5$ rad/s and $u_{2M} = 0.1$ m/s. Note that each plot shows the waveforms for 4 robots, and the legend in Fig. 3.15g applies to all plots.

3.5 Conclusions

This chapter presents two fixed-time VFO control algorithms for a distributed multi-vehicle system composed of nonholonomic mobile robots, which solve the problem of distributed formation control. The stability of the closed-loop dynamics was formally analyzed, and the performance of the proposed algorithms was verified through numerical simulations and experimental tests using physical mobile robots. Thus, the second objective has been confirmed, namely the VFO methodology can be successfully used to design control laws for distributed nonholonomic multi-vehicle systems that take into account the control input constraints and task-execution time constraints.

Compared to other solutions available in the literature, the proposed control laws result in non-oscillatory and chattering-free control signals. Furthermore, they ensure oscillation-free vehicle motion trajectories. Moreover, for the proposed algorithms, the maximum absolute values of the control inputs are explicitly set by the designer, and the presence of these control input constraints has been taken into account when determining the upper bound of the settling times.

A common feature of the two proposed control algorithms is the use of a consensus mechanism to create formations. However, the proposed algorithms differ in the way they use this mechanism: the observer-based approach addresses the consensus problem *a priori* – that is, this problem is solved by the distributed observers before the robots start their movement. The advantage of this approach is that it enables *a priori* knowledge of the desired configurations for each vehicle. However, a significant drawback is the lack of flexibility and the inability to respond to the robots' current behavior – the observer determines the desired configurations based on the initial configurations, and then the vehicles stop communicating with each other. A characteristic feature of this approach is also a three-stage control process in which three successive stages can be distinguished: *observation*, *pre-orientation*, and *motion*.

In contrast, in the consensus-based approach, the consensus problem is solved continuously, that is, based on the current configurations of individual vehicles. A consequence of this approach is that the desired positions remain unknown until they are reached. However, a significant advantage is the system's greater flexibility, which stems from the fact that communication between the vehicles is maintained at all times. It should also be noted that vehicles maintain communication throughout the entire movement, which results in a more noticeable impact of communication-related disturbances on control performance, however, at the same time, it improves the system's overall safety.

The next chapter will summarize the entire dissertation and present a discussion of potential directions for the further development of the proposed algorithms.

Chapter 4

Discussion and conclusions

4.1 Advantages and limitations of the proposed solutions

This dissertation presents control laws for nonholonomic mobile robots that solve the set-point control problem and the reference path-following problem, as well as two control algorithms for a distributed nonholonomic multi-vehicle system that solve the formation control problem. The proposed solutions are based on the VFO control design methodology and employ the concept of *fixed-time stability*, combining the advantages and limitations of both approaches.

Among the most important advantages is that the resulting control laws ensure task completion within the time constraints, while guaranteeing that the control inputs satisfy the imposed constraints. Moreover, the control signals are free of chattering, and there are no oscillations in the vehicles' motion trajectories. The dissertation demonstrates that it is possible to develop control algorithms in accordance with the concept of *fixed-time stability* while preserving the VFO control philosophy, in which two stages can be distinguished: *orienting* and *pushing* along the convergence vector field. It has also been shown that previous results regarding the VFO methodology remain valid, for example those concerning *integral curves* (cf. [26, 27]), which can also be used in the fixed-time set-point control problem. In light of the existing literature, it should be emphasized that a key advantage of the developed control algorithms is their ability to simultaneously handle the task-execution time constraints and the control input constraints without any computationally demanding procedures, such as online optimization. This makes the proposed algorithms suitable for implementation on low-cost physical robots, that is, those with limited computational capacity.

The main practical limitations of the proposed control algorithms concern the estimation of the upper bound of the system error settling time. First, it should be noted that the two-stage method of control synthesis (that is, first defining a *nominal* control law that does not satisfy the imposed control input constraints, and next post-processing it to obtain control signals that meet the imposed constraints) means that the upper bounds depend on the value of the scaling function $s(t)$ used in the scaling procedure. However, the value of $s(t)$ depends on the current values of the *nominal* control signals and is therefore time-varying (cf. (1.7)). In the dissertation, it is proposed to use the smallest possible value of $s(t)$ that is independent of time, however, this value is unknown *a priori* and must be estimated. So far, a method

for *a priori* estimation of the smallest value within a given set of admissible initial conditions has been developed only for the fixed-time set-point control law (see Section 2.2.3). The other proposed control algorithms can also be applied in practice, however, the development of a method for *a priori* estimation of the upper bounds of the system error settling times remains an open issue.

An important limitation that should be addressed is the conservatism in the estimation of the upper bound of the settling times. Several sources of this conservatism have been identified, the main ones being as follows:

1. The *fixed-time stability* concept itself – this concept guarantees that it is possible to estimate an upper bound of the settling times that will be valid for all initial conditions belonging to a given set of admissible initial conditions, in contrast to the *finite-time stability* concept, which guarantees an upper bound that depends on a particular initial condition. It is clear that this idea must lead to a certain degree of conservatism.
2. Selection of the Lyapunov function for a stability analysis – based on Lemmas 1-4, it can be observed that both the Lyapunov function and the bound on its time derivative directly influence the estimated upper bound of the settling times. Consequently, choosing a different function may lead to a different upper bound with a different level of conservatism.
3. The use of the smallest value of the function $s(t)$ – the scaling function $s(t)$ is time-varying and converges to 1 as the vehicles approach to the desired configuration. Using its lowest value over all admissible initial conditions allows one to obtain the upper bound of the settling times valid for the entire set of admissible initial conditions (according to the *fixed-time stability* concept). However, it introduces conservatism, as it implicitly assumes that the vehicles used this smallest value during the entire motion, which is generally not the case (except when the smallest value of the function $s(t)$ is 1, that is, when the control inputs are never saturated for the considered set of initial conditions).

Based on the above discussion, it can be concluded that the conservative nature of the estimation of the upper bound of the setting times is not unique to the algorithms presented in this dissertation, but is instead a common feature of solutions developed within the framework of the *fixed-time stability* concept. Thus, reducing this conservatism at the level of a control law design may be challenging.

The obtained results successfully expand the family of VFO controllers by integrating the properties of the *fixed-time stability* concept. Furthermore, this approach has been effectively extended to design distributed control algorithms for multi-vehicle systems. The effectiveness of the proposed control laws has been verified both through numerical simulations in the Matlab-Simulink environment and through laboratory-scale experiments conducted on physical mobile robots.

4.2 Further research directions

The solutions presented in this dissertation do not cover all aspects of control law design within the VFO methodology when simultaneously considering the task-execution time constraints and the control input constraints. Further research directions may include, among others:

- Development of a method for *a priori* estimation of the upper bound of the settling times for the remaining control algorithms presented in this dissertation, that is, for the path-following controller and the consensus-based formation algorithm. Such methods would increase a practical usefulness of the algorithms.
- Development of control algorithms for other motion tasks, such as trajectory tracking for a single mobile robot or motion tasks performed by a multi-vehicle formation.
- Formal robustness analysis of the proposed algorithms.
- More in-depth analysis of the collision avoidance problem.
- Extension towards algorithms based on the *predefined-time stability* concept (see, for example, [123]), where the upper bound of the settling times is a design parameter. To date, some preliminary results have been obtained for a *nominal* set-point predefined-time VFO controller (see [118]), however, no results have yet been obtained that also take into account control input constraints.
- Consideration of another vehicle kinematic model, such as car-like vehicles, and adaptation of the developed algorithms to such systems using, for example, the method presented in [77].

In conclusion, the directions for future research outlined above demonstrate that the results of this dissertation provide a solid foundation for the further development of fixed-time VFO control algorithms.

Bibliography

[1] Robot Operating System (ROS) website. [Online]. Available: https://www.ros.org/

[2] R. Aldana-López, D. Gómez-Gutiérrez, M. Defoort, J. D. Sánchez-Torres, and A. J. Muñoz-Vázquez, "A class of robust consensus algorithms with predefined-time convergence under switching topologies," *International Journal of Robust and Nonlinear Control*, vol. 29, no. 17, pp. 6179–6198, 2019.

[3] R. Aldana-López, D. Gómez-Gutiérrez, E. Jiménez-Rodríguez, J. D. Sánchez-Torres, and M. Defoort, "Enhancing the settling time estimation of a class of fixed-time stable systems," *International Journal of Robust and Nonlinear Control*, vol. 29, no. 12, pp. 4135–4148, 2019.

[4] V. Andrieu, L. Praly, and A. Astolfi, "Homogeneous approximation, recursive observer design, and output feedback," *SIAM Journal on Control and Optimization*, vol. 47, no. 4, pp. 1814–1850, 2008.

[5] M. Basin, Y. Shtessel, and F. Aldukali, "Continuous finite- and fixed-time high-order regulators," *Journal of the Franklin Institute*, vol. 353, no. 18, pp. 5001–5012, 2016.

[6] S. P. Bhat and D. S. Bernstein, "Finite-time stability of continuous autonomous systems," *SIAM Journal on Control and Optimization*, vol. 38, no. 3, pp. 751–766, 2000.

[7] A. Bloch and S. Drakunov, "Stabilization of a nonholonomic system via sliding modes," in *Proceedings of 1994 33rd IEEE Conference on Decision and Control*, vol. 3, 1994, pp. 2961–2963 vol.3.

[8] A. M. Bloch, *Nonholonomic Mechanics and Control*, 2nd ed., ser. Interdisciplinary Applied Mathematics. New York: Springer, 2015, vol. 24.

[9] V. Borkar and P. Varaiya, "Asymptotic agreement in distributed estimation," *IEEE Transactions on Automatic Control*, vol. 27, no. 3, pp. 650–655, 1982.

[10] R. W. Brockett, "Asymptotic stability and feedback stabilization," *Differential geometric control theory*, vol. 27, no. 1, pp. 181–191, 1983.

[11] E. F. Camacho and C. Bordons, *Model Predictive Control*, 2nd ed. Springer London, 2007.

[12] G. Campion, G. Bastin, and B. Dandrea-Novel, "Structural properties and classification of kinematic and dynamic models of wheeled mobile robots," *IEEE Transactions on Robotics and Automation*, vol. 12, no. 1, pp. 47–62, 1996.

[13] F. Chen and W. Ren, *Distributed Average Tracking in Multi-agent Systems*, 1st ed. Springer Cham, 2020.

[14] M. Chen, W. Lan, A. Cristofaro, and X. Yu, "Decentralized leader-following formation control of nonholonomic mobile robots by local measurement: A small-gain approach," *Systems & Control Letters*, vol. 205, p. 106253, 2025.

[15] M. L. Corradini and A. Cristofaro, "Nonsingular terminal sliding-mode control of nonlinear planar systems with global fixed-time stability guarantees," *Automatica*, vol. 95, pp. 561–565, 2018.

[16] M. Cui, H. Liu, W. Liu, R. Huang, and Y. Qin, "An adaptive unscented Kalman filter-based adaptive tracking control for wheeled mobile robots with control constrains in the presence of wheel slipping," *International Journal of Advanced Robotic Systems*, vol. 13, no. 5, 2016.

[17] P. De Villeros, J. D. Sánchez-Torres, M. Defoort, and A. Loukianov, "A predefined-time framework for average consensus and distributed optimization," *Nonlinear Dynamics*, vol. 114, no. 145, pp. 1–14, 2026.

[18] M. Defoort, G. Demesure, Z. Zuo, A. Polyakov, and M. Djemai, "Fixed-time stabilisation and consensus of non-holonomic systems," *IET Control Theory & Applications*, vol. 10, no. 18, pp. 2497–2505, 2016.

[19] L. Ding, Q.-L. Han, X. Ge, and X.-M. Zhang, "An overview of recent advances in event-triggered consensus of multiagent systems," *IEEE Transactions on Cybernetics*, vol. 48, no. 4, pp. 1110–1123, 2018.

[20] H. Du, G. Wen, Y. Cheng, Y. He, and R. Jia, "Distributed finite-time cooperative control of multiple high-order nonholonomic mobile robots," *IEEE Transactions on Neural Networks and Learning Systems*, vol. 28, no. 12, pp. 2998–3006, 2017.

[21] M. Duan and H. Zhu, "Constrained consensus of multiple autonomous vehicles with nonconvex constraints," in *2018 International Conference on Intelligent Rail Transportation (ICIRT)*, 2018, pp. 1–3.

[22] D. Efimov and A. Polyakov, "Finite-time stability tools for control and estimation," *Foundations and Trends in Systems and Control*, vol. 9, no. 2-3, pp. 171–364, 12 2020.

[23] K. Garg, E. Arabi, and D. Panagou, "Fixed-time control under spatiotemporal and input constraints: A quadratic programming based approach," *Automatica*, vol. 141, p. 110314, 2022.

[24] T. Gawron and M. M. Michałek, "Planning the waypoint-following task for a unicycle-like robot in cluttered environments," *Journal of Automation Mobile Robotics and Intelligent Systems*, vol. 9, 2015.

[25] ——, "VFO feedback control using positively-invariant funnels for mobile robots travelling in polygonal worlds with bounded curvature of motion," in *2017 IEEE International Conference on Advanced Intelligent Mechatronics (AIM)*, 2017, pp. 124–129.

[26] ——, "A G3-continuous extend procedure for path planning of mobile robots with limited motion curvature and state constraints," *Applied Sciences*, vol. 8, no. 11, 2018.

[27] ——, "The VFO-driven motion planning and feedback control in polygonal worlds for a unicycle with bounded curvature of motion," *Journal of Intelligent & Robotic Systems*, vol. 89, pp. 265–297, 01 2018.

[28] ——, "VFO path following control strategy for constrained motion of car-like robots with invariant funnels computed using the SOS optimization," in *2018 IEEE Conference on Control Technology and Applications (CCTA)*, 2018, pp. 94–100.

[29] T. Gawron, M. Mydlarz, and M. M. Michalek, "Algorithmization of constrained monotonic maneuvers for an advanced driver assistant system in the intelligent urban buses," in *2019 IEEE Intelligent Vehicles Symposium (IV)*, 2019, pp. 232–238.

[30] C. Gong, Y. Su, F. Jia, D. Zhang, and X. Hu, "Fixed time prescribed performance dynamic positioning control design for surface vessels," *Ocean Engineering*, vol. 287, p. 115615, 2023.

[31] R. Gonzalez, M. Fiacchini, T. Alamo, J. L. Guzman, and F. Rodriguez, "Adaptive control for a mobile robot under slip conditions using an lmi-based approach," *European Journal of Control*, vol. 16, no. 2, pp. 144–155, 2010.

[32] I. Gradshteyn and I. Ryzhik, *Table of Integrals, Series, and Products*, 7th ed., A. Jeffrey and D. Zwillinger, Eds. Academic Press, 2007.

[33] L. Guevara, M. M. Michałek, and F. A. Cheein, "Collision risk reduction of N-trailer agricultural machinery by off-track minimization," *Computers and Electronics in Agriculture*, vol. 178, p. 105757, 2020.

[34] D. Gómez-Gutiérrez, "On the design of nonautonomous fixed-time controllers with a predefined upper bound of the settling time," *International Journal of Robust and Nonlinear Control*, vol. 30, no. 10, pp. 3871–3885, 2020.

[35] H. R. Hertz, *The Principles of Mechanics Presented in a New Form.* London: MacMillan, 1899, (English translation of: *Die Prinzipien der Mechanik in neuem Zusammenhange dargestellt*, Leipzig: Barth, 1894).

[36] M. Hong, B. Wu, J. Wang, X. Zhang, Y. Qi, and J. Wang, "Cooperative control of the UGV formation in complex and dynamic environments," *IEEE Transactions on Intelligent Transportation Systems*, vol. 26, no. 11, pp. 18 762–18 774, 2025.

[37] J. Huang, C. Wen, W. Wang, and Z.-P. Jiang, "Adaptive stabilization and tracking control of a nonholonomic mobile robot with input saturation and disturbance," *Systems & Control Letters*, vol. 62, no. 3, pp. 234–241, 2013.

[38] A. Isidori, *Nonlinear Control Systems II.* Springer London, 1999.

[39] Z.-P. Jiang, E. Lefeber, and H. Nijmeijer, "Saturated stabilization and tracking of a nonholonomic mobile robot," *Systems & Control Letters*, vol. 42, no. 5, pp. 327–332, 2001.

[40] E. Jiménez-Rodríguez, A. Muñoz-Vázquez, J. Sánchez-Torres, M. Defoort, and A. Loukianov, "A Lyapunov-like characterization of predefined-time stability," *IEEE Transactions on Automatic Control*, vol. 65, pp. 4922–4927, 2019.

[41] E. Jiménez-Rodríguez, A. Muñoz-Vázquez, J. Sánchez-Torres, and A. Loukianov, "A note on predefined-time stability," *IFAC-PapersOnLine*, vol. 51, pp. 520–525, 2018.

[42] Z. Jin, C. Wang, D. Liang, S. Wang, and Z. Ding, "Fixed-time consensus for multiple tractor-trailer vehicles with dynamics control: A distributed internal model approach," *IEEE Transactions on Intelligent Vehicles*, vol. 9, no. 1, pp. 656–669, 2024.

[43] I. Kolmanovsky and N. McClamroch, "Developments in nonholonomic control problems," *IEEE Control Systems Magazine*, vol. 15, no. 6, pp. 20–36, 1995.

[44] W. Kowalczyk, M. Michałek, and K. Kozłowski, "Trajectory tracking control with obstacle avoidance capability for unicycle-like mobile robot," *Bulletin of the Polish Academy of Sciences. Technical Sciences*, vol. 60, no. 3, pp. 537–546, 2012.

[45] ——, "Trajectory tracking control and obstacle avoidance for a differentially driven mobile robot," *IFAC Proceedings Volumes*, vol. 44, no. 1, pp. 1058–1063, 2011.

[46] M. Labbadi, S. Boubaker, M. Djemai, S. K. Mekni, and A. Bekrar, "Fixed-time fractional-order global sliding mode control for nonholonomic mobile robot systems under external disturbances," *Fractal and Fractional*, vol. 6, no. 4, 2022.

[47] K. Łakomy and M. M. Michałek, "Robust output-feedback VFO-ADR control of underactuated spatial vehicles in the task of following non-parametrized paths," *European Journal of Control*, vol. 58, pp. 258–277, 2021.

[48] K. Łakomy, M. M. Michałek, and W. Adamski, "Scaling of commanded signals in a cascade control system addressing velocity and acceleration limitations of robotic UAVs," *IFAC-PapersOnLine*, vol. 52, no. 12, pp. 73–78, 2019.

[49] T.-C. Lee, K.-T. Song, C.-H. Lee, and C.-C. Teng, "Tracking control of unicycle-modeled mobile robots using a saturation feedback controller," *IEEE Transactions on Control Systems Technology*, vol. 9, no. 2, pp. 305–318, 2001.

[50] A. Levant, "Robust exact differentiation via sliding mode technique," *Automatica*, vol. 34, no. 3, pp. 379–384, 1998.

[51] ——, "On fixed and finite time stability in sliding mode control," in *52nd IEEE Conference on Decision and Control*, 2013, pp. 4260–4265.

[52] Z. Li, Z. Duan, G. Chen, and L. Huang, "Consensus of multiagent systems and synchronization of complex networks: A unified viewpoint," *IEEE Transactions on Circuits and Systems I: Regular Papers*, vol. 57, no. 1, pp. 213–224, 2010.

[53] J. Liu, Y. Zhang, Y. Yu, H. Liu, and C. Sun, "A zeno-free self-triggered approach to practical fixed-time consensus tracking with input delay," *IEEE Transactions on Systems, Man, and Cybernetics: Systems*, vol. 52, no. 5, pp. 3126–3136, 2022.

[54] T. Liu, R. Chai, S. Chai, F. Arvin, J. Zhang, and B. Lennox, "Fast collision-free multi-vehicle lane change motion planning and control framework in uncertain environments," *IEEE Transactions on Industrial Electronics*, vol. 71, no. 12, pp. 16 602–16 613, 2024.

[55] W. Liu, G. Wang, and X. Wang, "Modular formation control for multi-mobile robots with collision avoidance and communication maintenance,"

IEEE Transactions on Automation Science and Engineering, vol. 23, pp. 4477–4487, 2026.

[56] X. Liu, J. Cao, and C. Xie, "Finite-time and fixed-time bipartite consensus of multi-agent systems under a unified discontinuous control protocol," *Journal of the Franklin Institute*, vol. 356, no. 2, pp. 734–751, 2019.

[57] M. Livne and A. Levant, "Proper discretization of homogeneous differentiators," *Automatica*, vol. 50, no. 8, pp. 2007–2014, 2014.

[58] F. Lopez-Ramirez, D. Efimov, A. Polyakov, and W. Perruquetti, "Finite-time and fixed-time input-to-state stability: Explicit and implicit approaches," *Systems & Control Letters*, vol. 144, p. 104775, 2020.

[59] A. M. Lyapunov, "The general problem of the stability of motion," *International Journal of Control*, vol. 55, no. 3, pp. 531–534, 1992.

[60] N. A. Lynch, *Distributed Algorithms*. San Francisco, CA, USA: Morgan Kaufmann Publishers Inc., 1996.

[61] J. Lyu, J. Qin, D. Gao, and Q. Liu, "Consensus for constrained multi-agent systems with input saturation," *International Journal of Robust and Nonlinear Control*, vol. 26, no. 14, pp. 2977–2993, 2016.

[62] Q. Meng, Q. Ma, and Y. Shi, "Adaptive fixed-time stabilization for a class of uncertain nonlinear systems," *IEEE Transactions on Automatic Control*, vol. 68, no. 11, pp. 6929–6936, 2023.

[63] M. Michałek, "VFO control for mobile vehicles in the presence of skid phenomenon," in *Robot Motion and Control 2007*, K. Kozłowski, Ed. London: Springer London, 2007, pp. 57–66.

[64] ——, "Application of the VFO method to set-point control for the N-trailer vehicle with off-axle hitching," *International Journal of Control*, vol. 85, no. 5, pp. 502–521, 2012.

[65] M. Michałek, P. Dutkiewicz, M. Kiełczewski, and D. Pazderski, "Trajectory tracking for a mobile robot with skid-slip compensation in the Vector-Field-Orientation control system," *International Journal of Applied Mathematics and Computer Science*, vol. 19, no. 4, pp. 547–559, 2009.

[66] M. Michałek and M. Kiełczewski, "Helping a driver in backward docking with N-trailer vehicles by the passive control-assistance system," in *16th International IEEE Conference on Intelligent Transportation Systems (ITSC 2013)*, 2013, pp. 1993–1999.

[67] ——, "Cascaded VFO set-point control for N-trailers with on-axle hitching," *IEEE Transactions on Control Systems Technology*, vol. 22, no. 4, pp. 1597–1606, 2014.

[68] M. Michałek and K. Kozłowski, "Tracking controller with vector field orientation for 3-D nonholonomic manipulator," in *Proceedings of the Fourth International Workshop on Robot Motion and Control (IEEE Cat. No.04EX891)*, 2004, pp. 181–189.

[69] ——, "Asymptotic stabilization for the 3-D chained system: the vector field orientation approach," in *Proceedings of the Fifth International Workshop on Robot Motion and Control, 2005. RoMoCo '05.*, 2005, pp. 97–104.

[70] ——, "Trajectory tracking for a threecycle mobile robot: the Vector Field Orientation approach," in *Proceedings of the 44th IEEE Conference on Decision and Control*, 2005, pp. 1119–1124.

[71] ——, "Finite-time VFO stabilizers for the unicycle with constrained control input," in *Robot Motion and Control 2009*. Springer, 2009, pp. 23–34.

[72] ——, "Motion planning and feedback control for a unicycle in a way point following task: The VFO approach," *International Journal of Applied Mathematics and Computer Science*, vol. 19, no. 4, p. 533, 12 2009.

[73] ——, "Vector-Field-Orientation feedback control method for a differentially driven vehicle," *IEEE Transactions on Control Systems Technology*, vol. 18, no. 1, pp. 45–65, 2010.

[74] ——, "Finite-time and asymptotic stabilization of car-like kinematics with amplitude-limited control input," *IFAC Proceedings Volumes*, vol. 44, no. 1, pp. 3497–3502, 2011.

[75] ——, "Unified approach to trajectory tracking and set-point control for a front-axle driven car-like mobile robot," in *Proceedings of the 2011 American Control Conference*, 2011, pp. 1112–1117.

[76] ——, "The VFO state-constrained stabilisation of the nonholonomic manipulator with limited control input," *International Journal of Control*, vol. 84, no. 10, pp. 1678–1694, 2011.

[77] ——, "Feedback control framework for car-like robots using the unicycle controllers," *Robotica*, vol. 30, no. 4, p. 517–535, 2012.

[78] ——, "Convergence analysis for the orientation error of the unicycle in the VFO set-point control system," 2014, complementary note available on https://maciej.michalek.pracownik.put.poznan.pl/PublikacjePliki/UMRComplementaryNote.pdf.

[79] M. M. Michałek, "Robust visual servoing for mobile robots with the VFO-ADRC system," in *2022 17th International Conference on Control, Automation, Robotics and Vision (ICARCV)*, 2022, pp. 1–6.

[80] M. M. Michałek, P. Dutkiewicz, M. Kiełczewski, and D. Pazderski, "Vector-Field-Orientation tracking control for a mobile vehicle disturbed by the skid-slip phenomena," *Journal of Intelligent & Robotic Systems*, vol. 59, no. 3, pp. 341–365, 2010.

[81] M. M. Michałek and T. Gawron, "VFO path following control with guarantees of positionally constrained transients for unicycle-like robots with constrained control input," *Journal of Intelligent & Robotic Systems*, vol. 89, no. 1, pp. 191–210, 2018.

[82] M. M. Michałek and M. Kiełczewski, "The concept of passive control assistance for docking maneuvers with N-trailer vehicles," *IEEE/ASME Transactions on Mechatronics*, vol. 20, no. 5, pp. 2075–2084, 2015.

[83] M. M. Michałek, M. Kiełczewski, and T. Jedwabny, "Cascaded VFO control for non-standard N-trailer robots," *Journal of Intelligent & Robotic Systems*, vol. 77, no. 3, pp. 415–432, 2015.

[84] M. M. Michałek, K. Łakomy, and W. Adamski, "Robust output-feedback cascaded tracking controller for spatial motion of anisotropically-actuated vehicles," *Aerospace Science and Technology*, vol. 92, pp. 915–929, 2019.

[85] M. M. Michałek, R. M. Sobański, and M. Defoort, "Fixed-time VFO control for a unicycle," in *Prace Naukowe. Elektronika, Tom I,.* Warszawa: Oficyna Wydawnicza Politechniki Warszawskiej, 2022, vol. 197, pp. 191–200.

[86] M. M. Michałek, R. Wang, and X. Zhang, "VFO controller for set-point visual servoing of unicycle-like mobile robots equipped with a camera of an uncertain depth scale factor," in *2019 12th International Workshop on Robot Motion and Control (RoMoCo)*, 2019, pp. 184–190.

[87] P. Morin and C. Samson, *Motion Control of Wheeled Mobile Robots.* Berlin, Heidelberg: Springer Berlin Heidelberg, 2008, pp. 799–826.

[88] N. Moshtagh and A. Jadbabaie, "Distributed geodesic control laws for flocking of nonholonomic agents," *IEEE Transactions on Automatic Control*, vol. 52, no. 4, pp. 681–686, 2007.

[89] E. Moulay, V. Léchappé, E. Bernuau, and F. Plestan, "Robust fixed-time stability: Application to sliding-mode control," *IEEE Transactions on Automatic Control*, vol. 67, no. 2, pp. 1061–1066, 2022.

[90] E. Moulay and W. Perruquetti, *Finite-Time Stability and Stabilization: State of the Art.* Berlin, Heidelberg: Springer Berlin Heidelberg, 2006, pp. 23–41.

[91] A. Nedic, A. Ozdaglar, and P. A. Parrilo, "Constrained consensus and optimization in multi-agent networks," *IEEE Transactions on Automatic Control*, vol. 55, no. 4, pp. 922–938, 2010.

[92] B. Ning and Q.-L. Han, "Prescribed finite-time consensus tracking for multiagent systems with nonholonomic chained-form dynamics," *IEEE Transactions on Automatic Control*, vol. 64, no. 4, pp. 1686–1693, 2019.

[93] E. Nuño, A. Loría, A. I. Paredes, and T. Hernández, "Consensus-based formation control of multiple nonholonomic vehicles under input constraints," *IEEE Control Systems Letters*, vol. 6, pp. 2767–2772, 2022.

[94] K.-K. Oh, M.-C. Park, and H.-S. Ahn, "A survey of multi-agent formation control," *Automatica*, vol. 53, pp. 424–440, 2015.

[95] R. Olfati-Saber and R. Murray, "Consensus problems in networks of agents with switching topology and time-delays," *IEEE Transactions on Automatic Control*, vol. 49, no. 9, pp. 1520–1533, 2004.

[96] R. Olfati-Saber, J. A. Fax, and R. M. Murray, "Consensus and cooperation in networked multi-agent systems," *Proceedings of the IEEE*, vol. 95, no. 1, pp. 215–233, 2007.

[97] G. Oriolo, A. De Luca, and M. Vendittelli, "WMR control via dynamic feedback linearization: design, implementation, and experimental validation," *IEEE Transactions on Control Systems Technology*, vol. 10, no. 6, pp. 835–852, 2002.

[98] M. Ou, H. Sun, Z. Zhang, and S. Gu, "Fixed-time trajectory tracking control for nonholonomic mobile robot based on visual servoing," *Nonlinear Dynamics*, vol. 108, p. 251–263, 2022.

[99] M. Ou, H. Sun, Z. Zhang, L. Li, and X. ao Wang, "Fixed-time tracking control for nonholonomic mobile robot," *Kybernetika*, vol. 57, pp. 220–235, 2021.

[100] A. I. Paredes, E. Nuño, and A. Loría, "Output-feedback consensus-formation control of nonholonomic vehicles with input constraints and time-varying delays," *IEEE Transactions on Control of Network Systems*, vol. 12, no. 3, pp. 2361–2371, 2025.

[101] S. Parsegov, A. Polyakov, and P. Shcherbakov, "Nonlinear fixed-time control protocol for uniform allocation of agents on a segment," in *2012 IEEE 51st IEEE Conference on Decision and Control (CDC)*, 2012, pp. 7732–7737.

[102] Z. Peng, G. Wen, A. Rahmani, and Y. Yu, "Distributed consensus-based formation control for multiple nonholonomic mobile robots with a specified reference trajectory," *International Journal of Systems Science*, vol. 46, no. 8, pp. 1447–1457, 2015.

[103] A. Polyakov, "Nonlinear feedback design for fixed-time stabilization of linear control systems," *IEEE Transactions on Automatic Control*, vol. 57, no. 8, pp. 2106–2110, 2012.

[104] A. Polyakov, D. Efimov, and W. Perruquetti, "Robust stabilization of MIMO systems in finite/fixed time," *International Journal of Robust and Nonlinear Control*, vol. 26, no. 1, pp. 69–90, 2016.

[105] ——, "Finite-time and fixed-time stabilization: Implicit lyapunov function approach," *Automatica*, vol. 51, pp. 332–340, 2015.

[106] J.-B. Pomet, "Explicit design of time-varying stabilizing control laws for a class of controllable systems without drift," *Systems & Control Letters*, vol. 18, no. 2, pp. 147–158, 1992.

[107] C. Qian and W. Lin, "A continuous feedback approach to global strong stabilization of nonlinear systems," *IEEE Transactions on Automatic Control*, vol. 46, no. 7, pp. 1061–1079, 2001.

[108] Z. Qu, J. Wang, and R. A. Hull, "Cooperative control of dynamical systems with application to autonomous vehicles," *IEEE Transactions on Automatic Control*, vol. 53, no. 4, pp. 894–911, 2008.

[109] W. Ren and R. W. Beard, *Distributed Consensus in Multi-vehicle Cooperative Control: Theory and Applications*. London: Springer London, 2008.

[110] W. Ren, "Consensus tracking under directed interaction topologies: Algorithms and experiments," *IEEE Transactions on Control Systems Technology*, vol. 18, no. 1, pp. 230–237, 2010.

[111] A. Sen, S. R. Sahoo, and M. Kothari, "Circumnavigation on multiple circles around a nonstationary target with desired angular spacing," *IEEE Transactions on Cybernetics*, vol. 51, no. 1, pp. 222–232, 2021.

[112] S. Shi, S. Xu, and H. Feng, "Robust fixed-time consensus tracking control of high-order multiple nonholonomic systems," *IEEE Transactions on Systems, Man, and Cybernetics: Systems*, vol. 51, no. 3, pp. 1869–1880, 2021.

[113] K. Shojaei, "Output-feedback formation control of wheeled mobile robots with actuators saturation compensation," *Nonlinear Dynamics*, vol. 89, p. 2867–2878, 2017.

[114] J.-J. E. Slotine and W. Li, *Applied nonlinear control*. Englewood Cliffs, New Jersey: Prentice Hall, 1991.

[115] R. M. Sobański, M. Defoort, and M. M. Michałek, "Decentralized predefined-time leaderless consensus-formation VFO control for nonholonomic multi-agent systems," in *2024 13th International Workshop on Robot Motion and Control (RoMoCo)*, 2024, pp. 136–141.

[116] ——, "Observer-based fixed-time VFO control algorithm for leaderless multi-vehicle systems with directed communication topology," in *22nd Polish Control Conference*, 2026, (accepted).

[117] R. M. Sobański, M. M. Michałek, and M. Defoort, "VFO control design for a mobile robot in the presence of time and input constraints," in *2023 27th International Conference on Methods and Models in Automation and Robotics (MMAR)*, 2023, pp. 356–361.

[118] ——, "Predefined-time VFO control design for unicycle-like mobile robots," *Nonlinear Dynamics*, vol. 112, pp. 3591–3603, 2024.

[119] ——, "Fixed-time VFO control design for nonholonomic mobile robots with constrained control inputs," *IEEE Transactions on Cybernetics*, vol. 55, no. 7, pp. 3038–3050, 2025.

[120] ——, "Fixed-time path-following VFO control design for a unicycle-like mobile robot with constrained control inputs," in *23rd IFAC World Congress*, 2026, (accepted).

[121] O. Sordalen and O. Egeland, "Exponential stabilization of nonholonomic chained systems," *IEEE Transactions on Automatic Control*, vol. 40, no. 1, pp. 35–49, 1995.

[122] Y. Sun, F. Wang, Z. Liu, Y. Zhang, and C. L. P. Chen, "Fixed-time fuzzy control for a class of nonlinear systems," *IEEE Transactions on Cybernetics*, vol. 52, no. 5, pp. 3880–3887, 2022.

[123] J. D. Sánchez-Torres, D. Gómez-Gutiérrez, E. López, and A. Loukianov, "A class of predefined-time stable dynamical systems," *IMA Journal of Mathematical Control and Information*, vol. 35, 2018.

[124] B. Tian, H. Lu, Z. Zuo, and H. Wang, "Fixed-time stabilization of high-order integrator systems with mismatched disturbances," *Nonlinear Dynamics*, vol. 94, p. 2889–2899, 2018.

[125] E. Tolsted, "An Elementary Derivation of the Cauchy, Hölder, and Minkowski Inequalities from Young's Inequality," *Mathematics Magazine*, vol. 37, no. 1, pp. 2–12, 1964.

[126] J. Tsitsiklis, D. Bertsekas, and M. Athans, "Distributed asynchronous deterministic and stochastic gradient optimization algorithms," *IEEE Transactions on Automatic Control*, vol. 31, no. 9, pp. 803–812, 1986.

[127] C. Wang, H. Tnunay, Z. Zuo, B. Lennox, and Z. Ding, "Fixed-time formation control of multirobot systems: Design and experiments," *IEEE Transactions on Industrial Electronics*, vol. 66, no. 8, pp. 6292–6301, 2019.

[128] G. Wang, C. Wang, Q. Du, L. Li, and W. Dong, "Distributed cooperative control of multiple nonholonomic mobile robots," *Journal of Intelligent & Robotic Systems*, vol. 83, pp. 525–541, 2016.

[129] G. Wang, Z. Zuo, P. Li, and Y. Shen, "Controllers for multiagent systems with input amplitude and rate constraints and their application to quadrotor rendezvous," *IEEE Transactions on Automation Science and Engineering*, vol. 22, pp. 6354–6364, 2025.

[130] H. Wang, S. Shi, Z. Zhen, and J. Jiang, "Fixed-time switching tracking control for unmanned helicopter with multiple constraints," *ISA Transactions*, vol. 165, pp. 268–279, 2025.

[131] P. Wang, M. Chen, S. S. Ge, and X. Zhang, "Constrained finite-time and fixed-time stabilization for linear systems: Adaptive implicit lyapunov function-based control," *Automatica*, vol. 183, p. 112597, 2026.

[132] P. Wang and B. Ding, "Distributed rhc for tracking and formation of nonholonomic multi-vehicle systems," *IEEE Transactions on Automatic Control*, vol. 59, no. 6, pp. 1439–1453, 2014.

[133] Y. Wang, Y. Ji, W. Li, and X. Fang, "Fixed-time event-triggered control of nonholonomic mobile robots with uncertain dynamics and preassigned transient performance," *Mathematics*, vol. 12, no. 22, 2024.

[134] W. Yao, H. G. de Marina, B. Lin, and M. Cao, "Singularity-free guiding vector field for robot navigation," *IEEE Transactions on Robotics*, vol. 37, no. 4, pp. 1206–1221, 2021.

[135] W. Yao, B. Lin, B. D. O. Anderson, and M. Cao, "Topological analysis of vector-field guided path following on manifolds," *IEEE Transactions on Automatic Control*, vol. 68, no. 3, pp. 1353–1368, 2023.

[136] S. Yin, C. Chen, and Z. Xiang, "Distributed predefined-time leader–follower formation control for heterogeneous wheeled mobile robots," *IEEE Transactions on Automation Science and Engineering*, vol. 23, pp. 6687–6697, 2026.

[137] J. Zabczyk, "Some comments on stabilizability," *Applied Mathematics and Optimization*, vol. 19, no. 1, pp. 1–9, 1989.

[138] C. Zhang, G. Zhang, and Q. Dong, "Fixed-time disturbance observer-based nearly optimal control for reusable launch vehicle with input constraints," *ISA Transactions*, vol. 122, pp. 182–197, 2022.

[139] J. Zhu, J. Lu, and X. Yu, "Flocking of multi-agent non-holonomic systems with proximity graphs," *IEEE Transactions on Circuits and Systems I: Regular Papers*, vol. 60, no. 1, pp. 199–210, 2013.

[140] K. Zimenko, A. Polyakov, D. Efimov, and W. Perruquetti, "On simple scheme of finite/fixed-time control design," *International Journal of Control*, vol. 93, no. 6, pp. 1353–1361, 2018.

[141] A.-M. Zou, A. H. de Ruiter, and K. D. Kumar, "Distributed finite-time velocity-free attitude coordination control for spacecraft formations," *Automatica*, vol. 67, pp. 46–53, 2016.

[142] Z. Zuo, "Non-singular fixed-time terminal sliding mode control of non-linear systems," *IET Control Theory & Applications*, vol. 9, no. 4, pp. 545–552, 2015.

[143] Z. Zuo and L. Tie, "Distributed robust finite-time nonlinear consensus protocols for multi-agent systems," *International Journal of Systems Science*, vol. 47, no. 6, pp. 1366–1375, 2016.